Climate Change Adaption of Waterworks for Browning Surface Waters

Nano- and Ultrafiltration Membrane Applications for Drinking Water Treatment

Keucken, Alexander

2017

Document Version:
Publisher's PDF, also known as Version of record

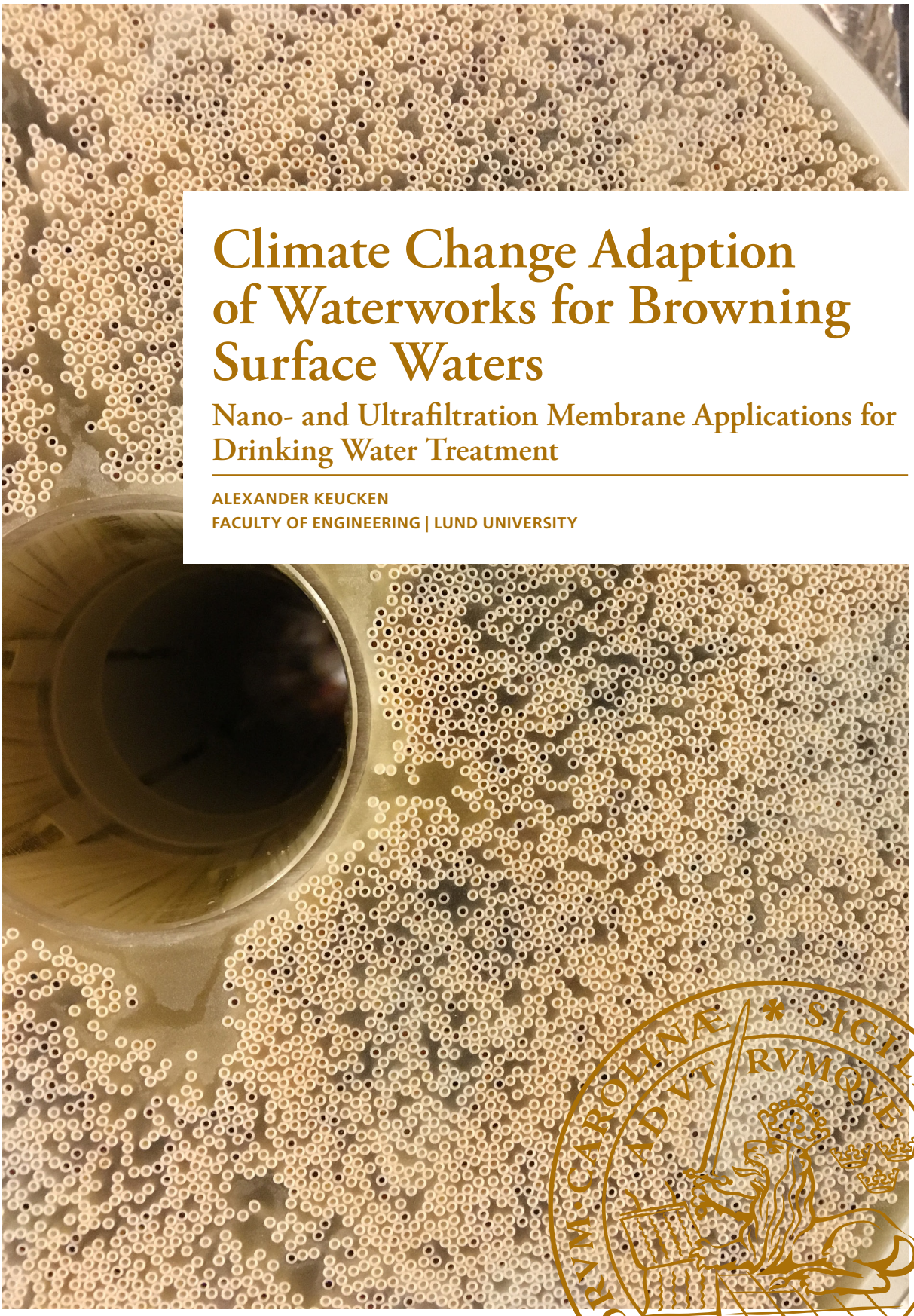

Climate Change Adaption of Waterworks for Browning Surface Waters

Nano- and Ultrafiltration Membrane Applications for Drinking Water Treatment

ALEXANDER KEUCKEN
FACULTY OF ENGINEERING | LUND UNIVERSITY

Climate Change Adaption of Waterworks for Browning Surface Waters

Climate Change Adaption of Waterworks for Browning Surface Waters

Nano- and Ultrafiltration Membrane Applications for Drinking Water Treatment

Alexander Keucken

LUND UNIVERSITY

DOCTORAL DISSERTATION
by due permission of the Faculty of Engineering, Lund University, Sweden.
To be defended at the Faculty of Engineering, V-building, John Ericssons väg 1, Lund, room V:A on Friday, 15th of December, 2017 at 10.15 a.m.

Faculty opponent
Prof. Dr. Riku Vahala

Organization LUND UNIVERSITY Water Resources Engineering Box 118 SE-221 00 Lund, Sweden	**Document name** DOCTORAL THESIS **Date of disputation** 2017-12-15
Author Alexander Keucken	**Sponsoring organizations** VIVAB, Sydvatten, Norrvatten, Tekniska Verken i Linköping, Gästrike Vatten, Sweden Water Research and Svenskt Vatten Utveckling

Title and subtitle

Climate Change Adaption of Waterworks for Browning Surface Waters – Nano- and Ultrafiltration Membrane Applications for Drinking Water Treatment

Abstract

Natural organic matter (NOM) is found in all surface, ground, and soil waters. During recent decades, reports worldwide show a continuing increase in the color and NOM of the surface water, which has an adverse effect on drinking water purification. For several practical and hygienic reasons, the presence of NOM is undesirable in drinking water. Various technologies have been proposed for NOM removal with varying degrees of success. Membranes are an exceptional barrier to particles, turbidity, microorganisms, and disinfectant by-product (DBP) precursors from drinking water. Significant improvements in membrane technology, design, and materials during the past three decades, has made the drinking water production processes nowadays more effective and environmentally friendly. Based on the research trend, it can be seen that membrane applications for NOM removal will play a more prominent role in the future.

This dissertation presents results for selective NOM removal by ultrafiltration (UF) and nanofiltration (NF) membrane configurations at two Swedish surface water treatment plants (WTPs). Extensive field testing with several customized and fully-automated pilot plants were carried out for evaluation of different membrane concepts for NOM removal. Modelling of membrane performance and retention behavior of hollow-fiber (HF) NF membranes using a solution-diffusion approach and two-dimensional axisymmetric computational fluid dynamics (CFD), provided accurate prediction of NOM removal. For this reason, it was used for full-scale process design and feasibility studies. Direct NF filtration of surface water indicated stable membrane performance and high average NOM removal rates (UV_{254}: 91.6–94.7 %; TOC: 82–92.2 %). The NF membrane retention was highest for biopolymers (>95% removal), followed by Humic Substances (HS) (>80% removal). Combined coagulation/UF processes removed approximately 30% of the DOC, and 50% of the HS and biopolymers. However, building blocks (BB) and low molecular weight acids (LMW_{acids}) remained unchanged compared with the NOM composition of the feed and permeate. For optimization of hybrid membrane processes, an automatic coagulant dosing system based on online measurements was successfully applied.

Autopsy results of HF-NF membranes after twelve months of continuous pilot operation with pretreated feed water (coagulation and rapid sand filtration), showed no substantial changes of the aged membranes from different module sections compared to virgin membranes. Rigorous analysis of the nanomechanical properties of HF-UF membranes harvested after 12–14 months pilot operation showed that the detected change in nanomechanical characteristics did not result in considerable impact on the macroscopic properties of the membranes. Comprehensive UF pilot trials resulted in improvements of the two-stage full-scale UF facility during the design phase and commissioning at Kvarnagården WTP.

Key words: natural organic matter, drinking water, ultrafiltration, nanofiltration, autopsy, modelling

Classification system and/or index terms (if any)

Supplementary bibliographical information	**Language:** English
ISSN and key title	**ISBN:** 978-91-7753-459-4 (print) 978-91-7753-460-0 (e-version)
Recipient's notes	**Number of pages:** 321 / **Price: -**
	Security classification

Climate Change Adaption of Waterworks for Browning Surface Waters

Nano- and Ultrafiltration Membrane Applications for Drinking Water Treatment

Alexander Keucken

LUND
UNIVERSITY

Cover photo (front) by Alexander Keucken

Cover photo (back) by Micael Goth, *Lime & Lemon Media*

Faculty of Engineering, Department of Building & Environmental Technology
Division of Water Resources Engineering

ISBN print: 978-91-7753-459-4
ISBN e-version: 978-91-7753-460-0
REPORT: 1072

Printed in Sweden by Media-Tryck, Lund University
Lund 2017

Dedicated to my beloved family: Maria – Alice – Robin

Contents

Acknowledgements

First and foremost, I would like to express my sincere gratitude to my supervisor Professor Kenneth M. Persson for convincing me to do a Ph.D. and for his committed support during the last five years. His tremendous expertise, practical understanding and inspiring coaching have been vital help during the intense time of field testing and completion of this thesis.

In my dual role as an industrial Ph.D. at Lund University and research manager for the public joint stock utility VIVAB, the immense support and recurring encouragement from my CEO, Margareta Björksund-Tuominen and from the Chairman, Peter Sjöholm have been essential for finalizing my thesis. Moreover, the realization of a full-scale membrane facility at Kvarnagården WTP as part of my research activities has been a highly motivating experience of combining theoretical approaches with practical needs.

I would also like to thank my academic colleagues, Angelica Lidén at the division of Water Resources Engineering (Lund University) and Elin Lavonen, Department of Aquatic Sciences (Swedish University of Agricultural Sciences), for productive collaboration and, fruitful discussions during various pilot trials and project meetings.

This research has been conducted in close collaboration with public water utilities, research institutes, and industrial partners. Special thanks go to Kristina Dahlberg, Per Ericsson, and Bertil Johansson who provided excellent practical help during my field studies at Görväln WTP, giving me, a commuter from the West Coast, always an essential feeling of home.

I would like to acknowledge all my co-authors and especially the collaboration with Stephan Köhler on NOM characterization and evaluation of online sensors; Yuan Wang and Keng Han Tng on membrane autopsies; Greg Leslie and Xuefei Liu on CFD modelling; Leo Guiterrez and Jean-Philippe Croué on membrane ageing; Tom Spanjer on NOM prediction and full-scale design; and Gerald Heinicke on feasibility studies and statistical analysis.

Since the core of my research activities is based on extensive long-term pilot trials, I was highly dependent on practical expertise and hands-on help. Therefore, I would like to thank Andrew Holmes (then at Purac AB) and Erik Scharenborg (Pentair) for priceless efforts during the commissioning and operations of complex pilot plants. Furthermore, I would like to acknowledge the operating staff at Kvarnagården WTP for practical assistance and their work installing of tricky solutions. Special thanks to Jennie Lindgren and Moshe Habagil for daily operations of the UF test facility.

Most importantly, I would like to thank my wife Maria, my daughter Alice and my son Robin for their understanding and the enormous support during my hectic Ph.D. period. Your patience and good spirit were very helpful for membrane sessions on weekends, numerous conference travels, and plenty of work off hours!

Finally, I acknowledge financial support by The Swedish Water and Wastewater Association (SVU 2015-20), VIVAB, Sydvatten, Norrvatten, Tekniska Verken i Linköping, Gästrike Vatten, Sweden Water Research, and Lund University.

List of Publications and Author´s Contributions

Appended papers

This thesis is based on the following papers, referred to by their Roman numerals in the body of the text. The papers are appended at the end of the thesis.

I. Evaluation of novel hollow fiber membranes for NOM removal by advanced autopsy

Keucken, A., Wang, Y., Tng, K.H., Leslie, G.L, Persson, K.M. and Spanjer, T. (2016).

Water Science and Technology: Water Supply 16 (3), 628–640. doi:10.2166/ws.2015.170.

Reprinted with kind permission of IWA Publishing, London, UK.

II. Impact of operation conditions, foulant adsorption, and chemical cleaning on the nanomechanical properties of ultra-filtration hollow fiber membranes

Gutierrez, L., **Keucken, A.**, Aubry, C., Zaouri, N., Teychene, B., Croué, J.-P. (2017).

In preparation (manuscript).

III. Optimizing hollow fibre nanofiltration for organic matter rich lake water

Keucken, A., Wang, Y., Tng, K.H., Leslie, G.L., Spanjer, T., Köhler, S.J. (2016).

Water, vol. 8 (10), 430. doi:10.3390/w8100430

Reprinted with kind permission of MDPI AG, Basel, Switzerland.

IV. Simulation of NOM removal by capillary NF: A numerical method for full-scale plant design

Keucken, A., Liu, X., Lian, B., Wang, Y.,Persson, K.M., Leslie, G. (2017).

Submitted to Journal of Membrane Science.

V. Combined coagulation and ultrafiltration process to counteract increasing NOM in brown surface water

Keucken, A., Heinicke, G., Persson, K.M., Köhler, S.J. (2017).

Water, vol. 9 (9), 697. doi:10.3390/w9090697

Reprinted with kind permission of MDPI AG, Basel. Switzerland.

VI. Upgrading coagulation with hollow-fibre nanofiltration for improved organic matter removal in drinking water

Köhler, S.J., Lavonen, E.E., **Keucken, A.**, Schmitt-Kopplin, P., Spanjer, T. and Persson, K.M. (2016).

Water Research, vol. 89, 232–240. doi:10.1016/j.watres.2015.11.048

Reprinted with kind permission of Elsevier Ltd., London, UK.

Author´s contribution to appended papers

I. The author planned the study together with the co-authors, performed the field studies (NF pilot operation and extraction of hollow fibers), analyzed the results, wrote the article together with the co-authors and did the final review of the paper. The membrane autopsy was conducted by Y. Wang and K.H. Tng.

II. The author planned the study together with the co-authors and performed the field studies (UF pilot operation and extraction of hollow fibers). The membrane autopsy was carried out by L. Gutierrez. The author contributed to the results and discussions of the paper, which was coordinated by J.P. Croué.

III. The author planned the study, performed the pilot trials and statistical analysis together with T. Spanjer. The author was the main contributor to the writing of all sections and the final review of the paper, while the co-authors provided useful commentary and discussion on the paper.

IV. The author planned the experiments and performed the pilot trials. The CFD modelling was carried out by X. Liu and B. Lian, while the author was responsible for the experimental calibration of the membrane trials. The author contributed to the results and discussions of the paper, which was coordinated by G. Leslie.

V. The author planned the study together with the co-authors, performed the pilot trials, analyzed the results, and was the main contributor to the writing of all sections and the final review of the manuscript, with the assistance of

the co-authors. Most of the analytical work was carried out at participating waterworks, commercial and research laboratories (SLU). Scenario analysis and UV sensor data evaluation were carried out by S.J. Köhler.

VI. The author planned the experiments and played a leading role in their execution. Most of the analytical work was carried out at participating waterworks, commercial and research laboratories (SLU). The author contributed with commentary and discussion of the paper, which was coordinated by S.J. Köhler.

Other related publications

Peer reviewed papers by the author not included in this thesis:

Uses of fluorescence excitation-emissions indices in predicting water treatment efficiency

Lidén, A., **Keucken, A.**, Persson, K.M. (2017).

Journal of Water Process Engineering 16, 249–257. doi:10.1016/j.jwpe.2017.02.003

The author planned and performed part of the pilot study together with the co-authors, contributed to the results and discussions of the paper, which was coordinated by A. Lidén.

Conference abstracts

NOM Characterization and Removal by Water Treatment Processes for Drinking Water and Ultra Pure Process Water

Keucken, A. and Heinicke, G.

4th IWA Speciality Conference on NOM, Costa Mesa (USA), 27-29 July, 2011.

Study of biopolymer retention, NOM fouling and microbial barrier effects in an UF pilot plant in Varberg, Sweden

Keucken, A. and Persson, K.M.

6th IWA Specialist Conference on Membrane Technology for Water & Wastewater Treatment, Aachen (Germany), 4-7 October, 2011.

Membrane fouling as revealed by advanced autopsy in a UF/coagulation pilot trial for enhanced NOM removal

Keucken, A. and Donose, B.C.

9th IWA Leading Edge Conference on Water and Wastewater Technologies, Brisbane (Australia), 3-7 June, 2012.

Study of biopolymer retention, NOM fouling and microbial barrier effects in pilot scale with ultrafiltration and combined coagulation

Keucken, A. and Persson, K.M.

IWA World Water Congress & Exhibition, Busan (South Korea), 16-20 September, 2012.

Advanced NOM monitoring of novel hollow fiber nanofiltration combined with activated carbon filters

Keucken, A., Spenkelink, F.J., Persson, K.M. and Köhler, S.J.

5th IWA SPC on NOM, Perth (Australia), 1-4 October, 2013.

Evaluation of Color Removal Package (CRP) for drinking water based on novel hollow fiber nanofiltration

Keucken, A., Ericsson, P., Persson, K.M., Dekker, R. and Köhler, S.J.

9th Nordic Drinking Water Conference, Helsinki (Finland), 2-4 June, 2014.

Enhanced NOM removal by hollow fiber nanofiltration combined with granular activated carbon filters

Keucken, A., Ericsson, P., Persson, K.M, Spanjer, T. and Dekker, R.

Singapore International Water Week, 1-5 June, 2014.

Evaluation of novel hollow fiber membranes for NOM removal by advanced autopsy

Keucken, A., Wang, Y., Tng, K.H., Leslie, G.L., Persson, K.M., Köhler, S.J. and Spanjer, T.

12th Leading Edge Conference on Water and Wastewater Technologies, Hong Kong (China), 30 May-3 June, 2015.

Enhanced NOM removal by direct filtration of surface water in Sweden using novel hollow fiber nanofiltration membranes

Keucken, A., Dekker, R. and Persson, K.M.

6th IWA SPC on NOM, Malmö (Sweden), 7-10 September, 2015.

The benefits of pilot trials for full-scale application of innovative two-stage UF membrane process at Kvarnagården WTP

Keucken, A. and Holmes, A.

10th Nordic Drinking Water Conference, Reykjavik (Island), 28-30 September, 2016.

Reports

GenoMembran. Slutrapport från projekt 2012–2015

Lidén, A., **Keucken, A.** and Persson, K.M.
Svenskt Vatten Utveckling, rapport 2015–20, Bromma, Sweden

Journals and Magazines

The rise of natural organic matter: a prompt for treatment progress

Persson, K.M., Köhler, S.J., Lavonen, E. and **Keucken, A.**
Water 21 Magazine of the International Water Association, April 2015, p25-27, ISSN 15619508.

Popular Summary

In recent decades, rising levels of organic natural material (NOM) have become a major challenge for water producers in countries with temperate climate. Increasing NOM concentrations have been reported primarily by waterworks with surface water sources, including (among others) northern USA, Canada, the Baltics, Russia, China, and Scandinavia. The raw water abstracted by waterworks contains primarily two types of humic substances, a terrestrial derived component (allochthonous NOM leached from soil that can be removed by flocculation) and a component derived from degradation processes of organic material within the water body (autochthonous NOM that is barely affected by flocculation). High NOM concentrations generally occur in surface waters with short residence time, mainly in southern and central Sweden, while brown-colored surface water is not very common in northern Sweden's inland (north of the river Dalälven) due to the lower turnover rate of water sources in this region. In drinking water treatment, elevated levels of NOM can cause negative effects on water quality such as color, bad taste, and offensive odor. In addition, the organic matter can be used by microorganisms as substrate so that microbial growth can be promoted within distribution networks, thus increasing the risk of hygiene problems. Furthermore, higher NOM levels increase the risk of the formation of cancerous disinfectant by-products, as disinfection with chlorine leads to formation of chlorinated compounds. Moreover, the complexing properties of humic substances present a risk of increased transport of heavy metals and adsorbed organic pollutants in the water. Increased levels of NOM in raw water adversely effect the microbiological and chemical barrier function of water treatment plants. In drinking water production, microbiological protection decreases due to increasing color (lower transmittance = increased absorption losses) in UV treatment, while chemical contaminants are not sufficiently retained by, for example, activated carbon filters due to the reduced adsorption capacity caused by already adsorbed humic substances. At present, there is no scientific evidence for decrease of the rising NOM levels in the near future. In view of this, Swedish drinking water producers are in need of robust and reliable treatment processes for efficient NOM removal. Recently, membrane technology has gained a boost as a new treatment process for removing organic matter and increasing the microbial barrier effect. Both ultrafiltration (UF) and nanofiltration (NF) can be used to reduce the NOM content in drinking water.

In order to achieve efficient NOM removal, UF must be combined either with pre-coagulation (i.e., flocculation and sedimentation) or direct coagulation (i.e., in-line dosing prior to membrane treatment), resulting in approximately the same degree of NOM reduction compared to conventional chemical flocculation. However, this membrane configuration requires lower dosing rates of coagulants, and results in shorter contact times (more compact plant design) and less chemical sludge. On the

other hand, NF achieves a NOM reduction of almost 90% compared to 50% by conventional flocculation and sedimentation, which mainly separate terrestrial humus (leaching products from soil environments such as forests). In contrast, NF allows for more selective NOM reduction, where only low molecular weight (LMW) NOM fractions pass through the membrane. Nevertheless, NF retains divalent ions such as calcium and magnesium, which needs to be considered for technical and health reasons in drinking water production.

UF and NF differ in terms of water recovery rate, backwash interval, system pressure, filtration capacity, and the need for cross-flow filtration. Unlike NF filters, UF filters have a higher capacity with flux rates up to 100 liters per square meter of active membrane surface (compared with approximately 20 liters for NF filters).

In the present research, UF and NF were applied at two Swedish waterworks with surface water sources in order to evaluate selective NOM removal for drinking water treatment. Extensive pilot trials were performed with several mobile and almost fully automated test facilities aiming to evaluate different membrane concepts for NOM reduction. Numerical models were established to simulate the separation properties of the membranes and to provide feasibility studies of the potential for full-scale application. Long-term pilot trials of direct NF filtration of surface water from Lake Mälaren (without pretreatment) indicated high and stable NOM reduction rates of 91.6–94.7 % for UV absorbance at 254 nm (UV_{254}) and 82–92.2 % for total organic carbon (TOC). Accordingly, the removal rate of high molecular weight NOM fractions was higher than 90%.

Test runs with UF combined with in-line coagulation on surface water from Lake Neden (mixed with 20% groundwater) resulted in a reduction of dissolved organic matter (DOC) corresponding to 30% and a removal rate of high molecular weight NOM fractions of approximately 50%. For this hybrid membrane application, an automatic dosing control system for coagulants was developed in order to optimize the NOM removal efficiency rate. Advanced analytical methods (so-called autopsy) of the membranes were applied after the experiments to detect deposits on the membrane surface and changes (deterioration) of membrane material (e.g., owing to exposure to cleaning chemicals or adverse operating conditions). After more than 12 months of continuous operation, membranes were extracted from different sections of the test modules and their physical and chemical properties analyzed. All autopsy results did not indicate any serious changes in the membrane properties or irreversible fouling layers. Finally, the specific findings from the pilot trials at the customized UF test facility contributed significant improvements during the design phase and commissioning of a full-scale two-stage UF plant at Kvarnagården WTP in Varberg, Sweden.

Abstract

Natural organic matter (NOM) is found in all surface, ground, and soil waters. During recent decades, reports worldwide show a continuing increase in the color and NOM of the surface water, which has an adverse effect on drinking water purification. For several practical and hygienic reasons, the presence of NOM is undesirable in drinking water. Various technologies have been proposed for NOM removal with varying degrees of success.

Membranes are an exceptional barrier to particles, turbidity, microorganisms, and disinfectant by-product (DBP) precursors from drinking water. Significant improvements in membrane technology, design, and materials during the past three decades, has made the drinking water production processes nowadays more effective and environmentally friendly. Based on the research trend, it can be seen that membrane applications for NOM removal will play a more prominent role in the future.

This dissertation presents results for selective NOM removal by ultrafiltration (UF) and nanofiltration (NF) membrane configurations at two Swedish surface water treatment plants (WTPs). Extensive field testing with several customized and fully-automated pilot plants were carried out for evaluation of different membrane concepts for NOM removal. Modelling of membrane performance and retention behavior of hollow-fiber (HF) NF membranes using a solution-diffusion approach and two-dimensional axisymmetric computational fluid dynamics (CFD), provided accurate prediction of NOM removal. For this reason, it was used for full-scale process design and feasibility studies. Direct NF filtration of surface water indicated stable membrane performance and high average NOM removal rates (UV_{254}: 91.6–94.7 %; TOC: 82–92.2 %). The NF membrane retention was highest for biopolymers (>95% removal), followed by Humic Substances (HS) (>80% removal). Combined coagulation/UF processes removed approximately 30% of the DOC, and 50% of the HS and biopolymers. However, building blocks (BB) and low molecular weight acids (LMW_{acids}) remained unchanged compared with the NOM composition of the feed and permeate. For optimization of hybrid membrane processes, an automatic coagulant dosing system based on online measurements was successfully applied.

Autopsy results of HF-NF membranes after twelve months of continuous pilot operation with pretreated feed water (coagulation and rapid sand filtration), showed no substantial changes of the aged membranes from different module sections compared to virgin membranes. Rigorous analysis of the nanomechanical properties of HF-UF membranes harvested after 12–14 months pilot operation showed that the detected change in nanomechanical characteristics did not result in considerable impact on the macroscopic properties of the membranes. Comprehensive UF pilot trials resulted in improvements of the two-stage full-scale UF facility during the design phase and commissioning at Kvarnagården WTP.

Populärvetenskaplig sammanfattning

De senaste decennierna har stigande halter av organiskt naturligt material (NOM) blivit en stor utmaning för vattenproducenter i länder med tempererat klimat. Stigande NOM halter har rapporterats av framförallt av ytvattenverk från bl.a. norra USA, Kanada, Baltikum, Ryssland, Kina och Skandinavien. NOM i råvattnet till vattenverk utgörs främst av två olika typer, humus från marken (alloktont NOM som kan avskiljas genom fällning) och humus från biologiska nedbrytningsprocesser i ytvatten (autoktont NOM som är svårfällningsbara fraktioner). Höga NOM halter förekommer generellt i ytvatten med korta uppehållstider främst i södra och mellersta Sverige, medan brunfärgade ytvatten är ovanligare i norra Sveriges inland (norr om Dalälven), pga. vattnets lägre omsättningshastighet. Inom dricksvattenberedningen kan NOM leda till missfärgning samt lukt- och smakstörningar. Dessutom kan det organiska materialet utgöra en substratkälla för mikroorganismer som in sin tur främjar mikrobiell efterväxt i distributionsnät och därmed ökar risken för hygieniska problem. Vid högre halter NOM i vattnet stiger även risken för bildandet av cancerogena desinfektionsbiprodukter, då desinfektion med klor medför bildning av klorerande föreningar. Dessutom kan humusämnenas komplexbildande egenskaper medföra en risk för ökad transport av metaller och organiska spårämnen såsom persistenta föreningar i vattnet. Ökade NOM halter i råvatten till ytvattenverk påverkar den mikrobiologiska och kemiska barriärverkan negativt. Det mikrobiella skyddet minskar pga. sämre transmittans (ökade absorptionsförluster) vid UV-behandling, samtidigt som kemiska föroreningar inte avskiljs genom t.ex. kolfilter med nedsatt adsorptionsförmåga pga. adsorberade humusämnen.

I dagsläge finns inga vetenskapliga bevis eller tecken på att de numera över tre decennier stigande NOM halterna skulle kunna minska inom snar framtid. Mot denna bakgrund är svenska vattenproducenter i stort behov av robusta och tillförlitliga reningsmetoder för effektiv NOM avskiljning. Den senaste tiden har membrantekniken fått ett uppsving som ny beredningsmetod för att både avskilja organiskt material och att öka den mikrobiella barriärverkan. Såväl ultrafilter (UF) som nanofilter (NF) kan användas för att minska NOM-halten i dricksvatten.

För att uppnå en effektiv NOM avskiljning måste ultrafiltrering kombineras antingen med förfällning eller med direktfällning, vilket resulterar i ungefär samma reduktionsgrad jämfört med konventionell fällning, förutom att denna membrankonfiguration kräver mindre fällningskemikalier och kortare kontakttider (kompaktare anläggningar) samt genererar mindre kemslam. Däremot uppnår nanofiltrering en NOM reduktion närmare 90 procent jämfört med 50 procent genom konventionell fällning som dessutom nästan enbart avskiljer terrester humus (urlakningsprodukter från markmiljöer, t.ex. skogsområden). Dessutom möjliggör

nanofiltering en både breddare och mer selektiv NOM avskiljning där enbart lågmolekylära NOM fraktioner passerar membranet. Icke desto mindre medför NF en avskiljning av mineraler i vattnet (t.ex. kalcium och magnesium), vilket måste beaktas ur teknisk och hälsomässig synvinkel inom dricksvattenproduktionen.

UF och NF filter skiljer sig vad gäller vattenutbyte, backspolningsbehov, systemtryck, ytbelastningar och tillämpning av tvärströmsfiltrering. Till skillnad från NF filter, har UF filter en högre kapacitet med flöden upp till 100 liter per kvadratmeter aktiv membranyta och timme (jämfört med drygt 20 liter per kvadratmeter och timme för NF filter).

I denna avhandling presenteras resultat från fältstudier på två svenska ytvattenverk där UF och NF har tillämpats för selektiv NOM avskiljning inom dricksvattenberedning. Omfattande pilotförsök genomfördes med ett antal mobila och delvis fullautomatiserade testanläggningar för att kunna utvärdera olika membrankoncept för NOM reduktion. Numeriska modeller upprättades dels för att kunna simulera membranens avskiljningsegenskaper och dels för genomförandestudier av potentiella storskaliga processanläggningar. Långtidsförsök med NF filtrering av ytvatten från sjön Mälaren (utan förbehandling) indikerade höga och stabila NOM reduktionsgrader motsvarande 91.6–94.7 % för UV absorbans vid 254 nm (UV_{254}) och motsvarande 82–92.2 % för totalt organiskt kol (TOC). Avskiljningen av NOM fraktioner med hög molekylärvikt uppmättes till drygt 90%. Testkörningar med UF kombinerad med direktfällning på ytvatten från sjön Neden (blandat med 20% grundvatten) resulterade i en reduktion av löst organiskt material (DOC) med motsvarande 30% samt 50% avskiljning av NOM fraktioner med hög molekylärvikt. En automatisk styrningsmodell för dosering av koagulanter utvecklades för optimering av NOM retention där UF processer kombineras med in-line fällningsmetoden. Avancerade mätmetoder (s.k. autopsi) användes för detektion av både ev. avlagringar på membranytan och förändringar/försämringar av membranmaterial (t.ex. pga. rengöringskemikalier eller ogynnsamma driftförhållanden). Efter drygt 12 månader kontinuerlig drift, extraherades membran från olika testmoduler och analyserades med avseende på fysikaliska och kemiska egenskaper. Samtliga autopsier indikerade vare sig allvarliga förändringar av membranegenskaper eller irreversibla beläggningar. Slutligen bidrog resultaten från testkörningar med en UF pilotanläggning till avsevärda förbättringar vid projektering och idrifttagande av en storskalig två-stegs UF-anläggning på Kvarnagårdens vattenverk i Varberg.

Abbreviations

Term	Definition	Unit
ΔP	Transmembrane pressure	Pa
A	Area	m^2
AFM	Atomic force microscopy	-
AIT	Air integrity test	-
ALK	Alkalinity as HCO_3^-	mg L^{-1}
BB	Building blocks	ppb-C
BDOC	Biodegradable dissolved organic carbon	mg L^{-1}
BW	Backwashing of membranes	-
CEB	Chemically enhanced backwash	-
CEFF	Chemically enhanced forward flushing of membranes	-
CIP	Cleaning-in-place	-
C_m	Solute concentration at membrane surface	mg L^{-1}
COD	Chemical oxygen demand	mg L^{-1}
CP	Concentration polarization	-
C_p	Solute concentration in permeate	mg L^{-1}
CPF	Concentration polarization factor	-
Da	Dalton	-
DBP	Disinfection by-products	-
DOC	Dissolved Organic Carbon	mg L^{-1}
DW	Drinking water	-
EBCT	Empty bed contact time	min
EEM	Excitation-emission matrix	-
FI	Fluorescence index, calculated from an EEM	-
FNU	Formazin nephelometric unit	-
GAC	Granular activated carbon	-
GW	Groundwater	-
HCl	Hydrochloric acid	ppm
H_2SO_4	Sulfuric acid	ppm
HF-NF	Hollow fiber nanofiltration	-
HF-UF	Hollow fiber ultrafiltration	-
HIX	Humification index, calculated from an EEM	-
HS	Humic substances	-
J	Mass flux	L m^{-2} h^{-1}
J_s	Solute flux	mg m^{-2} h^{-1}
LC-OCD	Liquid chromatography-organic carbon detection	-

Term	Definition	Unit
LMW_{acids}	Low molecular weight acids	ppb-C
$LMW_{neutrals}$	Low molecular weight neutrals	ppb-C
MM	Molar Mass	-
MW	Molecular weight	-
MWCO	Molecular weight cut-off	-
NaCl	Sodium chloride	ppm
NaOCl	Sodium hypochlorite	ppm
NaOH	Sodium hydroxide	ppm
NF	Nanofiltration	-
NOM	Natural organic matter	-
NTU	Nephelometric turbidity units	-
PES	Polyether sulfone	-
P_s	Solute permeability coefficient	-
r	Distance to the axis of HF membrane	m
r_0	Internal radius of HF membrane	m
RSF	Rapid sand filtration	-
R_m	Membrane resistance	m^{-1}
SEM	Scanning electron microscopy	-
S_m	Mass source term	kg m^{-3} s^{-1}
SUVA	Specific ultraviolet absorbance (DOC-normalized absorbance at 254 nm)	L mg^{-1} m^{-1}
S_v	Momentum source term	kg m^{-2} s^{-2}
TMP	Transmembrane pressure	bar
TOC	Total organic carbon	mg L^{-1}
UF	Ultrafiltration	-
UV_{254}	UV-absorption at wavelength 254 nm	m^{-1}
UV-vis	Ultraviolet-visual	-
V_{CF}	Cross-flow velocity	m s^{-1}
WTP	Water treatment plant	-
β:α	Freshness index, calculated from an EEM	-

1. Introduction

The rise of natural organic matter (NOM) in raw water sources has become one of the main drivers for drinking water treatment progress worldwide and poses a challenge both for scientists and drinking water producers.

NOM can be seen as the footprint of the ecological status of waters such as aquifers, lakes, and rivers. A thorough analysis of the production of autochthone NOM (degradation within the aquatic environment of the organic material), allochthone NOM (leached from soil), and NOM changes can provide information about such as retention time, microbial composition, nutrient status, season, etc. NOM serves as a carbon substrate for many organisms in water systems and is continuously produced and consumed. In addition, NOM preserved in lake sediments offer a record of how the landscape has changed over time.

Rising organic matter concentrations in the surface waters of Scandinavia require adaptation of current drinking water treatment processes. In the work described in this thesis, two Swedish water utilities, Norrvatten and Vatten & Miljö i Väst AB (VIVAB) have browning surface water sources that have been the subject of investigations and feasibility studies on new treatment techniques based on different membrane concepts for efficient NOM removal.

1.1 NOM in surface water

In the late 1980s, an increase of natural organic matter (NOM) concentration was first reported in Swedish surface waters as a link between increased amount of humic substances (HS) and the darkening of Swedish lakes (Forsberg & Petersen, 1990). Over the last few decades, several other reports have confirmed that the occurrence of NOM in water (browning of surface waters) is a worldwide phenomenon (Eikebrokk *et al.* 2004; Worrall & Burt, 2007; Evans *et al.*, 2005). Changes in the climate (temperature, quality, and amount of precipitation) (Köhler *et al.*, 2009) and the decline in acid deposition are reasonable explanations for the increasing NOM concentrations (Delpla *et al.*, 2009). NOM is a complex mixture of organic compounds present in all fresh water, particularly surface water (Lavonen *et al.*, 2015).

Elevated NOM levels in surface waters presents a suite of problems for potable supplies, including (i) negative effects on water quality relevant to color, taste, and odor; (ii) increased disinfectant dose requirements, resulting in potential harmful disinfection by-product (DBP) production (Lavonen *et al.*, 2013); (iii) promoted biological growth in the distribution system; and (iv) increased levels of complex heavy metals and adsorbed organic pollutants (Jacangelo *et al.*, 1995).

In the southern part of Sweden, a general tendency of browning of the lakes has been noticed. Climate change may alter NOM character, because lake turnover-time has a profound impact on NOM characteristics (Köhler *et al.*, 2013). In Sweden, WTPs have to comply with a recommended limit of around 4 mg C L^{-1} organic matter measured as chemical oxygen demand (COD) for drinking water. The increasing color and COD in Swedish surface waters requires a more strict and reliable technique that can provide high quality drinking water in the future. Therefore, increasing the efficacy of drinking water treatment processes to deal with elevated NOM is critical.

Among the technologies available to remove NOM, the most common and economically feasible method involves coagulation and flocculation, followed by sedimentation/flotation and filtration. Other treatment options for NOM removal include the magnetic ion exchange resin (MIEX®) technique, activated carbon filtration, advanced oxidation processes, and membrane filtration (Jacangelo *et al.*, 1997; Singer & Bilyk, 2002; Matilainen *et al.*, 2006; Zularisam *et al.*, 2006; Toor & Mohseni, 2007; Matilainen & Sillanpää, 2010).

1.2 Membranes for NOM removal

Since the late 1980s, microporous membranes have been used widely to meet the stringent regulations, and provide climate-independent sources of high quality water (Lebeau *et al.*; 1998, Chae *et al.*; 2008, Tng *et al.*; 2015).

Membranes are an exceptional barrier to particles, turbidity, microorganisms, and disinfectant by-product (DBP) precursors from drinking water. Significant improvements in membrane technology, design, and materials during the past three decades, making these drinking water production processes nowadays more effective and environmentally friendly.

The characteristics of NOM that influence membrane filtration most greatly are its pore size distribution and acidic functional group content. The molar mass (MM) of NOM is in the colloidal size range from a few 100 Da (Daltons equals to grams per mole) to more than 100 kDa (Ericsson & Trägårdh, 1997), covering the pore sizes of NF, UF, and MF membranes. Although the size distribution of NOM varies

among different water sources, in general very high proportions of small molecules (<1 kDa) have been observed (Fan *et al.*, 2001; Kim & Yu, 2005; Zularisam *et al.*, 2007; Zularisam *et al.*, 2009). Thus, the average MM is quite low. Weight-averaged MM values of 833-1031 Da (Spain (de la Rubia *et al.*, 2008)), 1254-1493 Da (Australia (Fabris *et al.*, 2008)), 1442-1812 Da (Norway (Fabris *et al.*, 2008)), and 2190 Da (Georgia, USA (Chin *et al.*, 1994) have been reported for surface waters. The smallest NOM fractions consist of hydrophilic compounds, organic acids, and building blocks (BBs), which are degradation products of humic substances (HS) (Huber *et al.*, 2011). Polysaccharides, proteins, and aromatic compounds (i.e., lignin and tannin derivatives) are abundant in the intermediate-high MM fractions of NOM (Lankes *et al.*, 2008).

In addition to size exclusion, membrane rejection depends on solute-solute and solute-membrane interactions, and hydrodynamic conditions. Rejection can be greater than what is expected according to the nominal cut-off value of the membrane if there is a repulsive electrostatic force between the membrane and solutes. Therefore, the properties of both the membrane and NOM are important factors in NOM removal, including acidic group content and hydrophobic/hydrophilic character. Other physiochemical effects that affect rejection when charge repulsion is used are pH, ionic strength, and divalent cation content (especially Ca^{2+}).

1.2.1 Capillary nanofiltration

High pressure (>10 bar), NF membranes with low molecular weight cut-off (<300 Da) have been used for a number years to remove organic matter for drinking water purposes (Meylan *et al.*, 2007). These tight membranes are efficient in removing DOC and hardness (e.g. Ca^{2+}, Mg^{2+}, >80% removal) as well as a number of organic micro-pollutants (Zhang *et al.* 2006). Commercially available spiral wound NF membranes are designed for DOC removal at the expense of undesirable retention of hardness for drinking water production from soft raw waters. Furthermore, the spiral wound membranes are characterized by low chlorine stability, limited disinfection and chemical cleaning possibilities, e.g. pH 3-8 for cellulose acetate filters as compared to pH 2-12 for polysulfonate (Regula *et al.* 2014). Intensive pre-treatment is necessary due to limited hydraulic cleaning options. Capillary, hollow fiber NF membranes have been applied for direct filtration of highly colored surface water during the last decade (Meylan *et al.* 2007). One of the latest concepts in NF for highly effective removal of organic matter is based on capillary NF membranes, combining the chemical resistance of hollow fiber membranes with the organic carbon retention of spiral wound units (De Grooth, 2015). These innovative hollow fiber nanofiltration (HF-NF) membranes are applied as an inside-out filtration

process and can directly be fed with raw surface water without further pretreatment other than 300 µm safety screen (Futselaar *et al.*, 2002).

Recently, several studies have focused on evaluating NOM removal by capillary nanofiltration (NF) in Swedish surface water sources. It has been reported that direct NF of lake water (Lake Bolmen and Lake Ringsjön) resulted in 93% removal of UV-absorbance (UV_{254}), and 88% total organic carbon (TOC) (Lidén & Persson, 2015).

1.2.2 Hybrid membrane processes

However, membrane processes often need pre-treatment for enhanced NOM removal and decreased membrane fouling. Hybrid processes may therefore be superior to the individual processes. The integration of coagulation with membrane filtration has two main advantages: enhanced removal of NOM molecules and reduction of membrane fouling.

Coagulants are used to create "pin flocs" (i.e., flocs of limited size) for the operation of the hybrid membrane process. On the one hand, these pin flocs are of sufficient size to be retained by the membranes and to create a relatively open cake structure on the membrane surface. On the other hand, the floc size required could be limited because the removal of solids is determined by the size difference between the flocs and the membrane pores, and does not depend on gravitational separation.

The most recent mode of combining coagulant with microfiltration (MF) (Meyn *et al.*, 2008; Cho *et al.*, 2006; Loi-Brugger *et al.*, 2006) or ultrafiltration (UF) (Barbot *et al.*, 2008; Blankert *et al.*, 2007; Zularisam *et al.*, 2009; Konieczny *et al.*, 2009) is to add coagulant into the feed stream immediately prior to the membrane process, without removal of the coagulated solids (in-line coagulation). The advantages of in-line coagulation are the reduced treatment plant footprint and lower coagulant dose, as settleable flocs are not needed (Jung & Kang, 2003). Coagulant selection and dosing can be optimized specifically for NOM removal, as particle removal is assured by the membrane (Vickers *et al.*, 1995). Careful dosing is required to produce large enough flocs to avoid pore blocking, while avoiding increased fouling (Tran *et al.*, 2006).

Aluminium- and iron-based coagulants are ideal for charge neutralization and sweep flocculation and, therefore, known to preferentially remove hydrophobic, charged, and larger-sized (>10 kDa) substances (Jung & Kang, 2003; Tran *et al.*, 2006), (Choi & Dempsey, 2004; Maartens, *et al.*, 1999; Carroll *et al.*, 2000; Wang & Wang, 2006; Chen *et al.*, 2007). Both charge neutralization and sweep coagulation conditions have been found effective for the removal of NOM and turbidity by in-line coagulation-UF (Choi & Dempsey, 2004). For the neutral hydrophilic fraction,

coagulation has shown poor removal efficiency in all molecular weight (MW) fractions (Chen *et al.*, 2007). Li *et al.*, 2011 noticed that aluminium coagulant could improve significantly the removal of colloidal forms of humic acids with MW above 10 kDa (from 85 to 99%), as well as those between 1 and 5 kDa (from 63 to 71%) by using UF with a 0.03 μm nominal pore size membrane. However, the removal of compounds smaller than 1 kDa increased only marginally (4%). Tran *et al.*, 2006 compared various coagulants in a coagulation-UF process. They noticed that polysilicato-iron (PSI) coagulant was more effective in removing NOM and in improving fouling conditions than were the aluminium-based coagulants. A DOC removal of 82–89 % was obtained with the PSI coagulant in comparison with the 67–86 % removal with the aluminium-based coagulants. The coagulant type and dosage have been found the most significant factors in NOM removal, followed by raw water SUVA, and the pH of dosing (Kabsch-Korbutowicz, 2005; Zularisam *et al.*, 2009).

1.3 Prediction of NOM retention

In order to optimize membrane processes (i.e., power consumption, water recovery, and permeate quality), a detailed understanding of NOM rejection is required as a function of design flux and cross flow velocity.

The literature teaches that NOM rejection in this filtration process will depend on: (i) transport through concentration polarization (CP) layer, (ii) partitioning phenomena at membrane interfaces and, (iii) solute transport through membrane pores (Déon *et al.*, 2007). Previous numerical models for the NF process include empirical mass-balance/black box approach to models based on irreversible thermodynamics (Levenstein *et al.*, 1996) and deterministic models based on the Extended Nernst–Planck equation (ENP) (Tsuru *et al.*, 1991). Deterministic models account for properties of both the membrane and hydraulic conditions in the module that can alter the spatial concentrations. For example, mass transfer models derived from space charge (SC) modeling (Gross & Osterle, 1968) assume radial homogeneity of ionic concentration and potential across the pores, which is valid in the case of small surface charge densities and sufficiently narrow pores, maintained under most NF conditions. Pore transport models have also been built upon the ENP equation. Bowen and Mukhtar suggested a hybrid model based on ENP with a Donnan condition at membrane-electrolyte interfaces and the hindered nature of transport through membranes (Bowen & Mukhtar, 1996). This hybrid model was subsequently modified to include a "Donnan-steric-pore model" (DSPM) (Bowen *et al.*, 1997). Further modifications to the DSPM account for the effects of pore size distribution on the rejection of uncharged solutes and sodium chloride (NaCl) for

hypothetical NF membranes incorporating dielectric constant variations between bulk and pore to calculate ionic distribution between bulk and pore solutions (Bowen *et al.*, 2002). Different approaches are proposed to include dielectric exclusion (DE) in the modeling, namely DSPM&DE (Bandini & Vezzani, 2003) and SEDE (steric-electric-dielectric exclusion) (Szymczyk & Fievet, 2005). However, all these mathematical models simplify the hydraulic conditions that influence the NOM convection and diffusion and ignore the effects of module geometry. This limited the application of these models for predicting NOM transport in complicated hollow fiber membrane modules.

1.3.1 Numerical models (Solution-diffusion model)

The transport of NOM through NF membrane pores is influenced either by convection or diffusion, depending on the hydrodynamic conditions and electrostatic interactions between the membrane surface and NOM molecules. Different mechanisms influencing the removal of small organic compounds have been suggested. The polarity and differences in diffusion rates in a non-porous structure may influence the rejection of small organic compounds in NF (van der Bruggen *et al.*, 1999; van der Bruggen & Vandecasteele, 2003). The solution-diffusion model is the most widely used model of permeation in non-porous polymer membranes (Wijmans & Baker, 1995; Wijmans, 2004; Hoek & Elimelech, 2003), while the Donnan steric pore model and dielectric exclusion model have also been used to describe mass transfer of electrolytes and neutral solutes through nanofiltration membranes (Bandini & Vezzani, 2003) as well as to predict rejections of trace organics by NF membranes (Wang *et al.*, 2015; Kong *et al.*, 2016). The ability of the solution-diffusion model to describe all non-porous membrane separation processes has been the subject of several reviews even in the past (Wijmans & Baker, 1995; Kataoka *et al.*, 1991; Nagy *et al.*, 2011). Since the selected capillary NF membrane for this study has been deemed to be a non-porous membrane (Spenkelink *et al.*, 2012), the solution-diffusion model is used to obtain a design tool for prediction of permeate quality for different settings regarding filtration flux, cross-flow velocity, recovery and for different staging configurations.

1.3.2 Computational Fluid Dynamics modelling

Computational Fluid Dynamics (CFD) methods have been used to link rejection fundamentals with hydraulic conditions to predict NOM transport in NF systems (Geraldes *et al.*, 2001). CFD modelling of NF process requires the coupling of water and NOM transport modelling in a specific module geometry with a transmembrane model for water and NOM transport across the membrane. However, a feature of

CFD models for NF processes is the assumption that the membrane behaves as an impermeable, "no-slip" wall (Cortés-Juan *et al.*, 2011). This approach neglects the water flux and concentration polarization near membrane surface. Recently, Liang *et al.* (2014) developed a 2D simulation of an electro-osmosis enhanced bench-scale membrane filtration by combinng a permeable wall model, based on the approach of Kedem & Katchalsky (1963), to simulate the water flux and a solute mass balanced model based on Neumann boundary conditions (Liang *et al.*, 2014; Liang *et al.*, 2016) for solute mass balance on membrane surface. This permeable wall model required the simulation of flow field in membrane which resulted in significant computational effort. A dissolving wall boundary condition was used recently to simulate water and solute transfer in a NF small device (Completo *et al.*, 2016). The successful development of numerical models for bench-scale NF process indicates the potential to evaluate the performance of full scale, multi-stage NF plant designs using CFD techniques. The challenge is to verify the accuracy of the model by validating simulated data with independent empirical observations using full scale membrane modules.

1.4 NOM characterization techniques

For several practical and hygienic reasons, the presence of NOM is undesirable in drinking water. The properties and amount of NOM, however, can significantly affect the efficiency of technologies for NOM removal. In order to improve and optimize these technologies, the characterization and quantification of NOM at different purification and treatment processes stages is important. Furthermore, it is of great importance to be able to understand and predict the reactivity of NOM or its fractions in different steps of the treatment. A number of new methods have been introduced during the recent years to describe the nature of NOM. Existing methods and techniques have simultaneously been improved (Matilainen *et al.*, 2011). These updated collections of characterization methods are used to study the composition of NOM prior to the treatment and during the different steps of treatment processes (Chen *et al.*, 2007; Sarathy & Mohseni, 2007; Her *et al.*, 2008; Liu *et al.*, 2008, 2010; Tercero Espinoza *et al.*, 2009; Zhao *et al.*, 2009). The diversity of molecules that constitute NOM and the relative low concentrations of NOM in water often make characterization difficult. Therefore, methods that can either accurately characterize NOM in these dilute solutions, or isolated or concentrated NOM, are essential.

Another approach for the characterization of NOM is the study of its reactivity towards DBP formation and the occurrence of different DBPs in drinking water (Culea *et al.*, 2006; Kanokkantapong *et al.*, 2006; Chen *et al.*, 2008; Cooper *et al.*,

2008; Richardson *et al.*, 2008; Blodau *et al.*, 2009). The binding-potential of NOM with inorganic and organic micro-pollutants may also be important topics in relation to drinking water treatment (Gjessing *et al.*, 2007; Laborda *et al.*, 2009; Park, 2009).

Most of the methods used in NOM characterization related to drinking water treatment, and their advantages and disadvantages have been reviewed recently (Matilainen *et al.*, 2011). In general, NOM characterization methods for drinking water can be divided in bulk parameters, spectroscopic methods, chromatographic methods, and mass spectrometric methods.

Methods used in the characterization of NOM include resin adsorption, size exclusion chromatography (SEC), nuclear magnetic resonance (NMR) spectroscopy, and fluorescence spectroscopy. The amount of NOM in water has been predicted with parameters including UV–Vis, total organic carbon (TOC), and specific UV-absorbance (SUVA). Recently, methods by which NOM structures can be more precisely determined have been developed; pyrolysis gas chromatography-mass spectrometry (Py-GC–MS), multidimensional NMR techniques, and Fourier transform ion cyclotron resonance mass spectrometry (FTICR-MS).

High-performance liquid chromatography (HPLC), thus called HPSEC (Fukano *et al.*, 1978) has been very popular for size fractionation of NOM with a number of different detection procedures (Matilainen *et al.*, 2006; Allpike *et al.*, 2007; Fabris *et al.*, 2008; Chow *et al.*, 2009a,b; Tercero Espinoza *et al.*, 2009; Zhao *et al.*, 2009). NMR spectroscopy has also been extensively used during the last decades for the study of NOM structures and other properties (Barron & Wilson, 1981). The role of MS has considerably increased since coupling with HPLC, allowing direct analysis of NOM with MS, without prior destruction or derivatization of the NOM molecules (Wong *et al.*, 2002). Recently the development of FTICR-MS has allowed the analysis of NOM at the molecular level, enabling the separation of molecular species from very complex NOM structures (Reemtsma, 2009). The multidimensional NMR techniques (Deshmukh *et al.*, 2007; Mao *et al.*, 2007a,b) together with FTICR-MS are new and apparently promising set of methods that may characterize the major fractions of NOM. Through these methods new insights into the structural and functional features of NOM and fractionated NOM can be illustrated.

However, besides the need for enhanced knowledge about the practical, hygienic and ecological consequences of NOM related to drinking water treatment, it is crucial for the water sector to have access to reproducible characterization methods, rather than aiming at the chemical structure of NOM.

1.5 Membrane autopsy techniques

1.5.1 Membrane fouling

The major problem in drinking water production by membrane processes is the decrease of flux and yield over time resulting from concentration polarization and fouling. Membrane fouling is the term used to describe the undesirable formation of deposits on membrane surfaces. Various membrane fouling types can be broadly classified as organic fouling, inorganic fouling, particulate deposition (colloidal) and biofouling. Some of the important mechanisms of membrane fouling are, adsorption of feed components, clogging of pores, chemical interaction between solutes and membrane material, gel formation, and bacterial growth. The fouling caused by organic macromolecules may overlap organic, colloidal, and microbial fouling.

NOM is believed to be the major membrane foulant in drinking water treatment plants using surface water. A propensity for fouling depends on the composition of NOM. In comparison to allochthonous NOMs, the autochthonous types have greater fouling potential (Amy, 2008). These NOM types consist of more extracellular and intracellular macromolecules and cellular debris. Surface water dominated by autochthonous NOM can cause serious fouling when algae bloom occurs, particular during the spring season (Plottu *et al.*, 2003). Furthermore, several authors observed that biopolymers cause more fouling than humic substances (Amy, 2008; Kennedy *et al.*, 2008; Lee *et al.*, 2006; Jermann *et al.*, 2008; Her *et al.*, 2008; Zazouli *et al.*, 2010).

1.5.2 Membrane ageing

In general, fouling can be controlled by suitable pre-treatment of the feed and membrane cleaning strategies. Over long-term operation, membrane fouling is not completely reversible by simple physical cleaning (i.e., backwash and relaxation). Therefore, chemical cleaners are used to remove remaining foulants from the membrane surface and restore the permeate flux. Generally, polymeric membranes are naturally hydrophobic and must be blended with additives and pore-formers to increase their hydrophilicity (i.e., polyvinlypyrrolidone, PVP). However, the major concern associated with chemical cleaning remains the potential membrane degradation (or ageing) upon repeated fouling-cleaning cycles.

Despite cleaning being a required step in most membrane processes, there have been many more studies directed to understand fouling basics than those on cleaning (Porcelli & Judd, 2010; Regula *et al.*, 2014, 2013b; Weis *et al.*, 2003). As a result,

cleaning procedures are usually carried out mainly based on manufacturer guidelines, and sometimes under excessive dosages, temperatures and exposure times, which leads to the shortening of membrane lifetime and to an increase in the operating costs (Muñoz-Aguado *et al.*, 1996; Regula *et al.*, 2014).

Sodium hypochlorite (NaClO) is the most studied ageing chemical (Gaudichet-Maurin & Thominette, 2006; Regula *et al.*, 2013a; Rouaix *et al.*, 2006). It is widely used as disinfectant but has a strong oxidation character, resulting in the degradation of polymeric membranes. However, ageing has been considered less extensively for acidic (Bégoin *et al.*, 2006; Paugam *et al.*, 2013, 2006; Wemsy Diagne *et al.*, 2013) and alkaline (Tian *et al.*, 2010; Weis *et al.*, 2005; Zhu & Nyström, 1998) reagents.

Often, membrane degradation is determined by comparing the permeability and sometimes the molecular weight cut-off (MWCO) of the membrane before and after exposure to the chemical reagent (Abdullah & Berube, 2013; Arkhangelsky *et al.*, 2007; Jung *et al.*, 2004; Platt & Nystrom, 2007; Qin *et al.*, 2003). Nevertheless, other membrane surface characterization methods have also been successfully employed to determine the membrane condition before and after the treatment. Some of these techniques are the scanning electron microscopy (SEM) and the atomic force microscopy (AFM), which provide information of the membrane surface morphology (Väisänen *et al.*, 2002). Another physicochemical technique widely employed is the attenuated total reflection Fourier transform infrared (ATR-FTIR) spectroscopy, which provides an insight on the chemical functional groups of the membrane surface (Bégoin *et al.*, 2006). An additional characterization parameter, which has also been considered in cleaning and ageing studies, is the contact angle which can be related to the hydrophobicity of the membrane (Abdullah & Berube, 2013; Arkhangelsky *et al.*, 2007).

Initially, these methods were used to help membrane manufacturers to create new types of membranes, and improve their filtration properties. Then these methods have been quickly applied to the study of fouled membranes in order to understand the mechanisms involved in the build-up of the fouling.

Previous research has been done on identification of fouling of UF membranes during NOM removal (Combe *et al.* 1999; Jones & O'Melia 2000; Yuan & Zydney 1999; Lee *et al.* 2004); using coagulant to reduce fouling (Lin *et al.* 2000 and Carroll *et al.* 2000) and improve NOM removal; and cleaning strategies (Lee *et al.* 2001). Most of the studies on NOM removal, and the effects of NOM on membrane fouling were based on lab scale experiments using synthetic water, or with limited time of operation (hours or days). So far, little is known on the nascent changes occurring at the molecular and structural level of membranes in progressive membrane ageing over prolonged operational period. Therefore, ageing has become the new bone of contention of studies dedicated to membrane characteristics and researches.

1.5.3 Nanomechanical membrane properties

The Atomic Force Microscopy (AFM) is a versatile tool extensively used for the investigation of surfaces at the nanoscale (Butt *et al.*, 2005). A wide range of use offered by AFM could be considered in terms of membrane characterization (Dietz *et al.*, 1992; Fritzsche *et al.*, 1992, 1993; Khayet & Matsuura, 2003; Kim *et al.*, 1999; Wyart *et al.*, 2008) as well as in terms of assessment of membrane cleaning/disinfection and membrane ageing.

This technique was primarily used to probe surface topography and interactions on the atomic-molecular scale (Bowen & Doneva, 2000). It has been used extensively to characterize the structure and morphology/topography of various types of clean MF and UF membranes. James *et al.* (2003) used AFM coupled with SEM and X-ray photoelectron microscopy to visualize the fouling layer. Al-Amoudi & Lovitt (2007) showed an accumulation of the particles in the valleys of rough membranes causing more severe flux decline than smooth membranes. Väisänen *et al.* (2002) used AFM to compare roughness of UF membranes made of different materials. However, it should be noted that AFM images are distorted by convolution between pore shape and cantilever tip shape and, therefore, the quantitative determination of pore size from an AFM image is not always straightforward (Singh *et al.*, 1998). Moreover, one of the main drawbacks of the AFM is the relatively small area which can be scanned at any given time. Such a limited scan-size makes it difficult to determine how representative the measured image of the surface is at large (Koyuncu *et al.*, 2006). However, the development of pulse-force AFM mode has provided a significant advantage in the quantitative calculation of surface characteristics, e.g., stiffness, adhesion, and Young's modulus (Rosa-Zeiser *et al.*, 1997; Vanlandingham *et al.*, 1997). Remarkably, the recent introduction of PeakForce^{TM} Quantitative Nanomechanical Mapping (QNM^{TM}) technique (Bruker, USA) has offered enhanced benefits for the nanoscale characterization of materials (Foster, 2012). Specifically, QNM technique quantitatively distinguishes between adhesion, dissipation, deformation, and modulus while simultaneously generating a topographic image of a surface.

At present, QNM technique has been used in several fields of research, i.e., medical and cement research (Sweers *et al.*, 2011; Young *et al.*, 2011; Adamcik *et al.*, 2011; Trtik *et al.*, 2012; Pakzad *et al.*, 2012). Interestingly, although mechanical properties of modified, virgin, and industrially fouled membranes have been studied by AFM colloidal probe technique and nanoindentation, the analytical advantages of QNM have not been majorly exploited in the field of membrane science and technology (Powell *et al.*, 2017; Homaeigohar *et al.*, 2012).

2. Objectives

The overall aim of this thesis was to evaluate the efficacy of UF and NF membrane configurations for improved NOM removal at two Swedish surface water treatment plants. The main cornerstones for this dissertation were:

- Pilot trials of membrane concepts for NOM removal
- Prediction of membrane performance and NOM retention
- Autopsy studies of new and aged membranes
- Extensive NOM characterization.

The aspects of membrane filtration for treatment of brownish surface water investigated in this work were to include:

- Evaluation of hollow fiber UF and NF concepts for enhanced NOM removal by field testing with respect to membrane performance and feasibility of full-scale applications for high quality drinking water supply (Papers III, V, and VI).
- Combination of several NOM characterization techniques to elucidate the retention of specific NOM fractions as a function of varying operation conditions (Papers I, III, V, and VI).
- Analysis and evaluation of surface properties and integrity of aged UF/NF membranes after long-term pilot trials using a suite of membrane autopsy techniques (Papers I and II).
- Prediction of NOM retention by NF membranes using numerical methods and models for different staging configurations of full-scale applications (Papers III and IV).

3. Background, Materials, and Methods

3.1 Research project: GenoMembran

The work presented in this thesis has been carried out as part of the Swedish national research project, GenoMembran ("through membranes"), funded by the Swedish Water & Wastewater Association. During a four-year period (2012–2015) three separate doctoral projects were finalized focusing on improved NOM removal by membrane filtration for drinking water treatment. This research project resulted in a broad collaboration between three universities (Lund University, Swedish University of Agriculture Sciences, and Chalmers University), a Norwegian research institute (SINTEF), membrane suppliers (Purac AB and Pentair), and five water utilities, namely Norrvatten (Görväln WTP, Stockholm), VIVAB (Kvarnagården WTP, Varberg), Tekniska Verken (Råberga WTP, Linköping), Sydvatten (Ringsjö WTP, Lund) and Gästrike Vatten AB (Sätra WTP).

In the winter of 2010–2011, massive waterborne outbreaks of *cryptosporidium* in the northern part of Sweden underlined the urgent need of improved microbiological barriers in the municipal drinking water supply. Furthermore, the on-going browning of surface water sources due to climate change, poses a challenge for drinking water producers to provide high quality drinking water in the future. For this reason, GenoMembran aimed to investigate UF and NF membranes for both reliable microbiological barrier function and improved NOM removal in drinking water production. Practical and operational experience of membrane concepts combined with analytical NOM characterization were achieved by long-term pilot trials at several drinking water plants of the participating utilities.

My role in this project has been to perform various test runs on site (Görväln WTP and Kvarnagården WTP) based on different membrane pilot plants. Furthermore, I have been responsible for evaluation of field testing, as well as the autopsy and feasibility studies of various membrane applications.

3.2 Membrane test modules

In this study two types of membrane modules have been the subject of various pilot trials, a) hollow fiber NF membranes (HF-NF) and b) hollow fiber UF membranes (HF-UF). Both membranes are made of PES and are applied for the inside-out filtration process. Eight-inch commercial HF-NF and HF-UF membrane test modules, manufactured by Pentair X-Flow, were mounted in different pilot plants for specific test runs.

3.2.1 HF-NF membrane (Papers I, III, IV and VI)

The HFW1000 membrane is designed for enhanced and selective removal of organics from surface water. This membrane is based on a capillary nanofiltration platform developed by X-Flow and recently commercialized by Pentair. According to SEM pictures (Figure 1), the structure becomes denser towards the membrane surface which is advantageous for an inside-out filtration process.

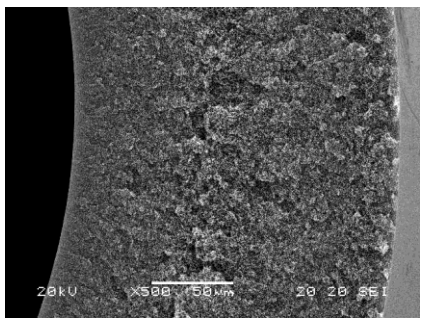

Figure 1 SEM images of the HFW1000 membrane: Cross-section. Figure from Paper III.

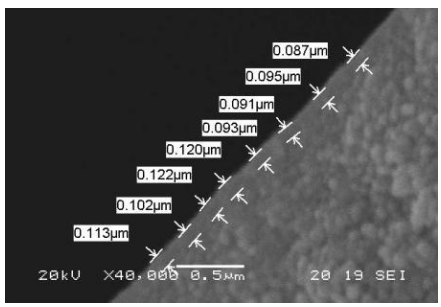

Figure 2 SEM images of the HFW1000 membrane: Top-layer with replicated measurements of layer thickness. Figure from Paper III.

Figure 2 illustrates the integrated top-layer with a thickness of approximately 100 nm. By optimizing the membrane production and polymer blend, a thin nanolayer is created at the inner wall of the membrane, which is completely integrated with the open membrane backbone structure and provides the strength required to withstand the forces applied during the filtration process and hydraulic membrane cleaning. Contrary to conventional spiral wound membrane modules, the integrated top-layer allows hydraulic cleaning of the HFW1000 membrane by backwashing. Since the membrane material is based on modified PES, the HFW1000 membrane properties can be characterized as highly chemical-tolerant and chlorine resistant. The presence of sulfonate groups on the benzene ring structure renders them hydrophilic and leads to a negative zeta potential at pH >5. In this study, the pH interval of the raw water was 7.4–7.8, which resulted in a further decrease of the zeta potential to around −20 mV. Therefore, the membrane effectively rejects molecules with negatively charged functional groups such as DOC (De Grooth, 2015). The main characteristics of the selected test membrane are presented in Papers I, III, and VI.

3.2.2 HF-UF membrane (Papers II and V)

Typical applications for the Pentair-X-Flow XIGA 55 and AQUAFLEX 55 modules are the filtration of surface water for large-scale drinking and process water production.

The hydrophilic membrane is a blend of polyvinylpyrrolidone and polyethersulfone with an asymmetric, microporous structure. The hollow fiber UF membrane is operated in dead-end filtration and adsorbed substances on the membrane surface are removed by acidic and caustic chemical cleaning. Furthermore, direct coagulation with inorganic coagulants can be applied to achieve high removal of organics. The membrane key performance parameters and properties of the HF-UF membranes are described in detail in Papers II and V.

3.3 Pilot plants

For field testing of membrane modules three pilot plants (supplied by Pentair X-Flow) of different sizes and configurations were used in this study.

3.3.1 NF QuickScan pilot (Papers I and VI)

For test runs of HF-NF for pretreated surface water from Lake Mälaren, a simplified and customized pilot plant was used.

The pilot was designed as a mobile, open construction with PVC piping and electrical enclosure mounted on a glass-fiber reinforced polyester frame. One standard size full-scale membrane module (8 inch in diameter and 1.5 meter in height) was vertically placed on the frame. The pilot facility ran automatically and used pre-programmed filtration sequences. An ordinary filtration cycle was followed by a forward flush; no backwashing function was provided. Instead, chemical cleaning in place (CIP) could be performed manually. In this study, all necessary process parameters were logged and trends recorded by an external SCADA system.

The NF pilot plant was equipped with several online sensors including an s::can absorbance probe (spectro:lyser™; s:can Messtechnik GmbH, Wien, Austria), pH-meter, pressure transmitters, and a conductivity probe (Figure 3). Absorbance spectra were acquired with the s::can sensor using a flow cell with 4 cm path length in the wavelength range of 230–750 nm. Empirical relationships from particle rich waters were used to calibrate the absorbance measurements against both TOC and turbidity.

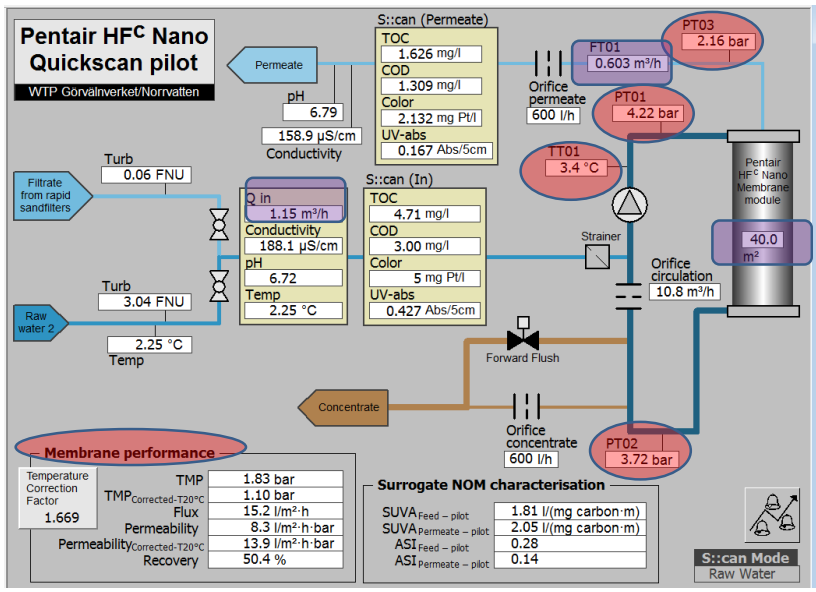

Figure 3 SCADA for NF QuickScan pilot at Görväln WTP, graphical interface & process flow schematic.

The pilot set up did not include a separate feed tank; therefore, the hose feed was directly connected to a pressurized feed water pipe on site. During the testing period, the pilot was equipped with a HF-NF module. The feed water was fed into the upper side of the module. An internal circulation pump created a cross-flow velocity along the membrane surface in order to decrease the effect of concentration polarization. During a filtration cycle, the hydraulics (feed, permeate, and concentrate flow) were controlled by specific orifices in the piping system. The pilot plant was constructed to provide treatment capacity of 29 m^3 d^{-1} (14.4 m^3 d^{-1} permeate production).

3.3.2 NF container pilot (Paper III)

For pilot tests of HF-NF by direct filtration of surface water from Lake Mälaren, a 20-foot-long container pilot setup was used with a treatment capacity similar to the NF QuickScan pilot. The pilot plant was designed as a stand-alone unit and equipped with one element adapter for 8-inch commercial membrane modules. The pilot plant is thoroughly described in Paper III. For the particular pilot trials, the feed water section was connected to an external feed pump located in the inlet of the Görväln WTP. Regular membrane cleaning was performed by hydraulic backwash/forward flushing (every 60 minutes) and chemically enhanced backwash (CEB) with NaOCl and sodium hydroxide (NaOH) (after 72 hours).

3.3.3 UF container pilot (Paper V)

For pilot tests of HF-UF combined with coagulation for filtration of surface water from Lake Neden, a 40-foot-long container pilot was used. Similar to the NF container pilot, the UF pilot plant was designed as a stand-alone unit with a two-stage UF membrane system including three 8-inch commercial UF membrane modules (primary UF stage: two modules, secondary UF stage: one module). The pilot plant was constructed to provide treatment capacity of 170 m^3 d^{-1} (150 m^3 d^{-1} permeate production).

The pilot plant is described in detail in Paper V. For the particular pilot trials, the raw water was supplied from the intake of Kvarnagården WTP by a pressurized line to the primary feed tank of the pilot plant.

In addition to the hydraulic cleaning of the membranes with a combined backwash and forward flush, several automatic cleaning sequences were pre-programmed for specific cleaning protocols. In general, cleaning took place on an elapsed-time interval. A cleaning cycle consisted of flushing with clean water (permeate), followed by soaking with a maximum of two cleaning agents (acidic and caustic). For the CEBs, dosing systems for sulfuric acid (H_2SO_4), NaOH, and NaOCl were

available. The dosing points were placed in the backwash inlet line, and were used by both the primary and secondary units.

3.4 Pilot studies at Görvälnverket WTP

Initially, a pilot study with module prototypes based on capillary NF membranes was performed at Görväln WTP from June 2012 to June 2013. These test membranes were modified for enhanced NOM removal and limited retention of bivalent metal ions from the feed water.

After the launch by Pentair of commercialized HF-NF membranes for selective NOM removal, comprehensive field testing of a specific membrane (Pentair X-Flow HFW1000) was conducted on site during August 2013 to July 2014. The main drivers of the water utility for the evaluation of this filtration concept were to i) increase the NOM removal (with less than 20% of hardness removal), and ii) to investigate the potential for improved performance of existing GAC filters as a chemical barrier. At present, the NOM remaining in the feed water leads to saturation of the GAC filter and blockage of the sorption sites within approximately two months after regeneration. Consequently, improved NOM removal prior to treatment with GAC filters may decrease irreversible fouling by NOM compounds, which diminishes the ability of GAC filters to remove micro-pollutants such as perfluorooctanesulfonic acid (PFOS), algal degradation products, or petroleum residues, contaminants that all occur in the surface water source. The evaluation of HF-NF was carried out in two separate studies using the HFW1000 membrane for a) NF after pretreatment with coagulation and rapid sand filtration and b) NF by direct treatment of surface water. Furthermore, after 12 months of operation an autopsy of the aged membrane samples from the NF membrane module with pretreated feed water was performed.

3.4.1 Raw water source: Lake Mälaren

Görväln WTP is located in eastern Sweden, close to the outlet of Lake Mälaren, where water from a northern basin (16%) and the large western basin (84%) is mixed. Varying water quality in the raw water intake is caused by different degradation of DOC within the lake (Köhler *et al.* 2013). A large number of biological and chemical parameters are routinely measured during the treatment process at the WTP. The raw water from Lake Mälaren (2002–2013) is characterized by high pH (7.6–7.8), high alkalinity (1.3 mM), and chemical oxygen demand with permanganate (COD_{Mn}) varying between 8–12 mg L^{-1}. Raw water turbidity varies between 2 and 10 FNU depending on the raw water intake depth (−4

or −22 m). A more detailed description of the water quality and different water sources that contribute to the raw water at Görväln WTP can be found in Ericsson *et al.* (1984).

3.4.2 Full-scale drinking water plant

The raw water (RAW) from Lake Mälaren is abstracted at two different intake depths (−4 and −22 m) depending on seasonal variations of the water quality. After passing a micro sieve (200 mm nominal pore size) the surface water is coagulated with $Al_2(SO4)^3$ at doses varying from 40 to 70 mg L^{-1}, followed by rapid sand filtration (RSF) (0.6 m h^{-1}) to remove residual flocs. The coagulant dose is controlled by online turbidity measurement after RSF. In addition, the water is filtered through a Norit 1240 W GAC bed (CF), and then disinfected with UV irradiation (25 mJ cm^{-2}) and monochloramine (NH_2Cl; 0.2–0.35 mg L^{-1}) to produce drinking water (DW), as shown in Figure 4. Görvälnverket WTP is operated by the water utility, Norrvatten, and provides drinking water for about 500,000 people in the northern part of the Swedish capital of Stockholm.

3.4.3 NF Pilot trial 1 with pretreatment (Papers I and VI)

An extensive pilot facility (membrane combined with GAC) was established at Görvälnverket WTP for various long-term trials (August 2013 to July 2014). The test facility consisted of a QuickScan NF pilot plant equipped with an 8-inch full-scale HFW1000 membrane module (40 m^2 of effective membrane surface area) followed by a pilot scale GAC filter (CF2). The feed water for the NF pilot was recovered from the RSF full-scale plant as displayed in Figure 4. A sub-stream of the sand filtrate was filtered directly by another GAC filter (CF4) so that the effect of the NF permeate quality on the activated carbon filter could be compared under the same conditions regarding GAC age and adsorption capacity (Figure 4). The GAC test columns of approximately 2.5 m height were filled with 1 m of GAC (Norit 1240 W) and operated at a hydraulic load of 10 m h^{-1}. These settings resulted in an empty bed contact time for the GAC test columns of approximately 6 min at a flow rate of 1 L min^{-1} in accordance with the full-scale plant conditions.

The NF pilot had a capacity of 600 L h^{-1} (permeate production). During the various pilot trials, the HFW1000 membrane was continuously operated at a feed flow rate of 1.2 m^3 h^{-1} with a flux range of around 15 L m^{-2} h^{-1}, a cross-flow velocity of 0.5 m s^{-1}, an intermittent forward flushing interval of every 60 min, and a recovery rate of 50% (initially, higher recovery rates of up to 80% were successfully tested). With operating pressures around 4 bar and permeability rates of 10 L m^{-2} h^{-1} bar^{-1} the transmembrane pressure typically increased with 0.17 bar and the permeability

decreased with 1.0 L m^{-2} h^{-1} bar^{-1} at low water temperature (around 1–3 °C) during a typical filtration period. CIP was carried out every four to seven weeks on a preventive basis with respect to TMP profiles to avoid irreversible fouling. The CIP solution consisted of 200 ppm NaOCl in the presence of NaOH to reach a pH of 12.4.

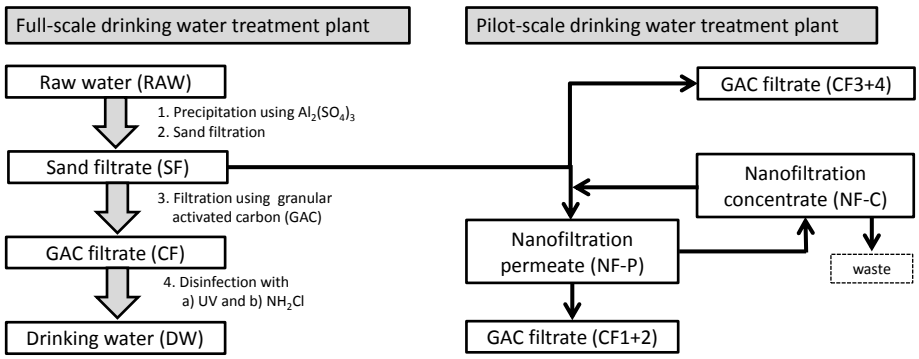

Figure 4 Water treatment train for the full-scale drinking water plant and the pilot scale plant at Görväln WTP. The codes for raw water (RAW), sand filter (SF), full-scale activated carbon filter (CF), nanofilter concentrate (NF-C), nanofilter permeate (NF-P), the GAC test columns (CF2 and CF4) and drinking water (DW) are used throughout the dissertation. Figure from Paper VI.

3.4.4 NF Pilot trial 2 with direct filtration of surface water (Paper III)

Pilot trials of HF-NF by direct filtration of surface water from Lake Mälaren were performed from January 2014 to June 2014 at Görväln WTP. Comprehensive performance tests, with a fully automated membrane container pilot plant equipped with a full-scale test module (HFW1000, 40 m^2 membrane surface), were conducted in stages.

At first, twenty short-term (<2 hours) experiments, at a fixed recovery of 50%, with sufficient variations in filtration flux (5–25 L m^{-2} h^{-1}) and cross-flow velocity (0.25–1.0 m s^{-1}) were performed to determine the solute diffusion coefficient and solute permeability coefficient to predict NOM retention (i.e., DOC). Thereafter, these short-term experiments were complemented with a long-term performance test of direct filtration at fixed filtration flux (20 L m^{-2} h^{-1}) and fixed cross flow (0.5 m s^{-1}) but at varying recoveries (50–90 %). For particular pilot trials, the feed water section of the pilot plant was connected to an external feed pump located in the inlet of the Görväln WTP. Regular membrane cleaning was performed using hydraulic backwash/forward flushing (every 60 minutes) and CEBs with NaOCl and NaOH (after 72 hours).

After an initial system stabilization period in February 2014 (Trial 1) at 10 and 15 L m^{-2} h^{-1} and fixed recovery of 50%, a large number of short term trails were conducted (Trial 2, "short term"). Five sets of experiments with different cross-flow velocities from 0.25 to 1.0 m s^{-1} at filtration fluxes of 5–25 L m^{-2} h^{-1} were performed in random order to minimize the effect of changing water quality. During those experiments, the system recovery was kept constant at 50%. Subsequently, experiments increasing filtration flux at a fixed cross flow of 0.5 m s^{-1} (Trial 3" filtration flux") were performed. The final two trials consisted of a longer-term performance test in March and April 2014 (Trial 4, "long-term") at 20 L m^{-2} h^{-1} at 50% recovery and a period where recovery was changed while keeping the filtration flux constant (Trial 5, "recovery"). Operating conditions during pilot trials can be found in Table 1.

Table 1 Operating conditions and process parameters during different NF pilot trials with direct filtration of surface water from Lake Mälaren. Table from Paper III.

Parameters	Unit	Short Term Trial	Filtration Flux Trial	Recovery Trial
Filtration time (tF)	(min)	90–180	60–90	60–90
Filtration flux (JF)	(L m^{-2} h^{-1})	5–25	15–20	20
V_{CF} (cross flow velocity)	(m s^{-1})	0.25–1	0.5	0.5
R (recovery during filtration)	(%)	50	50	50–90
tBW (backwash time)	(s)	60	60	60
JBW (backwash flux)	(L m^{-2} h^{-1})	40	40	40
tCEFF (CEFF interval)	(days)	0	3	1–3
CEFF dosing solution	(-)		200 ppm NaOCl @ pH 12 with NaOH	200 ppm NaOCl @ pH 12 with NaOH
tSOAK (Soak time CEFF)	(min)	0	60	60

*CEFF—Chemically Enhanced Forward Flushing.

During the short-term trials, samples were taken from four sample points: feed water from Lake Mälaren (pre-filtered with 300 µm strainer), circulation loop, concentrate, and permeate (Figure 5). Steady state conditions at the moment of sampling were ensured by online measurements of conductivity in the circulation loop and permeate line. In between two experiments, the concentrate and permeate side were completely drained, including the membrane module, to diminish the influence of previous experiments.

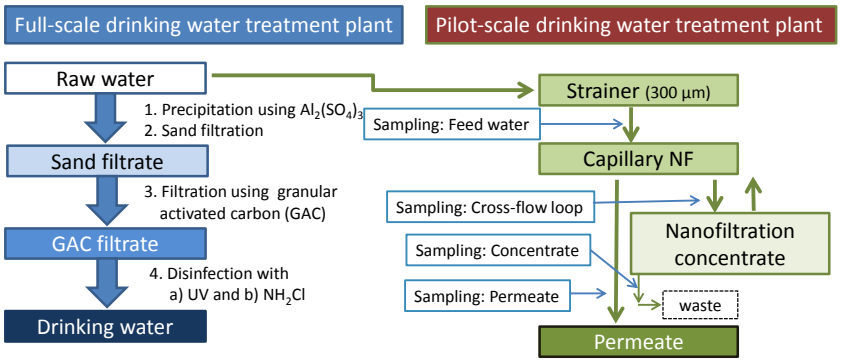

Figure 5 Schematic diagram of the NF container pilot plant for direct filtration of surface water from Lake Mälen and sampling points.

Average feed water parameters during the comprehensive pilot trials at Görväln WTP, are shown in Table 2.

Table 2 Average feed water quality during NF pilot trials with direct filtration of surface water at Görväln WTP (Table from Paper III).

Parameters	Unit	Range
Temperature	°C	2–12
pH	(-)	7.2–8.2
Turbidity	(NTU)	2–5
Conductivity	(µS cm^{-1})	150–230
UV_{254}	(5 cm^{-1})	1.09–1.44
Pt-Co	(mg Pt L^{-1})	28–33
DOC	(mg C L^{-1})	7.3–9.8
TOC	(mg C L^{-1})	7.3–9.9

3.5 Pilot studies at Kvarnagården WTP (Paper V)

The Kvarnagården WTP located in Varberg, Sweden and operated by the utility, VIVAB, supplies drinking water to both the municipality of Varberg and to the nuclear power plant Ringhals.

During the establishment of the nuclear power plant Ringhals near the City of Varberg in the early 1970's, an agreement between the utility company Vattenfall and the municipality of Varberg was signed for the supply of municipal drinking water. This agreement governs the conditions of water supply (quantity and quality) and the financing of co-owned infrastructure (WTP and distribution network). Of the approximately 5 million m^3 of drinking water produced annually at

Kvarnagården WTP, more than 1 million m^3 are delivered to Ringhals. About one third of this amount of water is used for internal process water (e.g., reactor cooling and production of steam).

In order to meet the requirements for ultra-pure water, Ringhals has its own treatment plant for desalination of municipal drinking water. The desalination plant comprises ion exchangers with cation, anion, and mixed polishing resin beds followed by a membrane filtration plant for Reverse Osmosis (RO). The quality of the feed water to the internal processes must correspond to a conductivity of <0.1 µS cm^{-1} and a low content of organic pollutants (<50 ppb TOC).

From 2005, staff at Ringhals noticed a gradual deterioration of the internal water treatment in terms of increasing conductivity and TOC concentrations. As a result, the desalination plant could not operate at full capacity. Operational problems have been traced to rising levels of HS in the drinking water from Kvarnagården WTP. Humic fractions caused deposits on the ion-exchange resins, which reduced the capacity of the ion exchange process and increased the organic matter concentration in the treated water.

Over the years, a number of measures were taken at the nuclear power plant Ringhals to improve the availability and degree of purification of the existing treatment plant. More frequent changes of ion exchange resins and interim trials for increasing the capacity of the RO plant have proved to be only temporary solutions, while the operational problems of the ion exchangers still remain. Thus, an improvement of the feed water to the ion exchangers is a longer-term solution. Therefore, Ringhals and VIVAB cooperated in the investigation options to upgrade the treatment process at Kvarnagården WTP in order to achieve enhanced NOM removal.

Furthermore, more stringent microbiological requirements for drinking water over the years required an additional microbiological barrier function for the existing water treatment process at Kvarnagården WTP.

In view of this, preliminary pilot trials with one-stage UF (UF-HF-P1) and HF-NF (NF-HF-P) were performed from June 2010 to May 2012 (Keucken & Heinicke, 2011; Keucken *et al.*, 2012). In the context of the GenoMembran project, more extensive field testing with a two-stage UF pilot plant was carried out from January 2015 to July 2017. In addition, the nanomechanical properties of two UF membrane test modules were investigated by advance autopsy methods after 12–14 months under different feed and operating conditions. An overview of the pilot studies is given in Table 3.

Table 3 Summary of different pilot studies at Kvarnagården WTP. HF: hollow fiber; NF: nanofiltration; PES: polyethersulfone; UF: ultrafiltration. Modified table from Paper V.

Pilot Plant Type (Module Type)	Code	Scale	Start	End	Membrane Type
UF HF one-stage (KOCH, HF 10-48 35)	UF-HF-P1	Pilot	1 June 2010	15 August 2011	PES
UF-HF two-stage (Pentair, XIGA/AquaFlex)	UF-HF-P2	Pilot	1 January 2015	Running	PES
NF (Pentair, HFW 1000)	NF-HF-P	Pilot	2 November 2011	4 May 2012	PES
UF-HF two-stage HF (Pentair, XIGA/AquaFlex)	UF-HF-F	Full	15 February 2017	Running	PES

3.5.1 Raw water source: Lake Neden

The raw water source used in this study was a mixture (20/80 %) of water from a nearby alkaline groundwater well (pH 8, TOC = 0.6 mg L^{-1}, σ = 380 µS cm^{-1}) and a slightly acidic clear-water lake (pH = 6.7, TOC = 3.4 mg L^{-1}, and σ = 60 µS cm^{-1}). The surface water source was an oligotrophic lake, surrounded by mixed woodland.

Lake Neden was heavily contaminated by acid rain during the 1980s and 1990s, and was subsequently treated with lime, as were most of the lakes in that area of southwestern Sweden. As a result, the organic matter concentration was suppressed temporarily but is currently recovering to its natural values, similar to many other lakes in the area (Valina *et al.*, 2015). In this specific region (Hallands Län), it was observed that the water color (mg Pt L^{-1}) more than doubled during 2007–2012 (Vattenkvalitet i Hallands Sjöar, 2012). In addition, it is assumed that prolonged vegetation periods will cause higher concentrations of organic matter in the future (Finstad *et al.*, 2016). Compared with the other lakes in the area, the water of Lake Neden is clear, low in TOC (3.4 ± 0.4 mg L^{-1}), and has a comparatively low SUVA value (3.2 ± 0.4). The removal of organic matter by flocculation is limited by the amount of HS in the water.

3.5.2 Full-scale drinking water plant

The Kvarnagården WTP is the largest municipal water treatment plant for the municipality of Varberg. The facility provides drinking water to 60,000 residents. The mixed raw water (80% surface water and 20% groundwater) is transported in a 20 km long pipeline from the water source to the plant.

Consistent with the continuing browning of lakes and rivers in large parts of Scandinavia, a rising trend in color and chemical oxygen demand (COD) has been

observed in the surface water abstracted by the Kvarnagården WTP. No significant NOM reduction was achieved with the old full-scale treatment process, consisting of rapid sand filtration, pH-adjustment, and UV irradiation.

Therefore, in November 2016, the WTP was upgraded with a UF facility (capacity of 1080 m^3 h^{-1} net permeate flow rate). In brief, the full-scale plant consists of a two-stage UF membrane filtration process, with in-line coagulation in a primary UF membrane stage that provides NOM retention and a barrier function against microorganisms (Figure 6). Owing to the fact that the sewer capacity of the site was limited and the backwash water contained coagulant residues, a second-stage UF membrane system was installed to increase the recovery of the plant to >99%.

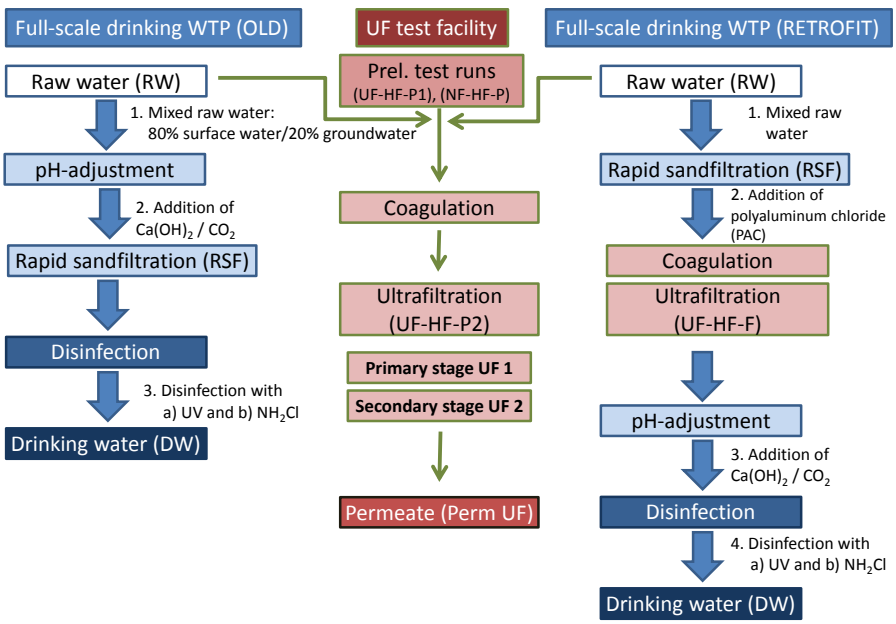

Figure 6 Treatment train for full-scale process and test facility at Kvarnagården WTP. Figure from Paper V.

3.5.3 UF Pilot trial with in-line coagulation

During the construction period of a full-scale membrane plant at Kvarnagården WTP, an extensive test facility was established for various long-term trials to verify the membrane performance of the full-scale design. For this purpose, a container pilot plant, designed as a stand-alone unit to mimic the full-scale UF plant, has been in operation since January 2015 (Figure 7).

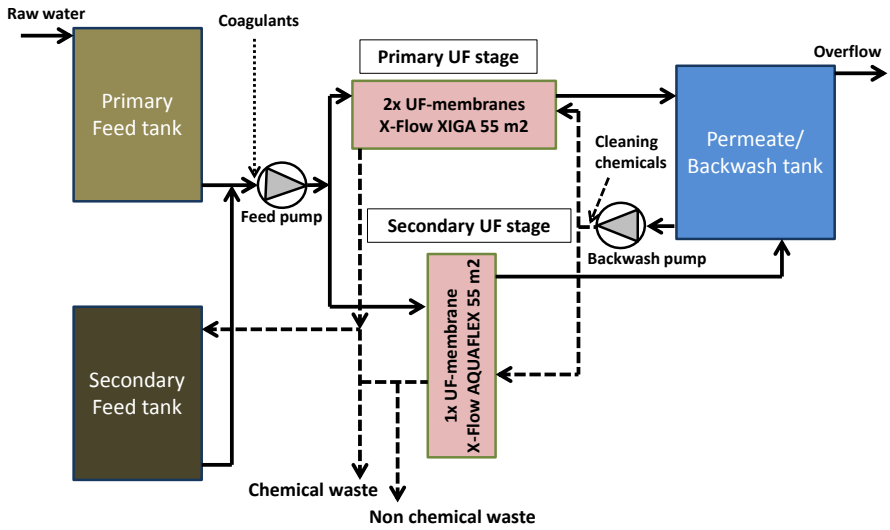

Figure 7 Schematic overview of the pilot plant process for the two-stage UF test facility (UF-HF-P2). Figure from Paper V.

The average feed water quality of the various pilot trials is described in Table 4.

Table 4 Feed water quality (median and standard deviations) of primary and secondary UF stages (UF-HF-P2). Table from supplementary info to Paper V.

Parameters	Unit	Range (UF-Stage 1)	Range (UF-Stage 2)
Temperature	°C	4.5 ± 0.7	4.6 ± 0.5
pH	(-)	7.4 ± 0.1	7.1 ± 0.2
Turbidity	(FTU)	0.6 ± 0.2	20.0 ± 2.9
Hardness	ºdH	1.5 ± 0.10	1.6 ± 0.15
Alkalinity	(mg HCO_3^- L^{-1})	19.0 ± 2.1	18.0 ± 3.0
COD	(mg O_2 L^{-1})	2.0 ± 0.1	25.0 ± 7,5
TOC	(mg C L^{-1})	2.9 ± 0.06	27.0 ± 3.2
DOC	(mg C L^{-1})	2.6 ± 0.1	4.4 ± 0.45
UV_{254}	(5 cm^{-1})	0.380 ± 0.22	3.955 ± 3.3
Pt-Co	(mg Pt L^{-1})	13 ± 1.0	15.0 ± 5.8
Conductivity	(µS cm^{-1})	110 ± 6.9	110 ± 5.7
Iron	(mg Fe L^{-1})	0.026 ± 0.02	0.57 ± 0.1
Manganese	(mg Mn L^{-1})	0.035 ± 0.01	0.044 ± 0.01

The applied cleaning protocols and operational conditions during long-term test runs are summarized in Table 5 and Table 6.

Table 5 Operating conditions and process parameters during long-term pilot trials at Kvarnagården WTP (UF-HF-P2). Table from supplementary info to Paper V.

Parameters	Unit	UF Primary	UF Secondary
Max. filtration time (t_F)	(min)	90	60
Max. filtration volume	(m^3)	8.4	1.65
Filtration flux (J_F)	(L m^{-2} h^{-1})	65–70	45
V_{CF} (cross flow velocity)	(m s^{-1})	-	0.5
R (recovery during filtration)	(%)	100	100
t_{BW} (backwash time)	(s)	30	30
J_{BW} (backwash flux)	(L m^{-2} h^{-1})	250	250
t_{CEFF} (CEB interval)	(days)	1.5	5
CEB1 dosing solution (caustic)	(-)	250–300 ppm NaOCl @ pH 12.2 with NaOH	250–300 ppm NaOCl @ pH 12.2 with NaOH
CEB2 dosing solution (acidic)	(-)	475 mg L^{-1} H_2SO_4 @ pH 2.4	475 mg L^{-1} H_2SO_4 @ pH 2.4
t_{SOAK} (Soak time CEB)	(min)	10	10

Table 6 Membrane key performance parameters during UF pilot trials at Kvarnagården WTP (UF-HF-P2). Table from supplementary info to Paper V.

Parameters	Unit	UF Primary	UF Secondary
Permeability	(L m^{-2} h^{-1} bar^{-1} @ 20 °C)	350–380	600–220
Transmembrane pressure	(bar)	0.18–0.28	0.12–0.25
Total number of CEBs	(-)	267	37
Module age before replacement	(months)	12	14
Total amount of filtration volume (feed water)	m^3	57.150 [1]	2.155 [2]

Notes: [1] 150 m^3 day^{-1} × 381 days, [2] 4.8 m^3 day^{-1} × 449 days.

Coagulant dosing system for UF test facility (Paper V)

The online measurements of turbidity and UV_{254} in feed water (UV_{Raw}) were used to control the coagulation dosing rate in the feed line in order to meet the target values for NOM removal and permeate quality. The dosing rate of coagulants could be adjusted depending on current feed water quality and flow rates, according to Eq. 1. The dependence was derived based on empirical evaluations of laboratory experiments and pilot studies, as part of the current study and previous studies by Keucken & Heinicke (2011).

$$Dos_{Coag} = A + B *^{(TURB)} + C *^{(UV\ abs)} \qquad \text{Eq. 1}$$

Where,

Dos_{Coag} is the coagulant dosing concentration (mg Metal L^{-1})

B is the conversion factor for turbidity [-] (was set to zero during the pilot trials)

C is the conversion factor for UV_{254} [-] (range: 0.005–0.035)

$TURB$ is the feed water turbidity (FTU)

$UV\ abs$ is the feed water UV_{254} (m^{-1})

A is a set point for the base coagulant dosage (range: 0.2–2.0).

Evaluation of coagulation efficiency (Paper V)

The variation of and differences in UV_{254} signals between the raw (UV_{Raw}) and permeate (UV_{Perm}) is the most efficient way to evaluate the removal efficiency of the UF flocculation process. The removal efficiency of UV_{254} at different coagulant dosing situations was evaluated by comparing the absolute change in UV absorbance (Eq. 2) – Eq. 4)).

$$\Delta\, UV = UV_{Raw} - UV_{Perm} \qquad \text{Eq. 2}$$

The observed values for UV_{254} were subsequently plotted as a function of the aluminium dose and fitted to a power relationship of the form:

$$\Delta\, UV = a + b * Al_{DOS} + c * Al_{DOS}{}^{2} \qquad \text{Eq. 3}$$

With *a*, *b*, and *c* used as empirical fitting factors to describe the observed curvature. In addition, a change in the UV_{254} removal efficiency that is normalized to the target coagulant dose (Al_{DOS*}) under regular operational conditions of 0.6 mg L^{-1} was calculated as:

$$UV_{norm} = \Delta \frac{UV}{Al_{DOS(t)}} * Al_{DOS*} \qquad \text{Eq. 4}$$

3.6 Membrane autopsy studies (Papers I and II)

The major concern associated with chemical cleaning remains the potential membrane degradation (or ageing) upon repeated fouling-cleaning cycles. For this reason, nascent changes occurring at the molecular and structural level of membranes in progressive membrane ageing over prolonged operational period are of great interest for WTPs. Furthermore, the assessment of current membrane cleaning protocols for polymeric microporous membranes, requires a deeper

understanding of the influence of NOM characteristics on membrane efficiency and membrane fouling. In this context, two membrane autopsy studies of full-scale test modules were performed after long-term pilot trials at Görväln WTP (HF-NF test module; feed water: filtrate from rapid sand filtration) and Kvarnagården WTP (HF-UF test modules; feed water: mixed raw water with in-line coagulation).

3.6.1 Autopsy of HF-NF test module (Görväln WTP)

After 12 months operation (August 2013 to July 2014) of an 8-inch commercial size hollow fiber NF membrane module (Pentair X-Flow HFW 1000), a membrane autopsy was conducted. The surface water from Lake Mälaren was pretreated with coagulation and sand filtration before feeding the test module.

A suite of membrane autopsy techniques, including tensile strength test, contact angle, atomic force microscopy (AFM), attenuated total reflectance Fourier transform infrared spectroscopy (ATR-FTIR), thermogravimetric analysis (TGA), and scanning electron microscopy (SEM) in conjunction with energy dispersive spectroscopy (EDS), were performed on the aged membrane samples and virgin membranes to evaluate the integrity of the membranes.

Membrane samples were collected from top, middle and bottom sections of the module after a final CIP. All samples were rinsed with deionized water and dried in a desiccator for at least 24 hrs prior to analysis.

Mechanical properties

Tensile strength of the membranes was measured using a TA-XT2 Tensile Analyzer (Stable Micro Systems, USA). The dried hollow fiber samples were cut into test samples of 80.0 ± 1.0 mm in length and subjected to a vertical elongation at a speed of 60 mm min^{-1} till the sample yielded and fractured. Five repeats per sample were performed and Young's Modulus and Breaking Force were calculated via the Stress-Strain curve obtained after each test.

Hydrophilicity

The hydrophilicity and wettability of the lumen side (i.e., the feed side) of the membranes were determined by static sessile drop contact angle analysis method using a goniometer (KSV CAM200 Contact Angle System). The reported contact angle was the average value of the left and right-side contact angles obtained for at least five different locations along the test sample.

Surface roughness

The roughness of both surfaces of the lumen and shell side of the membrane samples were analysed using AFM (Bruker Dimension Icon). An in-air, tapping mode, TM-

AFM at 1 Hz scan rate and 512 x 512 pixel resolution, was used to collect images from a 2 µm x 2 µm scanning area with a 13.5 µm Z-range. Images presented are with a 100 nm Z-range (-50 nm to 50 nm) and 200 nm Z-range (-100 nm to 100 nm) for lumen side and shell side, respectively. The Root Mean Squared (RMS) roughness, R_q, and the average roughness, R_a, were calculated from three different sections of each sample and the average values were reported.

Chemical degradation

The Perkin Elmer Spotlight 400 FTIR Microscope (Perkin Elmer, USA) equipped with an ATR crystal was used to analyse and detect any degradation of the polymer material's chemical composition due to chemical exposure during CIP. All spectra were collected with 32 scans at 1 cm^{-1} resolution from 650 cm^{-1} to 4000 cm^{-1}.

The thermal stability of the membrane material was analysed by Thermogravimetric analyser (Perkin Elmer, USA). An empty platinum pan was used as the reference for measuring the change in mass of the sample. Samples at room temperature were heated up to a temperature of 600 ºC at a constant rate of 50 ºC min^{-1} in a dry nitrogen atmosphere. Variation in the thermal decomposition profiles would help detect changes to the sample's chemical composition.

Membrane surface morphology and foulants characterisation

A Scanning Electron Microscopy (SEM, Hitachi S3400) was used to produce 2D images of the cross-section and surface (both lumen and shell side) morphology of the membranes. The elemental composition of the surfaces of the samples were analysed using Energy Dispersive Spectroscopy (EDS). All samples were sputter coated with a thin layer of carbon before SEM-EDS analysis.

3.6.2 Autopsy of HF-UF test module (Kvarnagården WTP)

Hollow fiber UF membranes were harvested from two 8-inch full-scale test modules (Pentair X-Flow XIGA 55 and Pentair X-Flow AQUAFLEX 55) after 12-14 months (XIGA module: February 2015 to February 2016; AQUAFLEX module: May 2015 to July 2016) of operation and subjected to different feed and operating conditions. In addition to mechanical and chemical modification assessment tools, Quantitative Nanomechanical Mapping (QNM) technique was used to distinguish between adhesion, dissipation, deformation, and modulus while simultaneously generating a topographic image of the membranes.

Briefly, the membrane samples were recovered after a final CEB from a) a primary UF unit (horizontal dead-end filtration) with two Xiga membrane modules, and b) a secondary UF unit (vertical dead-end filtration and cross-flow) with one Aquaflex membrane module (Figure 8 and Figure 9).

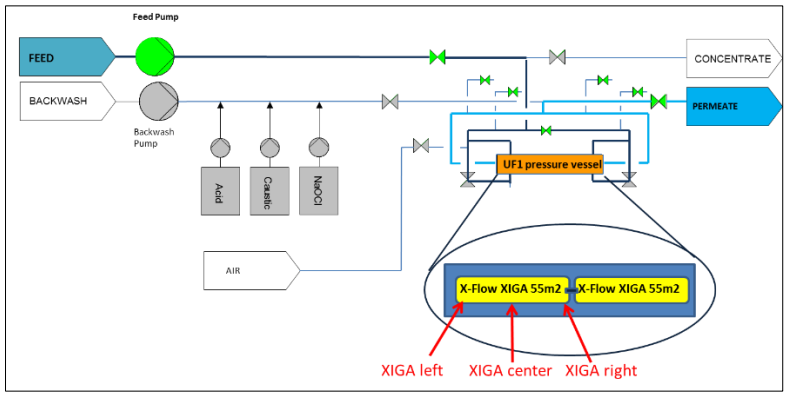

Figure 8 Sampling points for membrane autopsy: XIGA membranes with dead-end filtration. Modified figure from supplementary info to Paper II.

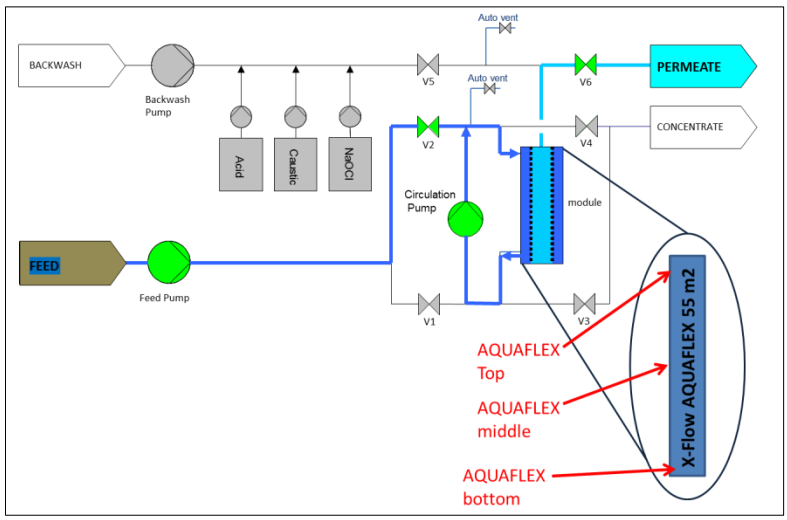

Figure 9 Sampling points for membrane autopsy: AQUAFLEX membranes with dead-end filtration and cross-flow. Modified figure from supplementary info to Paper II.

The primary UF unit received a coagulated water consisted of 80% surface water and 20% ground water (turbidity: 0.3–2.0 NTU; DOC: 2.0–8.1 mg L^{-1}; TOC: 2.3–8.3 mg L^{-1}). The backwash water of the primary UF unit was the feed water of the secondary UF unit (turbidity: 20.0–25.0 NTU; DOC: 4.0–4.9 mg L^{-1}; TOC: 22.0–28.0 mg L^{-1}). The total filtration volumes were 57,150 m^3 and 2,155 m^3 operated in dead-end or cross-flow mode for the primary and secondary unit, respectively. Membrane samples were collected at specific locations of these modules, and termed as: a) Xiga virgin, b) Xiga right, c) Xiga center, d) Xiga left, e) Aquaflex virgin, f) Aquaflex top, g) Aquaflex middle, and h) Aquaflex bottom.

Ageing experiments

Ageing experiments (i.e., chemical cleaning of virgin membranes) were performed using an automated bench scale filtration system (Touffet *et al.*, 2015). These experiments were conducted to assess the impact of chemical cleaning on the nanomechanical properties (NP) of membranes under controlled conditions. Two hollow fiber membranes of approximately 20 cm in length were potted in epoxy with one end cut open to allow inside out dead-end filtration. The mini hollow fiber modules were soaked overnight in ultrapure water (resistivity: 18.2 MΩ cm, Millipore, USA). Prior to aging experiment, each module was flushed with ultrapure water and the pure water flux measured by the flux step method (Filloux *et al.*, 2012). The chemical aging process was performed in inside-out filtration mode at 2 ml min^{-1}, 250 ppm NaOCl, and pH 12 for 10 h. The corresponding C.t exposition dose was 2500 mg h L^{-1}. The resulting membrane samples were termed as: i) Xiga virgin-chemically cleaned, and j) Aquaflex virgin-chemically cleaned.

Pyrolysis GC/MS, AR-FTIR, SEM, and EDS analysis of membrane samples

Used, virgin, and virgin-chemically cleaned UF hollow fiber membrane samples were dissected in halves with the assistance of an optic microscope under aseptic conditions to expose the inner-membrane surface. Virgin hollow fiber membranes were rinsed overnight in ultrapure water to remove any preservative/additive from their surfaces. All membrane samples were analyzed with a SEM Quanta 250 (FEI, Netherlands), working in environmental mode (ESEM). Pressure of water vapor was maintained at a constant value of 500 Pa allowing the removal of any charging effect due to the non-conductive nature of the membranes. Chemical analyzes were conducted with an EDS detector from EDAX at the same condition as for ESEM imaging.

SEM high-resolution images of virgin membrane samples were acquired with a NovaNano SEM (FEI, Netherlands) working in immersion mode. First, membrane coupons were coated by sputtering a 10 nm thick layer of Au/Pd on the sample (PECS 628, Gatan) to avoid any charging effect due to the non-conductive nature of the samples. The images were analyzed by ImageJ software (National Institute of Health, USA) to determine pore size distribution. A threshold filter was used to discriminate pores from the membrane surface. The data was statistically analyzed by probability density functions to extract the pore size distribution.

Also, cross-sectioning of membrane coupons were conducted using a FIB Quanta 3D dual beam FIB (FEI, Netherlands). Prior sample etching, a 50 nm protective layer of Au/Pd was deposited on the sample surface to preserve it from any damage caused by the ion beam. During this process, samples were tilted 45° to enhance the coating of the cross-section. An additional protective layer was added on virgin coupon by depositing a 2.5 µm thick band (25 µm in length and 2.5 µm in width) on the Au/Pd layer using the gas injection system (GIS). Samples were then etched

with FIB until a cross-section was observable. Finally, samples were coated with a 10 nm thick layer of Au/Pd to image the cross-section with high resolution SEM.

Foulant material recovered from Xiga virgin, Xiga center, Aquaflex virgin, and Aquaflex middle was subjected to Pyrolysis GC/MS analysis. Approximately 2.5 g of hollow fiber membranes dissected in halves were placed in 50 mL of ultrapure water and sonicated for 20 minutes. The aqueous phase was separated from the membrane fibers that easily settled and lyophilized. A small mass (few milligrams) of dry material was recovered from each set of membranes. Approximately 0.5 mg of material was placed into the pyrolysis quartz tube and analyzed according to the flash pyrolysis protocol previously described by Greenwood et al., 2012.

Quantitative nanomechanical mapping (QNM)

The development of pulse-force AFM mode has provided a significant advantage in the quantitative calculation of surface characteristics, such as: stiffness, adhesion, and Young's modulus. Remarkably, the recent introduction of PeakForce™ Quantitative Nanomechanical Mapping (QNM) technique (Bruker, USA) has offered enhanced benefits for the nanoscale characterization of materials. Specifically, QNM technique quantitatively distinguishes between adhesion, dissipation, deformation, and modulus while simultaneously generating a topographic image of a surface.

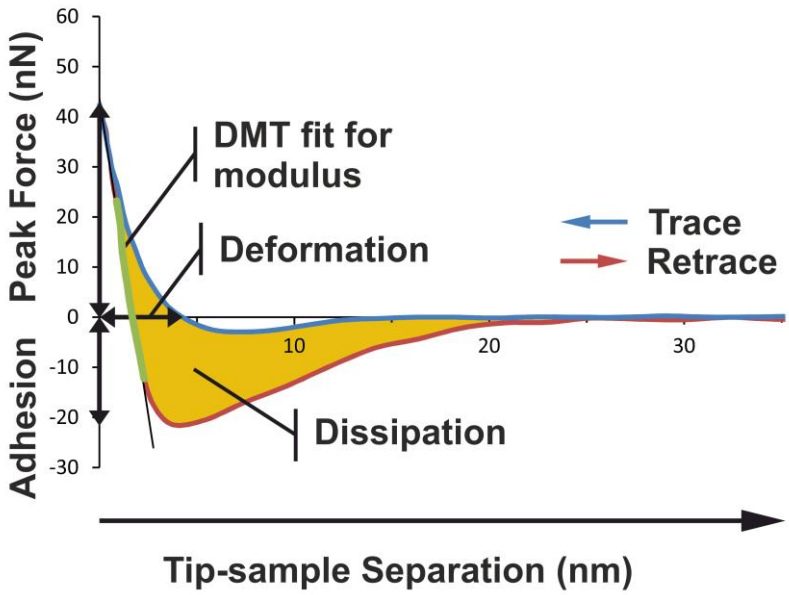

Figure 10 Principle of PeakForce™ Quantitative Nanomechanical Mapping (QNM).

Unlike tapping mode, the tip of the AFM probe interacts with the sample and force vs. distance curves are generated (Figure 10). In addition to a topographic map (as in tapping mode), a quantitative map of the nanomechanical properties of the sample is generated. Materials of different characteristics (i.e., membrane vs. foulant) show different nanomechanical properties (NP). Additionally, compounds of different characteristics "interact" differently with the AFM tip, generating force vs. distance curves of different NP. This latter remark is particularly valid with the used of functionalized tips (i.e., OH, COOH, CH3, humic-coated, colloids-coated, etc.). The interactions of these functionalities with virgin membrane and fouled (chemically-cleaned or not) membranes are expected to differ (i.e., although to an unknown extent). Macromolecules are identified (i.e., molecular recognition) based on their interactions with these modified tips.

Electrolyte solutions were prepared immediately before QNM experiments with ultrapure water and analytical grade reagents, and then filtered through a 0.22 µm membrane. A Dimension FastScan AFM (Bruker, USA) with an Icon Head were used for QNM analysis in solution of the following hollow fiber membrane samples: a) Xiga virgin, b) Xiga right, c) Xiga center, d) Xiga left, e) Xiga virgin-chemically cleaned, f) Aquaflex virgin, g) Aquaflex top, h) Aquaflex middle, i) Aquaflex bottom, and j) Aquaflex virgin-chemically cleaned.

Sharp Nitride Lever AFM probes (SNL-10 A, k: 0.35 N/m, silicon nitride cantilever, Bruker, USA) were used. This type of probe was selected as a function of the characteristics of the membrane samples themselves (i.e., soft polymeric surface); specifically, based on the capacity of probes to cause enough deformation without damaging the sample while still retaining sensitivity.

The calibration of the AFM probes was conducted as follows. Briefly, the deflection sensitivity of the AFM probes was measured in air conditions and using mica as a control substrate. The spring constant (k) of the cantilevers were determined by the Thermal Tuning method, where deflection (V) was converted to force (nN) in accordance to Hooke's law (Butt *et al.*, 2005). The calculation of the radius of curvature of the probes was performed by scanning a titanium model surface (Bruker, USA) in air conditions via Tip Qualification function in the NanoScope Analysis Software V1.5 (Bruker, USA). Dissected membrane samples were immobilized concave up on a glass slide (i.e., to expose their inner-membrane surface) using double-sided tape. The glass slide was placed on the AFM stage and examined with the AFM high resolution camera to verify the correct position of the membrane sample and to locate a suitable area to scan at the center of the membrane (Figure 11).

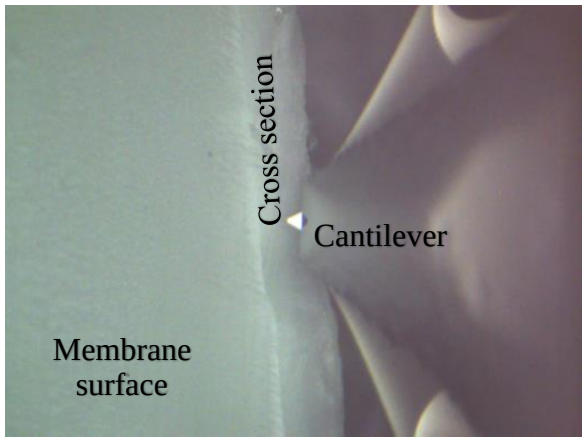

Figure 11 Membrane surface area selected for quantitative nanomechanical mapping. Images were acquired using the high-resolution camera of the AFM. Figure from supplementary info to Paper II.

The QNM images of the membrane samples were acquired in 1 mM NaCl solution, at a scan rate of 0.5 kHz, over an area of 2×2 μm, and at 512 samples/line, while the ScanAssyst Auto Control was set ON (i.e., Peak Force Setpoint was automatically controlled by the software). Between 15 to 25 locations were randomly selected in every hollow fiber membrane sample for QNM analysis (i.e., the images shown in this study are considered as representative). The following parameters (channels) were generated: topography, Peak Force error, adhesion, deformation, dissipation, and LogDMT Modulus.

Briefly, the deformation channel measures the maximum deformation (nm) of the polymeric structures of the membrane caused by the AFM probe during approaching regime, while the adhesion channel measures the maximum adhesion force (nN) between the membrane surface and AFM probe during retraction regime.

The LogDMT Modulus describes the tensile elasticity of the polymeric structures of the membrane sample. In PeakForce^{TM} QNM^{TM}, Young's modulus is calculated using Derjaguin-Muller-Toporov (DMT) model (i.e., modified Hertzian model which considers adhesion forces between tip and surfaces) (Derjaguin *et al.*, 1975). However, LogDMT Modulus (i.e., used in the current investigation) is calculated as the logarithm of the elastic modulus of the sample based on the DMT model. The Peak Force error channel generates a map of the peak force measured during the scan.

Finally, the dissipation channel describes the mechanical energy lost per approaching-retracting cycle; for instance, pure elastic deformation of the membrane corresponds to very low dissipation. Every image of a specific characteristic (e.g., height, LogDMT Modulus, adhesion, dissipation, or

deformation) was processed by Image Quadratic Mean (R_q) analysis and using NanoScope Software V1.5 (Bruker, USA). These values were statistically analyzed by probability density functions, where mean (μ) and variance (σ) were calculated. This statistical analysis provides the advantage of detecting peak values deviating from the distribution. These peak values would indicate regions of the membrane with properties differing from the probability density function (i.e., taking virgin membranes as a baseline). Every generated image was also inspected for the presence of foulants.

Additionally, a topographic and phase analysis of the membrane samples by Soft-Tapping Mode™ (Bruker, USA) in air conditions using TESPA AFM probes (silicon tip, k: 42 N/m, f: 320 kHz, Bruker, USA) was conducted. Specifically, phase analysis provided supplementary information on the characteristics of membrane samples (i.e., phase imaging allows chemical mapping of surfaces based on these material differences).

3.7 NOM characterization techniques (Papers V and VI)

In this study, the nature of the organics presented in the raw water to the WTPs, feed water to the pilot plants, and effluent from the WTPs and the treated water from the pilot plants were characterized by using both a suite of laboratory methods and online sensors.

3.7.1 Characterization of organic fractions in process water

Determination of bulk parameter UV_{254}, TOC, and DOC

UV_{254} was measured with a 5-cm cuvette ($UV_{\text{Lab2 unfilt}}$) using a Hach DR 5000 *UV*-Vis spectrophotometer (Loveland, CO, USA). The TOC and dissolved organic carbon (DOC) were determined using an Elementar Vario TOC Cube analyser (Langenselbold, Germany), with precision of 0.2 mg L^{-1}. All three characterization methods for unfiltered water samples were done by a commercial laboratory.

The composition of the organics in the water samples were characterized by using DOC-LABOR liquid chromatography-organic carbon detection (LC-OCD). The LC-OCD technique is based on a polymethacrylate size-exclusion column (Toso, Japan), coupled with three detectors (organic carbon, organic nitrogen, and *UV*-absorbance). This technique facilitates the subdivision of organic matter into six major subfractions: biopolymers, HS, building blocks, LMW_{acids}, $LMW_{neutrals}$, and hydrophobic organic carbon. Detailed information on the LC-OCD technique is published by Huber *et al.* (2011).

Absorbance and Fluorescence Characterization and Additional DOC and TOC

The presence of organic carbon was determined on unfiltered (TOC) and filtered samples (DOC) by using pre-combusted (4 h at 450 °C) GF/F filters (effective pore size of 0.7 μm) and acidified to pH 2 by using 37% HCl on a Shimadzu TOC-VCPH (Kyoto, Japan).

Fluorescence excitation emission matrices (EEMs) were collected by using an Aqualog (Horiba, Edison, NJ, USA) spectrofluorometer (Lavonen *et al.*,2015). Previously established indices were calculated from the corrected EEMs, namely humification index (HIX), fluorescence index (FI), and freshness index (β:α) according to (Cory & McKnight, 2005; Ohno & Bro, 2006; and Parlanti *et al.*, 2000). The freshness index (β:α) has been shown to be particularly valuable for the characterization of coagulation (Lavonen *et al.*, 2015; Köhler *et al.*, 2016).

Optical Sensors for Online Process Control and Dosing

In this study UV/vis spectrophotometers were used for online measurement of NOM surrogates in order to provide information of the treatability of the water source regarding NOM removal by coagulation and subsequent solids separation.

During the NF pilot trials at Görväln WTP, absorbance spectra were acquired with two UV sensors (spectro:lyser™, s::can Messtechnik GmbH, Vienna, Austria) using a flow cell with 4 cm path length in the wavelength range of 230-750 nm.

For control of in-line coagulation, two UV sensors (i::scan™; s::can Messtechnik GmbH, Vienna, Austria) were installed in the UF pilot plant at Kvarnagården WTP to detect the changes in the UV_{254}, colour, and turbidity in the feed water after the groundwater and lake water had been mixed (UF_{Feed}), and alternatively, in the permeate from both UF stages (UF_{Perm}). The absorbance spectra in the wavelength range 230–350 nm were acquired, with the online sensors using a flow-cell with a path length of 35 mm.

The empirical relationships from particle-rich waters were used to calibrate the absorbance measurements against both TOC and turbidity, with algorithms developed by the probe manufacturer (so-called global calibration).

The presence of particles probably led to deposition on the sensor, particularly on the raw water side. To prevent the degradation of the online signals, the UV sensors were cleaned at regular intervals by following the procedures suggested by the manufacturer. For automatic cleaning, a rotating brush was mounted inside the flow cell of the i::scan sensors in such way that the brush fibers reached the measuring windows on both sides of the measurement path of the spectrometer probes. Manual cleaning of all probes was carried out preventively once a month by using a mild alkaline cleaning agent provided by the manufacture and cleaning tissue. In the event of persistent fouling, pure alcohol (ethanol) and 3% hydrochloric acid (HCl)

(to prevent a mineral film/residue forming on the measuring windows) were used as cleaning liquids. The observed changes in UV_{254} and the calculated turbidity before and after manual cleaning typically ranged between 0.2 – 0.3 m^{-1} and 0.1 – 0.2 FTU, respectively (i.e., UF pilot trials at Kvarnagården WTP).

Quality control of Optical Sensors for in-line coagulation

Since UV probes were used in the UF pilot plant for control of dosing rate for coagulants, the quality of the online measurements was crucial to guarantee stable operational conditions with regard to NOM retention and membrane performance. Therefore, the correctness of the absorbance values of the online sensors was monitored by using three independent UV_{254} measurements. On a biweekly basis, the UV_{254} was measured directly in unfiltered water samples by the operators at the WTP, using a 4-cm cuvette ($UV_{\text{Lab1 unfilt}}$) and at a commercial laboratory ($UV_{\text{Lab2 unfilt}}$). Furthermore, the filtered water samples were sent to an external research laboratory and measured by using a 1-cm flow-through cuvette ($UV_{\text{Lab3 filt}}$) in combination with a high-precision combined fluorescence/absorbance spectrophotometer (Aqualog Horiba Jobin Yvon). During the second year of the UF pilot study, an internal standard (60 ppm K-phthalate, with approximately A = 0.7 @ 254 nm) was added to all the sample runs to determine whether UV lamp drift had occurred.

The correctness of the calculated turbidity values of the online sensors were monitored with regular laboratory measurements of turbidity, using a HACH Model 2100N IS® Turbidimeter (Loveland, CO, USA), designed for turbidity measurement in accordance with ISO 7027.

3.8 Modelling of NOM prediction (Papers III and IV)

3.8.1 Solution Diffusion model for HF-NF test membrane

Since the HFW1000 test membrane in this study is positioned between a dense UF and an open NF (MWCO: ~1000 Da), both the convection and solution diffusion models might be applicable for modelling the separation process. Recent studies of capillary nanofiltration membranes for determination of source specific model parameters showed a good fit of experimental results based on the solution diffusion model (Spenkelink, *et al.*, 2012b; Romera & Davis; 1988; Thorsen, 2004). According to previous research, the selected test membrane in this study can be described as a non-porous membrane. Therefore, the solution-diffusion model, which is based on the film theory, was used for modelling the active membrane layer.

When a driving force is applied on the feed solution, the solvent starts to permeate freely while the solute is partially retained by the membrane. As a result, the solute concentration in the permeate (C_p) will be lower compared with the bulk solution (C_b). A schematic illustration of the concentration polarization phenomena (CP) is given in Figure 12.

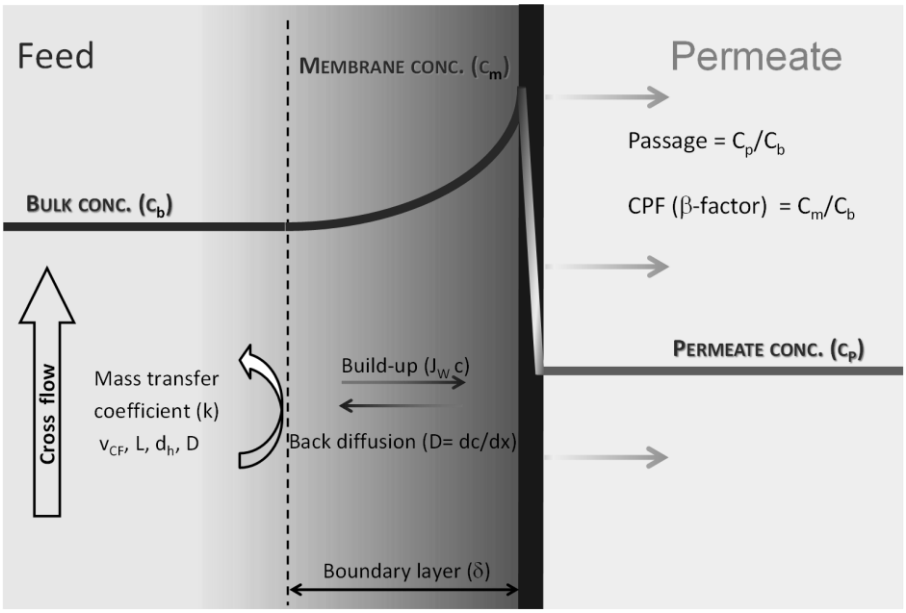

Figure 12 Concentration polarization phenomena (Mulder, 1996). Figure from Paper III.

The solution diffusion model differs from the convection model in how solute transport through the membrane is defined. The driving forces for solute permeation are assumed to rely solely on diffusion due to a solute concentration difference between permeate (c_p) and concentration at the membrane surface (c_m). The rate of solute permeation is determined by the solute permeability coefficient (B) expressed in (m s^{-1}). By performing a mass balance across the concentration polarization layer, the film model is obtained (Eq. (5)). Subsequent substitution of the rate of solute permeation yields Eq. (6) which describes the passage for the solution diffusion model (Mulder, 1996).

$$\frac{C_m - C_p}{C_b - C_p} = e^{\left(\frac{J\delta}{D}\right)} = e^{\left(\frac{J_W}{k}\right)} \qquad \text{Eq. 5}$$

$$\frac{c_p}{c_b} = \frac{e^{\left(\frac{J_W}{k}\right)}}{\frac{J_w}{B} + e^{\left(\frac{J_W}{k}\right)}} \quad \text{Eq. 6}$$

$$\frac{C_m}{C_b} = \frac{e^{\left(\frac{J_W}{k}\right)}}{1 + \frac{1}{\frac{J_W}{B} + 1} - \frac{1}{\frac{J_W}{B} + 1} e^{\left(\frac{J_W}{k}\right)}} \quad \text{Eq. 7}$$

$$k = 1.62 v^{\frac{1}{3}} d^{-\frac{1}{3}} D^{\frac{2}{3}} L^{-\frac{1}{3}} \quad \text{Eq. 8}$$

where,

C_p = Concentration in the permeate (e.g., TOC in mg L^{-1} or UV extinction in m^{-1})

C_b = Concentration in the bulk (actual feed)

C_m = Concentration at the membrane surface

J_w = Filtration flux (m^3 m^{-2} s^{-1})

k = Mass transfer coefficient (m s^{-1})

v = Cross flow velocity (m s^{-1})

d = Hydraulic membrane diameter (m)

L = Membrane length (m)

B = Solute permeability coefficient (m s^{-1})

D = Solute diffusion coefficient (m^2 s^{-1})

The solution diffusion model has two unknown parameters, the solute diffusion coefficient, *D*, and the solute permeability coefficient, *B*. These two latter parameters were fitted using the experimental results from short-term NF pilot trials at Görväln WTP.

Model fitting was performed through an iterative process with the initial value of solute diffusion coefficient, *D,* based on the literature value reported by Park & Cho, 2008. Mass transfer coefficients, *k,* were calculated using Eq. (8) for laminar flow conditions at four different crossflow velocities, ranging from 0 to 1.0 m s^{-1} with corresponding Reynolds numbers of 0 to 2400 for 0.8 mm membrane fibers.

According to previous studies (Spenkelink *et al.*, 2012b), TOC analysis can be used as a key parameter for the determination of the solute diffusion coefficient (D) and the solute permeability coefficient (B). As for membrane retention, TOC can be divided into three fractions; (I) 100% retained, (II) partially retained (based on current process conditions, membrane geometry and membrane properties), and (III) 0% retained. It should be noted that only the concentrations of fraction (II) of the TOC were used for the model calibration in this study as fraction (I) was only present in the feed water and concentrate, and fractions (III) was present in the same quantitative amount in the feed water and permeate. The TOC and UV_{254} of the permeate were calculated using Eq. (5) and compared with experimentally measured values. The final model fitting parameters of *D*, and *B* were determined using the Least Square Error method through the 'Generalized Reduced Gradient' (GRG2) algorithm in Excel (Solver).

3.8.2 Prediction of removal efficiency of full-scale NF Plant

In order to predict the removal efficiency of the first stage and full-scale NF processes, mass balance calculations were used. The full-scale design was not based on the full-scale flow and only illustrated the mass balances over the different membrane stages. The objective of staging was to lower the average bulk concentration at the feed side. This was achieved with the first stages operating at a lower overall recovery compared to that of an equivalent single stage process.

Different mass balances were calculated for all three TOC fractions. The TOC levels of feed water and permeate were corrected in order to eliminate the influence of fractions (I) and (III). Since fraction (I) was only present in the feed water and concentrate, the TOC level of the feed was corrected by subtracting fraction (I) from the total feed TOC value. Fraction (III) was present in the same quantitative amount in the feed and permeate, and therefore, was also subtracted to obtain the corrected TOC concentration for fraction (I) and (III). Correction factors (C) were determined via a Pentair-developed design tool that utilized trend-line regression. The design tool took into account the effects of filtration flux, and cross-flow velocity on the membrane retention. Based on the fixed membrane retention, the design tool then calculated removal efficiencies for the first stage and a typical 4-stage, full-scale process (Eq. (9) and Eq. (10)). The number of membrane modules per stage only indicates the ratio of membrane modules over the stages. For example, with the current module ratio 20-10-6-4 (40 modules), a skid could be designed with 80-40-24-16 modules (160 modules in total) for stage 1 to 4.

$$\eta_{First\ Stage} = 1 - (x_{II}(1 - C_{mem \rightarrow 1Stage}) + x_{III}) \qquad \text{Eq. 9}$$

$$C_{mem\rightarrow 1Stage} = 0.4542\eta_{mem}^{3} - 0.0187\eta_{mem}^{2} + 0.5633\eta_{mem} - 0.0026$$

$$\eta_{Full-scale} = 1 - (x_{II}(1 - C_{mem\rightarrow Full-scale}) + x_{III})$$

$$C_{mem\rightarrow Full-scale} = 0.7415\eta_{mem}^{4} - 0.5488\eta_{mem}^{3} + 0.5439\eta_{mem}^{2} + 0.2617\eta_{mem}$$

Eq. 10

where,

η = Removal efficiency (%);

χ_{II} = Partly-retained feed fraction;

χ_{III} = Non-retained feed fraction;

C = Correction Factor.

In the applied design tool, in each stage, two modules were operated in series. In this double-pass loop, the concentrate of the first module was the feed for the second module. Between the second and the first module, the circulation pump, pressurized feed line and concentrate line were connected. This setup halves the circulation flow rate, because two modules were operated in series, which resulted in smaller circulation pipes/headers. The disadvantage of this setup was the different TMP for both the modules, due to the pressure drop over the two modules. This caused a filtration flux deviation between the first and second module, which depended on the membrane permeability, filtration flux and cross-flow velocity. The first module was thereby running at the highest filtration flux and limiting the design based on the maximum allowable filtration flux. For the full-scale design, the pilot data and solution diffusion models were used to calculate the mass balances.

3.8.3 CFD modelling of HF-NF test membrane

In this study, a novel "mass jump" method (Lian *et al.*, 2016) was applied in a CFD model to assess NOM removal efficiency of the single HF-NF test membrane and HF-NF test modules operated in a double-pass loop mode. The model was validated using experimental data derived from previous short-term experiments and long-term pilot trials at the Görväln WTP (Keucken *et al.*, 2016, Paper III). Additionally, the model was subsequently used to predict the performance of a full-scale multi-stage NF membrane system. Mass transfer was simulated by mass and momentum balance, with experimentally calibrated submodels and coefficients including solute diffusion coefficient for solute transfer in bulk, solvent permeation model for solvent transfer through membrane and solute permeability model for solute transfer through membrane (Figure 13).

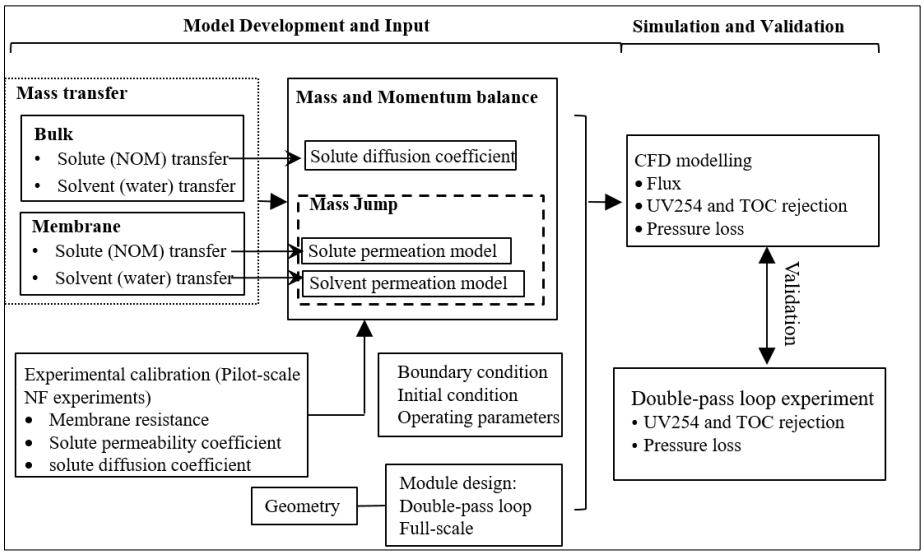

Figure 13 Workflow diagram for CFD modelling of hydraulic properties of NF process. Figure from Paper IV.

In terms of governing equations, the transport of solvent and solute through membrane can be expressed by the Navier-Stokes (NS) equations with mass and momentum source terms (S_m and S_v, respectively), expressed as,

$$S_m = -\frac{J \cdot A}{V}, at\ r = r_0; \qquad \text{Eq. 11}$$

$$S_v = -\frac{J \cdot A \cdot v}{V}, at\ r = r_0. \qquad \text{Eq. 12}$$

Where, A is area. Solvent transport is driven by the difference between transmembrane pressure and osmotic pressure, and expressed as a mass flux J using the approach of Kedem and Katchalsky as,

$$J = \frac{1}{\mu R_m}(\Delta P - \Delta \Pi) \qquad \text{Eq. 13}$$

Where, R_m is membrane resistance, μ is fluid viscosity, ΔP is transmembrane pressure, ΔΠ is osmotic pressure induced by solute concentration at membrane surface.

Comparatively, solute transportation in bulk was solved by conservation equation with consideration of the convection-diffusion effects, expressed as,

$$\frac{\partial \rho}{\partial t} + \nabla \cdot (\rho v) = -\nabla \cdot J_{sd} \quad \text{Eq. 14}$$

Where, J_{sd} is the diffusion flux. Solute permeation through the non-porous NF membrane was simulated by adding a mass sink at membrane surface, S_s, expressed as,

$$S_s = -\frac{J_s \cdot A}{V}, at\ r = r_0 \quad \text{Eq. 15}$$

Solute permeation through the non-porous NF membrane is driven by the concentration difference between permeate and the concentration at membrane surface. For a neutral solute at low concentration (i.e., NOM in surface water), the solute flux, J_s, can be calculated using an expression intuitively related to Fick's Law (Hines & Maddox, 1985), defined as,

$$J_s = P_s(C_m - C_p) \quad \text{Eq. 16}$$

Where, P_s is the solute permeability coefficient, C_p is the solute concentration in permeate.

Laminar flow in the HF-NF test membrane was simulated by applying the laminar model. Solute mixing was simulated using the volume-weighted mixing law. The membrane filtration process was simulated using the "mass jump" method developed by Lian *et al.* (2016), which utilizes source terms S_m and S_v to define mass and momentum sinks of the water and solute at the membrane and feed interface.

For the CFD simulation of the HF-NF test membrane, five inflation layers with a first layer thickness of 5×10^{-5} m and a growth rate of 1.2 × per layer were set near the liquid-membrane interfaces, ensuring that the zones where concentration polarization and transport phenomena occur were simulated by using a higher mesh resolution. A grid size of 0.4 mm, was employed universally across the remainder of the membrane lumen, resulting in a total of 50000 elements and an average aspect ratio of 0.25.

The obtained CFD model was calibrated using data from NF pilot scale short-term experiments with varying cross-flow velocities from (0.25 to 1.0 m s^{-1}) and filtration fluxes (10 - 25 L m^{-2} h^{-1}) conducted at Görväln WTP.

The solute diffusion coefficient and the solute permeability coefficient (Table 7), deduced from previous studies (Keucken *et al.*, 2016, Paper III) were used to calibrate the diffusion coefficient in Eq. (14) and Eq. (16), and experimentally measured membrane resistance were imported in Eq. (13). Most importantly, this model could not predict long-term membrane performance, since the short-term experimental data neglected membrane fouling.

Furthermore, experimentally measured solute retention and pressure drop along the fiber length of the HF-NF test membrane (Keucken *et al.*, 2016, Paper III) were used for model validation.

Table 7 Parameters for CFD model calibration. Table from Paper IV.

Parameters	Values
Membrane resistance $*10^{13}$ (m^{-1})	2.65
TOC diffusion coefficient (m^2 s^{-1})	1.65 $x10^{-10}$
UV_{254} diffusion coefficient (m^2 s^{-1})	1.74 $x10^{-10}$
TOC permeability coefficient (m s^{-1})	1.69 $x10^{-7}$
UV_{254} permeability coefficient (m s^{-1})	1.01 $x10^{-7}$

3.8.4 CFD simulation of HF-NF full-scale process

A two-dimensional axisymmetric model of the NF test module configured with HFW 1000 membranes was developed using commercial CFD software ANSYS Fluent (version 16.2). The model was used to evaluate the impact of the double-pass loop operation mode on NOM removal efficiency. Elements of the model of the single module were expanded to evaluate the performance of various multi-stage full-scale NF plant operations.

The operation in the double-pass loop mode was based on two membrane modules connected in series. The concentrate of the first module was the feed for the second module, while the concentrate of the second module was circulated back to the feed of the first module. The purpose of this setup was to halve the circulation flow rate resulting in smaller circulation pipes/headers.

The full-scale NF plant was designed to be comprised of stages which were connected in series, so that the concentrate of the previous stage was the feed for the later stage. In each stage, membrane modules were operated in the double-pass loop mode and in parallel. The performance of a full-scale NF plant in a configured 10:5:3:2 four stage array was compared to a typical three-stage full plant configured in a stage ratio of 10:5:3.

3.9 Feasibility studies and scenario analysis (Papers III and V)

3.9.1 Full-scale process design for direct NF of surface water

Based on the results of NF pilot trials, feasibility studies and sensitivity analyses have been conducted with the aim to develop a preliminary full-scale process design for direct nanofiltration at Görväln WTP. For this purpose, the characteristics for feed water, the required permeate quality and minimum recovery rate were defined. For calculation of mass balances obtained pilot data and specific requirements by the water utility, Norrvatten, were used as listed in Table 8.

Table 8 Design criteria for preliminary NF full-scale process design for direct filtration at Görväln WTP. Table from Paper III.

Design Parameter	Design Value
Overall system retention, based on UV_{254}	80%
Overall system recovery, based on the raw feed	85%
Average design temperature	5.73 °C
Membrane permeablility	10 L m^{-2} h^{-1} bar^{-1} @ 20 °C
Max. filtration flux	20 L m^{-2} h^{-1}
Max Chemical enhanced forward flushing (CEEF) interval	2 days
Cross-flow velocity (at the end of the 2nd module)	0.5 m s^{-1}

The most important design criteria for process optimization have been ranked as follows:

1. Permeate quality
2. Recovery rate
3. Operational costs (including energy) and investments

3.9.2 Process validation and effect of climate change on UF

Numerous pilot trials with a two-stage UF process coupled with coagulation were performed to identify the optimal operating conditions for the upcoming full-scale UF plant at Kvarnagården WTP. At the design flux of 65 L m^{-2} h^{-1} and with a CEB interval after 20 filtration cycles, the primary UF stage showed stable operational conditions at permeability of approximately 400 L m^{-2} h^{-1} bar^{-1} @ 20 °C over a period of 30 months. In this context, three episodes were analysed further, as they related to the robustness of the process. These are:

1. Impact of in-line coagulation on NOM removal and membrane performance
2. Effect of operation at high flux (maximum flux and subsequent regaining of permeability)
3. Varying feed water quality (e.g., surface water only or variation in surface water NOM content).

Furthermore, climate scenario analyses for constant rise of DOC in raw water at Kvarnagården WTP were performed. In this projection, it was assumed that the current character of DOC in the raw water sources from Lake Neden and the current groundwater well (i.e., SUVA) would not change over time, while a steady increase for DOC was defined with 0.05 mg L^{-1} per year in the surface water from Lake Neden. The impact on coagulant dosing rates and drinking water quality were studied for change of DOC and increasing ratio of groundwater to the mixed raw water (i.e., 20% and 25%, instead of the current 15% contribution).

4. Results and Discussion

4.1 Membrane performance (Papers I, III, V and VI)

4.1.1 NF Pilot trial 1 with pretreated feed water

Variations of transmembrane pressure (TMP), permeability and temperature for 90 days (1 January 2014 – 30 April 2014) of NF pilot plant operation at Görväln WTP with pretreated feed water (i.e., sand filtration (SF) filtrate) were shown in Figure 14. During long-term trials a manual CEB interval of 40 to 50 days was applied by operating the membrane pilot continuously at flux levels of 15 L m^{-2} h^{-1} with crossflow velocity of 0.5 m s^{-1}, intermittent forward flushing every 60 minutes and permeate recovery rates around 50 %. As shown in Figure 14 the TMP increased by 0.26 bar (1.47 to 1.73 bar) during an operation cycle of 38 days, while permeability (Figure 15) decreased by 1.48 L m^{-2} h^{-1} bar^{-1} @ 20 °C (9.28 to 7.80 L m^{-2} h^{-1} bar^{-1} @ 20 °C) at low water temperatures (1 to 3 °C). During this operational period, the feed water turbidity remained at 0.059 (± 0.005) FNU (Figure 15). Furthermore, periodic CIPs were capable to restore the membrane's permeability after prolonged filtration. These results indicated that membrane filtration of sand filtered water (SF) allowed long filtration cycles with no risk of irreversible membrane fouling.

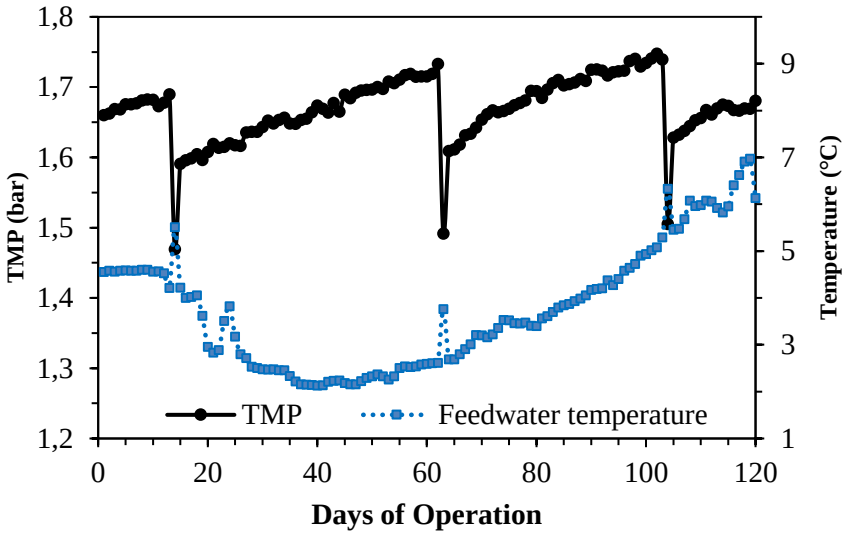

Figure 14 TMP and feed water temperature profiles of NF pilot plant before and after CIPs: January 2014 – April 2014. Figure from Paper I.

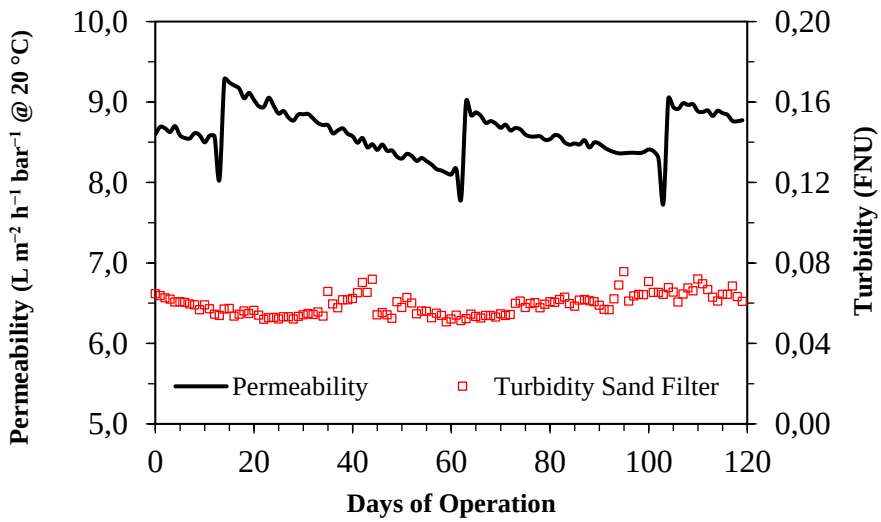

Figure 15 Permeability and turbidity profiles of NF pilot plant before and after CIPs: January 2014 – April 2014. Figure from Paper I.

4.1.2 NF Pilot trial 2 with direct filtration of surface water

According to Figure 16, membrane resistance data indicated a stable filtration performance of the NF test module during the entire pilot period with direct filtration of surface water from 23 January 2014 to 12 June 2014, except for the period from 10 May 2014 till 15 May 2014 (red dotted circle). During this period, a scaling issue occurred due to precipitation while dosing the chemical cleaning solution. The membrane scaling was caused by the insufficient rinsing of the concentrate loop in the pilot plant, before the caustic/oxidizer cleaning solution was dosed. Scaling was removed by one standard chemical cleaning with HCl at pH 2 and an extended soak time of 60 min. A subsequent adjustment of pilot automation alleviated the scaling issue and the process appeared to be stable with only caustic/oxidizer chemical cleanings for the remaining trial period.

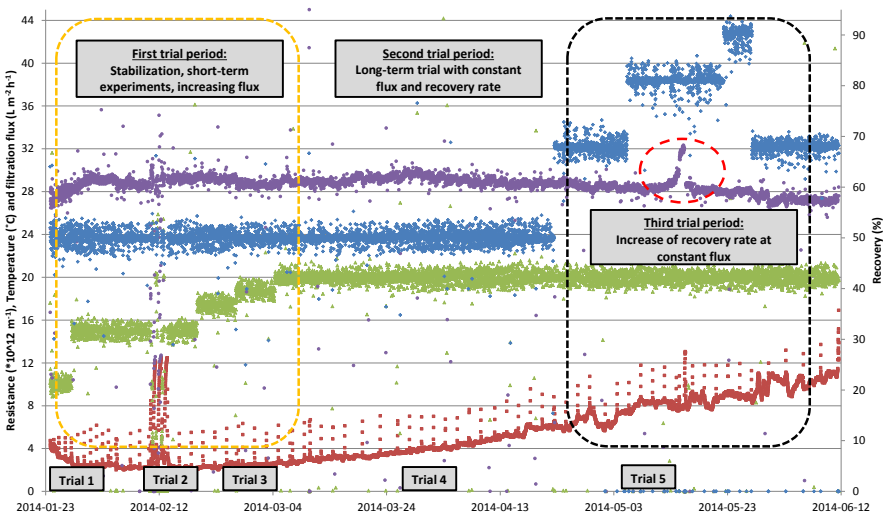

Figure 16 Hydraulic performance of the capillary NF container test module for time period January to June 2014 at Görväln WTP, Norrvatten. Periods of increase infiltration flux and increase of recovery rate are marked with orange and black frames respectively. Membrane resistance (*10^12 m^{-1}) (●), temperature (°C) (■) and flux rate (L m^{-2} h^{-1}) (▲) on the left y-axis; and recovery rate (%) (♦) on the right y-axis.

During the first trial period with increasing filtration fluxes from 10 to 20 L m^{-2} h^{-1}, an increase in the membrane resistance built-up was observed over time between two chemical cleanings. The increased membrane resistance was caused by the higher filtration fluxes (higher local forces towards the membrane) and larger filtration volumes per filtration run. However, this specific increase was not major and chemical cleaning could easily restore the membrane resistance to ensure stable filtration performances. In the third trial period with increasing recoveries from 50% to 90 %, an increase in the resistance built-up was not observed over time between

two chemical cleanings, which suggested that the fouling rate was probably independent of the recovery up to 90%, while the bulk concentration of the organics significant increased with increasing recovery. These results are also in line with the measured pressure drop over the module, which was stable during the entire pilot period, indicating no significant risk for fiber plugging during filtration and cleaning (Table 9).

Table 9 Variation of membrane performance and parameters during long-term NF pilot trials of direct filtration of surface water from Lake Mälaren. Table from Paper III.

Parameters	Unit	Range
Membrane permeability	(L m^{-2} h^{-1} bar^{-1} @ 20°C)	11–13.6
Membrane resistance * 10^{13}	(m^{-1})	2.65–3.23
Trans membrane pressure	(bar)	1.1–2.8
Pressure loss module (V_{CF} = 0.5 m s^{-1})	(bar)	0.5–0.7

4.1.3 UF Pilot trials with in-line coagulation

Episode 1 — Effect of in-Line Coagulation

Initial trials with various coagulants (PAX XL 100 and PLUSPAC 1465) and varying doses resulted in long-term settings for coagulant dosing, Dos_{coag} = 0.6 mg Al L^{-1} (base coagulants dosage, A = 0.25; and a correction factor for UV_{254}, C = 0.035).

Over a period of four days (7–11 December 2015), the UF pilot plant was operated without coagulant dosing, at a flux of 65 L m^{-2} h^{-1}. During that time, the permeability before the daily CEB quickly decreased from approximately 400 to below 250 L m^{-2} h^{-1} bar^{-1} @ 20 °C. After two extended CEBs, the permeability started increasing slowly again prior to the daily CEB. However, the initial permeability of 400 L m^{-2} h^{-1} bar^{-1} @ 20 °C could not be restored completely within a week after the incident (Figure 17).

The simulated shutdown of coagulant dosing caused an instant decrease in the permeability of the primary UF, which could not be recovered fully by subsequent CEBs. The membrane obviously had lower "critical flux" without the coagulant. Therefore, the critical flux of the membrane should be quantified for relevant feed water quality and coagulant dosing conditions in order to avoid irreversible loss of permeability in the future. Furthermore, investigations should be conducted to determine whether the permeability lost during such incidents could be recovered by a CIP. Moreover, process strategies for full-scale plant operation should be formulated on whether to reduce the flux automatically when a sudden loss of coagulant dosage occurs.

Once the UF full-scale plant is in stable operation at Kvarnagården WTP, the pilot plant could be used to adjust the CEB and CIP conditions to ensure effective yet mild cleaning of the membranes.

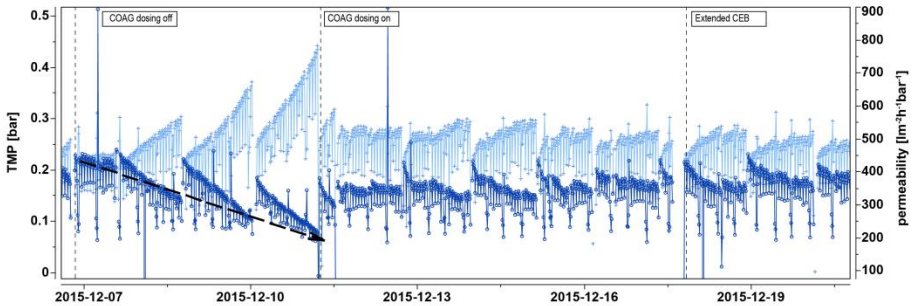

Figure 17 Hydraulic performance of the UF stage-1 container test modules at Kvarnagården WTP for the period 7–19 December 2015. Periods with an increase in transmembrane pressure (TMP; bar) (light blue on left y-axis) and a decrease in permeability (L m^{-2} h^{-1} bar^{-1} @ 20 °C) (dark blue on right y-axis) are shown in relation to in-line coagulation (before, during, and after a stop in coagulant dosing, as displayed with vertical lines) and chemically-enhanced backwashing (CEB) cycles. Figure from Paper V.

Episode 2 — High-Flux Testing

Over a period of six days (15–21 March 2016), the flux over UF stage-1 was increased from 65 to 70 L m^{-2} h^{-1} (i.e., by 7.7%), with a coagulation dosing concentration of 0.6 mg Al L^{-1} (Figure 18). Before this specific episode, the permeability was stable at approximately 400 L m^{-2} h^{-1} bar^{-1} @ 20 °C, with only minor reduction during a filter run, and 80 L m^{-2} h^{-1} bar^{-1} @ 20 °C between daily CEBs. In addition, the permeability was restored by the CEB and was maintained in the long term. At 70 L m^{-2} h^{-1}, the permeability drop during a filter run was more rapid (40 L m^{-2} h^{-1} bar^{-1} @ 20 °C), and there was a tendency toward decreasing permeability with every passing day (120 L m^{-2} h^{-1} bar^{-1} @ 20 °C between daily CEBs). There was a strong indication that a certain maximum flux should not be exceeded in the long-term operation. These boundaries should be quantified by using the pilot plant for varying raw water qualities and temperatures in the future. At the end of the high-flux testing period, a change in the raw water quality occurred (increase of UV_{254} from 10 to 11.5 m^{-1}), which resulted in a further decrease in permeability (below 300 L m^{-2} h^{-1} bar^{-1} @ 20 °C), although the coagulant dose was automatically adapted to 0.7 mg Al L^{-1} in accordance with the current UV correction factor and ordinary flux settings (65 L m^{-2} h^{-1}). The membrane system recovered first, after a further two days of normal operation, regaining levels of permeability and TMP comparable with the operational conditions prior to the testing period.

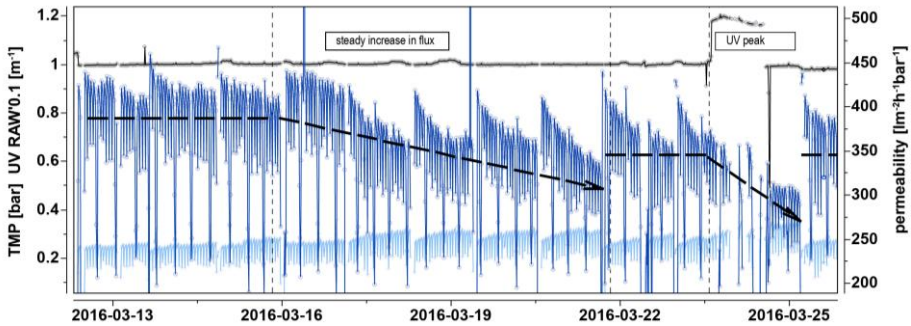

Figure 18 Hydraulic performance of the UF stage-1 container test modules at Kvarnagården WTP for the period 13 to 25 March 2016. The increase in flux was 65 to 70 L m^{-2} h^{-1} during the period 15 to 21 March 2016. The TMP and permeability before, during, and after the increase in flux and *UV* absorbance are indicated with vertical lines. The TMP (bar) on the left-hand scale is indicated with light-blue lines, and permeability (L m^{-2} h^{-1} bar^{-1} @ 20 °C) on the right-hand scale with dark-blue lines. UV_{254} (0.1*m^{-1}) for feed water is indicated with black lines on the left-hand scale. Figure from Paper V.

Episode 3 — Varying Feed Water Quality

During a period of 21 h (23–24 March 2016), the feed water consisted of surface water only (no addition of alkaline groundwater). As shown in Figure 19, the change in the quality of the raw water resulted in an increase in TMP from 0.18 to 0.35 bar at a flux rate of 65 L m^{-2} h^{-1}. Despite recurring backwashing and one CEB during this period, the TMP could not be stabilized and the high levels could not be brought down, even after the addition of mixed raw water. The change in the feed water had no further effect on the removal efficiency of NOM, but the filtration behavior indicated a tendency towards membrane fouling. Therefore, the cleaning protocols had to be adapted with regard to frequency and choice of cleaning chemicals.

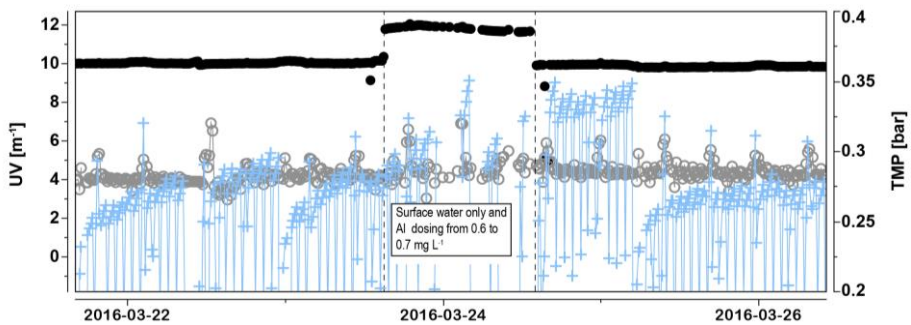

Figure 19 Membrane performance and natural organic matter (NOM) removal efficiency of the UF stage-1 container test modules at Kvarnagården WTP for the period 23 to 26 March 2016. A change occurred in the feed water quality for a period of 21 hrs. TMP (bar) is indicated on the right-hand scale (+), and *UV* absorbance (m^{-1}) on the left-hand scale: (●) UV_{Raw}, (○) UV_{Perm}. Figure from Paper V.

4.2 Selective removal of NOM (Papers I, III, V and VI)

4.2.1 NF Pilot trial 1 with pretreated feed water

DOC fractionation profiles suggested that NOM present in the feed water was effectively removed by the membranes (Figure 20, Figure 21, and Figure 22). The DOC concentration in the raw water from Lake Mälaren of around 8.1 to 11.1 mg C L^{-1} (10–90% quartiles respectively), mainly composed of approximately 70% HS), was reduced to below 0.6 mg C L^{-1} after NF. The full-scale treatment (conventional coagulation process) accounted for approximately 50% of this removal, while NF removed additionally 40% of the DOC, just slightly lower than what can be achieved using conventional spiral would membranes (Meylan *et al.*, 2007; Schafer *et al.*, 2004; Metsamuuronen *et al.*, 2014). The DOC concentration in the feed water to the GAC pilot plant (GAC pilot 2) was eight times lower compared to the feed water of the full-scale GAC and GAC pilot 4 (approximately 4 mg C L^{-1}). The overall removal rate across the NF/GAC pilot plants corresponded to 93% of incoming HS and 86% of incoming DOC.

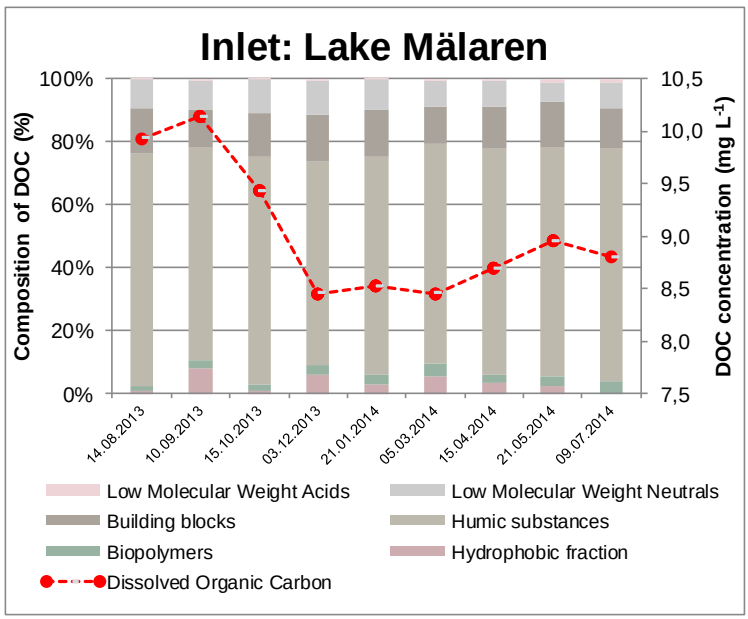

Figure 20 DOC fractionation of inlet water at Görväln WTP (raw water source: Lake Mälaren).

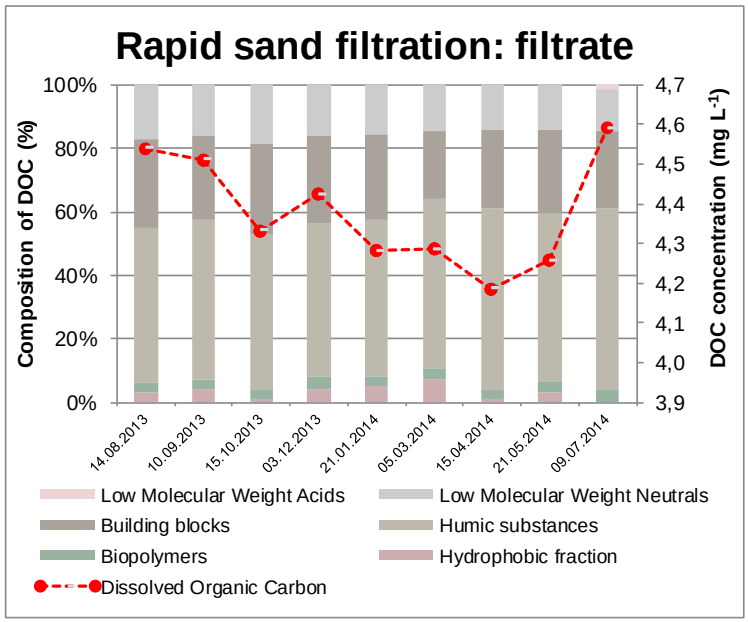

Figure 21 DOC fractionation of filtrate from full-scale rapid sand filtration (RSF) at Görväln WTP (feed water to NF-pilot plant).

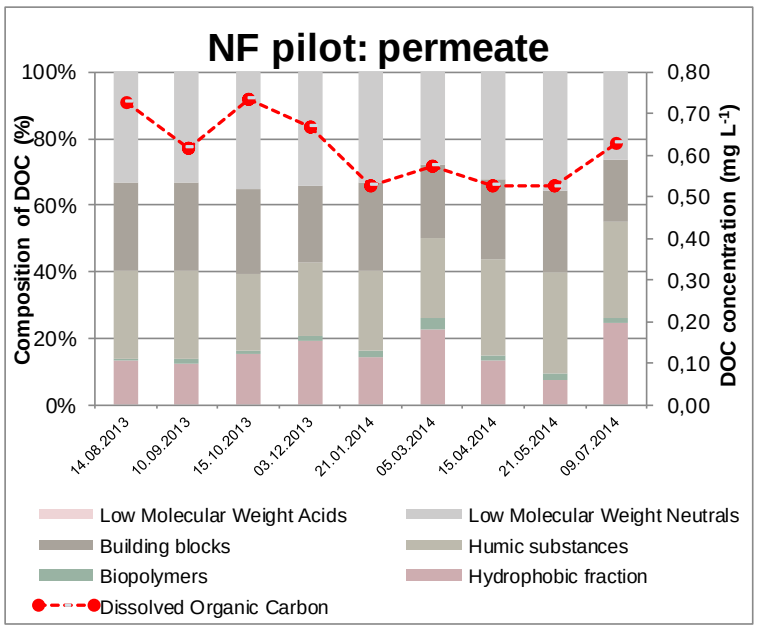

Figure 22 DOC fractionation of permeate from NF pilot plant at Görväln WTP (feed water: RSF filtrate from full-scale treatment).

The GAC pilot reference filter (GAC pilot 4) reduced 75% of the incoming DOC with fresh GAC, but after one month of operation the removal rate decreases to 11% (0.5 mg C L^{-1}). Moreover, the NOM removal rate stagnated after two months of operation (0.1 ± 0.8 mg C L^{-1}) and remained the same until the end of the test runs (Figure 23, Figure 24). The GAC pilot filter (GAC pilot 2) that was fed with NF permeate showed a similar tendency of decreased DOC removal over time. The DOC removal decreased from 1.4 mg C L^{-1} (72%) in the beginning with new GAC, to 0.5 mg C L^{-1} removal the next coming two months and thereafter the reduction in DOC was only 0.1 mg C L^{-1} until the end of the trial period, similar to the reference GAC pilot 4.

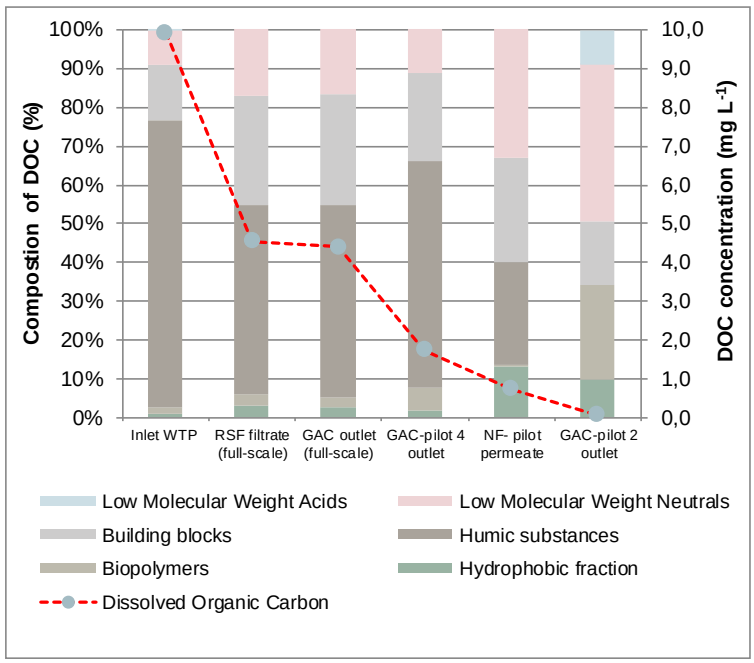

Figure 23 NOM profile of existing water treatment and NF/GAC-pilot plant at Görväln WTP. DOC fractionation was performed 18 hrs after start-up of pilot plants (14.08.2013).

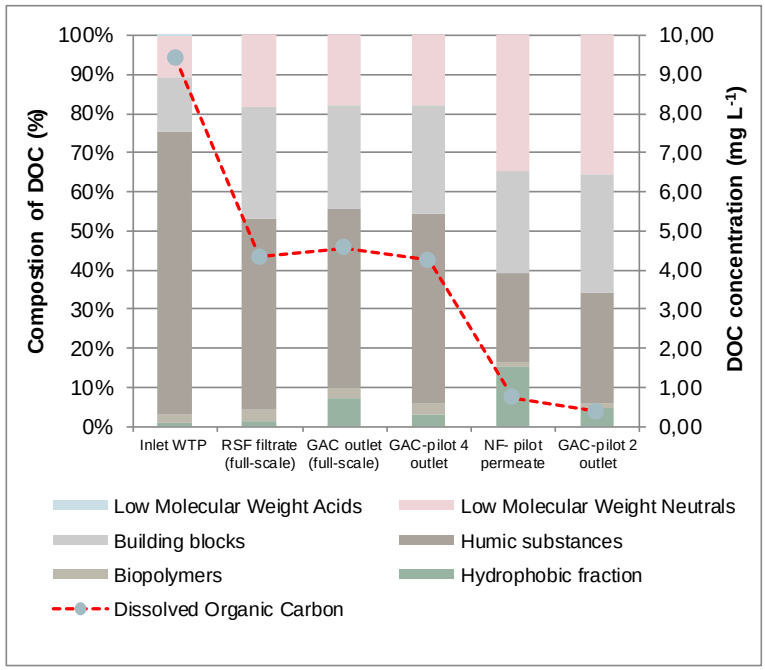

Figure 24 NOM profile of existing water treatment and NF/GAC-pilot plant at Görväln WTP. DOC fractionation was performed 62 days after start-up of pilot plants (15.10.2013).

Furthermore, NOM characterization during the test runs from August 2013 to July 2014 (Figure 25) showed that more than 85% of DOC in the sand filtered water was removed by the NF test membrane (from 4.4 mg C L^{-1} to 0.6 mg C L^{-1}), with less than 2% difference in removal efficiency throughout the 12 months' operational period. HS, which accounted for 53 (± 3) % of the hydrophilic chromatographic DOC, also reduced from 2.33 (± 0.14) mg C L^{-1} in the sand filtered water to 0.19 (± 0.03) mg C L^{-1} in the membrane filtrate, indicating membranes' stable performance on the rejection of organic matters.

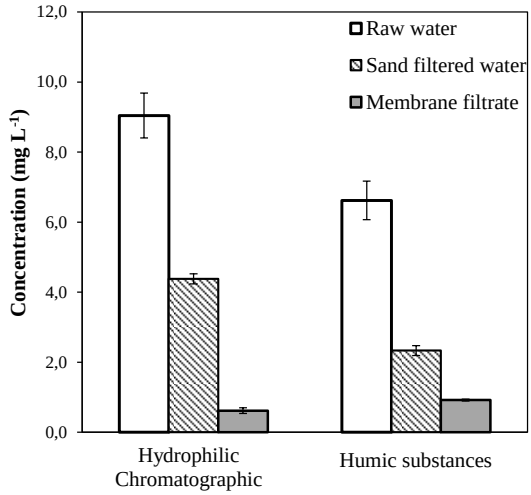

Figure 25 Comparison of average concentrations of DOC and humic substances in raw water (Lake Mälaren), RSF filtrate and NF permeate at Görväln WTP. Error bar indicates variations from August 2013 to July 2014. Figure from Paper I.

The extensive NOM characterization of various water samples from the existing treatment process and the membrane pilot (Keucken *et al.* 2014) indicated a relationship between biopolymers and DOC. As shown in Figure 26, biopolymers with larger molecular weight were removed proportionally over RSFs and completely removed by the membrane module. On the other hand, it was found that the BBs could not be removed by RSF. The proportional retention behavior by the membrane module is consistent to the specified MWCO of the membrane (500 - 700 Da) (Figure 27).

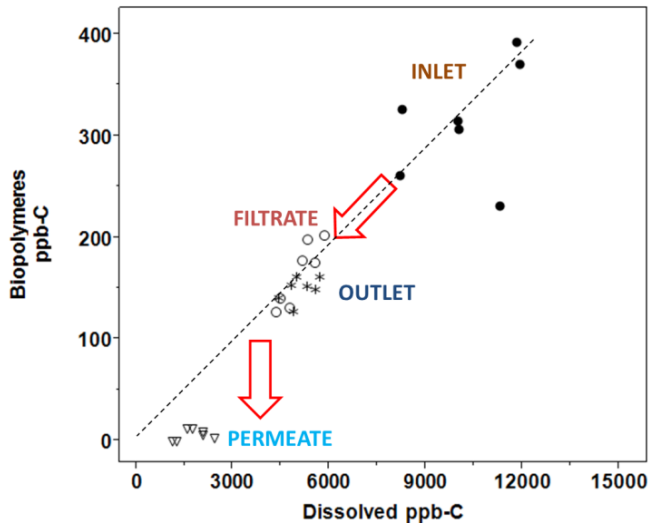

Figure 26 Linear regression of concentrations of different organic matters as a function of DOC concentration in different process streams; Biopolymer vs. DOC. Raw water from Lake Mälaren (●), rapid sand filter filtrate (O), NF permeate (∇), and drinking water from existing treatment process at Görväln WTP (∗). Figure from Paper I.

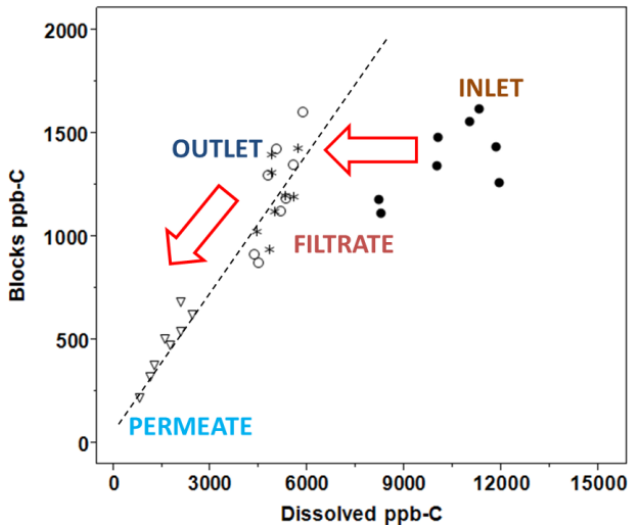

Figure 27 Linear regression of concentrations of different organic matters as a function of DOC concentration in different process streams; Building Blocks vs. DOC. Raw water from Lake Mälaren (●), rapid sand filter filtrate (O), NF permeate (∇), and drinking water from existing treatment process at Görväln WTP (∗).Figure from Paper I

4.2.2 NF Pilot trial 2 with direct filtration of surface water

For the entire pilot period (23 January 2014 to 12 June 2014) with direct filtration of raw water from Lake Mälaren, the recorded membrane filtration performance suggested that membrane retention behavior was strongly affected by the filtration flux and cross-flow velocity. Decreasing cross-flow and increasing recovery deteriorated water quality (Figure 28).

Membrane retention decreased with increasing filtration flux in the first trial period (trial 1-3). After the period with increasing filtration fluxes up to 20 L m^{-2} h^{-1}, the membrane resistance was stable and fluctuated only in a small range possibly due to measurement inaccuracies (trial 4). Even when the recovery was increased from 22 April 2014 (trial 5), the membrane resistance was constant over time. The membrane retentions for UV_{254} varied between 87.6–91.6 %, for Pt-Co between 87.5–97.5 % and for TOC between 82–89 % during the trial period. The range of membrane retentions achieved in the experimental matrix for modelling of solution diffusion coefficients (trial 2) were broader, with membrane retentions for UV_{254} between 88.0–94.7 %, for Pt-Co between 87.5–98.4 % and for TOC between 79.7–92.2 %.

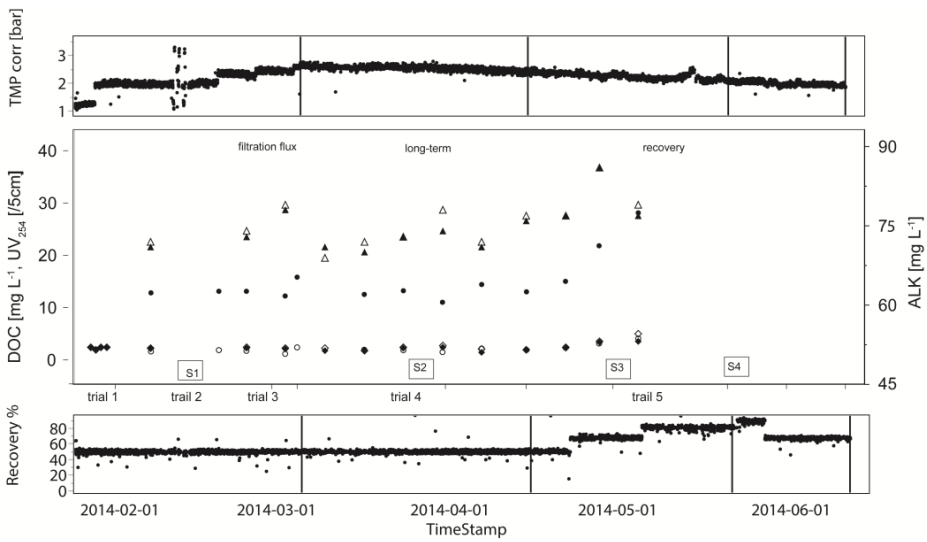

Figure 28 Membrane performance with respect to DOC (mg L^{-1}) (in ● and out ○), Alkalinity (right scale (mg L^{-1}) (ALK_{in} Δ, ALK_{out} ▲), and UV_{254} (UV_{in} ◇ and UV_{out} ◆) of the capillary NF container test module for time period January to June 2014 at WTP Görvälnverket, Norrvatten. S1–S4 samples were taken for LC-OCD analysis. Figure from Paper III.

The membrane retention was highest for biopolymers (>95% removal), followed by HS (>80% removal). This was in accordance with earlier experiments (NF pilot trial 1, paper VI) and previous studies using similar types of membranes (Laurell, *et al.*, 2015). According to LC-OCD analyses the molecular weight of HS in the feedwater was 660 Da, while the molecular weight of remaining HS in NF permeate was around 530 Dalton. Consequently, the removal rate for BBs (between 65–80 % removal) and LMW substances (<60%) was lower, due to MMs below 500 Da.

Both the $LMW_{neutrals}$ and the HS followed a similar pattern (Figure 29). At a cross flow velocity of 0.5 m s^{-1}, recovery rates of above 50% significantly deteriorated water quality. Permeate quality improved when the crossflow was increased to 0.8 m s^{-1}, above which no further improvement was observed.

Although the membrane retention increased with increasing cross-flow velocities, the relative DOC composition of NF permeate did not change in terms of retention behavior of HS and $LMW_{neutrals}$ (Figure 29). Increased cross-flow velocities (increased mass-transfer coefficients) affected the membrane retention on the several DOC fractions with comparable magnitudes, the lines in Figure 29 are close to parallel despite the molecular mass being significantly for those DOC fractions.

$LMW_{neutrals}$ were below the specific MWCO of the NF test membrane resulting in at least 40% passage on the permeate side. With a similar retention behavior for $LMW_{neutrals}$ (feedwater: 1300 ppb), 300 ppb were detected in NF permeate. Therefore, GAC filters could be an alternative for post treatment of these DOC fractions which has been shown in earlier experiments (NF pilot trial 1, paper VI) indicating a removal of at least half of the permeating LMW substances.

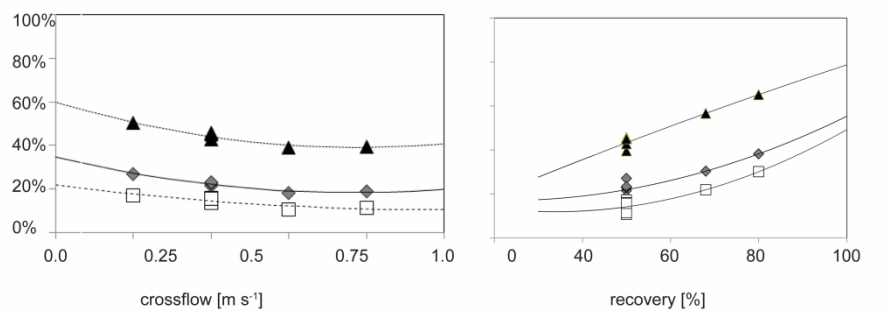

Figure 29 Effect of recovery rate on the fraction of DOC in the permeate for DOC (◆) , Humic substances (□) and $LMW_{neutrals}$ (▲) at a fixed cross flow of 0.5 m s^{-1} in the NF pilot plant (right, samples S1-S4 (LC-OCD analysis)) and effect of cross flow on the fraction of DOC in the permeate for DOC at fixed recovery of 50%, Humic substances and LMW_{acids}, $LMW_{neutrals}$ for the container plant experiments (left) The lines are second-degree order fits to the data to highlight the trends. Data points that overlap in the figures at crossflow of 0.5 m s^{-1} and at recovery of 50% are replicate samples at similar conditions but sampled under the short-term experiments (trial 2). Figure from Paper III.

4.2.3 UF Pilot trials with in-line coagulation

The temporal changes in the organic matter concentration and character of the raw water source of Lake Neden were minor compared with the other Swedish surface-water drinking-water plants in the GenoMembran project (i.e., Görväln WTP, Råberga WTP, and Ringsjö WTP) (Lidén & Persson, 2015; Lidén *et al.*, 2017). A lake turnover time of approximately five years probably allowed for substantial removal of terrestrial-derived carbon in Lake Neden, similar to the process observed in a larger Swedish lake, Lake Mälaren (Köhler *et al.*, 2013). The comparatively low SUVA (2.97 ± 0.05) and high freshness (0.63 ± 0.01) in the raw water (Table 10) were indicative of mixing both with groundwater with low SUVA (2.0 ± 0.18, Table 11) and with lake water containing internally produced carbon. This source water was more difficult to flocculate compared with many other boreal lakes, with shorter turnover times and a higher proportion of forest cover on the catchment. This notion is corroborated by the observation of a comparably high fraction (3%) of biopolymers in the lake water (Table 11**).**

The UV_{254} was measured with four different devices: online (UV_{Sensor}), in the laboratory of the WTP ($UV_{\text{Lab1 unfilt.}}$), in a commercial laboratory ($UV_{\text{Lab2 unfilt.}}$), and on filtered samples in a research laboratory ($UV_{\text{Lab3 filt.}}$). Owing to differences during the trials, the data were evaluated for the entire period and for each year (Table 10).

Table 10 Median and standard deviation for *UV* absorbance @254 nm (m^{-1}), DOC (mg L^{-1}), fluorescence index (FI), freshness index (β:α), and SUVA (L mg^{-1} m^{-1}) for the period 2015–2016. Regarding the *UV* absorbance, four different measurements are available, namely those of three laboratories ($UV_{Lab1–3}$) and the sensor data (UV_{Raw}). The samples for laboratory 3 are all filtered (0.7 µm glass fiber filters, GFF) samples. Missing results are marked n.d., and DELTA (%) is the percentage of removal of *UV* calculated as $\Delta UV_{Raw}/UV_{Perm}$. Table from Paper V.

Sample	UV_{Raw}	$UV_{Lab1\ unfilt.}$ $^{\$}$	$UV_{Lab2\ unfilt.}$ $^{\$}$	$UV_{Lab3\ filt.}$ $^{\#}$	DOC_{Lab3}	FI_{Lab3}	β/α_{Lab3}	$SUVA_{Lab3}$
Raw 2015	9.40 ± 0.46	9.23 ± 0.44	9.30 ± 0.38	8.57 ± 0.36	n.d.	n.d.	n.d.	n.d.
Raw 2016	9.90 ± 0.17	9.30 ± 0.37	9.04 ± 0.48	8.60 ± 0.39	n.d.	n.d.	n.d.	n.d.
Raw	9.80 ± 0.23	9.40 ± 0.45	9.11 ± 0.41	8.59 ± 0.37	2.89 ± 0.07	1.47 ± 0.02	0.63 ± 0.01	2.97 ± 0.05
Feed (with coagulants)	n.d.	n.d.	n.d.	5.93 ± 1.48	2.26 ± 0.30	1.58 ± 0.05	0.71 ± 0.03	2.51 ± 0.32
Perm	4.00 ± 0.78	4.00 ± 1.00	4.53 ± 1.02	4.41 ± 1.05	2.05 ± 0.22	1.61 ± 0.05	0.73 ± 0.03	2.12 ± 0.25
DELTA	59%	57%	50%	48%				
Perm 2015	4.10 ± 0.74	4.03 ± 0.76	4.50 ± 1.09	4.23 ± 1.07	n.d.	n.d.	n.d.	n.d.
Perm 2016	3.80 ± 0.34	4.01 ± 0.33	4.62 ± 0.95	4.43 ± 1.57	n.d.	n.d.	n.d.	n.d.

Notes: $^{\$}$ Measured in a 4-cm cuvette. $^{\#}$ Measured in a 1-cm cuvette.

On average, less than 30% of the DOC and slightly more than 50% of the UV_{254} (UV_{Raw}) were removed during the coagulation UF process (Table 10). The SUVA decreased from approximately 3 to close to 2. Most of the LC-OCD measurements conducted over the last five years indicated quite stable conditions for both ground- and lake water (Table 11). On average, the raw water consisted of approximately 60% humic acids, only half of which could be removed by the current process.

Table 11 Average and standard deviation of liquid chromatography-organic carbon detection (LC-OCD) analysis for (*n*) samples of the groundwater well (Well), the lake (Neden), the feed (Feed, values in bold for comparison), and the UF and NF permeate (Perm), NF concentrate (Conc), and the drinking water from the retrofitted UF full-scale water treatment plant (DW). Missing results are marked as n.d. LMW: low molecular weight. Table from Paper V.

Code	Sample	*n*	TOC (ppb-C)	DOC (ppb-C)	Biopolymers (ppb-C)	HS (ppb-C)	Building Blocks (ppb-C)	$LMW_{neutrals}$ (ppb-C)	LMW_{acids} (ppb-C)	SUVA ($L\ mg^{-1}\ m^{-1}$)
NF-HF-P	Lake	3	n.d.	3235 ± 81	121 ± 8	2034 ± 54	568 ± 67	398 ± 33	9 ± 9	3.92 ± 0.03
UF-HF-P1	Lake	4	3126 ± 202	3021 ± 204	100 ± 23	1919 ± 119	558 ± 49	401 ± 20	20 ± 9	3.82 ± 0.24
UF-HF-P1	GW	2	600 ± 73	546 ± 213	5 ± 26	260 ± 85	0 ± 7	0 ± 2	0 ± 0	2.02 ± 0.18
UF-HF-P1	**Feed**	**4**	**2578 ± 402**	**2423 ± 343**	**72 ± 37**	**1603 ± 273**	**444 ± 57**	**344 ± 33**	**23 ± 11**	**3.65 ± 0.8**
UF-HF-P1	Perm	3	1655 ± 85	1714 ± 111	35 ± 10	855 ± 140	418 ± 28	315 ± 38	5 ± 7	2.62 ± 0.18
UF-HF-F	**Feed**	**2**	**2541 ± 77**	**2337 ± 16**	**72 ± 10**	**1513 ± 10**	**409 ± 3**	**302 ± 5**	**42 ± 4**	**3.43 ± 0.22**
UF-HF-F	Perm	2	1679 ± 34	1496 ± 24	27 ± 4	756 ± 53	424 ± 68	281 ± 1	17 ± 9	2.31 ± 0.26
NF-HF-P	**Feed**	**3**	**n.d.**	**2593 ± 167**	**93 ± 2**	**1638 ± 55**	**508 ± 13**	**334 ± 19**	**0 ± 3**	**3.83 ± 0.04**
NF-HF-P	Perm	3	n.d.	1158 ± 268	7 ± 3	592 ± 185	244 ± 56	210 ± 49	0 ± 3	3.09 ± 0.18
NF-HF-P	Conc	3	n.d.	4502 ± 1317	162 ± 99	2940 ± 980	804 ± 171	476 ± 123	1 ± 0	4.09 ± 0.16
UF-HF-F	DW	2	1742 ± 194	1473 ± 7	31 ± 1	754 ± 66	411 ± 70	272 ± 4	11 ± 5	1.88 ± 0.41

On the one hand LC-OCD analysis indicated a lower DOC in the permeate (1.7 mg L^{-1}) compared with the classical DOC analysis listed in Table 10 (2.1 mg L^{-1}), but on the other hand a higher DOC in the feed (2.5 mg L^{-1}) was measured compared with the classical DOC analysis (2.3 mg L^{-1}). According to the LC-OCD, the combined coagulation/ultrafiltration processes removed approximately 30% of the DOC and 50% of the HS. However, other NOM compounds (BBs and LMW_{acids}) remained unchanged compared with NOM composition of the feed and permeate (Figure 30 and Figure 31). According to LC-OCD results, HS removal resulted in a decrease of SUVA from 3.4–3.7 to 2.3–2.6 (Table 11), compared with a decrease from 3 to 2 derived from classical DOC analysis (Table 10). The specific differences for SUVA were beyond the analytical error of the classical method. Despite comprehensive quality control, no plausible explanation was found for the consistently higher LC-OCD-derived SUVA values in this study.

Moreover, the LC-OCD results indicated that both the biopolymers and the $LMW_{neutrals}$ originated from the lake water. Half of the biopolymers but none of the LMW_{acids} were removed with in-line coagulation/UF treatment process. These carbon fractions have the potential to cause regrowth in the distribution system, which in view of climate change, could probably have implications for the future adaptation of the process.

All the results from the pilot-scale trial (UF-HF-P1) conducted in 2011 agreed with the data obtained from the most recent (2017) full-scale process (UF-HF-F). This is a most satisfactory result, as it indicates that a) the full-scale plant was successfully implemented and trimmed to resemble the pilot-scale plant closely and b) the LC-OCD results were reproducible over time.

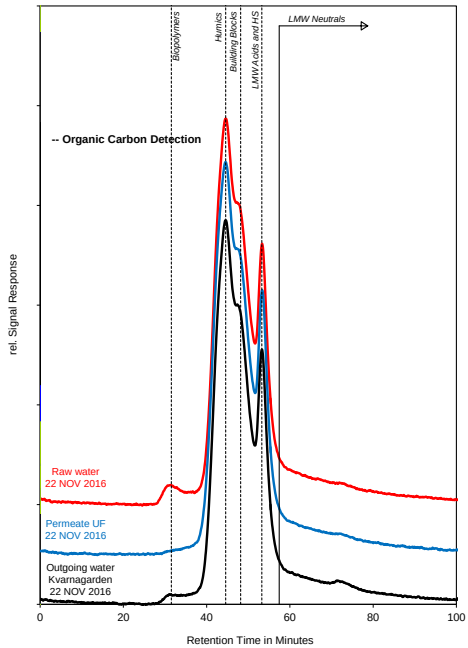

Figure 30 NOM profile: Kvarnagården WTP after retrofit (UF without in-line coagulation). LC-OCD chromatograms for raw water (red line), permeate (blue line) and outgoing drinking water (black line).

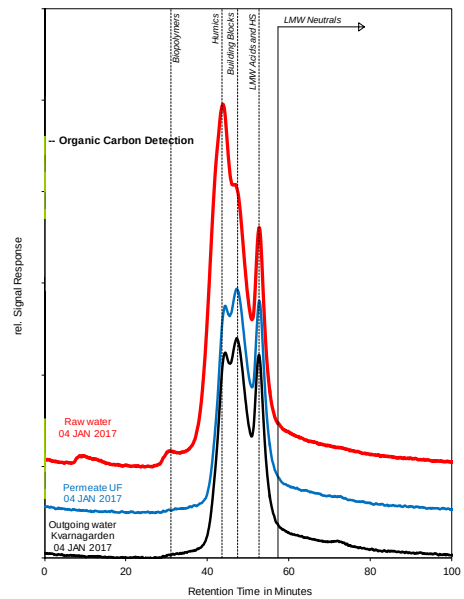

Figure 31 NOM profile: Kvarnagården WTP after retrofit (UF combined with in-line coagulation). LC-OCD chromatograms for raw water (red line), permeate (blue line) and outgoing drinking water (black line).

4.3 NOM removal efficiency: UF with in-line coagulation

During a 30-month UF pilot trial on the surface water of Lake Neden, automatic coagulant dosing based on online measurement was successfully applied.

The sensor data and coagulant dosing rates were used to identify the optimal coagulation conditions over the entire pilot period. For this purpose, the variation in the observed UV signals between the feed and permeate was plotted against the utilized coagulant dose. The observed relationship was nonlinear, with decreasing efficiency of UV_{254} removal when the Al dose was increased. This behavior could be mimicked with a second-degree curve, as shown in Figure 32.

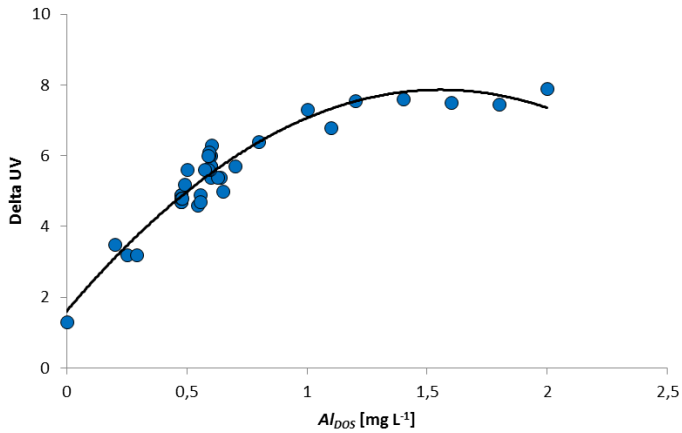

Figure 32 Sensor-based change in UV_{254} signal between the feed and permeate, as a function of added Al. $\Delta UV = 2.63 + 5.15*\text{Al dose} - 4.30*(\text{dose} - 0.529)^2$. Figure from Paper V.

Based on this relationship, all the results related to dosing could be benchmarked. According to Figure 33, episodes with removal rates (ΔUV) of at least 25% below the optimum removal (according to the fitted equation in Figure 32) are colored red, while episodes with removal rates of at least 10% below optimum removal (but within 25% of the optimal performance) are marked black. Correspondingly, the increasing coagulation efficiency as a function of time was evident. During the first three months of the trial period, a large number of data points indicated coagulation efficiency below 75% (initial trimming phase). However, almost all the data points showed coagulation efficiency above 90%, nine months after commissioning of the UF two-stage pilot plant.

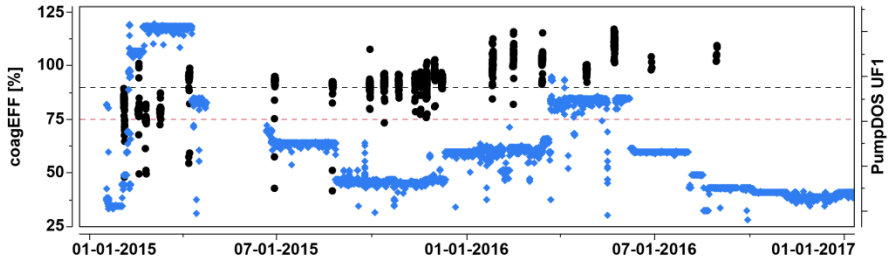

Figure 33 Change in coagulation efficiency and coagulant dosing signal as a function of time for the two-year UF pilot period (● coagEFF [%] and (♦) Al dosing [0–0.01 L h^{-1}]). The black and red horizontal lines highlight 90% and 75% of coagEFF. Figure from supplementary information to Paper V.

Furthermore, recorded sensor data during various test runs could be used to identify the potential limits of the coagulation dosing beyond 0.6 mg Al L^{-1} currently applied for both the UF pilot plant and UF full-scale facility at Kvarnagården WTP. While there was a somewhat linear relationship between the dose and change in *UV* (Delta *UV*) in the range 0 to 0.7 mg Al L^{-1}, the relationship flattened out at higher doses. Dosing above 1.2–1.4 mg Al L^{-1} did not result in further reductions of *UV* (Figure 32). This limit was related to the raw water content in the HS and the low SUVA, as was described earlier (Table 11).

Moreover, the evaluation of normalized coagulation efficiency (Eq. 4) could help to determine the efficiency of increasing the dosage compared with the current dose of 0.6 mg Al L^{-1}. These data revealed the sharply decreasing efficiency of Al addition (Figure 34), and in accordance with Figure 32, the curve flattened out at higher doses. It could be calculated how much UV_{254} was removed with an increase in the dose ($\Delta UV/\Delta Al$). Dosing at 0.95 mg Al L^{-1} (1.4 mg Al L^{-1}) resulted in only 80% (respectively 66%) of the *UV* removal efficiency per dose achieved by the current Al dose (0.6 mg Al L^{-1}).

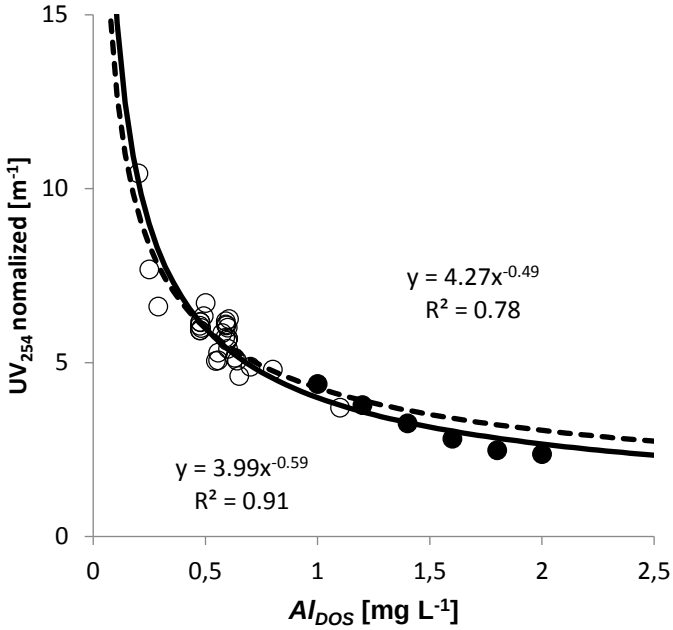

Figure 34 Estimation of normalized UV_{254} removal as a function of Al dose based on Eq.(4). Black circles (●) are additional high-dose experiments, while white circles (**O**) are derived from the optimization period during long-term UF pilot trials at Kvarnagården WTP. Two regression lines are depicted including (below) or excluding (above) the additional data points for high-dose test runs. Figure from supplementary information to Paper V.

However, higher doses produced more sludge, which from both an environmental and economical viewpoint was not a desired result. In view of the overall membrane performance during stress testing with maximum coagulation dosage (Table 12), it was concluded that the current process with the current raw water quality probably had an optimal technical and economic dosing limit of close to 0.95 mg L^{-1}. This dosing rate was even used for scenario analyses assessing the potential deterioration in raw water quality due to climate change.

Table 12 The effect of incremental increase of the coagulant dose on UV_{254} and membrane performance. Data for TMP and permeability relate to an ordinary filtration cycle for UF stage-1 and UF stage-2 of the UF test facility (UF-HF-P2) at Kvarnagården WTP. Table from Paper V.

Dose (mg Al L^{-1})	**1.00**		**1.40**		**1.60**		**1.80**		**2.00**	
UF stage	UF1	UF2	UF1	UF2	UF1	UF2	UF1	UF2	UF1	UF2
Flux (L m^{-2} h^{-1})	49	33	49	33	49	33	49	33	49	33
TMP (bar)	0.16–0.19	0.05–0.14	0.17–0.19	0.06–0.17	0.16–0.18	0.06–0.22	0.16–0.18	0.06–0.24	0.16–0.19	0.06–0.25
Permeability (L m^{-2} h^{-1} bar^{-1} @ 20 °C)	420–360	760–320	420–360	760–240	420–370	740–200	420–360	740–170	420–360	740–150
Feed water, UV_{254} (m^{-1})	10.02	n.a.	9.9	n.a.	9.8	n.a.	9.7	n.a.	10.05	n.a.
Permeate, UV_{254} (m^{-1})	2.70	4.1	2.3	3.2	2.3	2.8	2.25	2.7	2.15	2.8

4.4 Characterization of aged membrane properties (Papers I and II)

4.4.1 Properties of HF-NF test module

After 12 months´ continuous operation of the HF-NF test module (HFW1000) with pretreated feed water at Görväln WTP, the mechanical properties of extracted membrane fibers (from different module sections) and virgin membranes (reference) were compared by tensile strength analysis and independent samples t-tests. As for elasticity of the membranes, Young´s Modulus values of aged fibers from the top and bottom section were higher compared to the reference. These results indicated that the membranes became stiffer after multiple filtrations and cleaning cycles. In contrary, the middle section sample's Young's Modulus value was statistically unchanged (Figure 35). Moreover, not any significant changes in the force required to fracture the membrane were observed from the tensile strength analysis (Figure 36). In addition, subsequent t-tests showed no statistical differences in breaking force amongst the four samples at 95% confidence interval. Thus, it could be concluded that the increase in Young's Modulus values caused by repeated filtration and backwashing cycles did not have a significant impact on the membrane's mechanical strength, although periodic CIP was carried out during the pilot trials by using NaOCl (200 ppm) in the presence of NaOH (pH: 12.4). A previous study by Causserand *et al.* (2008) suggested no change to the mechanical properties of the membranes could be observed at this pH level because the hypochlorite solution at pH 12 would contain hypochlorite ion (OCl^-) only, which has less oxidising potential compared to the hypochlorous acid (HClO).

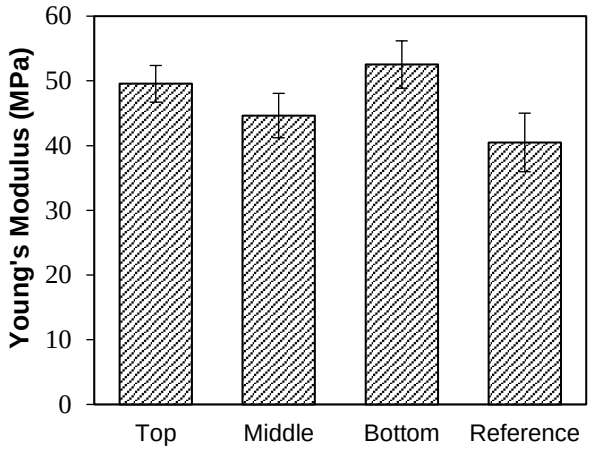

Figure 35 Mechanical properties of HF-NF membrane samples: Young's Modulus of aged fibers from NF test module (top, middle and bottom section) and virgin fibers (reference). Figure from Paper I.

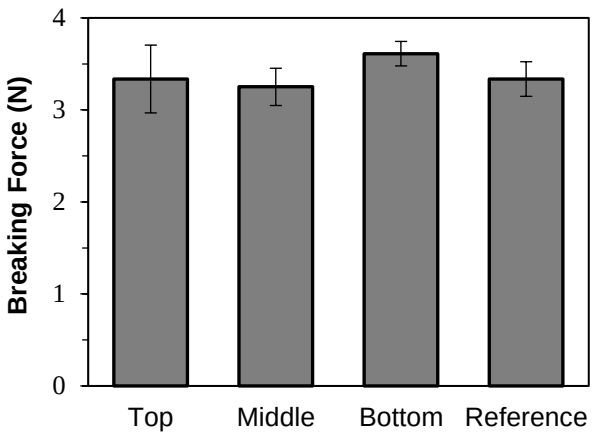

Figure 36 Mechanical properties of HF-NF membrane samples: Breaking Force of aged fibers from NF test module (top, middle and bottom section) and virgin fibers (reference). Figure from Paper I.

Contact angle measurements of the membrane samples indicated that the membrane's lumen surface (feed side) became less hydrophilic after prolonged operation and cleaning. Lumen side average contact angle increased from 62.06° (± 4.51°) to 69.73° (± 2.37°), 70.16° (± 5.45°), and 66.56° (± 4.02°) for the samples from the top, middle, and bottom section, respectively. Furthermore, a comparison of the contact angle results showed that fibers from the top, middle and bottom sections had similar hydrophilicity and wettability.

AFM investigations indicated an increase in lumen side surface roughness for samples from the top, middle and bottom sections compared to the reference membrane sample. The R_q value increased from 10.6 nm (reference sample) to 18.6 nm for the sample collected from the top section of the module. Furthermore, samples from the bottom section had a relatively lower roughness (R_q = 15.4 nm) compared to samples from top and middle sections. A similar trend was observed for the calculated average roughness of the aged samples (Table 13). Increase in roughness could indicate the possibility of the enlargement of pore size (Arkhangelsky *et al.* 2007).

Table 13 Roughness values of membrane samples for the lumen side surface: aged fibers from NF test module (top, middle and bottom section) and virgin fibers (reference). Table from Paper I.

Typ of sample	Top section	Middle section	Bottom section	Reference
RMS Roughness, R_q (nm)	18.6	18.4	15.4	10.6
Average Roughness, R_a (nm)	15.1	12.6	11.9	7.6

Moreover, the shell side (permeate) surface roughness increased significantly for the aged fibers compared to the virgin membrane. The R_q value increased from 23.5 nm (reference sample) to 28.1 nm, 35.6 nm, and 62.9 nm for the samples collected from the top, middle, and bottom section, respectively. Besides, the shell side surface also exhibited a higher roughness than the lumen side surface, which is due to the higher porosity.

ATR-FTIR spectroscopy has been previously applied to assess the chemical degradation of PES membranes. In this context, different mechanisms have been proposed for NaOCl attachment on PES membranes, including chain scission and formation of phenyl sulfonate (Arkangelsky *et al.* 2007), or the chain scission of the PES polymeric backbone into two parts with one end terminated by a sulfonic acid group and other part terminated by a phenyl chloride group (Yadav *et al.* 2009). None of those mechanisms were observed by ATR-FTIR spectra of the virgin and aged membrane samples as similar peaks were detected at their corresponding functional group's wavelengths. However, a significant change in the broad peak at around 3400 cm^{-1}, which was the hydrogen bonding stretching vibration, was noticed. This change could be attributed to the residual glycerol and water in the reference sample. Besides that, ATR-FTIR results suggested that no degradation to the membrane samples' polymer material composition had occurred (Figure 37).

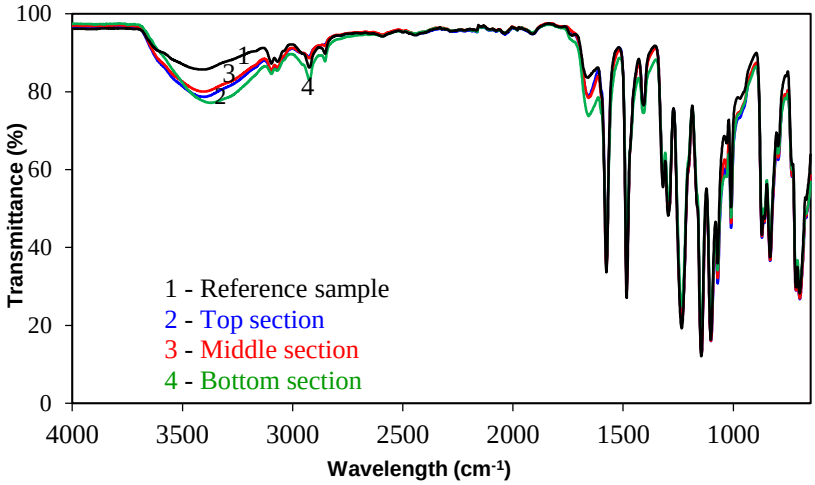

Figure 37 ATR-FTIR spectra of HF-NF membrane samples: virgin membrane (black line), aged membranes from top section (blue line), from middle section (red line), and from bottom section (green line). Figure from Paper I.

Additionally, TGA analysis was used to detect the changes in the mass of the membrane samples as a function of temperature. The TGA profiles of all four samples showed identical decomposition profiles indicating the absence of chemical degradation of the polymer material (Figure 38). However, for the reference membrane sample a decrease in mass was observed at around 280 °C, which can be attributed to the residual glycerol preservative agent present in the sample, with glycerol having a boiling point of 290 °C. In sum, the conclusions drawn from ATR-FTIR spectroscopy were cross-confirmed by TGA analysis.

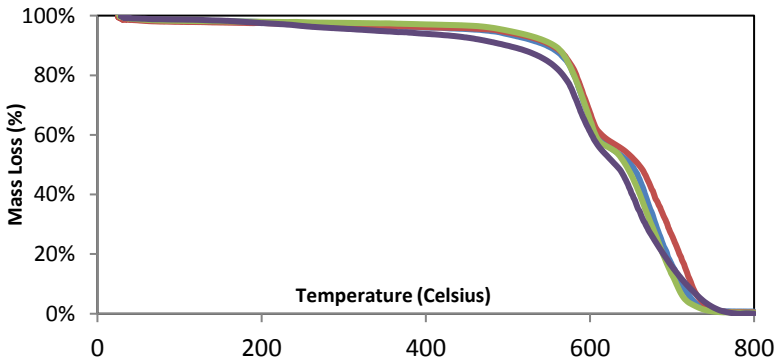

Figure 38 TGA profiles of HF-NF membrane samples: virgin membrane (purple line), aged membranes from top section (blue line), from middle section (red line), and from bottom section (green line). The plots of percentage mass loss as a function of temperature exhibited a two-step degradation mechanism. The mass loss due to decomposition of the polymer material started at around 450°C, with major mass loss occurring between 500 °C to 560 °C followed by a second degradation stage occurring between 630 °C to 650 °C. Figure from Paper I.

According to SEM investigations no significant defects, cracks, or deposits (foulants) were observed on the shell side surface samples. In accordance to AFM analysis, the lumen surface of the samples from top, middle and bottom section were identified by SEM to be rougher compared to the reference sample's surface.

A further EDS analysis on the elemental composition of the membrane surface detected similar spectra with three elements, Carbon, Oxygen, and Sulphur. Given the fact that EDS detected no other elements, it can be concluded that there were neither signs of fouling on the lumen side surface of all the membrane fiber samples nor traces of CIP by-products.

4.4.2 Properties of HF-UF test module

After 12 to 14 months´ continuous pilot operation (two-stage UF container pilot at Kvarnagåden WTP), the change in nanomechanical properties of HF-UF test modules (Xiga and Aquaflex membranes) were analyzed by using Quantitative Nanomechanical Mapping (QNM) technique. Operation conditions were different for the test modules in terms of feed water quality, frequency of backwashing and chemical cleaning, flux rates, filtration volumes etc. Xiga membranes in the primary UF stage were exposed for in-line coagulation, while Aquaflex membranes in the secondary UF stage were fed with water of higher turbidity (coagulant flocs) and higher particulate organic carbon (POC) concentration.

Xiga virgin and Aquaflex virgin displayed a low roughness, i.e., μ:13.7 nm (σ:0.43) and μ:16.7 nm (σ:0.17), respectively, which were consistent to those obtained by tapping mode in air during morphological analysis.

The mean adhesion, Peak Force error, dissipation, LogDMT Modulus, and deformation of Xiga virgin were 0.19 nN, 0.12 nN, 54.9 eV±, 0.12 Log[Pa]±, and 12.2 nm; while for Aquaflex virgin were 0.36 nN, 0.18 nN, 59.7 eV±, 0.067 Log[Pa]±, and 7.7 nm, respectively.

Aquaflex virgin showed higher Peak Force error and adhesion, as well as lower modulus and deformation than Xiga virgin. The values of dissipated energy were similar for both virgin membranes. These results indicate virgin membranes of different properties; specifically, the surface of Aquaflex virgin showed more adhesion to the AFM silica probe and their polymeric structures were softer than those of Xiga virgin.

Harvested membrane samples that showed no adsorb foulants (i.e., locations where the cleaning process seemed effective) were selected by a rigorous morphological analysis using QNM-height sensor and Soft-Tapping Mode™, supported by adhesion and modulus analysis. Clean membrane surfaces (i.e., showing pores and a characteristic polymeric structure as seen in virgin membranes) were observed in

the six types of membrane samples analyzed: Xiga right, Xiga center, Xiga left, Aquaflex top, Aquaflex middle, and Aquaflex bottom, suggesting the efficiency of the CEB procedure. The properties of these membrane samples were statistically processed and analyzed by probability density functions.

Briefly, the mean roughness of the three Xiga samples were similar to that of Xiga virgin (i.e., Xiga left: 18.5 nm, Xiga center: 19.4 nm, and Xiga right: 14.9 nm), where no value significantly deviated from the fitting function. Conversely, the mean LogDMT Modulus of Xiga center and Xiga right (i.e., 0.33 and 0.21 log[Pa]±, respectively) were higher than that of Xiga virgin (0.12 log[Pa]±). Besides, high LogDMT Modulus values of up to 0.7, 1.4, and 1.0 were recorded for Xiga left, Xiga right, and Xiga center, respectively; indicating that Xiga membranes displayed stiffer surfaces after fouling and chemical cleaning. As an outcome of fouling and cleaning process, the stiffness of membranes increased and these surfaces would need more force to deform. This observation was also supported by the Peak Force values recorded. The Peak Force values of Xiga center, Xiga right, and Xiga left were higher compared to Xiga virgin (i.e., 0.34 nN, 0.17 nN, 0.20 nN, and 0.12 nN, respectively). Finally, the mean dissipation of Xiga right and Xiga left were lower than that of Xiga center (i.e., 36.6, 39.5, and 74.6 eV±, respectively).

The roughness values of clean Aquaflex membranes were lower than those of Aquaflex virgin, suggesting polymer degradation. The values of Peak Force, dissipation, and modulus of virgin and clean Aquaflex membranes were similar in magnitude. However, the adhesion of the AFM probe to Aquaflex bottom and Aquaflex middle were slightly higher than to Aquaflex top and Aquaflex virgin (i.e., 0.52 nN, 0.46 nN, 0.37 nN, and 0.36 nN, respectively). Additionally, the deformations of clean Aquaflex membranes (middle, top, and bottom) were slightly lower than that of virgin sample (i.e., 4.5 nm, 4.0 nm, 5.1 nm, and 7.7 nm, respectively). These results suggest that fouling and subsequent cleaning process did not significantly affect the surface properties of Aquaflex membranes.

Fouling and chemical cleaning exerted different impacts on the surface characteristics of both Xiga and Aquaflex membranes. In the case of Aquaflex membranes, only few (nanomechanical) properties were affected by fouling and chemical cleaning. However, this impact was significantly higher on Xiga membranes, and was evidenced by a change in mean mechanical properties (i.e. considering virgin membrane characteristics as a baseline). In particular, the Xiga membrane material (PES) might undergo physicochemical changes by reacting with the coagulants, cleaning agents and by the adsorption of foulant molecules. Besides, the Xiga test module was used more extensively than the Aquaflex module; filtering 57,150 m^3 and 2,155 m^3, respectively. Additionally, the Xiga test module was backwashed 267 times while the Aquaflex test module only 37 times using the same

CEB procedure. These operational conditions most likely have exerted a higher impact on the polymeric surface of Xiga membranes.

Furthermore, the morphology and nanomechanical characteristics of harvested XIGA and Aquaflex membrane samples were studied showing the presence of foulants after operation and CEB. The six samples showing adsorption of foulants were analyzed: Xiga center, Xiga right, Xiga left, Aquaflex top, Aquaflex middle, and Aquaflex bottom. At a nano-scale of selected scanning areas, foulant adsorption was heterogeneous in both morphology and mechanical properties. Therefore, these foulant properties could not be statistically described by probability density functions due to their high heterogeneity. Previous AFM investigations have observed the heterogeneous physicochemical characteristics of foulant layers during a kinetic study of RO membrane fouling (Khan *et al.*, 2013).

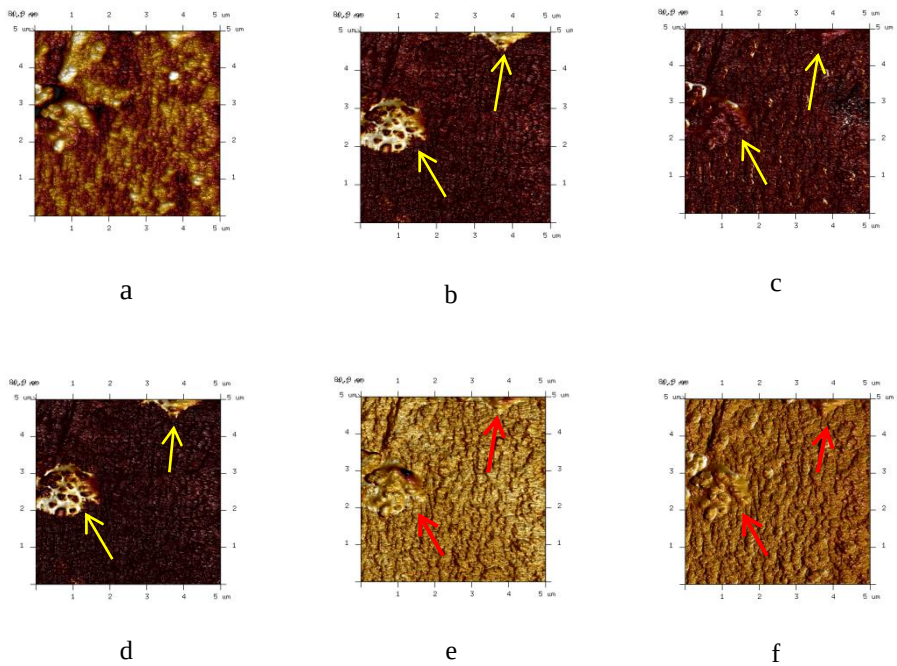

Figure 39 (a) Height sensor, (b) Adhesion, (c) Deformation, (d) Dissipation, (e) LogDMT Modulus, and (f) Peak Force error images of Xiga right membrane samples showing adsorption of foulant. Scan area: 5×5 μm. Figure from Paper II.

As shown in Figure 39, QNM technique also proved to be a powerful tool for discriminating foulants from membrane surface due to their different mechanical properties. Briefly, the roughness of an apparently clean area of Xiga right was 26.6 nm (Figure 39a). Nevertheless, in the adhesion channel (Figure 39b) two small areas (yellow arrows) displaying high adhesion forces of up to 1.8 nN were evident. The

values of Peak Force of the foulant were lower than those of the surrounding membrane (i.e., 0.151 nN vs. 0.241 nN) (Figure 39f, red arrows). Also, the LogDMT Modulus (Figure 39e, red arrows) of this foulant was lower than the surrounding membrane surface (i.e., 0.163 vs. 0.248 log[Pa]±, respectively), while the dissipation (605 eV±) was higher than the values typically observed for virgin membrane (Figure 39d). These results indicated a soft, adhesive, and less elastic foulant. Previous studies have reported foulants of lower elastic modulus compared to virgin membranes (Powell *et al.*, 2017). Moreover, the presence of this foulant after chemical cleaning and its high adhesion could be an indicative at a nano-scale of irreversible adsorption, as suggested in previous investigations (Yamamura *et al.*, 2008; Merle *et al.*, 2016). Furthermore, this QNM analysis also indicated that the detection of foulants solely using height sensor or phase channels can be incomplete and misleading.

Even fouled Aquaflex membranes showed heterogeneous morphologies, surface characteristics, and mechanical properties (Figure 40).

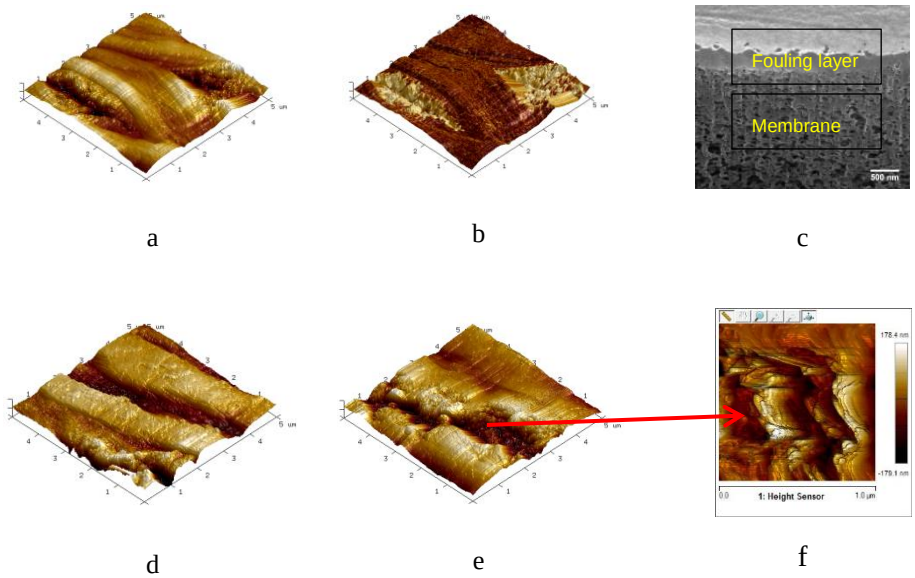

Figure 40 (a) Height sensor and (b) phase images of fouled Aquaflex middle section membrane (scan area: 5×5 µm). (c) SEM image of cross section of Aquaflex middle section membrane showing a ~300 nm fouling layer. (d) Height sensor of fouled Aquaflex membrane (scan area: 5×5 µm). Height sensor of (e) fouled Aquaflex membrane showing micro-cracks (scan area: 5×5 µm) and exposing (f) membrane surface (scan area: 1×1 µm). Figure from Paper II.

Particularly, fouling layers were recorded totally covering scanning areas, where micro-cracks were also detected, i.e., also evidenced in SEM images. Phase images of these fouling layers suggested materials of heterogeneous physicochemical characteristics (Figure 40b). Interestingly, these micro-cracks (i.e., observed in

Aquaflex top, middle, and bottom samples) provided crucial information regarding the thickness of the fouling layers. The depth of these crack ranged from 23 nm to 239 nm, where no membrane material was observed (Figure 40d). This latter result suggests fouling layers thicker than 239 nm. SEM images of cross sections showed foulant layers of similar thickness (Figure 40c). However, other samples showed cracks of few tens of nm where membrane material was detected (Figure 40e-f), indicating the high heterogeneity of fouling layers in terms of thickness. The mean roughness of the foulant layers of used Aquaflex membranes were highly variable, e.g., 130 nm (Figure 40a) or 93 nm (Figure 40d); while the mean LogDMT Modulus values ranged from 0.081 up to 0.372 log[Pa]± (Figure 40d). Although variable, the mean adhesion forces of these foulant layers were higher than Aquaflex virgin. However, the mean adhesion forces of foulant layers of Aquaflex membranes were also lower compared to those of Xiga membranes (e.g., ranging from 0.35 nN to 0.87 nN). Consequently, the dissipation energies of these foulant layers were also lower than those of Xiga membranes, i.e., 220 eV± to 598 eV±. Similar to fouled Xiga membranes, the fouling material of Aquaflex membranes was highly variable in characteristics and nanomechanical properties.

In sum, the QNM results indicated that the fouling layer of Aquaflex membranes were rougher, less adhesive, and slightly stiffer compared to the fouling layers of Xiga membranes. This latter result could be explained by the feed water quality of the UF-stages.

The pyrolysis GC/MS analysis was conducted on the material recovered from Xiga center. Comparison with the pyrochromatogram recorded from Xiga virgin confirmed the presence of foulant material accumulated at the membrane surface. Pyrolysis by-products such as cyclopentenone and methyl cyclopentenone were indicators of the presence of polysaccharides in the organic layer. Toluene, styrene, pyrrole, and methyl pyrrole confirmed the presence of proteins. The detection of furanmethanol, a DNA pyro-fragment, is an indicator of living or recently dead microorganisms (Bruchet *et al.*, 1990). The obtained pyrolysis fingerprint for XIGA center membrane samples demonstrated the biological origin (biofilm) of the foulant. Similar results were obtained with the foulant recovered from Aquaflex middle, however the pyro-fragments showed lower relative abundance.

Furthermore, the change of nanomechanical properties of virgin membranes after chemical cleaning was studied to control potential effects on the membrane surfaces due to reaction with applied cleaning agents. Briefly, the mean roughness and adhesion forces of Xiga virgin-chemically cleaned membranes were similar to those of Xiga virgin, while its mean LogDMT modulus was double in magnitude. Along with a slightly lower deformation and a higher Peak Force, this latter result suggested a stiffer Xiga membrane surface after chemical cleaning. However, an important conclusion extracted from these results is that the type of chemical

cleaning process performed in the current investigation did not impact the nanomechanical properties of Xiga virgin to the extent of causing peak values highly deviating from the probability density functions as seen in clean Xiga left, Xiga center, and Xiga right samples. Thus, these peak values in the mechanical properties of clean Xiga membranes might be the result of a combination of the effect of adsorbed foulant molecules and a more stringent chemical cleaning in the pilot unit (i.e., higher C.t, higher number of CEBs, and acid cleaning).

In the same way, the nanomechanical properties of Aquaflex membrane samples were not significantly impacted by the ageing process. The C.t of the ageing process was similar to that of the chemical cleaning used at the pilot unit. The roughness of Aquaflex virgin-chemically cleaned membranes was lower than Aquaflex virgin membranes (i.e., 8.2 nm and 16.7 nm, respectively), also observed for harvested Aquaflex membranes showing no adsorbed material. Additionally, the magnitudes of Peak Force, LogDMT Modulus, and adhesion were slightly higher for Aquaflex virgin-chemically cleaned membranes, while the magnitudes of deformation and dissipation were similar for both samples. These control experiment results indicated that both Aquaflex and Xiga membranes would maintain their mechanical properties after a chemical cleaning process as performed in the current study.

Finally, the stable operation conditions in terms of permeability and TMP during the long-term pilot trial period indicated that the applied cleaning protocol was always able to recover the initial performance of the test modules. Moreover, the stable membrane performance suggested a) an insignificant presence of irreversible foulants on membrane surface, and b) membrane characteristics slightly affected by the pilot-scale operation.

4.5 Prediction of NOM retention for HF-NF (Papers III and IV)

4.5.1 Solution diffusion model parameters and model validation

Calculations for prediction of membrane retention for the NF test module (NF pilot trial 2 – direct filtration of surface water from Lake Mälaren) were based on short-term experiments with varying flux rates and cross-flow velocities.

The estimated TOC fractions ((I) 100% retained, (II) partially retained and (III) 0% retained) and model parameters from the model fitting based on UV_{254} and TOC are listed in Table 14.

Table 14 Water fractions and model parameters for UV_{254} and TOC. Table from Paper III.

	Model parameter: UV_{254}	Model parameter: TOC
Fraction (I)	0	0
Fraction (II)	0.985	1
Fraction (III)	0.015	0
D (solute diffusion coefficient)	1.74×10^{-10} (m^2 s^{-1})*	1.65×10^{-10} (m^2 s^{-1})*
B (solute permeability coefficient)	1.01×10^{-7} (m s^{-1})	1.69×10^{-7} (m s^{-1})

Notes: *comparable with diffusion coefficients in the literature (Park & Cho, 2008).

According to the calculations of the model parameters, the solute diffusion coefficients were comparable for UV_{254} and TOC, while the solute permeability coefficient for TOC was higher compared with the permeability coefficient for UV_{254}. This resulted in lower TOC retentions compared to retentions based on UV_{254}, which was also expected.

The results of model fit for the NF test module with regard to membrane passage for TOC and UV_{254} are shown in Figure 41 and Figure 42. The four different data lines (Figure 41) indicated the predicted membrane performance for various cross-flow velocities. It can be seen that the measured and predicted membrane passages were well fitted with probably some outliers. For instance, the fitting was improved with 25%, based on the average error per data point, if the result for one short-term experiment was excluded from the model (vCF: 0.5 m s^{-1}, Jf: 15 L m^{-2} h^{-1}; passage 20%). Furthermore, it can be pointed out that the membrane passage increased if the cross-flow velocity is decreased. With a certain cross-flow velocity, the passage first decreases when the flux is increased. However, if the filtration flux was further increased the passage increased again. This effect is similar for the retention of UV_{254}, which is caused by the dilution effect (permeate flux) and concentration polarization (Figure 42). Based on the predicted membrane passages, the retention of the first stage (50% recovery) could be calculated by using mass balances. In Figure 43, the measured retentions (surface water to permeate) and predicted retentions were shown for the applied cross-flow velocities. The predicted retentions fitted well with the measured retentions with an outlier at 65% retention and filtration flux of 15 L m^{-2} h^{-1}. Moreover, the calculations indicated that the expected first stage retentions, with 0.5 m s^{-1} cross-flow velocity and filtration fluxes between 10–20 L m^{-2} h^{-1}, were in the range of 78–80 % based on TOC. The first stage retentions could be increased further to 83% by increasing the cross-flow velocity towards 1 m s^{-1}. From an operational perspective, a cross-flow velocity of 0.5 m s^{-1} with a flux-range from 8 to 22 L m^{-2} h^{-1} was considered to be the most optimal setting based on the passage and energy consumption.

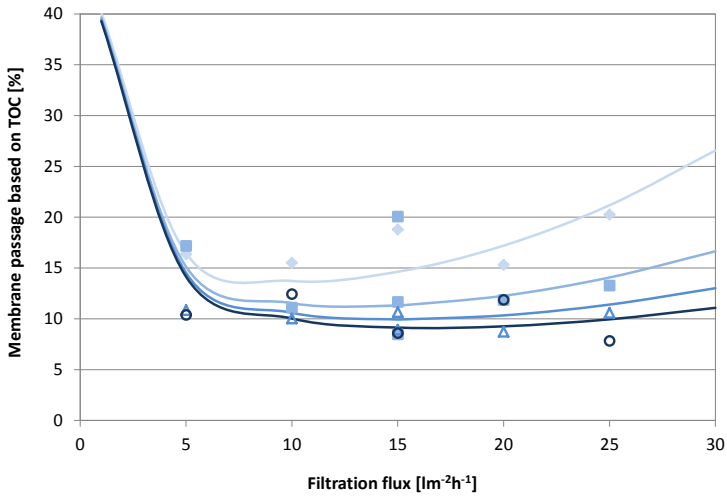

Figure 41 Model fit of membrane passage of capillary NF pilot test module. Influence of flux and cross-flow velocity on membrane passage based on TOC. Incremental increase of cross-flow velocity: (♦) 0.25, (■) 0.5, (▲) 0.75 and (○) 1.0 m s^{-1}. Measured membrane passages (data points) and predicted membrane passages (data lines). Predicted membrane passage for increasing cross-flows (0.25 to 1.0 m s^{-1}) from light to dark blue (●,●,●,● from top to bottom).

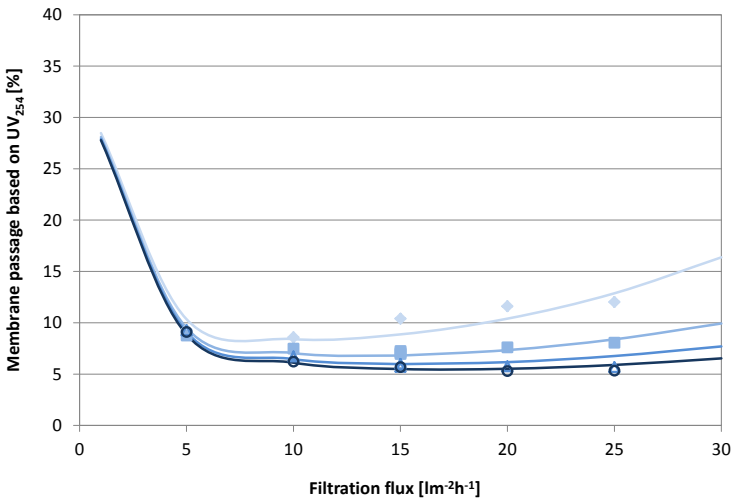

Figure 42 Model fit of membrane passage of capillary NF pilot test module. Influence of flux and cross-flow velocity on membrane passage based on UV_{254}. Incremental increase of cross-flow velocity: (♦) 0.25, (■) 0.5, (▲) 0.75 and (○) 1.0 m s^{-1}. Measured membrane passages (data points) and predicted membrane passages (data lines). Predicted membrane passage for increasing cross-flows (0.25 to 1.0 m s^{-1}) from light to dark blue (●,●,●,● from top to bottom).

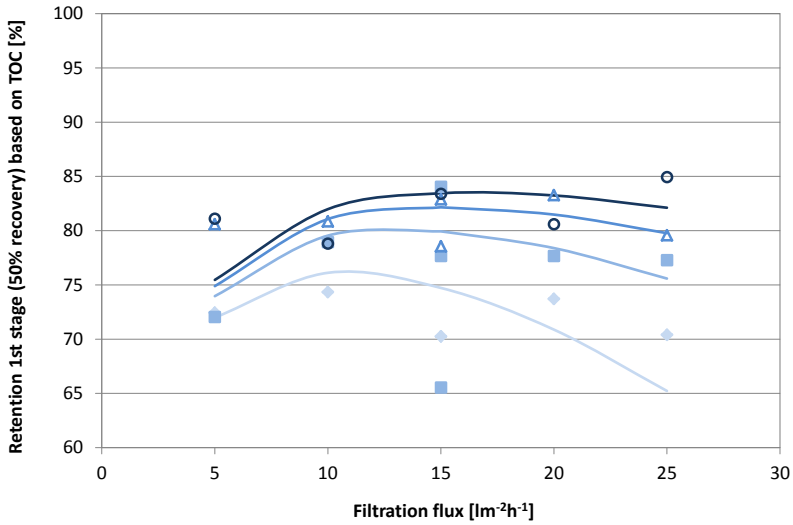

Figure 43 Model fit of membrane passage of capillary NF pilot test module. Influence of flux and cross-flow velocity on membrane passage based on TOC (first stage: 50% recovery rate). Incremental increase of cross-flow velocity: (♦) 0.25, (■) 0.5, (Δ) 0.75 and (○) 1.0 m s^{-1}. Measured membrane passages (data points) and predicted membrane passages (data lines). Predicted membrane passage for increasing cross-flows (0.25 to 1.0 m s^{-1}) from light to dark blue (●,●,●,● from bottom to top).

4.5.2 CFD model validation

In accordance with the solution diffusion model parameters, the CFD model was calibrated based on the same short-term experimental data derived from test runs with different cross-flow velocities from 0.25 to 1.0 m s^{-1} at filtration fluxes between 10 to 25 L m^{-2} h^{-1} performed on NF container pilot plant at Görväln WTP (NF pilot trial 2).

Simulated performance differed from experimental observation by 1.9% for retention of UV_{254} (Figure 44a), 2.1% for retention of TOC (Figure 44b) and 1.0 % for pressure drop (Figure 44c).

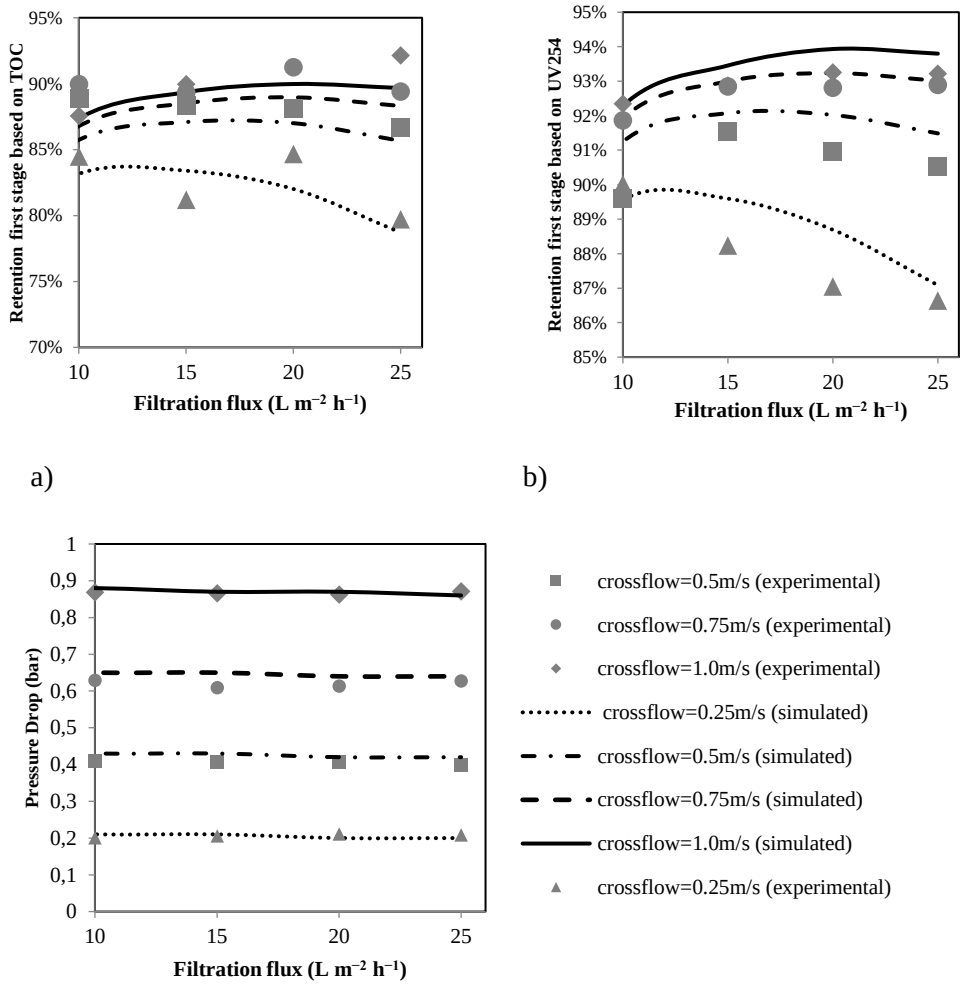

Figure 44 Comparison between experimental and simulated (a) TOC retention, (b) UV_{254} retention and (c) pressure drop at different cross-flow velocities ranging from 0.25 to 1.0 m s^{-1} at filtration fluxes between 5 - 25 L m^{-2} h^{-1}. Figure from Paper IV.

The simulated solute retention based on TOC and UV254 was found to be larger than 78.7% and 87.1%, respectively, for all cases with different cross-flow velocities from 0.25 to 1.0 m s^{-1} at filtration fluxes between 10 - 25 L m^{-2} h^{-1} (Figure 44a and Figure 44b).

A significant increase of cross-flow velocity at constant flux rate of 25 L m^{-2} h^{-1}, resulted in an increase of TOC retention from 78.7% at 0.25 m s^{-1} to 89.4% at 1.0

m s^{-1}. However, the impact of different flux rates on NOM retention was more complicated. At comparatively higher cross-flow velocity (i.e., vCf: 1.0 m s^{-1}), the solute retention based on TOC increased gradually from 87.6% to 89.4% with increasing flux rate from 10 to 25 L m^{-2} h^{-1}. On contrary, an opposite trend was observed at 0.25 m s^{-1} cross-flow velocity with decreasing TOC retention from 83.2% at flux rate of 10 L m^{-2} h^{-1} to 78.7% at flux rate of 25 L m^{-2} h^{-1}.

A similar but less pronounced trend was obtained for retention behavior of UV_{254}. Accordingly, the largest UV_{254}-retention (from 87.1% to 93.2%) was obtained by increasing the cross-flow velocity from 0.25 to 1.0 m s^{-1} at a flux rate of 25 L m^{-2} h^{-1}. These results indicated that an increase of cross-flow velocity contributed more to the removal of colorless NOM fractions.

Furthermore, it could be noted that the pressure drop along the membrane fiber length at a constant flux rate of 10 L m^{-2} h^{-1} increased significantly by increasing the cross-flow rate (from 0.21 bar at vCF: 0.25 m s^{-1} to 0.88 bar at vCF: 1.0 m s^{-1}). As shown in Figure 44c, an increase of flux rate from 10 to 20 L m^{-2} h^{-1} at different cross-flow velocities from 0.25 to 1.0 m s^{-1} had no impact on pressure drop. This behavior was expected, since the maximum flux is approximately 2.2×10^{-3} times lower than the minimum cross-flow velocity. Therefore, the flux rate has a negligible impact on pressure drop for this specific inside-out HF-NF test membrane.

4.6 Modelling of NF full-scale process design (Papers III and IV)

4.6.1 Solution diffusion approach for NF full-scale design

A preliminary full-scale process design for direct nanofiltration at Görväln WTP has been developed based on predicted full-scale retentions of HF-NF modules (solution diffusion approach) for a multi-stage membrane process (three-stage and four-stage configuration).

The predicted full-scale retentions for a typical three stage process were based on an overall recovery rate of 82.5%, whereby all stages operated at 50% recovery. Figure 45 showed the predicted full-scale TOC retention for different applied cross-flow velocities (0.25–1.0 m $s^{-1)}$. The predicted overall TOC retention, with 0.5 m s^{-1} cross-flow velocity and filtration fluxes between 10–20 L m^{-2} h^{-1}, was in the range of 67–69 %. Furthermore, the overall TOC retention could be increased for

this type of full-scale installation to 74% by increasing the cross-flow velocity to 1 m s^{-1}.

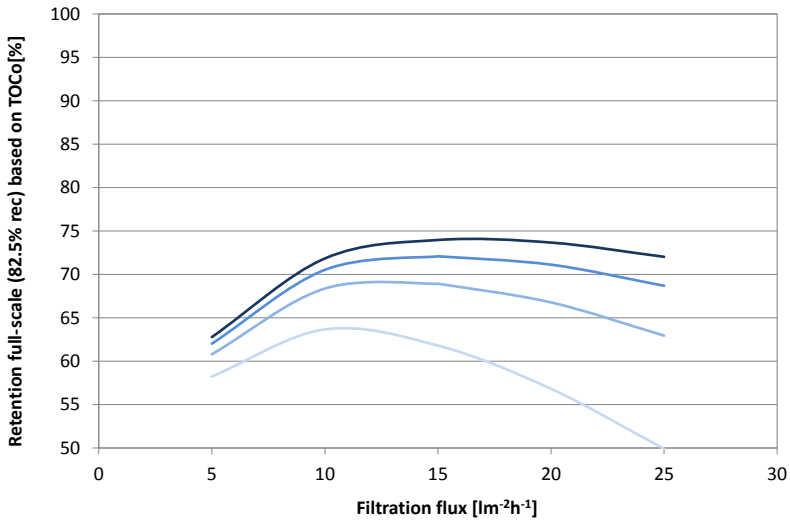

Figure 45 Influence of filtration flux (5–25 L m^{-2} h^{-1}) and cross-flow velocity (0.25–1.0 m s^{-1}) for a full-scale three-stage process with 82.5% overall recovery on predicted membrane passage of TOC. Predicted membrane passage (data lines) for increasing cross-flows from light to dark blue (●) 0.25, (●) 0.5, (●) 0.75 and (●) 1.0 m s^{-1} (from bottom to top).

In general, the TOC retention with a cross-flow velocity of 0.5 m s^{-1} was 10% lower compared to the UV retention (78%).

In addition, the specific ranges of membrane retentions, achieved in the experimental matrix, were used to calculate process retentions of a four-stage system with 90.2% recovery during filtration. Calculations for predicted membrane (process-) retention were on average 88–95 % (72–87 %) for UV_{254}, 88–98 % (72–96 %) for color (mg Pt L^{-1}) and between 80–92 % (58–81 %) for TOC (mg C L^{-1}).

In order to meet the defined design criteria of the water utility, a four-stage membrane system was proposed.

Preliminary calculations indicated a total membrane surface area in the range of 314,000 to 524,000 m^2 for the given flow rates of the actual plant capacity for Görväln WTP. The NF plant design consisted of 7862 modules for 120.000 m^3 day^{-1} and 13,103 modules for 200.000 m^3 day^{-1} with an estimated module ratio of 10-5-3-2 for stage 1 to 4. More precisely, a 160-module membrane skid could be designed with 80-40-24-16 per stage configuration. For the full-scale design of the membrane plant, it was assumed that two modules were operated in series for each membrane

stage. Consequently, the selected process configuration enabled a double-pass loop operation (the concentrate of the first module would be the feed water of the second module). The circulation pump as well as the pressurized feed and concentration line were connected between the second and first module, resulting in smaller pipes and headers due to lower circulation flow rates. However, this setup resulted in different TMPs for both of the modules due to the pressure drop over the two modules. Furthermore, a filtration flux deviation between the first and second module occured, depending on the membrane permeability, filtration flux and cross-flow velocity. In other words, the first module was running at the highest flux and thus, limited the process design based on the filtration flux. The output of the projection tool (provided by the membrane supplier Pentair X-Flow) for the proposed retrofit of Görväln WTP, is summarized in Table 15.

Table 15 Calculated design parameters for retrofit of Görväln WTP with four-stage HF-NF process for direct filtration of raw water from Lake Mälaren. Table from Paper III.

Design Parameter	**Output of Design Tool**
Overall system retention, based on UV_{254}	80.0%
Overall plant recovery, based on the raw water flow rate	85.1%
Net permeate flux	15.9 L m^{-2} h^{-1}
Recovery during filtration in the 1st stage	45.1%
Overall recovery during filtration in the 2nd stage	67.6%
Overall recovery during filtration in the 3rd stage	81.2%
Overall recovery during filtration in the 4th stage	90.2%
Membrane permeability	10 L m^{-2} h^{-1} bar^{-1} @ 20 °C
Average TMP (@5.73 °C)	2.65 bar
Pressure loss over the two modules in double-pass loop (@5.73 °C)	1.27 bar
Filtration flux, 1st module in the double-pass loop	20.0 L m^{-2} h^{-1}
Filtration flux, 2nd module in the double-pass loop	15.7 L m^{-2} h^{-1}
Average cross-flow velocity	0.53 m s^{-1}
Overall pump efficiency	75%
Pressure loss over the membrane skid	0.2 bar
Additional pressure loss over the circulation line	0.2 bar
Energy consumption for pressurization*	0.12 kWh m^{-3} produced water
Energy consumption for circulation*	0.42 kWh m^{-3} produced water
Total energy consumption*	0.54 kWh m^{-3} produced water

*corrected calculation with the additional pressure losses over skids and circulation line; and for pump efficiencies of 75%.

In addition, sensitivity analyses were performed to investigate the effects of several design parameters on the full-scale process. For example, the energy consumption was significantly affected by the current feed water temperature Varying temperatures of 0.5, 5.73 and 18 °C resulted in an energy demand of 0.63, 0.54 and 0.4 kWh m^{-3} of produced water respectively. Given the fact that the defined average feed water temperature was 5.73 °C, the predicted average energy consumption would be 0.54 kWh m^{-3} of produced water for the proposed full-scale process at Görväln WTP.

4.6.2 CFD modelling approach for NF full-scale design

As a continuation of the CFD modelling, the performance of a three-stage full-scale NF plant configured with 7200 NF modules in a module ratio of 10-5-3 was compared to a 10:5:3:2 four-stage configuration (Table 16).

Table 16 The predicted performance of three stage vs. four-stage NF full-scale process based on CFD modelling. Table from Paper IV.

Full-scale NFplant	Stage No	Number of modules	TOC retention	UV_{254} retention	Water recovery
3-stage NF plant configuration	Stage 1	4000	80.9%	86.9%	50.3%
	Stage 2	2000	65.0%	75.3%	25.1%
	Stage 3	1200	22.7%	42.5%	15.1%
	Overall	**7200**	**66.8%**	**76.3%**	**90.5%**
4-stage NF plant configuration	Stage 1	3600	82.3%	88.0%	45.3%
	Stage 2	1800	71.8%	80.5%	22.6%
	Stage 3	1080	54.9%	67.8%	13.6%
	Stage 4	720	19.8%	40.9%	9.1%
	Overall	**7200**	**69.3%**	**78.4%**	**90.5%**

The NF process simulations were based on feed water containing 8.0 mg L^{-1} of TOC. Previous simulations of water flux distribution in membrane modules for operation under a double-pass loop mode showed that 1.5 m NF test modules in series could be operated at higher flux rates and produced better permeate quality. Therefore, a double-pass loop mode with an initial TMP of 2.42 bar at the inlet of the 1st membrane module for each stage and a cross flow velocity of 0.57 m s^{-1} were used as defined process configuration.

The predicted NOM removal rate for a three-stage NF plant (overall recovery rate of 90.5%, with each stage set to a recovery rate of 50.3%) was estimated to 66.8% (based on TOC) and 76.3% (based on UV_{254}). In contrast, a four-stage NF plant simulation indicated a slightly higher NOM removal of 69.3% (based on TOC) and 78.4% (based on UV_{254}) at the same overall recovery rate (90.5%), but with a single stage recovery of only 45.3%.

Moreover, the low recovery rate for each stage in the four-stage configuration resulted in a reduced recycle rate of the retentate of the 2nd module to the inlet of the 1st module (double-pass filtration at constant cross flow velocity of 0.57 m s^{-1}). This operation mode reduced the NOM concentration at the feed side and resulted in an increased NOM removal rate. For example, the TOC retention in module stage 1 of the three-stage NF plant (with a recycle rate of 4.75) was estimated to be 80.9%. In comparison, the estimated TOC retention obtained for module stage 1 of the four-stage NF plant (with a recycle rate of 3.7) was predicted to 82.3%.

More importantly, a lower recycle rate reduced energy consumption. Therefore, the four-stage full-scale NF plant (capacity: 110.000 m^3 day^{-1}; overall recovery rate of 90.5%) is predicted to achieve a higher NOM removal rate by using less energy, compared to the three-stage full-scale NF plant at the same recovery rate.

4.7 From pilot scale to two-stage UF full-scale plant

Based on the results and operational experiences of various UF pilot trials at Kvarnagården WTP, the water utility VIVAB decided to retrofit the existing facility with a two-stage UF membrane process combined with in-line coagulation. As for procurement, specific site requirements were defined in order to guarantee microbiological barrier function, enhanced NOM removal and plant capacity (Table 17).

Table 17 Specific site requirements for UF full-scale plant at Kvarnagården WTP.

Category	Unit	Requirement
Capacity	m^3 h^{-1} (net permeate flow rate)	1080
NOM removal rate	% (UV_{254})	≥ 50
Color (permeate)	mg Pt L^{-1}	≥ 5
Reduction of protozoa	log	≥ log 6 (*Pseudomonas diminuta*)
Reduction of virus	log	≥ log 4 (MS2 coliphages)
Recovery rate	%	≥ 99
Energy consumption	(kWh m^3 permeate production)	≤ 0.12

Furthermore, three scenarios for operational conditions with respect to raw water quality and coagulant dosing were specified, including (i) average raw water quality, (ii) worst raw water quality; and (iii) worst raw water quality without access to in-line coagulation (Table 18 and Table 19).

Table 18 Specification of raw water quality for UF full-scale plant at Kvarnagården WTP.

Parameters	Unit	Average quality	Worst quality
Temperature	°C	5.3 ± 0.5	6.5 ± 0.5
pH	(-)	7.6 ± 0.1	7.8 ± 0.2
Turbidity	(FTU)	0.4 ± 0.2	2.0 ± 0.5
Hardness	ºdH	1.8 ± 0.10	2.0 ± 0.15
Alkalinity	(mg HCO_3^- L^{-1})	22.0 ± 2.0	26.0 ± 3.0
COD	(mg O_2 L^{-1})	2.3 ± 0.1	4.4 ± 0,5
TOC	(mg C L^{-1})	2.9 ± 0.1	8.3 ± 0.5
DOC	(mg C L^{-1})	2.6 ± 0.1	8.1 ± 0.5
UV_{254}	(m^{-1})	9.58 ± 1.25	21.66 ± 2.0
Pt-Co	(mg Pt L^{-1})	14 ± 1.0	31.0 ± 5.8
Conductivity	(µS cm^{-1})	120 ± 6.0	130 ± 6.0
Iron	(mg Fe L^{-1})	0.054 ± 0.02	0.42 ± 0.1
Manganese	(mg Mn L^{-1})	0.036 ± 0.01	0.072 ± 0.01

Table 19 Defined scenarios for operational conditions ofUF full-scale plant at Kvarnagården WTP.

Definition	Plant capacity	Microbiological barrier function	NOM removal	Recovery rate
Scenario I: Average raw water quality	Design value	According to requirements	According to requirements	≥ 99%
Scenario II: Worst raw water quality	Design value	According to requirements	According to requirements	≥ 97.5%
Scenario III: Worst raw water quality without in-line coagulation step	75% of design value	According to requirements	No requirements	≥ 97.5%

During planning phase of the full-scale plant, the UF container pilot was used for validation of proposed full-scale process design in order to minimize investment cost by early detection of possible optimization potential. In this context, important findings were made:

- Coagulant dosing on the secondary UF stage was not required to achieved overall NOM removal.
- Hydraulic backwash of HF-UF membranes prior to starting of an air integrity test (AIT) was crucial; otherwise, membrane fouling caused by floc particles would have required intensive cleaning procedures.

Accordingly, the programming of the full-scale process was adjusted to avoid operational problems and costs due to fouling issues.

- Stopping coagulant dosing on the primary UF stage required an alteration to the UF primary plant settings (i.e. flux rate and filtration volume), otherwise the negative impact on membrane performance and fouling, would have resulted in extensive cleaning protocols for membrane recovery. As a result, the full-scale plant was upgraded to automatically change the UF primary settings when coagulation system is not operational.
- Online sensors for UV_{254} and turbidity were successfully used to control coagulant dosing and NOM removal by implementing a feed forward control strategy. Consequently, the applied control system for coagulant dosing of the UF full-scale plant is based on online measurements by UV/vis spectrophotometers. Depending on current raw water quality, coagulant dosing rates are calculated by feed forward loop (UV_{254} and turbidity in feed water) and a feedback signal (UV_{254} in permeate) in order to achieve required NOM removal.
- After two years of constructions, the two-stage UF full-scale plant was commissioned in November 2016. So far, rigorous quality and performance tests have confirmed that current UF plant operations are meeting the specified site requirements according to final process design (Table 20).

Table 20 Process design ofUF full-scale plant at Kvarnagården WTP.

Parameter	Unit	Primary UF	Secondary UF
Type of UF unit		XIGA-55 (Pentair)	Aquaflex-55 (Pentair)
UF unit total		4	2
Housings/unit		21	n.a.
Spare housings/unit		3	n.a.
Elements/ housing		4	n.a.
Elements/unit		84	17
Spare elements/unit		12	3
Elements total		336	34
Area per element	m^2	55	55
Area per unit	m^2	4 620 (+ 660)	935 (+ 165)
Total membrane area	m^2	18 480 (+ 2 640)	1 870 (+ 330)
Scenario I (average raw water quality)			
Gross flux	$L\ m^{-2}\ h^{-1}$	64.5	44
Net flux	$L\ m^{-2}\ h^{-1}$	58.5	36.5
Filtration volume/cycle	m^3	350	27
Scenario II (worst raw water quality)			
Gross flux	$L\ m^{-2}\ h^{-1}$	69.5	42
Filtration volume/cycle	m^3	190	17
Scenario III (worst raw water quality, no coagulation)			
Gross flux	$L\ m^{-2}\ h^{-1}$	56.5	57.6
Filtration volume/cycle	m^3	110	63

4.7.1 Adaptation and resilience of full-scale process design (Paper V)

As part of the UF full-scale design a surface water quality scenario analysis was performed to evaluate the potential effects of on-going climate change.

Since DOC concentrations have been rising in large parts of the boreal zone, with trends reported to be in the range 0.1 to 0.2 mg L^{-1} per year, the scenario analysis was based on an initial UV_{254} value of 9.4 m^{-1} (obtained from measurements of the operational laboratory at Kvarnagården WTP) and a UV removal level down to approximately 4 m^{-1} using a coagulant dose of 0.6 mg Al L^{-1}. Furthermore, it was assumed that the current character of DOC in the raw water sources from Lake Neden and the current groundwater well (i.e., SUVA) would not change over time, while a steady increase for DOC was defined with 0.05 mg L^{-1} per year in the surface water from Lake Neden. In comparison with other lakes in the geographical region (Valinia *et al.*, 2015), the relatively low annual increase was chosen to account for the potential breakdown of terrestrial TOC during the five-year turnover time. Besides the change of DOC, the effect of increasing ratios for the fraction of

groundwater to raw water (i.e., 20% and 25%, instead of the current 15% contribution) was studied. As shown in Figure 46, the defined scenarios resulted in a change for coagulant dosing rates. In order to guarantee the same drinking water quality (UF permeate) for the different scenarios, a constant rise in DOC over time from the current DOC of 3 mg L^{-1} (2015) to 4.25 (2040) would imply a significant increase of the required Al dose. According to the model, the coagulant dosing rate would reach its maximum removal capacity (1.6 mg L^{-1}) with the current ratio of groundwater (15%) to surface water (85%) in year 2031; resulting in a decrease of the drinking water quality due to limited DOC removal. In contrary, an increase of the groundwater fraction from 15% to 20% would postpone this eventuality to year 2040 and even beyond year 2040, if 25% of the mixed raw water could be obtained from the groundwater source. Additionally, one scenario defined the economic limit of coagulant dosing rate to approximately 0.95 mg Al L^{-1}.

In this scenario, the maximum dosing rate was reached in year 2025, leading to a deterioration of the UV_{254} in the drinking water from the current 4 m^{-1} to approximately 6.3 m^{-1} in year 2040.

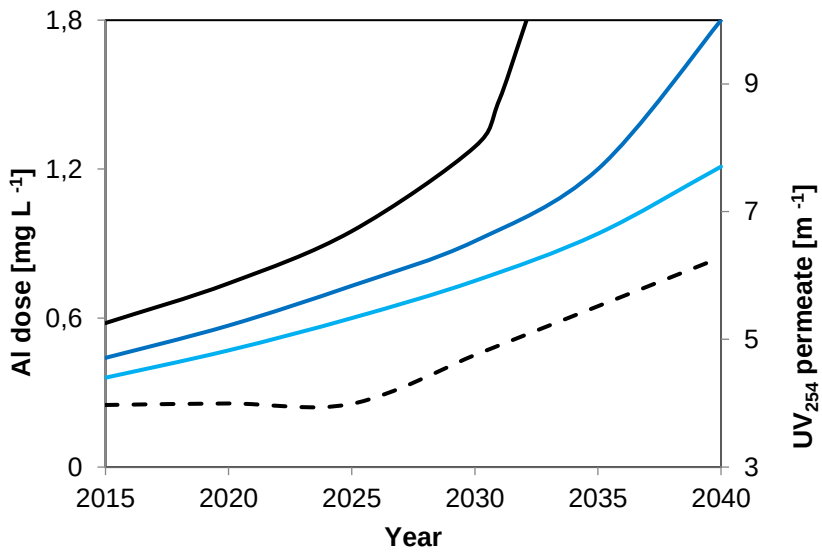

Figure 46 Predicted Al dose (left scale) as a function of time for current mixing conditions (15% groundwater (GW), 85% surface water, black line), optional (20% GW and 80% surface water, dark-blue line), and increased (25% GW and 75% surface water, light-blue line), assuming constant SUVA in both sources over time, but an increase of 0.05 mg DOC L^{-1} per year in the surface water (Lake Neden) over time. The black stippled line shows the predicted *UV* absorbance (right scale) in the UF permeate (UV_{254} permeate) from the retrofitted UF full-scale water treatment plant, if current mixing conditions were maintained and the maximum economically feasible dosing was assumed to be 0.95 mg Al L^{-1}. Figure from Paper V.

The specific scenario analysis clearly revealed that comparatively minor but reasonable changes in DOC over time owing to climate change or continuing recovery from acid rain would require future adaptations to the current process configuration. Consequently, an extended raw water monitoring is recommended in the future in order to obtain an early warning system for necessary operational adjustments at Kvarnagården WTP.

5. Conclusions, Limitations, and Future Perspectives

5.1 Conclusions

The results presented in this thesis show that ultra- and nanofiltration technology can be successfully applied to achieve selective NOM removal from drinking water either as a stand-alone process or as a technique to fulfill and enhance conventional treatment processes (e.g., coagulation, adsorption, and oxidation). Furthermore, membrane technology has great potential to replace and/or simplify conventional treatment chains of physicochemical and biological unit processes needed for compliance with stringent drinking water quality criteria in the future.

Predicted membrane retention for direct NF filtration of surface water from Lake Mälaren, calculated for a full-scale four-stage system with 90.2% recovery rate were on average 88–95 % for UV_{254}, 88–98 % for color (mg Pt L^{-1}), and between 80 and 92 % for TOC (mg C L^{-1}). In contrast, a hybrid membrane process applied for filtration of surface water from Lake Neden, achieved an average DOC retention rate of 30% (maximum UV retention rate: 78%, at 2.0 mg Al L^{-1} coagulant dosing rate). According to climate scenario analysis, UF combined with coagulation would be insufficient after year 2031 to meet drinking water quality standards for Kvarnagården WTP. Therefore, either an increase of the groundwater fraction to surface water is necessary or additional NF treatment would be required.

The key findings of the NF/UF pilot trials, process modelling, NOM characterizations, and membrane autopsies can be summarized in the following general conclusions.

- NOM characterization of various water samples from the existing treatment processes and the membrane pilots indicated a relationship between biopolymers and DOC. Biopolymers with larger molecular weight were removed proportionally by RSF and completely removed by the NF test module. In contrast, building blocks (BBs) could not be removed by RSF, but the proportional retention behavior by the NF test module was consistent with the specified MWCO of the membrane (500–700 Da).

- The overall removal rate across the NF/GAC pilot plants corresponded to 93% of incoming HS and 86% of incoming DOC. The GAC pilot filter that was fed with NF permeate showed limited retention behavior similar to the full-scale GAC (initial DOC removal rate of 72% decreased to 14% after two months of operation and stagnated).
- The NF/GAC pilot plant showed significant differences, with slower saturation rate and large changes in DOC character, compared to the current full-scale GAC filters at Görväln WTP. Therefore, this setup, should improve removal of emerging pollutants in the raw water resulting in enhanced chemical barrier function of the WTP.
- Direct NF filtration of surface water during long-term trials indicated stable membrane performance and high NOM removal average rates (UV_{254}: 91.6–94.7 %; TOC: 82–92.2 %). The NF membrane retention was highest for biopolymers (>95% removal), followed by HS (>80% removal). Due to molecular weights <500 Da, lower removal rates for building blocks (65–80 % removal) and low molecular weight substances (<60%) were achieved.
- Combined coagulation and ultrafiltration processes removed approximately 30% of the DOC, and 50% of the HS and biopolymers. However, BBs and LMW_{acids} remained unchanged compared with the NOM composition of the feed and permeate. These carbon fractions have the potential to cause regrowth in the distribution system, which in view of climate change, probably would have implications for the future adaptation and limitation of the process.
- Determination of source specific model parameters for prediction of NOM removal showed a good fit of experimental results based on the solution diffusion model. The validated model parameters allowed deducing of optimal operation conditions and predicting NOM removal efficiency of a hypothetical four-stage NF full-scale design.
- A two-dimensional axisymmetric CFD model of the NF test module was developed and calibrated with both experimental data and calculated source specific parameters (solution diffusion approach). The CFD model provided accurate prediction for NOM removal over a wide range of operating conditions, compared to results from the pilot trials. Consequently, this model was used to assist the design and evaluation of different full-scale HF-NF configurations for direct filtration of surface water.
- The membrane configuration is an important factor for the overall process performance. Based on CFD modelling, a four-stage full-scale NF process operated at 90.5% water recovery was found to remove 69.3% of TOC and

78.4% of UV_{254} from the feed water, which is superior to a typical three-stage full-size plant operated at the same overall recovery.

- Autopsy results of HF-NF membranes after twelve months of continuous pilot operation with pretreated feed water (coagulation and RSF), showed no substantial change of aged membranes from different module sections compared to virgin membranes. Only minimal changes in the Young's Modulus and the lumen surface contact angle were detected, with insignificant impact on the membrane's overall integrity and performance.
- Rigorous analysis of the nanomechanical properties of HF-UF membranes harvested after 12 to 14 months continuous pilot operation showed that the change detected in the nanomechanical characteristics did not considerable impact the macroscopic properties of the membranes.
- Quantitative Nanomechanical Mapping (QNM) revealed that the differences in operation conditions, feed water quality, and cleaning frequency for the primary and secondary UF-stage, played an important role in the change of nanomechanical properties of the test modules from the two-stage UF pilot plant.
- Detected foulant layers on HF-UF membranes displayed high roughness, adhesion forces, and dissipation (low elastic deformation), as well as variable modulus. However, the fouling layers of the membranes from the secondary UF-stage were rougher, less adhesive, and slightly stiffer compared to membranes from the primary UF-stage. This difference in characteristics could be explained by the feed water quality of the UF-stages.
- Fouling and chemical cleaning (CEBs) exerted different impacts on harvested HF-UF membranes during the pilot tests. The nanomechanical properties of the harvested UF membranes (secondary UF-stage) showed no adsorption of foulants and were only slightly affected compared to virgin membrane. Conversely, the properties of UF membranes (primary UF-stage) were highly impacted.
- For optimization of hybrid membrane processes, an automatic coagulant dosing system based on online measurement was successfully applied. Online sensor data were used to identify the current optimal aluminum coagulation conditions (0.5–0.7 mg L^{-1}) and the potential boundaries (0.9–1.2 mg L^{-1}) for efficient future (2040) NOM removal at Kvarnagården WTP.
- Comprehensive UF pilot trials resulted in important findings and consequent improvements of the two-stage full-scale UF facility during design phase and commissioning at Kvarnagården WTP.

5.2 Limitations of the study and future work

In view of the limited time frame for the GenoMembran-project, certain aspects of this thesis could not be completely covered due to time restrictions and lack of resources.

5.2.1 Membrane ageing

For example, the autopsy studies were performed on aged test modules after continuous operation of only 12 to 14 months. From a scientific perspective and operational view, it would have been desirable to conduct ageing studies after several years of pilot trials linked to longer periods of stress-testing, specific cleaning protocols, and operational strategies for enhanced membrane performance. In general, more environment-friendly cleaning/disinfection protocols are needed. However, even if at the current stage, the basic principles governing the key requirements for the most effective and the least harmful membrane cleaning/disinfection have been identified and are generally well-known, there is still a continuous need for investigation to elucidate the cleaning/disinfection mechanisms and incorporate them into qualitative and quantitative cleaning/disinfection models. Furthermore, it is essential for such cleaning studies to be conducted under conditions that mimic the industrial process and have sufficiently long run lengths (including repeated periods), to ensure the best match between findings from the research activities and the needs of industrial practitioners.

In particular, the water utility VIVAB is in need of further long-term assessments of membrane ageing for the two-stage UF full-scale plant at Kvarnagården WTP. This is because a specific membrane warranty for a 10-year time period has been issued by the membrane supplier. In this context, two definitions of ageing should be taken into account for future investigations of membrane filtration: membrane ageing and module ageing. In other words, restricting membrane ageing to polymer ageing only can be questioned. Indeed, the manufacturers guarantee the compatibility between detergent and polymer but in certain configurations the detergent also comes into contact with the often-sensitive glue and spacer materials (Bégoin *et al.*, 2006). More precisely, membrane ageing corresponds to the ageing of the materials which constitute the membrane. Furthermore, it depends on the operating conditions of both the production and cleaning/disinfection steps and results in a decrease of productivity, an increase in backwash or cleaning/disinfection step frequency, a modification of the physical-chemical properties of the membrane (elasticity/plasticity of the membrane, membrane surface zeta potential), an alteration of the membrane selectivity, and a loss of

integrity. While the definition of module ageing includes the integrity of all the elements constituting the membrane module, the potting zones in particular, have to be taken into account.

5.2.2 Impact of selected NOM removal on distribution networks

Despite comprehensive NOM characterization and evaluation of selective NOM removal for different membrane concepts, the impact of NF/UF permeate quality on microorganisms in the distribution network (i.e., regrowth potential related to biodegradable dissolved organic carbon: BDOC, loss of biofilm, etc.) has not been covered in this thesis due to time limitations. For example, the water utility VIVAB had concerns that the retrofitted hybrid membrane process (in-line coagulation combined with UF) could have a temporary impact on the biofilm of the distribution system due to enhanced NOM removal (e.g., release of biofilm or unfavorable biofilm function that might affect water quality and safety). Therefore, a full-scale study of the biofilm community and its function has been initiated at Lund University (Division of Applied Microbiology) in collaboration with VIVAB and Sweden Water Research. Briefly, biofilm studies, including DNA-based flow cytometry (FC), next generation sequencing (NGS), and quantitative PCR (qPCR), are used to obtain in-depth knowledge of the biofilm community from a long-term perspective (2016–2019), before and after commissioning of UF treatment combined with in-line coagulation.

5.2.3 Innovative control systems for membrane filtration

Although this thesis is based on results from fully automated container pilots, complete mimicking of full-scale operation is limited. Therefore, careful long-term evaluation of operational conditions and practical experience with upcoming full-scale plants are crucial for process validation and optimization. For example, commissioning procedures and trouble-shooting of recently built UF full-scale facilities in Sweden could give future guidelines on the operating conditions and productivity of proposed process design for water utilities in Scandinavia.

In addition, the implementation of self-adapting control systems for optimization of filtration processes would be of great interest for water utilities in the future. Therefore, new control systems for membrane filtration are necessary, combining the thinking patterns of a skilled operator, in-depth knowledge of energy-dissipation characteristics of pumps, and real-time data processing capabilities of SCADA systems.

5.2.4 Scenario analysis for climate change impact on water sources

As for adaption and resilience of membrane applications for NOM removal, more specific scenario analyses are necessary to assess the impact of climate change on raw water quality, the removal efficiency of different membrane types, and requirements for pre-treatment. In this context, the implementation of UV/vis spectrophotometers is highly recommended to obtain online fingerprints of NOM dynamics in raw water sources and for selective NOM removal in drinking water treatment. Moreover, this study has underlined the usefulness of optical sensors for online dosing of coagulants to control NOM removal and to optimize membrane performance. Nevertheless, more in-depth studies should be pursued in the future, focusing on strategic use and evaluation of UV measurements for online monitoring of NOM and for prediction of the potential for DBPs formation during drinking water treatment (Korshin, *et al.*, 2009; Li *et al.*, 2016).

5.2.5 Predictive NF modelling

Regarding NOM prediction, the established CFD model in this thesis is not suitable for assessment of long-term membrane fouling behavior. This is because the experimental set-up for the short-term trials neglected membrane fouling due to recurrent hydraulic backwashing cycles prior to each experiment. This limitation was caused by practical considerations (pre-programmed sequences for pilot plant operation) and time constraints.

The challenge for the future of NF modelling must be to gain further understanding of the fundamental phenomena occurring during the NF process, but also to develop accurate yet simplified models and design methodologies for concentrated multi-component feed streams that may be used by non-specialist scientists, engineers, and industrial practitioners.

5.2.6 New applications of NF/UF membranes

For NOM retention, based on the research trend, it can be seen that the integrated and hybrid processes of NF and UF in NOM removal applications will play more prominent roles in the future. Standalone NF/UF processes might not be able to produce water that meets the requirements, but after coupling them with other processes or membranes, the overall process should perform well. In addition, future work should focus on the development of "tailor-made" membranes for specific site requirements rather than standardized membrane solutions.

Due to their wide range of salt selectivity, as well as organic solute selectivity, NF membranes will continue to be explored for various other applications (e.g., removal of cyanotoxins and emerging pollutants such as pharmaceuticals, personal care products (PPCPs), perfluorinated compounds, and hormones). However, investigation of micro pollutant removal by NF test membranes was not the subject of this thesis. For example, the specific HFW1000 test membrane would most likely remove at least some of the larger hydrophilic micro pollutants such as microcystines and large PFCAs (perfluorodecanoate 513 Da) and PFOS (perfluorooctane sulfonic acid 500 Da). Other typically occurring, smaller compounds such as ketoprofene (pKa = 4.5, 250 Da), or danofloxazine (pKa = 6.0, 360 Da) might pass through the membrane. Consequently, future research studies at Görväln WTP will focus more specifically on the chemical barrier function of existing and innovative water treatment configurations. Therefore, in the future, the fate of a number of micro pollutants will be analyzed in order to evaluate the removal efficiency of NF and subsequent GAC filters.

Since the water resources are slowly depleting, NF/UF membranes are expected to be used more for water recycling and reuse. Studies have shown that water recycling will incur much less cost than for desalination (Harrison, *et al.*, 2007; AlTaee & Sharif, 2011; Liu, *et al.*, 2013; Ang, *et al.*, 2015). Nevertheless, in order to obtain sustainable NF/UF applications, energy integration from renewable resources would be necessary.

5.2.7 Fouling control and prevention

In this thesis, most of the fouling monitoring assessments were based on permeate flux rates. This approach involves time gaps because by the time obvious fouling is observed, the fouling is already fully established. Consequently, fouling mitigation and control strategies require more extensive research to develop fouling mitigation plans that cover from the start to the end of the membrane process. Therefore, early fouling detection strategies could play an important role in preventing the problem of membrane fouling. Once the membrane process is started, some mitigation strategies could be taken to reduce the fouling propensity of the process. For example, several approaches have been attempted to reduce the adverse effects of concentration polarization on membrane fouling, including the use of pulsating flow induced by pulse pumps or valve sequences (Najarian & Bellhouse, 1996), air sparging (Cui, *et al.*, 2003), intermittent jets and use of novel type spacers (Schwinge *et al.*, 2004), flow reversals (Hargrove, *et al.*, 2003), and low frequency ultrasonic irradiation (Patel & Nath, 2013).

From previous studies, it can be seen that rejection of solutes may change due to different types of fouling mechanisms (Fane & Beatson, 2000; Wang *et al.*, 2005)

Hence, modelling for solute rejection could provide valuable prediction for the mechanisms involved in fouling. Probably, future studies combining early detection methods of retention changes with standard fouling monitoring, could give a better perspective on fouling and rejection mechanisms for NF/UF membranes.

References

Abdullah, S.Z., Berube, P.R., 2013. Assessing the effects of sodium hypochlorite exposure on the characteristics of PVDF based membranes. Water Res. 47, 5392–5399.

Adamcik, J., Berquand, A., Mezzenga, R., 2011. Single-step direct measurement of amyloid fibrils stiffness by peak force quantitative nanomechanical atomic force microscopy, Appl. Phys. Lett. 98, 3701.

Al-Amoudi, A., Lovitt, R.W., 2007. Fouling strategies and the cleaning system of NF membranes and factors affecting cleaning efficiency. J. Membr. Sci. 303, 4–28.

Allpike, B.P., Heitz, A., Joll, C.A., Kagi, R.I., 2007. A new organic carbon detector for size exclusion chromatography. J. Chromatogr. A 1157, 472–476.

AlTaee, A., Sharif, A.O., 2011. Alternative design to dual stage NF seawater desalination using high rejection brackish water membranes, Desalination 273, 391–397.

Amy, G., 2008. Fundamental understanding of organic matter fouling of membranes. Desalination 231, 44–51.

Ang, W, Mohammad, A, Hilal, N, Leo, C., 2015. A review on the applicability of integrated/hybrid membrane processes in water treatment and desalination plants. Desalination 363, 2–18.

Arkhangelsky, E., Kuzmenko, D., Gitis, V., 2007. Impact of chemical cleaning on properties and functioning of polyethersulfone membranes. J. Membr. Sci. 305, 176–184.

Bandini, S., Vezzani, D., 2003. Nanofiltration modeling: the role of dielectric exclusion in membrane characterization, Chemical engineering science 58, 3303–3326.

Barbot, E., Moustier, S., Bottero, J., Moulin, P., 2008. Coagulation and ultrafiltration: understanding of the key parameters of the hybrid process. J. Membr. Sci. 325, 520–527.

Barron, P.F., Wilson, M.A., 1981. Humic soil and coal structure study with magic-angle spinning ^{13}C CP NMR. Nature 289, 275–276.

Bégoin, L., Rabiller-Baudry, M., Chaufer, B., Hautbois,M.-C., Doneva, T., 2006. Ageing of PES industrial spiral-wound membranes in acid whey ultrafiltration. Desalination 192, 25–39.

Blankert, B., Betlem, B., Roffel, B., 2007. Development of a control system for in-line coagulation in an ultrafiltration process. J. Membr. Sci. 301, 39–45.

Blodau, C., Bauer, M., Regenspurg, S., Macalady, D., 2009. Electron accepting capacity of dissolved organic matter as determined by reaction with metallic zinc. Chem. Geol. 260, 186–195.

Bowen, W.R., Doneva, T.A., 2000. Atomic force microscopy characterisation of ultrafiltration membranes: correspondence between surface pore dimensions and molecular weight cut-off. Surf. Interface Anal. 29, 544–547.

Bowen, W.R., Mohammad, A.W., Hilal, N., 1997. Characterisation of nanofiltration membranes for predictive purposes–use of salts, uncharged solutes and atomic force microscopy, Journal of Membrane Science, 126, 91–105.

Bowen, W.R., Mukhtar, H., 1996. Characterisation and prediction of separation performance of nanofiltration membranes, Journal of Membrane Science, 112, 263–274.

Bowen, W.R., Welfoot, J.S., Williams, P.M., 2002. Linearized transport model for nanofiltration: development and assessment, AIChE journal, 48, 760–773.

Butt, H.J., Cappella, B., Kappl, M., 2005. Force measurements with the atomic force microscope: Technique, interpretation and applications. Surf. Sci. Rep., 59, 1–152.

Carroll, T., King, S., Gray, S., Bolto, B., Booker, N., 2000. The fouling of microfiltration membranes by NOM after coagulation treatment. Water Research 34, 2861–2868. doi:10.1016/S0043-1354(00)00051-8

Causserand, C., Rouaix, S. Lafaille, J-P., Aimar, P., (2008). Ageing of polysulfone membranes in contact with bleach solution: Role of radical oxidation and of some dissolved metal ions. Chem. Eng. Process. 47, 48–56.

Chae, S-R., Yamamura, H., Ikeda, K., Watanabe, Y.,2008. Comparison of fouling characteristics of two different polyvinylidene fluoride microfiltration membranes in a pilot-scale drinking water treatment system using precoagulation/sedimentation, sand filtration, and chlorination, Wat. Res. 42, 2029–2042.

Chen, C., Zhang, X., He, W., Lu, W., Han, H., 2007. Comparison of seven kinds of drinking water treatment processes to enhance organic material removal: a pilot test. Sci. Total Environ. 382, 93–102.

Chen, C., Zhang, X., Zhu, L., Liu, J., He, W., Han, H., 2008. Disinfection by-products and their precursors in a water treatment plant in North China: seasonal changes and fraction analysis. Sci. Total Environ. 397, 140–147.

Chen, Y., Dong, B. Z., Gao, N. Y., Fan, J. C., 2007. Effect of coagulation pretreatment on fouling of an ultrafiltration membrane. Desalination 204(1-3), 181–188. doi:10.1016/j.desal.2006.04.029

Chin, Y., Aiken, G., O´Loughlin, E., 1994. Molecular weight, polydispersity, and spectroscopic properties of aquatic humic substances. Environ. Sci. Technol. 28, 1853–1858.

Cho, M.-H., Lee, C.-H., Lee, S., 2006. Effect of flocculation conditions on membrane permeability in coagulation-microfiltration. Desalination 191, 386–396.

Choi, K. Y., Dempsey, B. A., 2004. In-line coagulation with low-pressure membrane filtration. Water Research 38, 4271–4281. doi:10.1016/j.watres.2004.08.006

Chow, C.W.K., Kuntke, P., Fabris, R., Drikas, M., 2009a. Organic characterisation tools for distribution system management. Water Sci. Technol. 9 (1), 1–8.

Chow, C.W.K., von Leeuwen, J.A., Fabris, R., Drikas, M., 2009b. Optimised coagulation using aluminium sulfate for the removal of dissolved organic carbon. Desalination 245, 120–134.

Combe, C., Molis, E., Lucas, P., Riley, R. & Clark, M., 1999 The effect of CA membrane properties on adsorptive fouling by humic acid. J. Membr. Sci. 154, 73–87.

Completo, C., Semiao, V., Geraldes, V., 2016. Efficient CFD-based method for designing cross-flow nanofiltration small devices, Journal of Membrane Science, 500, 190–202.

Cooper, W.J., Song, W., Kalnina, D., Gonsior, M., Mezyk, S.P., Peake, B.M., 2008. Recent advances in structure and reactivity of dissolved organic matter in natural waters. Water Sci. Technol. 8 (6), 615–623.

Cortés-Juan, F., Balannec, B., Renouard, T., 2011. CFD-assisted design improvement of a bench-scale nanofiltration cell, Separation and purification technology, 82, 177–184.

Cory, R., McKnight, D., 2005. Fluorescence spectroscopy reveals ubiquitous presence of oxidized and reduced quinones in dissolved organic matter. Environ. Sci. Technol. 39, 8142–8149.

Cui, Z.F., Chang, S., Fane, A.G., 2003. The use of gas bubbling to enhance membrane processes. J. Membr. Sci. 221, 1–35.

Culea, M., Cozar, O., Ristoiu, D., 2006. Methods validation for the determination of trihalomethanes in drinking water. J. Mass Spectrom. 41, 1594–1597.

De Grooth, J., 2015. A Tale of Two Charges: Zwitterionic Polyelectrolyte Multilayer Membranes., Ph.D. Thesis, Twente University, Twente.

de la Rubia, Á., Rodríguez, M., León, V.M., Prats, D., 2008. Removal of natural organic matter and THM formation potential by ultra- and nanofiltration of surface water. Water Res. 42, 714–722.

Delpla, I., Jung, A.-V., Baures, E., Clement, M., Thomas, O., 2009. Impacts of climate change on surface water quality in relation to drinking water production. Environ. Int. 35, 1225–1233.

Déon, S., Dutournié, P., Bourseau, P., 2007. Transfer of monovalent salts through nanofiltration membranes: A model combining transport through pores and the polarization layer, Industrial & Engineering Chemistry Research, 46, 6752–6761.

Derjaguin, B.V., Muller, V.M., Toporov, Y.U.P, 1975. Effect of contact deformations on the adhesion of particles. J. Colloid Interface Sci. 53.

Deshmukh, A.P., Pacheco, C., Hay, M.B., Myneni, S.C.B., 2007. Structural environments of carboxyl groups in natural organic molecules from terrestrial systems. Part 2: 2D NMR spectroscopy. Geochim. Cosmochim. Acta 71, 3533–3544.

Dietz, P., Hansma, P.K., Inacker, O., Lehmann, H.-D., Herrmann, K.-H., 1992. Surface pore structures of micro- and ultrafiltration membranes imaged with the atomic force microscope. J. Membr. Sci. 65, 101–111.

Eikebrokk, B., Vogt, R., Liltved, H., 2004. NOM increase in Northern European source waters: Discussion of possible causes and impacts on coagulation/contact filtration processes. Water Sci. Technol. Water Supply 4, 47–54.

Ericsson, B., Trägårdh, G., 1997. Treatment of surface water rich in humus – membrane filtration vs. conventional treatment. Desalination 108, 117–128.

Ericsson, P., Hajdu, S., Willén, E., 1984. Vattenkvaliteten i Görväln. En dynamisk Mälarfjärd. Vattenkemi och växtplankton i ett fyrtioårigt perspektiv. Vatten 40, 193–211 (In Swedish).

Evans, C.D., Monteith, D.T., Cooper, D.M., 2005. Long-term increases in surface water dissolved organic carbon: Observations, possible causes and environmental impacts. Environ. Pollut. 137, 55–71.

Fabris, R., Chow, C.W.K., Drikas, M., Eikebrokk, B., 2008. Comparison of NOM character in selected Australian and Norwegian drinking waters. Water Res. 42, 4188–4196.

Fan, L., Harris, J.L., Roddick, F.A., Booker, N.A., 2001. Influence of the characteristics of natural organic matter on the fouling of microfiltration membranes. Water Res. 35, 4455–4463.

Fane, A.G., Beatson, P., Li, H, 2000. Membrane fouling and its control in environmental applications. Water Sci. Technol. 41, 303–308.

Filloux, E., Gallard, H., Croué, J.-P., 2012. Identification of effluent organic matter fractions responsible for low-pressure membrane fouling. Water Res. 46, 5531–5540.

Finstad, A., Blumentrath, S., Tømmervik, H., Andersen, T., Larsen, S., Tominaga, K., Hessen, D., De Wit, H., 2016. From greening to browning: Catchment vegetation development and reduced S-deposition promote organic carbon load on decadal time scales in Nordic lakes. Sci. Rep. 6, 1–8, doi:10.1038/srep31944

Forsberg, C., Petersen, R., Jr., 1990. A darkening of Swedish lakes due to increased humus inputs during the last 15 years. Verhandlungen des Internationalen Verein Limnologie 24, 289–292.

Foster, B., 2012. New atomic force microscopy (AFM) approaches life sciences gently, quantitatively, and correlatively, Am. Lab. 44, 24–28.

Fritzsche, A.K., Arevalo, A.R., Moore, M.D., Elings, V., Kjoller, K., Wu, C.M., 1992. The surface structure and morphology of polyvinylidene fluoride microfiltration membranes by atomic force microscopy. J. Membr. Sci. 68, 65–78.

Fritzsche, A.K., Arevalo, A.R., Moore, M.D., Elings, V., O'Hara, C., 1993. The surface structure and morphology of polyacrylonitrile membranes by atomic force microscopy. J. Membr. Sci. 81, 109–120.

Fukano, K., Komiya, K., Sasaki, H., Hashimoto, T., 1978. Evaluation of new supports for high-pressure aqueous gel permeation chromatography: TSK-gel SW type columns. J. Chromatogr. 166, 47–54.

Futselaar, H., Schonewille, H., Meer, W.V.D, 2002. Direct filtration nanofiltration – A new high-grade purification concept. Desalination 145, 75–80.

Gaudichet-Maurin, E., Thominette, F., 2006. Ageing of polysulfone ultrafiltration membranes in contact with bleach solutions. J. Membr. Sci. 282, 198–204.

Geraldes, V.T., Semião, V., de Pinho, M.N., 2001. Flow and mass transfer modelling of nanofiltration, Journal of Membrane Science, 191, 109–128.

Gjessing, E.T., Steiro, C., Becher, G., Christy, A., 2007. Reduced analytical availability of polychlorinated biphenyls (PCB's) in coloured surface water. Chemosphere 66, 644–649.

Greenwood, P.F., Berwick, L.J., Croué, J.-P., 2012. Molecular characterisation of the dissolved organic matter of wastewater effluents by MSSV pyrolysis GC–MS and search for source markers. Chemosphere 87, 504–512.

Gross, R.J., Osterle, J., 1968. Membrane transport characteristics of ultrafine capillaries, The Journal of chemical physics, 49, 228–234.

Hargrove, S.C., Parthasarathy, H., Ilias, S., 2003. Flux enhancement in cross-flow membrane filtration by flow reversal: a case study on ultrafiltration of BSA. Sep. Purif. Technol. 38, 3133–3144.

Harrison, C, Le Gouellec, Y., Cheng, R., Childress, A., 2007. Bench-scale testing of nanofiltration for seawater desalination. J. Environ. Eng. 133, 1004–1014.

Her, N., Amy, G., Chung, J., Yoon, J., Yoon, Y., 2008. Characterizing dissolved organic matter and evaluating associated nanofiltration membrane fouling. Chemosphere 70, 495–502.

Hines, A.L., Maddox, R.N, 1985. Mass transfer: fundamentals and applications, Prentice-Hall Englewood Cliffs, NJ.

Hoek, E.M.,Elimelech, M., 2003. Cake-enhanced concentration polarization: A new fouling mechanism for salt-rejecting membranes. Environ. Sci. Technol. 37, 5581–5588.

Homaeigohar, S., Koll, J., Lilleodden, E.T., Elbahri, M., 2012. The solvent induced interfiber adhesion and its influence on the mechanical and filtration properties of polyethersulfone electrospun nanofibrous microfiltration membranes. Sep. Purif. Technol. 98, 456–463.

Huber, S.A., Balz, A., Abert, M., Pronk, W., 2011. Characterisation of aquatic humic and non-humic matter with size-exclusion chromatography–organic carbon detection–organic nitrogen detection (LC-OCD-OND). Water Res. 45, 879–885.

Jacangelo, J., DeMarco, J., Owen, D., Randtke, S., 1995. Selected processes for removing NOM: An overview. J. Am. Water Works Assoc. 87, 64–77.

Jacangelo, J.G., Rhodes Trussell, R., Watson, 1997. M. Role of membrane technology in drinking water treatment in the United States. Desalination 113, 119–127.

James, B.J., Jing, Y., Dong Chen, X., 2003. Membrane fouling during filtration of milk-a microstructural study. J. Food Eng. 60, 431–437.

Jermann, D., Pronk, W., Meylan, S., Boller, M., 2007. Interplay of different NOM fouling mechanisms during ultrafiltration for drinking water production. Water Res. 41, 1713–1722.

Jones, K., O'Melia, C., 2000. Protein and humic acid adsorption onto hydrophilic membrane surface: effects of pH and ionic strength. J. Membr. Sci. 165, 31–46.

Jung, B., Yoon, J.K., Kim, B., Rhee, H.-W., 2004. Effect of molecular weight of polymeric additives on formation, permeation properties and hypochlorite treatment of asymmetric polyacrylonitrile membranes. J. Membr. Sci. 243, 45–57.

Jung, C.-W., Kang, L.-S., 2003. Application of combined coagulation-ultrafiltration membrane process for water treatment. Korean J. Chem. Eng. 20, 855–861.

Kabsch-Korbutowicz, M., 2005. Effect of Al coagulant type on natural organic matter removal efficiency in coagulation/ultrafiltration process. Desalination 185 (Desalination and the Environment), 327–333. doi:10.1016/j.desal.2005.02.083

Kanokkantapong, V., Marhaba, T.F., Pavasant, P., Panyapinyophol, B., 2006. Characterization of haloacetic acid precursors in source water. J. Environ. Manage. 80, 214–221.

Kataoka, T, Tsuru, T., Nakao, S.I., Kimura, S., 1991. Permeation equations developed for prediction of membrane performance in pervaporation, vapour permeation and reverse osmosis based solution-diffusion model. J. Chem. Eng. Jpn. 24, 326.

Kedem, O. & Katchalsky, A., 1963. Permeability of composite membranes. Part 1. – Electric current, volume flow and flow of solute through membranes. Transactions of the Faraday Society. 59, 1918, ISSN: 00147672.

Kennedy, M.D., Kamanyi, J., Heijman, B.G.J., Amy, G., 2008. Colloidal organic matter fouling of UF membranes: role of NOM composition & size. Desalination 220, 200–213.

Keucken, A., Donose, B.-C., Persson, K.-M., 2012. Membrane fouling revealed by advanced autopsy. In Proceedings of the 8th Nordic Drinking Water Conference, Stockholm, Sweden, 18–20 June 2012.

Keucken, A., Ericsson, P., Persson, K.M., Dekker, R., Köhler, S.J., 2014. Evaluation of Color Removal Package (CPR) for drinking water based on novel hollow fiber nanofiltration. Proceedings of the 9th Nordic Drinking Water Conference (NORDIWA), Helsinki, Finland.

Keucken, A., Heinicke, H., 2011. NOM characterization and removal by water treatment processes for drinking water and ultra pure process water. In Proceedings of the 4th IWA Speciality Conference on Natural Organic Matter, Costa Mesa, CA, USA, 27–29 July 2011.

Khan, M.T., de O Manes, C.-L., Aubry, C., Gutierrez, L., Croue, J.-P., 2013. Kinetic study of seawater reverse osmosis membrane fouling. Environ. Sci. Technol. 47 10884–10894.

Khayet, M., Matsuura, T., 2003. Determination of surface and bulk pore sizes of flat-sheet and hollow-fiber membranes by atomic force microscopy, gas permeation and solute transport methods. Desalination 158, 57–64.

Kim, J.Y., Lee, H.K., Kim, S.C., 1999. Surface structure and phase separation mechanism of polysulfone membranes by atomic force microscopy. J. Membr. Sci. 163, 159–166.

Kim, M.H., Yu, M.J., 2005. Characterization of NOM in the Han River and evaluation of treatability using UF-NF membrane. Environ. Res. 97, 116–123.

Köhler, S.J., Buffam, I., Seibert, J., Bishop, K.H., Laudon, H., 2009. Dynamics of stream water TOC concentrations in a boreal headwater catchment: Controlling factors and implications for climate scenarios. J. Hydrol. 373, 44–56.

Köhler, S.J., Kothawala, D., Futter, M.N., Liungman, O., Tranvik, L., 2013. In-Lake Processes Offset Increased Terrestrial Inputs of Dissolved Organic Carbon and Color to Lakes. PLoS ONE 8, 1–12.

Köhler, S.J., Lavonen, E.E., Keucken, A., Schmitt-Kopplin, P., Spanjer, T., Persson, K.M., 2016. Upgrading coagulation with hollow-fibre nanofiltration for improved organic matter removal during surface water treatment. Water Res. 89, 232–240.

Kong, F.X., Yang, H.W., Wang, X.M., Xie, Y.F., 2016. Assessment of the hindered transport model in predicting the rejection of trace organic compounds by nanofiltration. J. Membr. Sci. 498, 57–66.

Konieczny, K., Sakol, D., Plonka, J., Rajca, M., Bodzek, M., 2009. Coagulation-ultrafiltration system for river water treatment. Desalination 240, 151–159.

Korshin, G., Chow, C. W., Fabris, R., Drikas, M., 2009. Absorbance spectroscopy-based examination of effects of coagulation on the reactivity of fractions of natural organic matter with varying apparent molecular weights. Water Res., 43, 1541–1548. doi:10.1016/j.watres.2008.12.041

Koyuncu, I., Brant, J., Lüttge, A., Wiesner, M.R., 2006. A comparison of vertical scanning interferometry (VSI) and atomic force microscopy (AFM) for characterizing membrane surface topography. J. Membr. Sci. 278, 410–417.

Laborda, F., Ruiz-Beguería, S., Bolea, E., Castillo, J.R., 2009. Functional speciation of metal-dissolved organic matter complexes by size exclusion chromatography coupled to inductively coupled plasma mass spectrometry and deconvolution analysis. Spectrochim. Acta B 392, 392–398.

Lankes, U., Lüdemann, H.D., Frimmel, F.H., 2008. Search for basic relationships between "molecular size" and "chemical structure" of aquatic natural organic matter - answers from ^{13}C and ^{15}N CPMAS NMR spectroscopy. Water Res. 42, 1051–1060.

Laurell, P., Sivonen, K., Poutanen, H., Vuoriletho, V.-P., Hesampour, M., Kettunen, V., Tuutijärvi, T., Vahala, R., 2015. Applicability of loose nanofiltration membranes for the removal of natural organic matter from soft surface water. In Proceedings of the 6th IWA Specialist Conference on Natural Organic Matter in Water, Malmö, Sweden, 7–10 September 2015.

Lavonen, E.E., Gonsior, M., Tranvik, L.J., Schmitt-Kopplin, P., Köhler, S.J., 2013. Selective Chlorination of Natural Organic Matter: Identification of Previously Unknown Disinfection Byproducts. Environ. Sci. Technol. 47, 2264−2271, doi:10.1021/es304669p.

Lavonen, E.E., Kothawala, D.N., Tranvik, L.J., Gonsior, M., Schmitt-Kopplin, P., Köhler, S.J., 2015. Tracking changes in the optical properties and molecular composition of dissolved organic matter during drinking water production. Water Res. 85, 286–294.

Lebeau, T., Lelièvre, C., Buisson, H., van der Venter, L. W., Côté, P., 1998. Immersed membrane filtration for the production of drinking water: combination with PAC for NOM and SOCs removal, Desalination, 117, 219–231.

Lee, H., Amy, G., Cho, J., Yoon, Y., Moon, S.-H., Kim, I. S., 2001. Cleaning strategies for flux recovery of an ultrafiltration membrane fouled by natural organic matter. Wat. Res. 35, 3301–3308.

Lee, N., Amy, G., Croué, J.-P., 2006. Low-pressure membrane (MF/UF) fouling associated with allochthonous versus autochthonous natural organic matter. Water Res. 40, 2357–2368.

Lee, N., Amy, G., Croué, J.-P., Buisson, H., 2004. Identification and understanding of fouling in low-pressure membrane (MF/UF) filtration by natural organic matter (NOM). Wat. Res. 38, 4511–4523.

Levenstein, R., Hasson, D., Semiat, R., 1996. Utilization of the Donnan effect for improving electrolyte separation with nanofiltration membranes, Journal of Membrane Science, 116, 77–92.

Li, W.-T., Jin, J., Li, Q., Wu, C.-F., Lu, H., Zhou, Q., Li, A.-M., 2016. Developing LED UV fluorescence sensors for online monitoring DOM and predicting DBPs formation potential during water treatment. Wat. Res. 93, 1–9, doi: 10.1016/j.watres.2016.01.005.

Li, Y., Wang, J., Zhang, W., Zhang, X., Chen, C., 2011. Effects of coagulation on submerged ultrafiltration membrane fouling caused by particles and natural organic matter (NOM). Chinese Science Bulletin 56(6), 584–590, doi:10.1007/s11434-010-4296-8.

Lian, B., Wang, Y., Le-Clech, P., Chen, V., Leslie, G., 2016. A numerical approach to module design for crossflow vacuum membrane distillation systems, Journal of Membrane Science, 510, 489–496.

Liang, Y.Y, Chapman, M.B., Fimbres Weihs, G.A., Wiley, D.E., 2014. CFD modelling of electro-osmotic permeate flux enhancement on the feed side of a membrane module, Journal of Membrane Science, 470, 378–388.

Liang, Y.Y, Fimbres Weihs. G.A., Setiawan, R, Wiley, D.E., 2016. CFD modelling of unsteady electro-osmotic permeate flux enhancement in membrane systems, Chemical Engineering Science, 146, 189–198.

Lidén, A., Keucken, A., Persson, K.M., 2017. Uses of fluorescence excitation-emissions indices in predicting water efficiency. J. Water Proc. Eng. 16, 249–257.

Lidén, A., Persson, K.M., 2015. Comparison between ultrafiltration and nanofiltration hollow-fiber membranes for removal of natural organic matter–A pilot study. J. Water Supply Res. Technol. AQUA 65 (1), 43–53. doi:10.2166/aqua.2015.065.

Lin, C. F., Lin, T. Y., Hao, O. J., 2000. Effects of humic substance characteristics on UF performance. Water Res. 34 (4), 1097–1106.

Liu, J., Yuan, J., Xie, L., Ji, Z., 2013. Exergy analysis of dual-stage nanofiltration seawater desalination, Energy 62, 248–254.

Liu, S., Lim, M., Fabris, R., Chow, C., Chiang, K., Drikas, M., Amal, R., 2008. Removal of humic acid using TiO2 photocatalytic process – fractionation and molecular weight characterisation studies. Chemosphere 72, 263–271.

Loi-Brugger, A., Panglisch, S., Buchta, P., Hattori, K., Yonekawa, H., Tomita, Y., Gimbel, R., 2006. Ceramic membranes for direct river water treatment applying coagulation and microfiltration. Water Sci. Technol. Water Supply 6, 89–98.

Maartens, A., Swart, P., Jacobs, E., 1999. Feed-water pretreatment: Methods to reduce membrane fouling by natural organic matter. Journal of Membrane Science 163, 51–62. doi:10.1016/S0376-7388(99)00155-6

Mao, J., Cory, R.M., McKnight, D.M., Schmidt-Rohr, K., 2007a. Characterization of a nitrogen-rich fulvic acid and its precursor algae from solid state NMR. Org. Geochem. 38, 1277–1292.

Mao, J., Tremblay, L., Gagné, J.-P., Kohl, S., Rice, J., Schmidt-Rohr, K., 2007b. Humic acids from particulate organic matter in the Saguenay Fjord and St. Lawrence Estuary investigated by advanced solid-state NMR. Geochim. Cosmochim. Acta 71, 5483–5499.

Matilainen, A., Gjessing, E.T., Lahtinen, T., Hed, L., Bhatnagar, A., Sillanpää, M., 2011. An overview of the methods used in the characterisation of natural organic matter (NOM) in relation to drinking water treatment. Chemosphere 83, 1431–1442.

Matilainen, A., Iivari, P., Sallanko, J., Heiska, E., Tuhkanen, T., 2006. The role of ozonation and activated carbon filtration in the natural organic matter removal from drinking water. Environ. Technol. 27, 1171–1180.

Matilainen, A., Sillanpää, M., 2010. Removal of organic matter from drinking water by advanced oxidation processes: A review. Chemosphere 80, 351–365.

Merle, T., Dramas, L., Gutierrez, L., Garcia-Molina, V., Croué, J.-P., 2016. Investigation of severe UF membrane fouling induced by three marine algal species. Water Res. 93, 10–19.

Metsamuuronen, S., Sillanpaa, M., Bhatnagar, A., Manttari, M., 2014. Natural organic matter removal from drinking water by membrane technology. Sep. Purif. Rev. 43 (1), 1–61.

Meylan, S., Hammes, F., Traber, J., Salhi, E., von Gunten, U., Pronk, W., 2007. Permeability of low molecular weight organics through nanofiltration membranes. Water Res. 41 (17), 3968–3976.

Meyn, T., Bahn, A., Leiknes, T., 2008. Significance of flocculation for NOM removal by coagulation-ceramic membrane microfiltration. Water Sci. Technol. Water Supply 8, 691–700.

Muñoz-Aguado, M.J., Wiley, D.E., Fane, A.G., 1996. Enzymatic and detergent cleaning of a polysulfone ultrafiltration membrane fouled with BSA and whey. J. Membr. Sci.117, 175–187.

Nagy, E., Kulcsár, E., Nagy, A., 2011. Membrane mass transport by nanofiltration: Coupled effect of the polarization and membrane layers. J. Membr. Sci. 368, 215–222.

Najarian, S., Bellhouse, B.J., 1996. Effect of liquid pulsation on protein fractionation using ultrafiltration processes. J. Membr. Sci. 114, 245–253.

Ohno, T., Bro, R., 2006. Dissolved organic matter characterization using multiway spectral decomposition of fluorescence landscapes. Soil Sci. Soc. Am. J. 70, 2028–2037. doi:10.2136/sssaj2006.0005

Pakzad, A., Simonsen, J., Yassar, R.S., 2012. Gradient of nanomechanical properties in the interphase of cellulose nanocrystal composites. Compos. Sci. Technol. 72, 314–319.

Park, J.-H., 2009. Spectroscopic characterization of dissolved organic matter and its interactions with metals in surface waters using size exclusion chromatography. Chemosphere 77, 485–494.

Park, N., Cho, J., 2008. Natural organic matter diffusivity for transport characterizations in nanofiltration and ultrafiltration membranes. J. Membr. Sci. 315, 133–140.

Parlanti, E., Woerz, K., Geoffroy, L., Lamotte, M., 2000. Dissolved organic matter fluorescence spectroscopy as a tool to estimate biological activity in a coastal zone submitted to anthropogenic inputs. Org. Geochem. 31, 1765–1781.

Patel, T.M., Nath, K., 2013. Alleviation of flux decline in cross flow nanofiltration of twocomponent dye and saltmixture by low frequency ultrasonic irradiation. Desalination 317, 132–141.

Paugam, L., Delaunay, D., Diagne, N.W., Rabiller-Baudry, M., 2013. Cleaning of skim milk PES ultrafiltration membrane: on the real effect of nitric acid step. J. Membr. Sci. 428, 275–280.

Paugam, L., Rabiller-Baudry, M., Delaunay, D., 2006. Physico-chemical effect of simple alkaline and acid solutions in cleaning sequences of spiral ultrafiltration membranes fouled by skim milk. Desalination 200, 192–194.

Platt, S., Nystrom, M., 2007. Cleaning of membranes fouled by proteins to evaluate the importance of fully developed flow. Desalination 208, 19–33.

Plottu, A., Houssais, B., Democrate, C., Gatel, D., Cavard, J., 2003. Autopsies of membranes fouled on Mery-sur-Oise pilot units: many lessons for the behavior of the water treatment plant. Desalination 157(1–3):367. doi:10.1016/S0011-9164(03)00418-1

Porcelli, N., Judd, S., 2010. Chemical cleaning of potable water membranes: a review. Sep. Purif. Technol. 71, 137–143.

Powell, L.C., Hilal, N., Wright, C.J., 2017. Atomic force microscopy study of the biofouling and mechanical properties of virgin and industrially fouled reverse osmosis membranes. Desalination 404, 313–321.

Qin, J.-J., Wong, F.-S., Li, Y., Liu, Y.-T., 2003. A high flux ultrafiltration membrane spun from PSU/PVP (K90)/DMF/1,2-propanediol. J.Membr. Sci. 211, 139–147.

Reemtsma, T., 2009. Determination of molecular formulas of natural organic matter molecules by (ultra-) high-resolution mass spectrometry – status and needs. J. Chromatogr. A 1216, 3687–3701.

Regula, C., Carretier, E., Wyart, Y., Gesan-Guiziou, G., Vincent, A., Boudot, D., Moulin, P., 2014. Chemical cleaning/disinfection and ageing of organic UF membranes: a review. Water Res. 56, 325–365.

Regula, C., Carretier, E., Wyart, Y., Sergent, M., Gésan-Guiziou, G., Ferry, D., Vincent, A., Boudot, D., Moulin, P., 2013b. Drinking water ultrafiltration: state of the art and experimental designs approach. Desalin. Water Treat. 51, 4892–4900.

Regula,C., Carretier, E., Wyart, Y., Sergent, M., Gésan-Guiziou, G., Ferry, D., Vincent, A., Boudot, D., Moulin, P., 2013a. Ageing of ultrafiltration membranes in contact with sodium hypochlorite and commercial oxidant: experimental designs as a new ageing protocol. Sep. Purif. Technol. 103, 119–138.

Richardson, S.D., Fasano, F., Ellington, J.J., Crumley, F.G., Buettner, K.M., Evans, J.J., Blount, B.C., Silva, L.K., Waite, T.J., Luther, G.W., McKague, A.B., Miltner, R.J., Wagner, E.D., Plewa, M.J., 2008. Occurrence and mammalian cell toxicity of iodinated disinfection byproducts in drinking water. Environ. Sci. Technol. 42, 8330–8338.

Romera, C.A., Davis, R.H., 1988. Global model of crossflow microfiltration based on hydrodynamic diffusion. J. Membr. Sci. 39, 117.

Rosa-Zeiser, A., Weilandt, E., Hild, S., Marti, O., 1997. The simultaneous measurement of elastic, electrostatic and adhesive properties by scanning force microscopy: pulsed-force mode operation, Meas. Sci. Technol., 8, 1333.

Rouaix, S., Causserand, C., Aimar, P., 2006. Experimental study of the effects of hypochlorite on polysulfone membrane properties. J. Membr. Sci. 277, 137–147.

Sarathy, S.R., Mohseni, M., 2007. The impact of UV/H2O2 advanced oxidation on molecular size distribution of chromophoric natural organic matter. Environ. Sci. Technol. 41, 8315–8320.

Schwinge, J., Wiley, D.E., Fane, A.G., 2004. Novel spacer design improves observed flux, J. Membr. Sci. 229, 53–61.

Singer, P., Bilyk, K., 2002. Enhanced coagulation using a magnetic ion exchange resin. Water Res. 36, 4009–4022.

Singh, S., Khulbe, K.C., Matsuura, T., Ramamurthy, P., 1998. Membrane characterization by solute transport and atomic force microscopy. J. Membr. Sci. 142, 111–127.

Spenkelink, F.J., Wennekes, W.B., Blankert, B., Knops, F., Dekker, R., Potreck, J., 2012. New Developments in Hollow Fiber Nanofiltration. In Proceedings of the 2nd Dissemination Workshop of the Nano4water Cluster, Chalkidiki, Greece, 24–25 April 2012.

Spenkelink, F.J., 2012b. Capillary Nanofiltration–Influence of Membrane Characteristics & Process Parameters on Permeate Quality. Master´s Thesis, UNESCO-IHE, Delft.

Sweers, K, van der Werf, K., Bennink, M., Subramaniam, V., 2011. Nanomechanical properties of α-synuclein amyloid fibrils: a comparative study by nanoindentation, harmonic force microscopy, and Peakforce QNM. Nanoscale Research Letters 6, 270.

Szymczyk, A., Fievet, P., 2005. Investigating transport properties of nanofiltration membranes by means of a steric, electric and dielectric exclusion model, Journal of Membrane Science, 252, 77–88.

Tercero Espinoza, L.A., ter Haseborg, E., Weber, M., Frimmel, F.H., 2009. Investigation of the photocatalytic degradation of brown water natural organic matter by size exclusion chromatography. Appl. Catal. B – Environ. 87, 56–62.

Thorsen, T., 2004. Concentration polarization by natural organic matter (NOM) in NF and UF. J. Membr. Sci. 233, 79–91.

Tian, J.Y., Chen, Z.L., Yang, Y.L., Liang, H., Nan, J., Li, G.B., 2010. Consecutive chemical cleaning of fouled PVC membrane using NaOH and ethanol during ultrafiltration of river water. Water Res. 44, 59–68.

Tng, K. H., Wang, Y., Audley, M., Koh, S. H., Currie, J., Roberts, C., Leslie, G. L., 2015. Performance Analysis of Advanced Water Treatment Plants Using Resilience Modelling Software, OzWater'15, Australia Water Association, Adelaide, Australia, 12–14 May 2015.

Toor, R., Mohseni, M., 2007. UV-H2O2 based AOP and its integration with biological activated carbon treatment for DBP reduction in drinking water. Chemosphere 66, 2087–2095.

Touffet, A., Baron, J., Welte, B., Joyeux, M., Teychene, B., Gallard, H., 2015. Impact of pretreatment conditions and chemical ageing on ultrafiltration membrane performances. Diagnostic of a coagulation/adsorption/filtration process. J. Membr. Sci., 489, 284–291.

Tran, T., Gray, S., Naughton, R., Bolto, B., 2006. Polysilicato-iron for improved NOM removal and membrane performance. J. Membr. Sci. 280, 560–571. doi:10.1016/j.memsci.2006.02.013

Trtik, P., Kaufmann, J., Volz, U., 2012. On the use of peak-force tapping atomic force microscopy for quantification of the local elastic modulus in hardened cement paste. Cem. Concr. Res. 42, 215–221.

Tsuru, T., Nakao, S.-I., Kimura, S., 1991. Calculation of ion rejection by extended Nernst–Planck equation with charged reverse osmosis membranes for single and mixed electrolyte solutions, Journal of chemical engineering of Japan, 24, 511–517.

Väisänen, P., Bird, M.R., Nystrom, M., 2002. Treatment of UFmembranes with simple and formulated cleaning agents. Food Bioprod. Process. 80,98–108.

Valinia, S., Futter, M., Fölster, J., Cosby, B., Rosén, P., 2015. Simple models to estimate historical and recent changes of total organic carbon concentrations in lakes. Environ. Sci. Technol. 49, 386–394. doi:10.1021/es503170r

Van der Bruggen, B., Schaep, J., Wilms, D., Vandecasteele, C., 1999. Influence of molecular size, polarity and charge on the retention of organic molecules by nanofiltration. J. Membr. Sci. 156, 29–41.

Van der Bruggen, B., Vandecasteele, C., 2003. Removal of pollutants from surface water and groundwater by nanofiltration: Overview of possible applications in the drinking water industry. Environ. Pollt. 122, 435–445.

Vanlandingham, M.R., McKnight, S.H., Palmese,G.R., Eduljee, R.F., Gillespie, J.W., McCulough, J.R.L., 1997. Relating elastic modulus to indentation response using atomic force microscopy, J. Mater. Sci. Lett. 16, 117–119.

Vattenkvalitet i Hallands Sjöar 2012. Resultat Från Omdrevsprogrammet 2007–2012 Länsstyrelsen i Hallands Län, Enheten för Naturvård & Miljöövervakning Meddelande, Vattenkvalitet i Hallands Sjöar: Hallands Sjöar, (In Swedish), 2013, ISSN 1101–1084.

Vickers, J., Thompson, M., Kelkar, U., 1995. The use of membrane filtration in conjunction with coagulation processes for improved NOM removal. Desalination 102, 57–61. doi:10.1016/0011-9164(95)00041-Y

Wang, J., Wang, X., 2006. Ultrafiltration with in-line coagulation for the removal of natural humic acid and membrane fouling mechanism. Journal of Environmental Sciences 18, 880–884. doi:10.1016/S1001-0742(06)60008-9

Wang, X.M., Li, B., Zhang, T., Li, X.Y., 2015. Performance of nanofiltration membrane in rejecting trace organic compounds: Experiment and model prediction. Desalination 370, 7–16.

Wang, Z., Zhao, Y., Wang, J., Wang, S., 2005. Studies on nanofiltration membrane fouling in the treatment of water solutions containing humic acids. Desalination 178,171–178.

Weis, A., Bird, M.R., Nystrom, M., 2003. The chemical cleaning of polymeric UF membranes fouled with spent sulphite liquor over multiple operational cycles. J. Membr. Sci. 216, 67–79.

Weis, A., Bird, M.R., Nyström, M., Wright, C., 2005. The influence of morphology, hydrophobicity and charge upon the long-term performance of ultrafiltration membranes fouled with spent sulphite liquor. Desalination 175, 73–85.

Wemsy Diagne, N., Rabiller-Baudry, M., Paugam, L., 2013. On the actual cleanability of polyethersulfone membrane fouled by proteins at critical or limiting flux. J. Membr. Sci. 425–426, 40–47.

Wijmans, J.G., 2004. The role of permanent molar volume in the solution-diffusion model transport equations. J. Membr. Sci. 237, 39–50.

Wijmans, J.G., Baker, R.W., 1995. The solution-diffusion model: A review, J. Membr. Sci. 107, 1–21.

Wong, S., Hanna, J.V., King, S., Carroll, T.J., Eldridge, R.J., Dixon, D.R., Bolto, B.A., Hesse, S., Abbt-Braun, G., Frimmel, F.H., 2002. Fractionation of natural organic matter in drinking water and characterization by ^{13}C cross-polarization magic-angle spinning NMR spectroscopy and size exclusion chromatography. Environ. Sci. Technol. 36, 3497–3503.

Worrall, F., Burt, T., 2007. Trends in DOC concentration in Great Britain. J. Hydrol. 346, 81–92.

Wyart, Y., Georges, G., Deumie´, C., Amra, C., Moulin, P., 2008. Membrane characterization by microscopic methods: multiscale structure. J. Membr. Sci. 315, 82–92.

Yadav, K. Morison, K., Staiger, M. P., 2009. Effects of hypochlorite treatment on the surface morphology and mechanical properties of polyethersulfone ultrafiltration membranes. Polym. Degrad. Stab. 94, 1955–1961.

Yamamura, H., Kimura, K., Okajima, T., Tokumoto, H., Watanabe, Y., 2008. Affinity of functional groups for membrane surfaces: Implications for physically irreversible fouling. Environ. Sci. Technol. 42, 5310–5315.

Young, T.J., Monclus, M.A., Burnett, T.L., Broughton, W.R., Ogin, S.L., Smith, P.A, 2011. The use of the PeakForce TM quantitative nanomechanical mapping AFM-based method for high-resolution Young's modulus measurement of polymers. Meas. Sci. Technol. 22, 125703 (6pp).

Yuan, W., Zydney, A., 1999. Humic acid fouling during microfiltration. J. Membr. Sci. 157, 1–12.

Zazouli, M.A., Nasseri, S., Ulbricht, M., 2010. Fouling effects of humic and alginic acids in nanofiltration and influence of solution composition. Desalination 250, 688–692.

Zhang, Y., Causserand, C., Aimar, P., Cravedi, J.P., 2006. Removal of bisphenol A by a nanofiltration membrane in view of drinking water production. Water Res. 40 (20), 3793–3799.

Zhao, Z.-Y., Gu, D.-J., Li, H.-B., Li, X.-Y., Leung, K.M.-Y., 2009. Disinfection characteristics of the dissolved organic fractions at several stages of a conventional drinking water treatment plant in South China. J. Hazard. Mater. 172, 1093–1099.

Zhu, H., Nyström, M., 1998. Cleaning results characterized by flux, streaming potential and FTIR measurements. Colloids Surf. 138, 309–321.

Zularisam, A., Ismail, A., Salim, R., 2006. Behaviours of natural organic matter in membrane filtration for surface water treatment—A review. Desalination 194, 211–231.

Zularisam, A.W., Ismail, A.F., Salim, M.R., Sakinah, M., Matsuura, T., 2009. Application of coagulation-ultrafiltration hybrid process for drinking water treatment: optimization of operating conditions using experimental design. Sep. Purif. Technol. 65, 193–210.

Zularisam, A.W., Ismail, A.F., Salim, M.R., Sakinah, M., Ozaki, H., 2007. The effects of natural organic matter (NOM) fractions on fouling characteristics and flux recovery of ultrafiltration membranes. Desalination 212, 191–208.

Appended papers: I-VI

Paper I:	Evaluation of novel hollow fiber membranes for NOM removal by advanced autopsy
Paper II:	Impact of operation conditions, foulant adsorption, and chemical cleaning on the nanomechanical properties of ultra-filtration hollow fiber membranes
Paper III:	Optimizing hollow fibre nanofiltration for organic matter rich lake water
Paper IV:	Simulation of NOM removal by capillary NF: A numerical method for full-scale plant design
Paper V:	Combined coagulation and ultrafiltration process to counteract increasing NOM in brown surface water
Paper VI:	Upgrading coagulation with hollow-fibre nanofiltration for improved organic matter removal in drinking water

Paper I

Evaluation of novel hollow fibre membranes for NOM removal by advanced membrane autopsy

A. Keucken, Y. Wang, K. H. Tng, G. L. Leslie, Kenneth M. Persson, Stephan J. Köhler and Tom Spanjer

ABSTRACT

A full-scale inside out hollow fibre membrane module was operated in a pilot-scale water treatment plant in Sweden for a period of 12 months from August 2013 to July 2014. Liquid chromatography–organic carbon detection (LC-OCD) chromatogram indicated the membranes could effectively remove 86% of dissolved organic carbon and 92% of humic substances from the feedwater. Routine cleaning-in-place was conducted to remove any fouling material accumulated on the membranes. Autopsy of the aged membrane samples after 12 months' operation suggested no significant changes were detected for the membrane samples obtained from the top, middle and bottom sections of the membrane module and were similar to the virgin membrane sample.

Key words | LC-OCD, membrane autopsy, natural organic matter (NOM) removal

A. Keucken (corresponding author)
Vatten & Miljö i Väst AB (VIVAB),
Box 110, 311 22 Falkenberg,
Sweden
E-mail: *alexander.keucken@vivab.info*

Y. Wang
K. H. Tng
G. L. Leslie
UNESCO Centre for Membrane Science and Technology,
University of New South Wales, Sydney 2052,
Australia

Kenneth M. Persson
Sydvatten AB,
Skeppsgatan 19, SE 211 19 Malmö,
Sweden

Stephan J. Köhler
Department of Aquatic Sciences and Assessment,
Swedish University of Agriculture Sciences,
Box 7050, 750 07 Uppsala,
Sweden

Tom Spanjer
Pentair X-Flow B.V.,
PO 739, 7500 AS Enschede,
The Netherlands

INTRODUCTION

In the southern part of Sweden, a general tendency of browning of the lakes has been noticed. The current drinking water supplies to Stockholm rely on conventional filtration (sand filters followed by granular activated carbon) and UV disinfection. The increasing colour and chemical oxygen demand (COD) in Swedish surface waters requires a more strict and reliable technique that can provide high quality drinking water. Climate change may alter natural organic matter (NOM) character, as lake turnover time has a profound impact on NOM characteristics (Köhler *et al.* 2013). Microporous membranes have been used widely in recent years to meet the stringent regulations, and provide climate-independent sources of high quality water (Lebeau *et al.* 1998, Chae *et al.* 2008, Tng *et al.* 2015). Membranes are an exceptional barrier to particles, turbidity, and microorganisms, provided that fouling of the membrane surface is kept to a minimum and the hollow fibres maintain their integrity.

Previous research has been done on identification of fouling of UF membranes during NOM removal (Combe *et al.* 1999; Yuan & Zydney 1999; Jones & O'Melia 2000; Lee *et al.* 2004), using coagulant to reduce fouling (Lin *et al.* 2000 and Carroll *et al.* 2000) and improve NOM removal and cleaning strategies (Lee *et al.* 2001). In addition, many membrane characterisation efforts have focused on evaluation of degradation of polyethersulfone (PES) membranes after hypochlorite treatment (Belfer *et al.* 2000; Thominette *et al.* 2006; Arkhangelsky *et al.* 2007; Levitsky *et al.* 2011; Regula *et al.* 2014). Most of the

doi: 10.2166/ws.2015.170

studies on NOM removal, and the effects of NOM on membrane fouling were based on laboratory-scale experiments using synthetic water, or with limited time of operation (hours or days). Therefore, it is important to assess the performance of membranes using real water and over a longer period. With regard to membrane degradation studies, the accelerated cleaning approach (i.e. cleaning using a high concentration of hypochlorite for a short period of time that gives an equivalent chlorine exposure (ppm·hr) as the real cleaning schedule used in water treatment plants (WTPs)) has been widely used. The current literature therefore shows a lack of data on membrane degradation and performance declines from real-time fouling/cleaning cycles.

The aim of this paper was to evaluate the performance (NOM removal, fouling, and integrity) of a commercial full-scale hollow fibre membrane module, and the feasibility of using such hollow fibre membrane filtration for high quality drinking water supply. A total of 12 months of operational data were collected from a pilot plant operated at Görvälnverket WTP, owned by the water utility, Norrvatten, which provides drinking water for the northern part of the Swedish capital of Stockholm. A suite of membrane autopsy techniques, including tensile strength test, contact angle, atomic force microscopy (AFM), attenuated total reflectance Fourier transform infrared spectroscopy (ATR-FTIR), thermogravimetric analysis (TGA), and scanning electron microscopy (SEM) in conjunction with energy dispersive spectroscopy (EDS), were performed on the aged membrane samples and virgin membranes to evaluate the integrity of the membranes after 12 months' operation.

MATERIAL AND METHODS

Pilot plants at Görvälnverket WTP

In the context of a national research project regarding NOM removal treatment processes, an extensive pilot facility (membrane combined with granulated activated carbon (GAC)) was established at Görvälnverket WTP in Sweden for various long-term trials (Figure 1). A membrane pilot plant with a treatment capacity of 29 m^3/day (14.4 m^3/day permeate production) was operated from August 2013 to July 2014. The surface water source feeding Görvälnverket WTP, is Lake Mälaren, the third largest lake in Sweden. The raw water was pretreated with sand filtration before feeding the pilot plant. The pilot plant was fitted with one 8 inch commercial size membrane module (Pentair X-Flow HFW1000) with an effective area of 40 m^2. Details of the membranes can be found in Table 1. The performance of the test module was monitored by continuously recording transmembrane pressure (TMP) over time. Regular membrane cleaning was performed by hydraulic backwash/forward flushing (every 60 minutes). Cleaning-in-place (CIP) was carried out every four to seven weeks on a preventive basis with respect to TMP profiles to avoid irreversible fouling. CIP solution consisted of 200 ppm sodium hypochlorite in the presence of sodium hydroxide to reach a pH of 12.4.

Characterisation of NOM in feed water and treated water

The nature of the organics presented in the raw water to the WTP, feedwater to the pilot plant, and effluent from

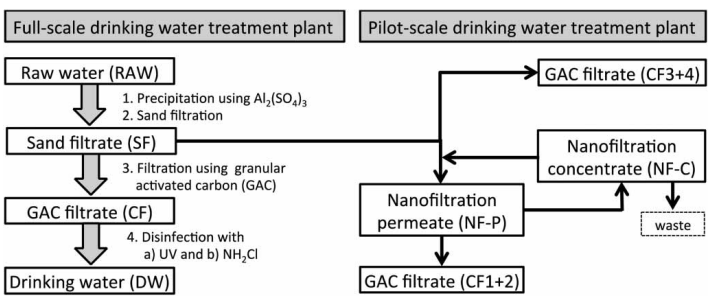

Figure 1 | Water treatment train for the full-scale drinking water plant and the pilot-scale drinking water plant at Görvälnverket WTP.

Table 1 | Intrinsic properties of the hollow fibre membrane and module

Membrane material	Sulfonated PES
Permeability (L/m^2 hr bar)	~10
MWCO based on PEG (Da)	~1,000
o.d./i.d. (mm)	1.15/0.80
Collapse pressure (bar)	>18
Burst pressure (bar)	>20
Membrane area (m^2)	40
Number of fibres	11,376
Module diameter (m)	0.20
Module length (m)	1.50

the WTP and the pilot plant were characterised using UV absorbance at 254 nm and liquid chromatography–organic carbon detection (LC-OCD). LC-OCD utilises size-exclusion coupled with three detectors (organic carbon, organic nitrogen and UV-absorbance). This technique allows for subdivision of organic matter into six major sub-fractions: biopolymers, humic substances (HS), building blocks, low molecular-weight acids, low molecular-weight neutrals, and hydrophobic organic carbon. From the results, the nitrogen content of the biopolymer and the HS can be estimated. The measurement of the protein content of the biopolymer fraction allows for the amount of bound nitrogen to be determined using the UV detector, while HS can be further characterised using the HS diagram which plots the aromaticity of HS against its nominal molecular weight. Detailed information of the LC-OCD technique can be found in the paper published by Huber *et al.* (2011).

Evaluation of membrane fouling and integrity

Membrane samples were collected from top, middle and bottom sections of the module after a CIP on 9 July 2014. All samples were rinsed with deionised water and dried in a desiccator for at least 24 hrs prior to analysis.

Mechanical properties

Tensile strength of the membranes was measured using a TA-XT2 Tensile Analyser (Stable Micro Systems, USA). The dried hollow fibre samples were cut into test samples of 80.0 ± 1.0 mm in length and subjected to a vertical elongation at a speed of 60 mm/min until the sample yielded and fractured. Five repeats per sample were performed and Young's Modulus and breaking force were calculated via the stress–strain curve obtained after each test.

Hydrophilicity

The hydrophilicity and wettability of the lumen side (i.e. the feed side) of the membranes were determined by static sessile drop contact angle analysis method using a goniometer (KSV CAM200 Contact Angle System). The reported contact angle was the average value of the left and right side contact angles obtained for at least five different locations along the test sample.

Surface roughness

The roughness of both surfaces of the lumen and shell side of the membrane samples were analysed using AFM (Bruker Dimension Icon). An in-air, tapping mode, TM-AFM at 1 Hz scan rate and 512×512 pixel resolution, was used to collect images from a $2\,\mu m \times 2\,\mu m$ scanning area with a 13.5 μm Z-range. Images presented are with a 100 nm Z-range (−50 nm to 50 nm) and 200 nm Z-range (−100 nm to 100 nm) for lumen side and shell side, respectively. The root mean squared (RMS) roughness, R_q, and the average roughness, R_a, were calculated from three different sections of each sample and the average values were reported.

Chemical degradation

The Perkin Elmer Spotlight 400 FTIR Microscope (Perkin Elmer, USA) equipped with an ATR crystal was used to analyse and detect any degradation of the polymer material's chemical composition due to chemical exposure during CIP. All spectra were collected with 32 scans at 1 cm^{-1} resolution from 650 to 4,000 cm^{-1}.

The thermal stability of the membrane material was analysed by thermogravimetric analyser (Perkin Elmer, USA). An empty platinum pan was used as the reference for measuring the change in mass of the sample. Samples at

room temperature were heated up to a temperature of 600 °C at a constant rate of 50 °C/min in a dry nitrogen atmosphere. Variation in the thermal decomposition profiles of would help detect changes to the sample's chemical composition.

Membrane surface morphology and foulants characterisation

A SEM (Hitachi S3400) was used to produce 2D images of the cross-section and surface (both lumen and shell side) morphology of the membranes. The elemental composition of the surfaces of the samples were analysed using EDS. All samples were sputter coated with a thin layer of carbon before SEM-EDS analysis.

RESULTS AND DISCUSSION

Membrane performance during filtration and cleaning

Membrane filtration performance of the pilot plant was monitored by continuously recording TMP and permeability over time. Figure 2 shows variation of TMP and temperature for 90 days of operation (1 January 2014–30 April 2014). During long-term trials a manual chemically enhanced

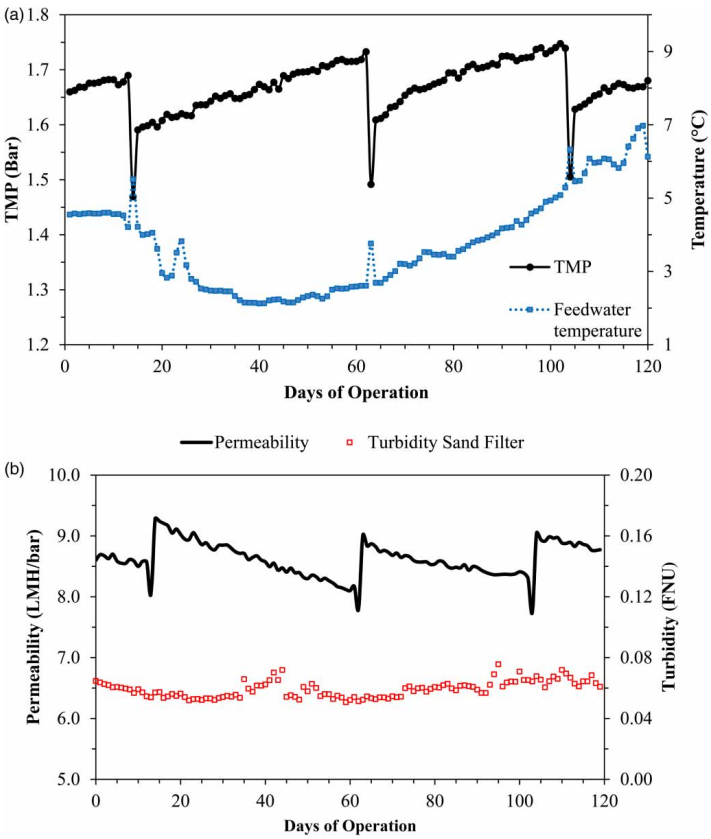

Figure 2 | TMP (a) and permeability (b) profiles of pilot plant before and after CIPs: January 2014–April 2014.

backwash (CEB) interval of 40 to 50 days was applied by operating the membrane pilot continuously at flux levels of 15 L/(m^2 h) (LMH) with crossflow velocity of 0.5 m/s, intermittent forward flushing every 60 minutes and permeate recovery rates around 50%. As shown in Figure 2(a) the TMP increased by 0.26 bar (1.47 to 1.73 bar) during an operation cycle of 38 days, while permeability (Figure 2(b)) decreased by 1.48 LMH/bar (9.28 to 7.80 LMH/bar) at low water temperatures (1 to 3 °C). During this operational period, the feedwater (i.e. sand filtration (SF) filtrate) turbidity remained at 0.059 (±0.005) Formazin Turbidity Unit (Figure 2(b)). Such low turbidity is comparable with the turbidity of microfiltration's permeate and with the CIPs restoring the membrane's permeability after prolonged filtration, further shows the low risk of membrane filtration of sand filter effluent for extended operating cycles. These results indicated that membrane filtration of sand filtered water allowed long filtration cycles with no risk of irreversible membrane fouling.

Characterisation of NOM

LC-OCD chromatogram suggested that NOM present in the feed water was effectively removed by the membranes (Figure 3). Raw water NOM (total organic carbon (TOC) = 8.8 ppm) consists of around 70% HS, two-thirds of which were removed in the flocculation/coagulation process (TOC after rapid SF was 4.3 ppm). Almost all remaining HS were removed during membrane filtration. Compounds smaller than HS (i.e. building blocks and LMW acids and neutrals) were also removed by the membranes. The combined process removed more than 93% of incoming TOC (average TOC after membrane filtration was 0.6 ppm).

Removal of NOM by the membranes also caused an increase in TMP. The TMP was recovered effectively after chemical cleaning (Figure 4).

The LC-OCD data can be used to quantify the contribution of HS in all water samples throughout the whole treatment steps. UV absorbance at 254 nm is tightly related to the measured content of HS (Figure 5). This is consistent with earlier findings (Erlandsson *et al.* 2012) and allows for quantification of the amount of HS that may be flocculated from the incoming raw water using absorbance values only. High precision measurement of absorbance in the membrane permeate will help to indicate problems with the incomplete separation of HS during membrane failure.

Data collected from August 2013 to July 2014 (Figure 6) showed that more than 85% of dissolved organic carbon (DOC) in the sand filtered water was removed by the membranes (from 4.4 to 0.6 mg/L), with less than 2% difference in removal efficiency throughout the 12 months' operational period. HS, which accounted for 53 (±3) % of the hydrophilic chromatographic DOC, also reduced from 2.33 (±0.14) mg/L in the sand filtered water to 0.19 (±0.03) mg/L in the membrane filtrate, indicating membranes' stable performance on the rejection of organic matters.

The extensive NOM characterisation of various water samples from the existing treatment process and the membrane pilot (Keucken *et al.* 2014) indicated a relationship between biopolymers and DOC. As shown in Figure 7(a) biopolymers with larger molecular weight were removed proportionally over the rapid sand filters and completely removed by the membrane module. On the other hand, it was found that the building blocks could not be removed by rapid sand filtration. The proportional retention behaviour by the membrane module is consistent with the specified molecular weight cut-off (MWCO) of the membrane (500–700 Da) (Figure 7(b)).

Mechanical properties

Tensile strength analysis and independent samples *t*-tests showed that the Young's Modulus of the top and bottom were higher than that of reference (virgin membrane) sample indicating that the samples became stiffer after multiple filtration/cleaning cycles while the middle sample's Young's Modulus was statistically unchanged (Figure 8(a)). No significant changes in the force required to fracture the membrane were observed from the tensile strength analysis (Figure 8(b)) and subsequent *t*-tests showed no statistical differences in breaking force amongst the four samples at a 95% confidence interval. Thus, it can be concluded that this increase in Young's Modulus caused by multiple filtration/cleaning cycles did not have an impact on the membrane's mechanical strength. It should be noted that during the pilot trials, chemical cleaning was carried out using a solution of pH 12.4. A previous study by Causserand *et al.* (2008) suggested that no change to the mechanical properties of the membranes could be observed at this pH

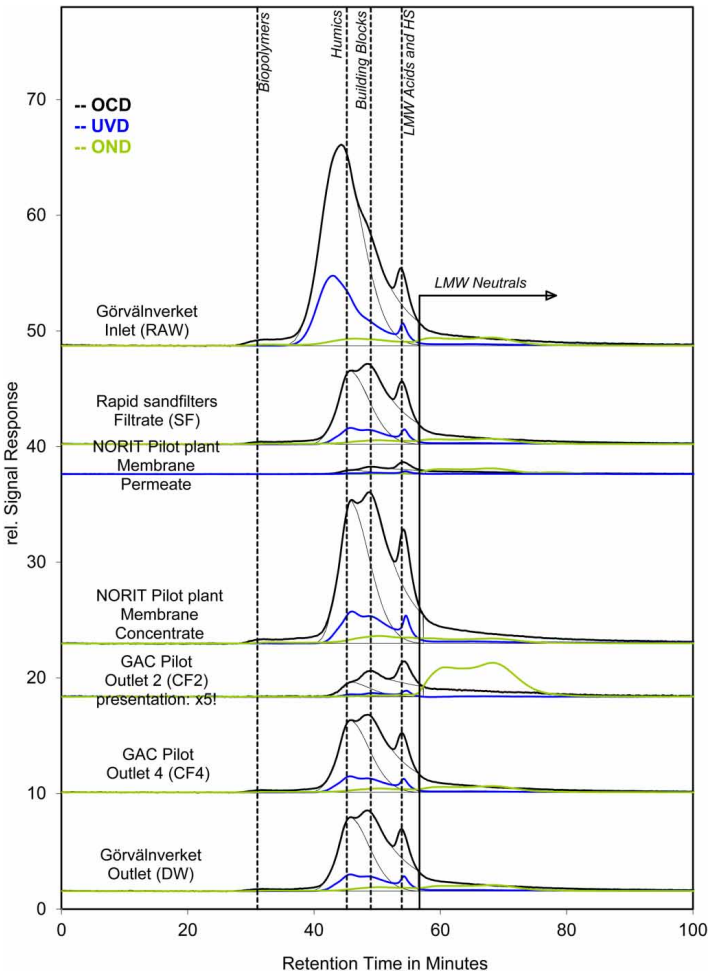

Figure 3 | LC-OCD chromatogram of sampling profile: full-scale drinking water plant vs. pilot plant.

because the hypochlorite solution at pH 12 would contain hypochlorite ion (OCl^-) only, which has less oxidising potential compared with the hypochlorous acid.

Hydrophilicity and surface roughness

Lumen (feed) side average contact angle increased from 62.06° (±4.51°) to 69.73° (±2.37°), 70.16° (±5.45°), and 66.56° (±4.02°) for the top, middle, and bottom samples, respectively, indicating that the membrane's lumen surface became less hydrophilic after prolonged operation and cleaning. Comparison of the contact angle also showed that the top, middle and bottom sections had similar hydrophilicity and wettability.

An increase in lumen side surface roughness was observed for the top, middle and bottom sections when

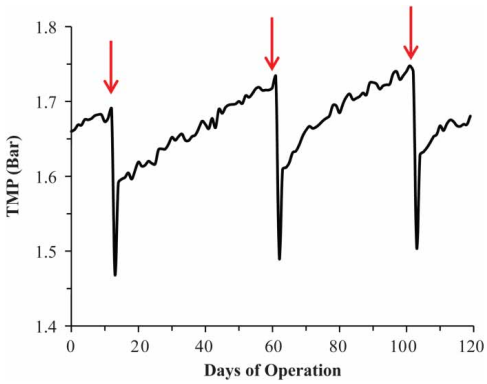

Figure 4 | TMP profiles of pilot plant before and after CIP cycles from 1 January to 30 April 2014 (arrows representing CIP events).

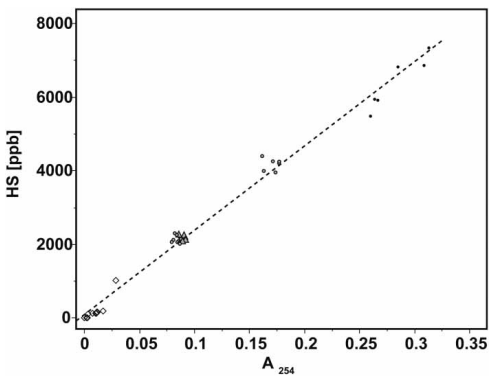

Figure 5 | Linear regression of HS concentration as a function of UV254 (LC-OCD data).

compared with that of the reference membrane sample with the R_q value, increasing from 10.6 nm for reference sample to 18.6 nm for the sample collected from the top section of the module. Bottom section samples had a relatively lower roughness ($R_q = 15.4$ nm) compared with samples from the top and middle sections. This trend was also observed for the calculated average roughness (Figure 9 and Table 2). Increase in roughness could indicate the possibility of the enlargement of pore size (Arkhangelsky *et al.* 2007).

An significant increase in shell side surface roughness was observed for the top, middle and bottom sections

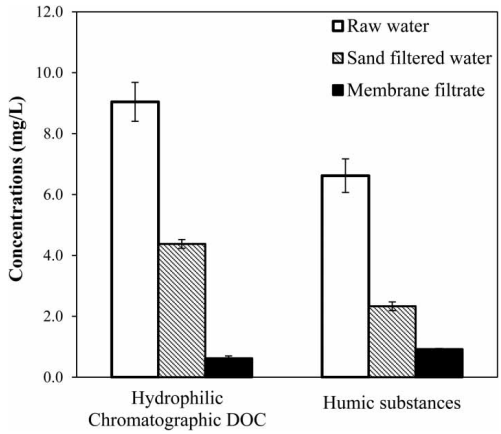

Figure 6 | Comparison of average concentrations of DOC and HS in different waters. Error bar indicates variations from August 2013 to July 2014.

when compared with that of the reference membrane sample (Figure 10) with the R_q value increasing from 23.5 nm for reference sample to 28.1 nm, 35.6 nm, and 62.9 nm for the sample collected from the top, middle, and bottom section, respectively. The shell side surface also exhibited a higher roughness than the lumen side surface, which is due to the higher porosity (Figure 10).

Chemical degradation

The ATR-FTIR spectra of the virgin and aged membrane samples are shown in Figure 11, and the peak assignments for PES membranes are given in Table 3.

Different mechanisms of NaOCl attachment on PES membranes have been proposed, including chain scission and formation of phenyl sulfonate (Arkhangelsky *et al.* 2007), or the chain scission of the PES polymeric backbone into two parts with one end terminated by a sulfonic acid group and other part terminated by a phenyl chloride group (Yadav *et al.* 2009). None of this was observed on the current membrane samples as similar peaks were detected at their corresponding functional group's wavelengths. A significant change in the broad peak at around 3,400 cm^{-1}, which was the hydrogen bonding stretching vibration, was observed. This could be attributed to the residual glycerol and water in the reference sample. The

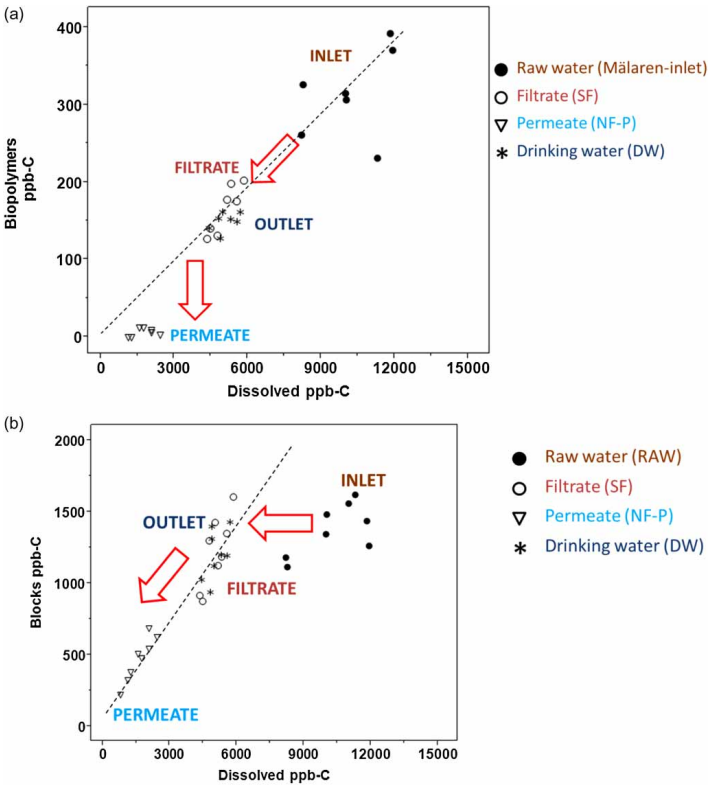

Figure 7 | Linear regression of concentrations of different organic matters as a function of DOC concentration in different process streams: (a) biopolymer vs. DOC; and (b) building blocks vs. DOC.

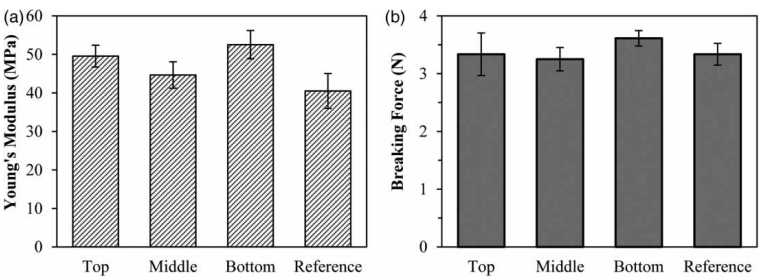

Figure 8 | Mechanical properties of tested samples: (a) Young's Modulus; and (b) breaking force.

ATR-FTIR results suggested that samples were chemically identical and that no degradation to the membrane samples' polymer material composition occurred.

The conclusions drawn from ATR-FTIR spectroscopy were cross-confirmed by measuring the changes in the mass of the sample as a function of temperature using

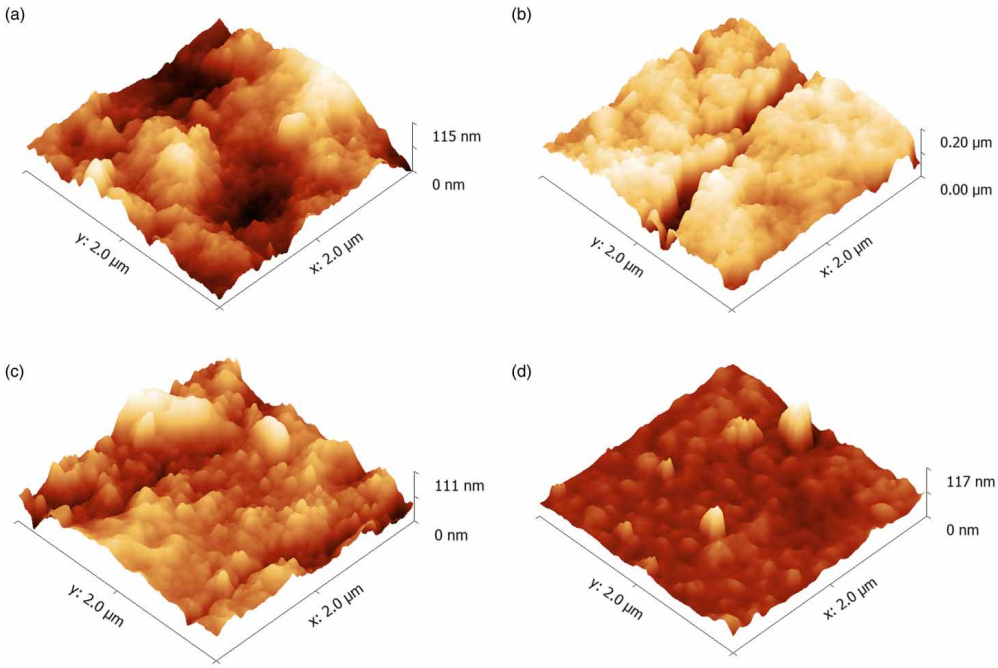

Figure 9 | Lumen side surface AFM topography images of: (a) top; (b) middle; (c) bottom; and (d) reference.

Table 2 | Roughness values of the lumen side surface

	Top	Middle	Bottom	Reference
RMS roughness, R_q (nm)	18.6	18.4	15.4	10.6
Average roughness, R_a (nm)	15.1	12.6	11.9	7.6

TGA. The TGA profiles of the all four samples have identical decomposition profiles indicating the absence of chemical degradation of the polymer material (Figure 12). The plot of percentage mass loss as a function of temperature for all the tested samples exhibited a two-step degradation mechanism. The mass loss due to decomposition of the material started at around 450 °C, with major mass loss occurring between 500 to 560 °C followed by a second degradation stage occurring between 630 to 650 °C. The weight loss patterns for all the test samples were very similar to the reference membrane sample suggesting the absence of any potential chemical degradation of the polymer material. However, the decrease in mass was observed at around 280 °C, for the reference membrane sample, can be attributed to the residual glycerol preservative agent present in the sample, with glycerol having a boiling point of 290 °C.

Surface morphology

The lumen and shell side surfaces as well as cross-sections of the hollow fibre samples were microscopically analysed for any signs of damage by high resolution SEM. Not any significant defects, cracks, or deposits (foulants) were observed on the shell side surface sample (at ~×1,000 magnification) and cross-sections (at ×800 magnification) (Figure 13).

SEM images of the lumen side surface showed that the lumen surface of the top, middle and bottom samples were visibly rougher compared with the reference sample's

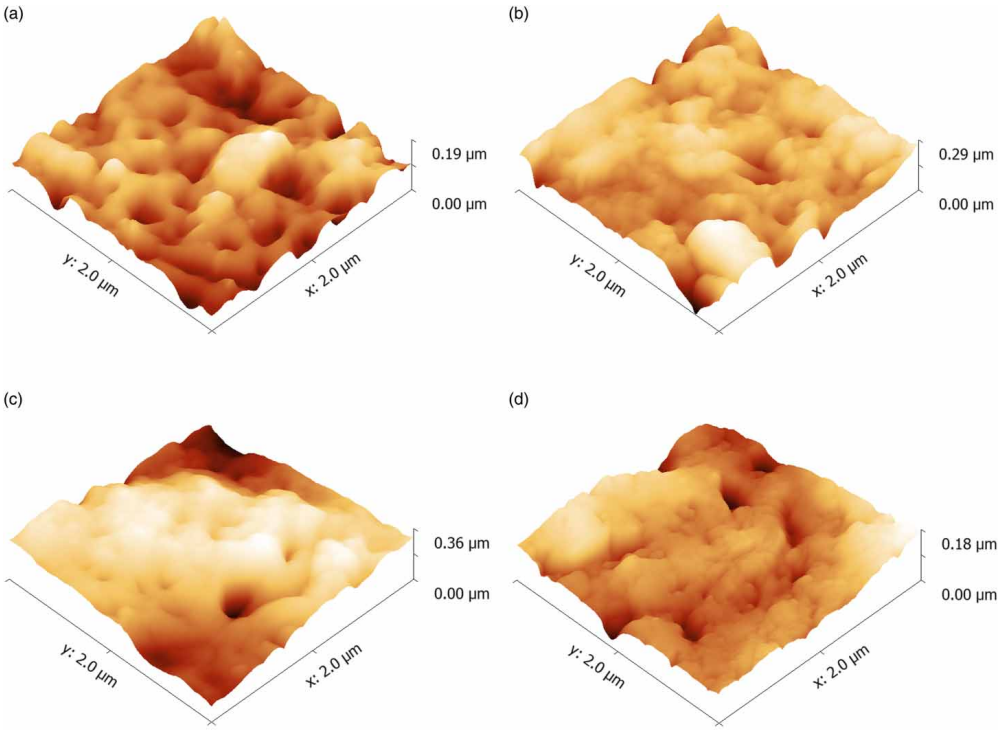

Figure 10 | Shell side surface AFM topography images of: (a) top; (b) middle; (c) bottom; and (d) reference.

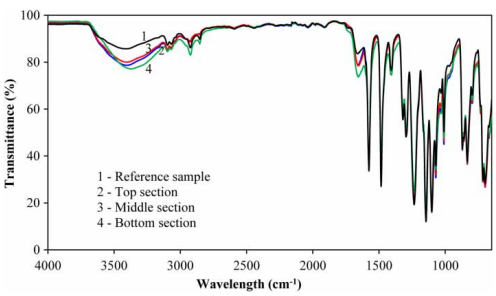

Figure 11 | ATR-FTIR spectra of membrane samples.

surface (Figure 14). This observation is consistent with the results obtained via AFM analysis. At a magnification levels of ~×1,000, tiny cracks were observed on all samples. It should be noted that these cracks could be caused by sample preparation and were unavoidable given the necessity for the samples to be cut to expose the lumen side surface for analysis.

Table 3 | Assignment of the relevant IR bands in the range of 1,800–1,100 cm^{-1} (Arkhangelsky *et al.* 2007; Belfer *et al.* 2000)

IR band (cm^{-1})	Range given in the literature	Assignment
1,642	1,620–1,680	Aromatic stretching vibrations
1,578	About 1,580	Aromatic systems
1,485	1,460–1,550	C–S stretch
1,320	1,310–1,350	SO_2
1,298	1,050–1,300	SO_2
1,241	1,200–1,275	C–O–C
1,148	1,120–1,160	SO_2 stretching
1,105	1,085–1,125	C–O stretching vibration

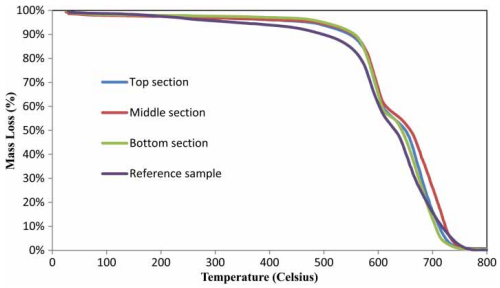

Figure 12 | TGA profiles of membrane samples.

A further analysis on the elemental composition was conducted using EDS. Similar spectra with three elements, carbon, oxygen, and sulphur, were obtained for all samples analysed (Figure 15). Given that EDS detected no other elements, it can be concluded that there were neither signs of fouling on the lumen side surface of all the membrane fibre samples nor traces of CIP by-products further reinforcing the conclusion that the cracks were caused by sample preparation and not by chemical ageing.

CONCLUSIONS

A total of 12 months' operational data were collected from a pilot plant located at Görvälnverket water treatment plant (WTP) in Sweden. The DOC removal efficiency was significantly improved by 87.8% using the hollow fibre membrane filtration when compared with the existing treatment (flocculation, sand filtration and granular activated carbon) currently used in the WTP. A membrane autopsy was conducted on samples obtained from the top, middle and bottom sections of the module. Autopsy results showed that no substantial changes were detected for samples obtained from the different sections of the aged membrane

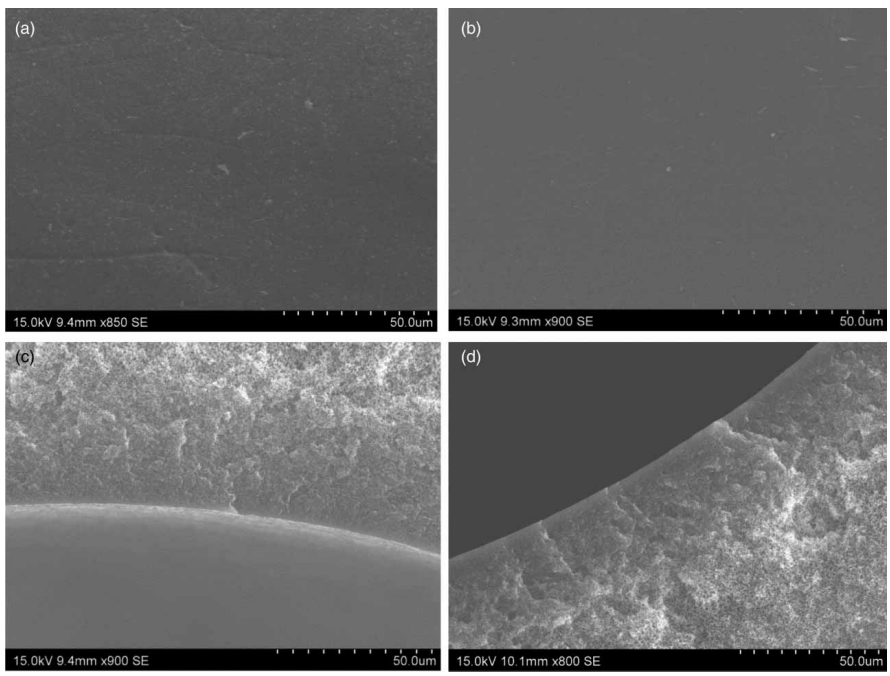

Figure 13 | SEM images of shell side surface and cross-sections of the hollow fibre samples: (a) shell side surface of virgin membrane; (b) shell side surface of the aged membrane; (c) cross-section of the virgin membrane; and (d) cross-section of the aged membrane.

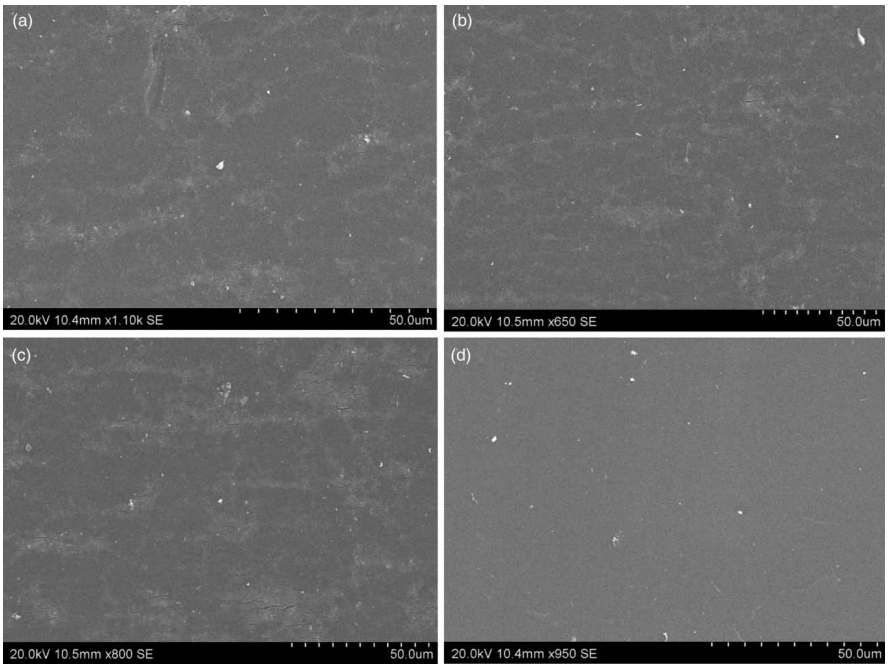

Figure 14 | SEM images of the lumen side surfaces of: (a) top; (b) middle; (c) bottom; and (d) reference.

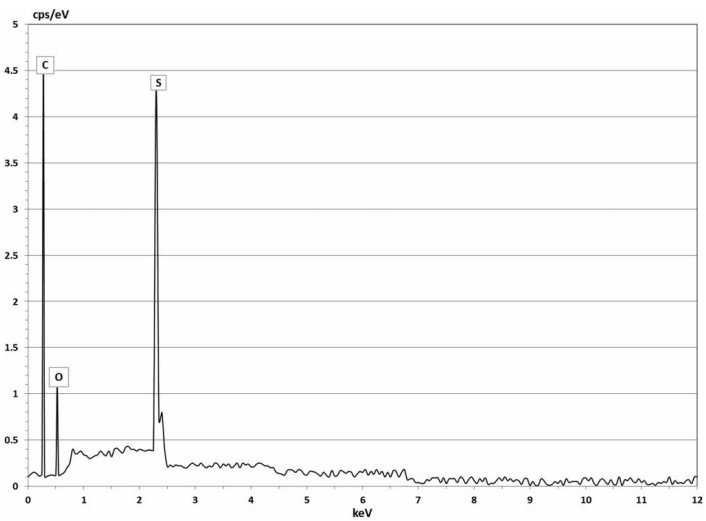

Figure 15 | EDS spectra of the lumen side surfaces.

and were very similar to the reference sample. Membrane ageing was the main cause for the minimal changes in the Young's Modulus and the lumen surface's contact angle. However, the effects of these changes would have an insignificant impact on the membrane's overall integrity and performance. Therefore, it can be concluded that the hollow fibre membranes are reliable and capable of providing safe drinking water for the northern part of the Swedish capital of Stockholm.

REFERENCES

Arkhangelsky, E., Kuzmenko, D. & Gitis, V. 2007 Impact of chemical cleaning on properties and functioning of polyethersulfone membranes. *J. Membr. Sci.* **305**, 176–184.

Belfer, S., Fainchtain, R., Purinson, Y. & Kedem, O. 2000 Surface characterization by FTIR-ATR spectroscopy of polyethersulfone membranes–unmodified, modified and protein fouled. *J. Membr. Sci.* **172** (1–2), 113–124.

Carroll, T., King, S., Gray, S. R., Bolto, B. A. & Booker, N. A. 2000 The fouling of microfiltration membranes by NOM after coagulation treatment. *Water Res.* **34** (11), 2861–2868.

Causserand, C., Rouaix, S., Lafaille, J.-P. & Aimar, P. 2008 Ageing of polysulfone membranes in contact with bleach solution: role of radical oxidation and of some dissolved metal ions. *Chem. Eng. Process.* **47**, 48–56.

Chae, S.-R., Yamamura, H., Ikeda, K. & Watanabe, Y. 2008 Comparison of fouling characteristics of two different polyvinylidene fluoride microfiltration membranes in a pilot-scale drinking water treatment system using precoagulation/sedimentation, sand filtration, and chlorination. *Wat. Res.* **42**, 2029–2042.

Combe, C., Molis, E., Lucas, P., Riley, R. & Clark, M. 1999 The effect of CA membrane properties on adsorptive fouling by humic acid. *J. Membr. Sci.* **154**, 73–87.

Erlandsson, M., Futter, M. N., Kothawala, D. & Köhler, S. J. 2012 Variability in spectral absorbance metrics across boreal lake waters. *J. Environ. Monit.* October, **14**(10), 2643–2652.

Huber, S. A., Balz, A., Abert, M. & Pronk, W. 2011 Characterisation of aquatic humic and non-humic matter with size-exclusion chromatography–organic carbon detection–organic nitrogen detection (LC-OCD-OND). *Water Res.* **45** (2), 879–885.

Jones, K. & O'Melia, C. 2000 Protein and humic acid adsorption onto hydrophilic membrane surface: effects of pH and ionic strength. *J. Membr. Sci.* **165**, 31–46.

Keucken, A., Spanjer, T., Ericsson, P., Persson, K. M. & Köhler, S. J. 2014 Evaluation of Color Removal Package (CPR) for drinking water based on novel hollow fiber nanofiltration. Proceedings of the 9th Nordic Drinking Water Conference (NORDIWA), Helsinki, Finland.

Köhler, S. J., Kothawala, D., Futter, M. N., Ljungman, O. & Tranvik, L. 2013 In-lake processes offset increased terrestrial inputs of dissolved organic carbon and color to lakes. *PLoS ONE* **8** (8), e70598. DOI: 10.1371/journal.pone.0070598.

Lebeau, T., Lelièvre, C., Buisson, H., van der Venter, L. W. & Côté, P. 1998 Immersed membrane filtration for the production of drinking water: combination with PAC for NOM and SOCs removal. *Desalination* **117**, 219–231.

Lee, H., Amy, G., Cho, J., Yoon, Y., Moon, S.-H. & Kim, I. S. 2001 Cleaning strategies for flux recovery of an ultrafiltration membrane fouled by natural organic matter. *Wat. Res.* **35**, 3301–3308.

Lee, N., Amy, G., Croue, J.-P. & Buisson, H. 2004 Identification and understanding of fouling in low-pressure membrane (MF/UF) filtration by natural organic matter (NOM). *Wat. Res.* **38**, 4511–4523.

Levitsky, I., Duek, A., Arkhangelsky, E., Pinchev, D., Kadoshian, T., Shetrit, H., Naim, R. & Gitis, V. 2011 Understanding the oxidative cleaning of UF membranes. *J. Membr. Sci.* **377**, 206–213.

Lin, C. F., Lin, T. Y. & Hao, O. J. 2000 Effects of humic substance characteristics on UF performance. *Water Res.* **34** (4), 1097–1106.

Regula, C., Carretier, E., Wyart, Y., Gésan-Guiziou, G., Vincent, A., Boudot, D. & Moulin, P. 2014 Chemical cleaning/disinfection and ageing of organic UF membranes: a review. *Wat. Res.* **56**, 325–365.

Thominette, F., Farnault, O., Gaudichet-Maurin, E., Machinal, C. & Schrotter, J. C. 2006 Ageing of polyethersulfone ultrafiltration membranes in hypochlorite treatment. *Desalination* **200** (1–3), 7–8.

Tng, K. H., Wang, Y., Audley, M., Koh, S. H., Currie, J., Roberts, C. & Leslie, G. L. 2015 Performance Analysis of Advanced Water Treatment Plants Using Resilience Modelling Software, OzWater'15, Australia Water Association, Adelaide, Australia, 12–14 May 2015.

Yadav, K., Morison, K. & Staiger, M. P. 2009 Effects of hypochlorite treatment on the surface morphology and mechanical properties of polyethersulfone ultrafiltration membranes. *Polym. Degrad. Stab.* **94**, 1955–1961.

Yuan, W. & Zydney, A. 1999 Humic acid fouling during microfiltration. *J. Membr. Sci.* **157**, 1–12.

First received 19 August 2015; accepted in revised form 9 November 2015. Available online 26 November 2015

Paper II

Impact of operation conditions, foulant adsorption, and chemical cleaning on the nanomechanical properties of ultrafiltration hollow fiber membranes

MANUSCRIPT

Leonardo Gutierrez[1,2], Alexander Keucken[3,4], Cyril Aubry[5], Noor Zaouri[6], Benoit Teychene[7], Jean-Philippe Croue[1*]

[1] Curtin Water Quality Research Centre, Department of Chemistry, Curtin University, Australia

[2] Facultad del Mar y Medio Ambiente, Universidad del Pacifico, Guayaquil, Ecuador

[3] Vatten & Miljö i Väst AB (VIVAB), Falkenberg, Sweden

[4]Water Resources Engineering, Faculty of Engineering, Lund technical University, Lund, Sweden

[5]Masdar Institute of Science and Technology, Masdar City, Abu Dhabi, United Arab Emirates

[6]Water Desalination and Reuse Center, King Abdullah University of Science and Technology, Saudi Arabia

[7] Universite de Poitiers, France

* Corresponding author: Tel.: +61 (0) 8 9266 9793
E-mail address: jean-philippe.croue@curtin.edu.au

29 pages, 7 figures, and a supporting information section are included in the current manuscript.

Abstract

This study analyzed the change in nanomechanical properties of Xiga and Aquaflex ultrafiltration hollow fiber membranes harvested from pilot-scale units after 12-14 months of operation and subjected to different feed and operating conditions. Quantitative Nanomechanical Mapping technique was used to distinguish between adhesion, dissipation, deformation, and modulus while simultaneously generating a topographic image of the membranes. Nanomechanical maps of virgin membranes evidenced surfaces of heterogeneous properties. Aquaflex virgin showed higher adhesion, and lower modulus and deformation than Xiga virgin; indicating membranes of different properties. Operating conditions and feed quality exerted different impacts on harvested membranes. Xiga modules were more extensively used and backwashed. However, the feed of Aquaflex modules was lower in quality. The nanomechanical properties of clean Xiga membranes were highly impacted, while Aquaflex membranes were slightly affected. The polymeric material of Xiga would undergo more severe physicochemical changes by foulants adsorption and reaction with cleaning agents. Foulant adsorption on membranes was heterogeneous in both morphology and mechanical properties; and could not be statistically described by probability density functions. Foulants displayed high roughness and adhesion forces, low elastic deformation, and variable modulus. This study advances our nanoscale understanding of the impact of fouling and operating conditions on membranes characteristics.

1. Introduction

The Atomic Force Microscope (AFM) is a versatile tool widely used for the investigation of surfaces at the nanoscale [1]. In addition to topographic analysis, the AFM can measure specific and non-specific interacting forces at the very interface between surfaces across a medium [1-3]. The non-destructive and non-invasive nature of this technique allows it to explore different types of samples (e.g., polymers, metal oxides, organics, bacteria) and their surface characteristics [4-7]. This latter AFM capability has been extensively exploited in previous studies as a semi-quantitative scanning technique, i.e., phase imaging and force modulation [8]. However, the development of pulse-force AFM mode has provided a significant advantage in the quantitative calculation of surface characteristics, e.g., stiffness, adhesion, and Young's modulus [9, 10]. Remarkably, the recent introduction of PeakForce^{TM} Quantitative Nanomechanical Mapping (QNM^{TM}) technique (Bruker, USA) has offered enhanced benefits for the nanoscale characterization of materials [11]. Specifically, QNM technique quantitatively distinguishes between adhesion, dissipation, deformation, and modulus while simultaneously generating a topographic image of a surface.

At present, QNM technique has been used in several fields of research. Briefly, the nanomechanical properties of amyloid fibrils of the human α-synuclein protein were determined by QNM. The elastic moduli of the α-synuclein fibrils obtained was consistent to those determined by single-point nanoindentation and harmonic force microscopy [12]. In a similar study, the modulus values of 12 different polymeric surfaces (i.e., most of them commonly used in filtration membranes: polycarbonate, polyethersulfone, polyvinylidene fluoride, polystyrene, etc.) obtained by PeakForce^{TM} QNM^{TM} using diamond and silicon sharp probes were in reasonable agreement with those measured by instrumented indentation testing (IIT) [13].

Furthermore, other previous studies have reported consistent Young's modulus values between QNM and indirect evaluation of β-lactoglobulin amyloid fibrils stiffness obtained by combining polymer physics and topological statistical analysis on fibrils' structural conformations [14]. In cement research, different phases in the cement paste microstructure that could not be distinguished from back-scattered electron images, were discriminated by the quantitative mapping of the local elastic modulus [15]. QNM has also been used to characterize deformation, adhesion, and modulus gradient of the interphase region in poly(vinyl alcohol)–poly(acrylic acid)–cellulose nanocrystal composites [16]. Interestingly, although mechanical properties of modified, virgin, and industrially fouled membranes have been studied by AFM colloidal probe technique and nanoindentation, the analytical advantages of QNM have not been majorly exploited in the field of membrane science and technology [17, 18].

Membrane treatment-based technologies (e.g., desalination, membrane bio-reactor, ceramic membranes) have become suitable alternatives to face the current challenges of water scarcity [19]. This technology has quickly evolved and expanded worldwide as an attempt to reduce pressure on local natural water resources. Nevertheless, the performance of membranes is still severely affected by inorganic/organic/bio fouling. Specifically, the interfacial interactions between membrane and foulants (i.e., leading to adsorption) changes the surface properties of the membrane, thus influencing subsequent fouling behavior [6]. This adsorption of foulants on membranes may be reversible or irreversible. The latter type of association causes a permanent change in membrane characteristics and performance [20]. Different procedures and techniques for membrane cleaning (e.g., by chemical, biochemical, or physical means) are currently used for removing these non-integral substances (foulants) from the membrane [21]. Remarkably, the cleaning process itself (e.g., chemical cleaning) may have an impact on the physicochemical

characteristics of the membranes. Different advanced autopsy techniques have been used to study this complex phenomena taking place at the membrane surface [22]. Despite extensive research, the adsorption of foulants, cleaning processes, and their effects on the (mechanical) properties of membranes are still poorly understood and have not yet been quantitatively measured at a nanoscale resolution.

The target of this investigation was to analyze the change in surface properties of ultrafiltration (UF) hollow fiber membranes harvested from pilot scale units after several months of continuous operation. The impact of the cleaning procedure on membrane surface characteristics received a special emphasis in this current study. PeakForce^{TM} Quantitative Nanomechanical Mapping (QNM^{TM}) technique was used to measure the nanomechanical properties (i.e., deformation, dissipation, modulus, adhesion) of UF hollow fiber membrane samples harvested from modules tested at pilot scale and virgin hollow fiber membranes subjected to chemical cleaning at bench scale. A rigorous statistical analysis was conducted to assess the change in membrane characteristics. Additionally, surface imaging by Scanning Electron Microscopy (SEM) coupled with Energy-dispersive X-ray Spectroscopy (EDS) and foulant characterization by Pyrolysis Gas Chromatography/Mass Spectrometry (GC/MS) were used as complementary tools. The methodology detailed in this investigation can be extended to numerous applications within the membrane science and technology field. Finally, the merit of this research is to advance our nanoscale understanding of the impact of foulant adsorption, operation conditions, and chemical cleaning on the surface characteristics of membranes.

2. Materials and Methods

2.1. Membranes samples and ageing experiments

The raw water quality parameters, full-scale plant operation, pilot-scale plant operation, and sampling points for membrane autopsy were described in detail in the SI section. Briefly, the membrane samples were recovered from UF hollow fiber (inside-out) modules harvested after a final Chemically Enhanced Backwash (CEB) from a pilot plant (Kvarnagården water treatment plant, Varberg, Sweden) consisting of: a) a primary UF unit (horizontal dead-end filtration) with two Pentair X-Flow Xiga membrane modules, and b) a secondary UF unit (vertical dead-end filtration) with one Pentair X-Flow Aquaflex membrane module (Figure S1-S2). The primary UF unit received a coagulated water consisted of 80% surface water and 20% ground water (turbidity: 0.3-2.0 NTU; DOC: 2.0-8.1 mg C/L; TOC: 2.3-8.3 mg C/L). The backwash water of the primary UF unit was the feed water of the secondary UF unit (turbidity: 20.0-25.0 NTU; DOC: 4.0-4.9 mg C/L; TOC: 22.0-28.0 mg C/L). The total filtration volumes were 57,150 m^3 and 2,155 m^3 operated in dead-end or cross-flow mode for the primary and secondary unit, respectively (Table S1-S3). Membrane samples were collected at specific locations of these modules, and termed as: a) Xiga virgin, b) Xiga right, c) Xiga center, d) Xiga left, e) Aquaflex virgin, f) Aquaflex top, g) Aquaflex middle, and h) Aquaflex bottom.

Ageing experiments (i.e., chemical cleaning of virgin membranes) were performed using the automated bench scale filtration system as previously described [23]. These experiments were conducted to assess the impact of chemical cleaning on the nanomechanical properties of membranes under controlled conditions. Two hollow fiber membranes of approximately 20 cm in length were potted in epoxy with one end cut open to allow inside out dead end filtration. The mini hollow fiber modules were soaked overnight in ultrapure water (resistivity: 18.2 MΩ·cm,

Millipore, USA). Prior to aging experiment, each module was flushed with ultrapure water and the pure water flux measured by the flux step method [24]. The chemical aging process was performed in inside-out filtration mode at 2 ml/min, 250 ppm NaOCl, and pH 12 for 10 h. The corresponding C.t exposition dose was 2500 $mg.h.L^{-1}$. The resulting membrane samples were termed as: i) Xiga virgin-chemically cleaned, and j) Aquaflex virgin-chemically cleaned.

2.2. Pyrolysis GC/MS, AR-FTIR, SEM, and EDS analysis of membrane samples

Used, virgin, and virgin-chemically cleaned UF hollow fiber membrane samples were dissected in halves with the assistance of an optic microscope under aseptic conditions to expose the inner-membrane surface. Virgin hollow fiber membranes were rinsed overnight in ultrapure water to remove any preservative/additive from their surfaces. All membrane samples were analyzed with a SEM Quanta 250 (FEI, Netherlands), working in environmental mode (ESEM). Pressure of water vapor was maintained at a constant value of 500 Pa allowing to remove any charging effect due to the non-conductive nature of the membranes. Chemical analyzes were conducted with an EDS detector from EDAX at the same condition as for ESEM imaging.

SEM high-resolution images of virgin membrane samples were acquired with a NovaNano SEM (FEI, Netherlands) working in immersion mode. First, membrane coupons were coated by sputtering a 10 nm thick layer of Au/Pd on the sample (PECS 628, Gatan) to avoid any charging effect due to the non-conductive nature of the samples. The images were analyzed by ImageJ software (National Institute of Health, USA) to determine pore size distribution. A threshold filter was used to discriminate pores from the membrane surface. The data was statistically analyzed by probability density functions to extract the pore size distribution. Also, cross-sectioning of membrane coupons were conducted using a FIB Quanta 3D dual beam FIB (FEI, Netherlands). Prior sample etching, a 50 nm protective layer of Au/Pd was deposited on the sample surface to preserve it from any damage caused by the ion beam. During this process,

samples were tilted 45° to enhance the coating of the cross-section. An additional protective layer was added on virgin coupon by depositing a 2.5 μm thick band (25 μm in length and 2.5 μm in width) on the Au/Pd layer using the gas injection system (GIS). Samples were then etched with FIB until a cross-section was observable. Finally, samples were coated with a 10 nm thick layer of Au/Pd to image the cross-section with high resolution SEM.

Foulant material recovered from Xiga virgin, Xiga center, Aquaflex virgin, and Aquaflex middle was subjected to Pyrolysis GC/MS analysis. Approximately 2.5 g of hollow fiber membranes dissected in halves were placed in 50 mL of ultrapure water and sonicated for 20 minutes. The aqueous phase was separated from the membrane fibers that easily settled and lyophilized. A small mass (few milligrams) of dry material was recovered from each sets of membrane. Approximately 0.5 mg of material was placed into the pyrolysis quartz tube and analyzed according to the flash pyrolysis protocol previously described [25].

2.3. Quantitative nanomechanical mapping (QNM)

Electrolyte solutions were prepared immediately before QNM experiments with ultrapure water and analytical grade reagents, and then filtered through a 0.22 μm membrane. A Dimension FastScan AFM (Bruker, USA) with an Icon Head were used for QNM analysis in solution of the following hollow fiber membrane samples: a) Xiga virgin, b) Xiga right, c) Xiga center, d) Xiga left, e) Xiga virgin-chemically cleaned, f) Aquaflex virgin, g) Aquaflex top, h) Aquaflex middle, i) Aquaflex bottom, and j) Aquaflex virgin-chemically cleaned. Sharp Nitride Lever AFM probes (SNL-10 A, k: 0.35 N/m, silicon nitride cantilever, Bruker, USA) were used. This type of probe was selected as a function of the characteristics of the membrane samples themselves (i.e., soft polymeric surface); specifically, based on the capacity of probes to cause enough deformation without damaging the sample while still retaining sensitivity. The calibration of the AFM probes

was conducted as follows. Briefly, the deflection sensitivity of the AFM probes was measured in air conditions and using mica as a control substrate. The spring constant (k) of the cantilevers were determined by the Thermal Tuning method, where deflection (V) was converted to force (nN) in accordance to Hooke's law [1]. The calculation of the radius of curvature of the probes was performed by scanning a titanium model surface (Bruker, USA) in air conditions via Tip Qualification function in the NanoScope Analysis Software V1.5 (Bruker, USA). Dissected membrane samples were immobilized concave up on a glass slide (i.e., to expose their inner-membrane surface) using double-sided tape. The glass slide was placed on the AFM stage and examined with the AFM high resolution camera to verify the correct position of the membrane sample and to locate a suitable area to scan at the center of the membrane (Figure S3). The QNM images of the membrane samples were acquired in 1 mM NaCl solution, at a scan rate of 0.5 kHz, over an area of 2×2 μm, and at 512 samples/line, while the ScanAssyst Auto Control was set ON (i.e., Peak Force Setpoint was automatically controlled by the software). Between 15 to 25 locations were randomly selected in every hollow fiber membrane sample for QNM analysis (i.e., the images shown in this study are considered as representative). The following parameters (channels) were generated: topography, Peak Force error, adhesion, deformation, dissipation, and LogDMT Modulus. Briefly, the deformation channel measures the maximum deformation (nm) of the polymeric structures of the membrane caused by the AFM probe during approaching regime, while the adhesion channel measures the maximum adhesion force (nN) between the membrane surface and AFM probe during retraction regime. The LogDMT Modulus describes the tensile elasticity of the polymeric structures of the membrane sample. In PeakForce^{TM} QNM^{TM}, Young's modulus is calculated using Derjaguin-Muller-Toporov (DMT) model (i.e., modified Hertzian model which considers adhesion forces between tip and surfaces) [26].

However, LogDMT Modulus (i.e., used in the current investigation) is calculated as the logarithm of the elastic modulus of the sample based on the DMT model. The Peak Force error channel generates a map of the peak force measured during the scan. Finally, the dissipation channel describes the mechanical energy lost per approaching-retracting cycle; for instance, pure elastic deformation of the membrane corresponds to very low dissipation. Every image of a specific characteristic (e.g., height, LogDMT Modulus, adhesion, dissipation, or deformation) was processed by Image Quadratic Mean (R_q) analysis and using NanoScope Software V1.5 (Bruker, USA). These values were statistically analyzed by probability density functions, where mean (μ) and variance (σ) were calculated. This statistical analysis provides the advantage of detecting peak values deviating from the distribution. These peak values would indicate regions of the membrane with properties differing from the probability density function (i.e., taking virgin membranes as a baseline). Every generated image was also inspected for the presence of foulants. Additionally, a topographic and phase analysis of the membrane samples by Soft-Tapping Mode™ (Bruker, USA) in air conditions using TESPA AFM probes (silicon tip, k: 42 N/m, f: 320 kHz, Bruker, USA) was conducted. Specifically, phase analysis provided supplementary information on the characteristics of membrane samples (i.e., phase imaging allows chemical mapping of surfaces based on these material differences).

3. Results and Discussion

3.1. Surface morphology of Xiga virgin and Aquaflex virgin membrane samples

As a first step, the morphology of Xiga virgin and Aquaflex virgin was studied. The pore size distribution was calculated from the SEM images (Figure S4a, S4d) using ImageJ software (Figure S4b). A statistical analysis by probability density function was used due to the heterogeneity of the pore size (Figure S4c, S4e). The mean pore size of Aquaflex virgin and Xiga virgin was calculated as 6.4 nm (i.e., σ: 0.63 and R^2: 0.99) and 7.0 nm (i.e., σ: 0.65 and R^2: 0.95), respectively. These values of pore size are smaller than those reported by the manufacturers (i.e., 20 nm nominal pore size for both membranes) and previous studies [27]. Topography (3D-height sensor) images acquired in tapping mode in air revealed the physically heterogeneous nature of the surfaces of Xiga virgin and Aquaflex virgin (Figure S5a, S6a). The roughness (R_{RMS}) of these membranes was measured as 14.3±3.7 nm (n=5) and 19.3±3.2 nm (n=6), respectively. Interestingly, phase images of Xiga virgin and Aquaflex virgin (i.e., chemical mapping of surfaces based on these material differences) suggested surfaces of different properties (Figure S5b, S6b).

3.2. Quantitative nanomechanical mapping of hollow fiber membrane samples

3.2.1. Xiga virgin and Aquaflex virgin hollow fiber membranes

The surface of Xiga virgin and Aquaflex virgin were analyzed by QNM. The following properties were collected: 1) Height sensor, 2) Peak Force error, 3) LogDMT Modulus, 4) Adhesion, 5) Deformation, and 6) Dissipation (Figure 1). Briefly, Xiga virgin and Aquaflex virgin displayed a low roughness, i.e., μ:13.7 nm (σ:0.43) and μ:16.7 nm (σ:0.17), respectively (Figure 2a, S14a, Table S4-S5), which were consistent to those obtained by tapping mode in air during morphological analysis.

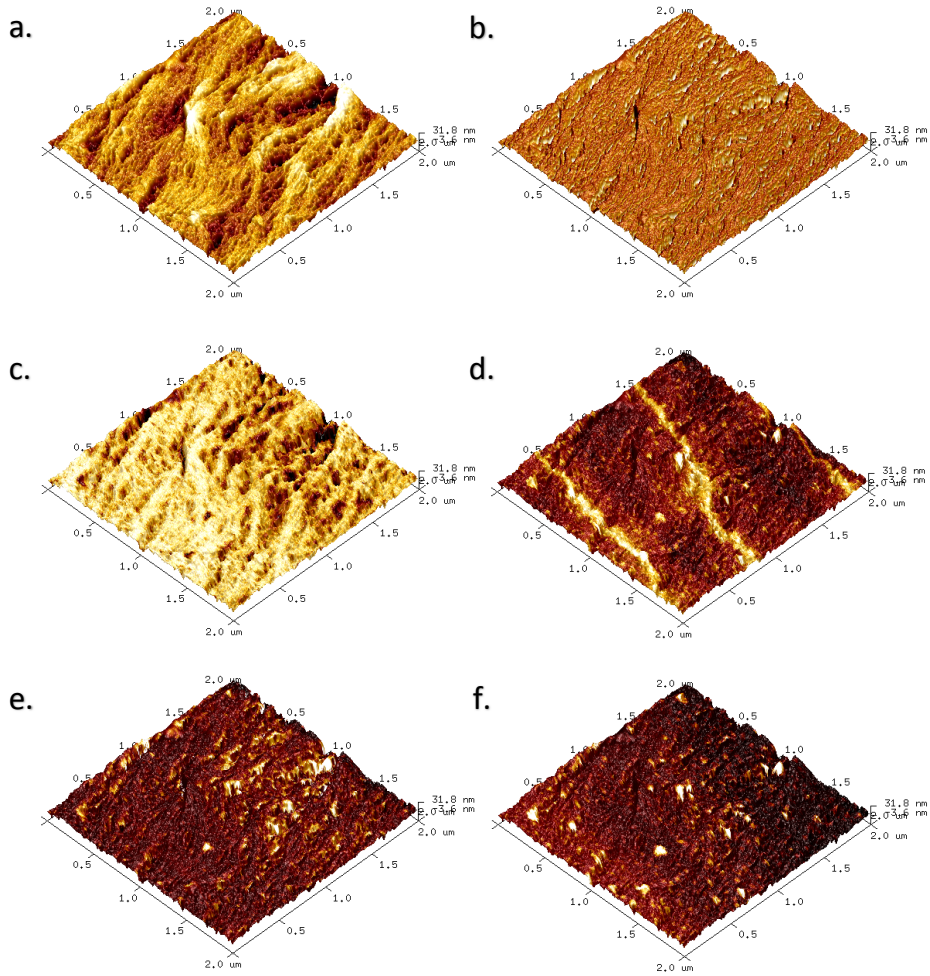

Figure 1. a) Height sensor, b) Peak Force error, c) LogDMT Modulus, d) Adhesion, e) Deformation, and f) Dissipation images of Aquaflex virgin membrane. Scan area: 2×2 µm.

Also, the surface morphologies of Xiga virgin and Aquaflex virgin acquired by QNM-Height sensor (Figure 1a, S7a, S8a) were similar to each other and to those observed in high-resolution SEM (Figure S4a, S4d). This result confirmed the capability of QNM to image surface structures at a nano-scale. The nanomechanical characteristics of virgin membranes extracted from QNM were statistically processed by normal distributions (i.e., Gauss, Log-Normal). This data could

not be processed by average and standard deviation due to the heterogeneity at the nano-scale of these mechanical properties; thus, resulting in high standard deviation values. Membranes have been previously described as physically and chemically heterogeneous surfaces by chemical force spectroscopy analysis [28].

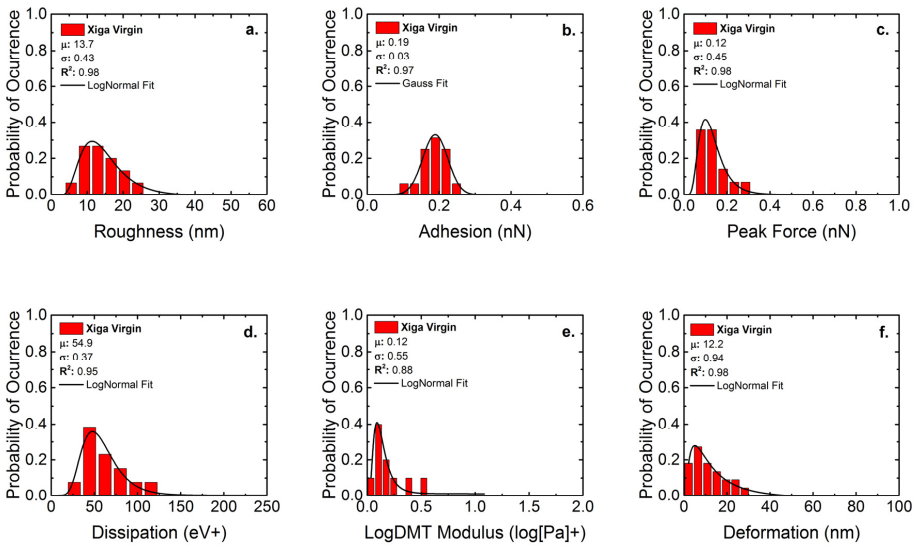

Figure 2. Probability density functions describing a) roughness, b) adhesion, c) Peak Force error, d) dissipation, e) LogDMT Modulus and f) deformation of Xiga virgin membrane

The mean adhesion, Peak Force error, dissipation, LogDMT Modulus, and deformation of Xiga virgin were 0.19 nN, 0.12 nN, 54.9 eV±, 0.12 Log[Pa]±, and 12.2 nm (Table S4, Figure 2a-f); while for Aquaflex virgin were 0.36 nN, 0.18 nN, 59.7 eV±, 0.067 Log[Pa]±, and 7.7 nm (Table S5, Figure S14a-f), respectively. No significant peak values were observed deviating from the probability density fitting functions for both virgin membranes. However, every nanomechanical map also evidenced surfaces of heterogeneous properties (Figure 1a-f, S7a-f, S8a-f). Aquaflex virgin showed higher Peak Force error and adhesion, as well as lower modulus and deformation than Xiga virgin. The values of dissipated energy were similar for both virgin membranes. These

results indicate virgin membranes of different properties; specifically, the surface of Aquaflex virgin showed more adhesion to the AFM silica probe and their polymeric structures were softer than those of Xiga virgin. Remarkably, QNM technique assisted in the discrimination of structural features differing from the surrounding polymeric structures, e.g., areas of dissimilar deformation (Figure 1d).

3.2.2. *Harvested hollow fiber membranes showing no adsorbed foulants*

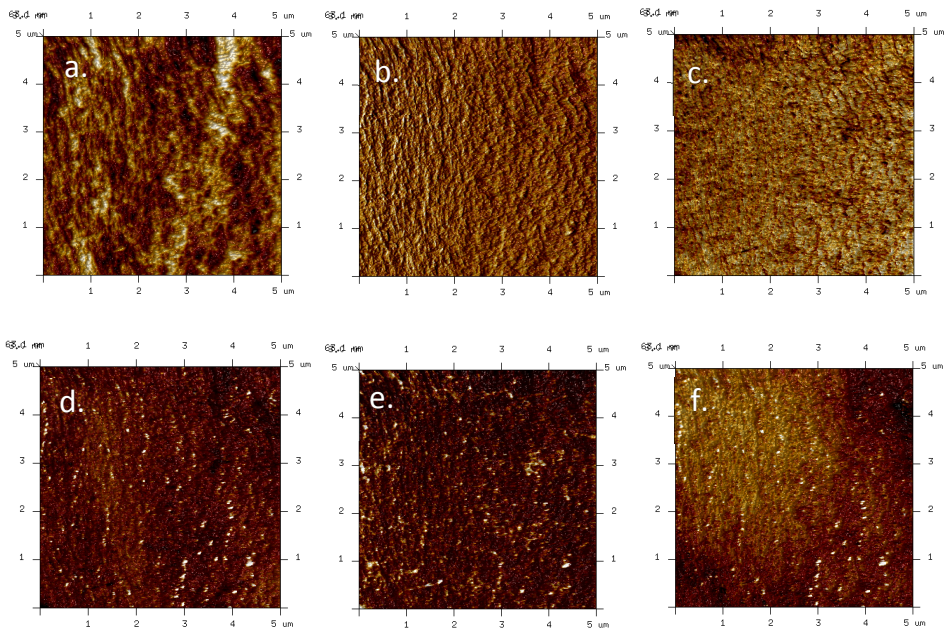

Figure 3. a) Height sensor, b) Peak Force error, c) LogDMT Modulus, d) Adhesion, e) Deformation, and f) Dissipation images of Xiga Center membrane. Scan area: 5×5 µm.

This section of the study focused on those harvested membrane samples that showed no adsorbed foulants (i.e., locations where the cleaning process seemed effective). The selection of these samples was conducted by a rigorous morphological analysis by QNM-height sensor (Figure 3a, 4a) and Soft-Tapping Mode™ (Figure S13b-c), and supported by adhesion and modulus analysis (Figure 3c-d, 4c-d). Clean membrane surfaces (i.e., showing pores and a characteristic polymeric

structure as seen in virgin membranes) were observed in the six types of membrane samples analyzed: Xiga right, Xiga center, Xiga left, Aquaflex top, Aquaflex middle, and Aquaflex bottom (Figure 3a, 4a, S13a), suggesting the efficiency of the CEB procedure. Their properties were statistically processed and analyzed by probability density functions (Figure S9-11, Figure S15-16, Table S4-S5). Briefly, the mean roughness of the three Xiga samples were similar to that of Xiga virgin (i.e., Xiga left: 18.5 nm, Xiga center: 19.4 nm, and Xiga right: 14.9 nm), where no value significantly deviated from the fitting function (Figure S9a, S10a, and S11a). The morphology of these samples showed physically heterogeneous at the nano-scale. Except for Xiga right (mean adhesion: 0.10 nN), the AFM tip mean adhesion to Xiga center and Xiga left were similar to that of Xiga virgin (Figure S9b, S10b, and S11b). Nevertheless, 30% and 28% of the recorded adhesions forces from Xiga center and Xiga right deviated from the fitting functions, where forces of up to 2.25 nN and 0.62 nN were observed, respectively (Figure S10b, S11b). These results suggest a change in surface characteristics in the samples displaying high adhesion forces (i.e., deviating from the probability density functions). Conversely, the mean LogDMT Modulus of Xiga center and Xiga right (i.e., 0.33 and 0.21 log[Pa]±, respectively) were higher than that of Xiga virgin (0.12 log[Pa]±). Besides, high LogDMT Modulus values of up to 0.7, 1.4, and 1.0 were recorded for Xiga left, Xiga right, and Xiga center, respectively (Figure S9e, S10e, and S11e); indicating that Xiga membranes displayed stiffer surfaces after fouling and chemical cleaning. Also, approximately 40% and 8% of the recorded LogDMT Modulus deviated from the fitting functions for Xiga left and Xiga Right, respectively. The mean deformation shown by chemically cleaned membranes was lower than that of Xiga virgin (i.e., although 40% and 12% of the recorded values for Xiga left and Xiga right deviated from the fitting functions, respectively) (Figures S9f, S10f, and S11f). As an outcome of fouling and

cleaning process, the stiffness of membranes increased and these surfaces would need more force to deform. This observation is also supported by the Peak Force values recorded (i.e., PeakForce^{TM} QNM mode uses peak force as a feedback signal; essentially, as a peak force Setpoint plus the error). The Peak Force of Xiga center, Xiga right, and Xiga left were higher than that of Xiga virgin (i.e., 0.34 nN, 0.17 nN, 0.20 nN, and 0.12 nN, respectively) (Figure 2c, S9c, S10c, and S11c). Finally, the mean dissipation (i.e., dissipated energy calculated by integrating the area between approaching and retracting curves) of Xiga right and Xiga left were lower than that of Xiga center (i.e., 36.6, 39.5, and 74.6 eV±, respectively). However, a considerable fraction of dissipation values of the three membrane samples deviated from the fitting functions, i.e., 26.6%, 22%, and 28% for Xiga left, Xiga center, and Xiga right, respectively. (Figure S9d, S10d, and S11d).

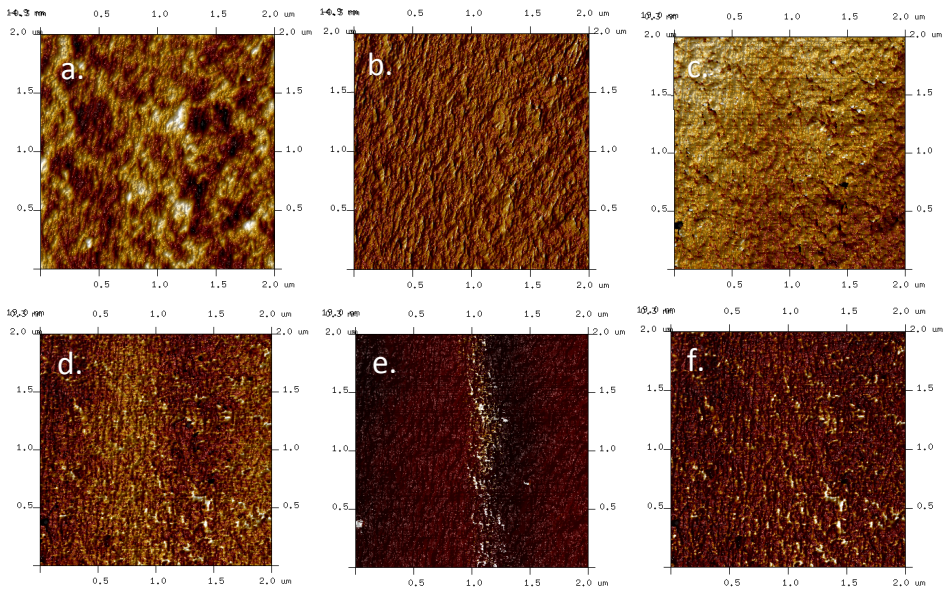

Figure 4. a) Height sensor, b) Peak Force error, c) LogDMT Modulus, d) Adhesion, e) Deformation, and f) Dissipation images of Aquaflex bottom membrane. Scan area: 2×2 μm.

Harvested Aquaflex membranes showing no foulant adsorption and the presence of polymeric structures and pores (Figure S13b-c) were also rigorously selected based on a morphological analysis by QNM-height sensor, Soft-Tapping Mode^{TM}, and SEM (i.e., this latter tool was used in the approximate locations where AFM images were recorded). Remarkably, AFM images were highly consistent with SEM micrographs, e.g., some Aquaflex samples displayed parallel structural features possibly caused by use, cleaning, or manufacturing processes (Figure 4a, S13d). Unlike Xiga samples, no significant value of the six properties measured for Aquaflex membranes significantly deviated from the probability density functions (Figure S15-S16). This result indicates that the values of the properties of clean Aquaflex membranes are less scattered than those of clean Xiga samples. The roughness of clean Aquaflex membranes were lower than those of Aquaflex virgin (Table S5), suggesting polymer degradation. The values of Peak Force, dissipation, and modulus of virgin and clean membranes were similar in magnitude. However, the adhesion of the AFM probe to Aquaflex bottom and Aquaflex middle were slightly higher than to Aquaflex top and Aquaflex virgin (i.e., 0.52 nN, 0.46 nN, 0.37 nN, and 0.36 nN, respectively). Additionally, the deformation of clean Aquaflex membranes (middle, top, and bottom) were slightly lower than that of virgin sample (i.e., 4.5 nm, 4.0 nm, 5.1 nm, and 7.7 nm, respectively). These results suggest that fouling and subsequent cleaning process did not significantly affect the surface properties of Aquaflex membranes. Remarkably, QNM proved again its versatility to detect regions of heterogeneous properties. For instance, small regions of different characteristics were discriminated in the LogDMT Modulus and adhesion channels, while undetected in the height sensor, Peak Force, and dissipation channels (Figure S18). These areas would be the result of fouling and cleaning process.

Fouling and chemical cleaning exerted different impacts on the surface characteristics of both Xiga and Aquaflex membranes. In the case of Aquaflex membranes, only few (nanomechanical) properties were affected by fouling and chemical cleaning. However, this impact was significantly higher on Xiga membranes, and was evidenced by a change in mean mechanical properties (i.e. considering virgin membrane characteristics as a baseline) and by peak values deviating from the probability density functions. Specifically, the Xiga membrane material (PES/PVP) might undergo physicochemical changes by reacting with the cleaning agent and by the adsorption of foulant molecules. The operation conditions would play an important role in this phenomenon (SI). Xiga modules were more extensively used than Aquaflex modules; filtering 57,150 m^3 and 2,155 m^3, respectively (Table S3). Additionally, Xiga modules were backwashed 267 times while Aquaflex only 37 times using the same CEB procedure (Table S2, S3). However, the average feed water quality of the secondary UF-stage (Aquaflex modules) was significantly lower than that of the primary UF-stage (Xiga Modules) (Table S1). These conditions would have exerted a higher impact on the polymeric surface of Xiga membranes.

3.2.3. Harvested membrane samples showing foulant adsorption

This second section presents an overview of the morphology and nanomechanical characteristics of membrane samples showing the presence of foulants after operation and CEB. The six samples analyzed: Xiga center, Xiga right, Xiga left, Aquaflex top, Aquaflex middle, and Aquaflex bottom showed adsorption of foulants. At a nano-scale, foulant adsorption was heterogeneous in both morphology and mechanical properties. Specifically, foulant partially coating a membrane surface (5×5 μm) (Figure 5), as well as foulant layers completely covering a scanning area (2×2 μm, 5×5 μm) (Figure 6, 7, S19-S22) were observed. In both cases, the morphology and mechanical properties of foulants highly differed from membranes and could

not be statistically described by probability density functions because of their high heterogeneity. Previous AFM investigations have observed the heterogeneous physicochemical characteristics of foulant layers during a kinetic study of RO membrane fouling [29].

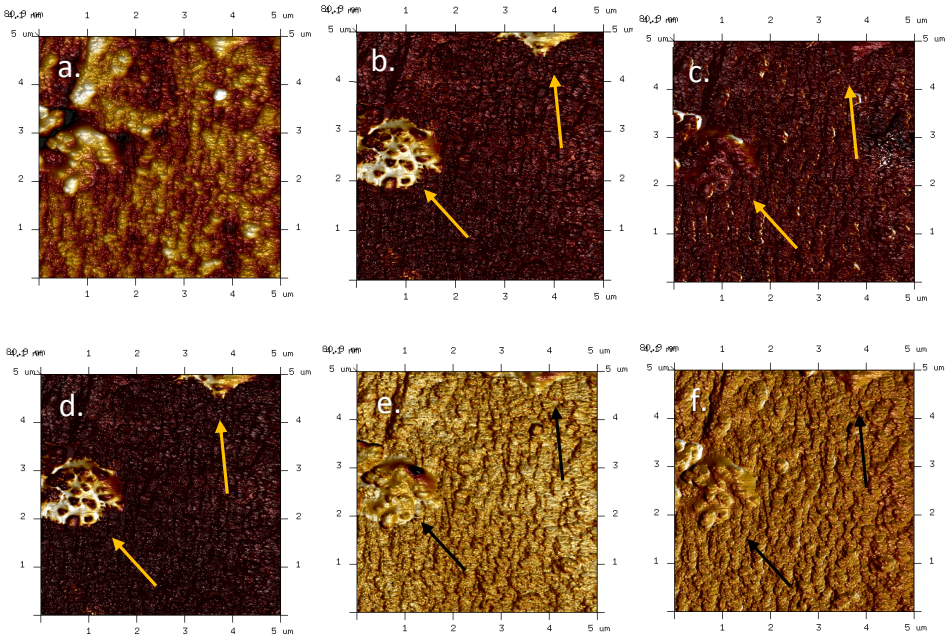

Figure 5. a) Height sensor, b) Adhesion, c) Deformation, d) Dissipation, e) LogDMT Modulus, and f) Peak Force error images of Xiga right membrane showing adsorption of foulant. Scan area: 5×5 µm.

QNM technique also proved to be a powerful tool for discriminating foulant from membrane surface due to their different mechanical properties (Figure 5). Briefly, the roughness of an apparently clean area of Xiga right was 26.6 nm (Figure 5a). Nevertheless, in the adhesion channel (Figure 5b) two small areas (yellow arrows) displaying high adhesion forces of up to 1.8 nN were evident. The values of Peak Force of the foulant were lower than those of the surrounding membrane (i.e., 0.151 nN vs. 0.241 nN) (Figure 5f). Also, the LogDMT Modulus (Figure 5e) of this foulant was lower than the surrounding membrane surface (i.e., 0.163 vs. 0.248 log[Pa]±, respectively), while the dissipation (605 eV±) was higher than the values

typically observed for virgin membrane. These results indicate a soft, adhesive, and less elastic foulant. Previous studies have reported foulants of lower elastic modulus compared to virgin membranes [17]. Moreover, the presence of this foulant after chemical cleaning and its high adhesion could be an indicative at a nano-scale of irreversible adsorption, as suggested in previous investigations [30, 31]. This QNM analysis also indicates that the detection of foulants solely using height sensor or phase channels can be incomplete and misleading.

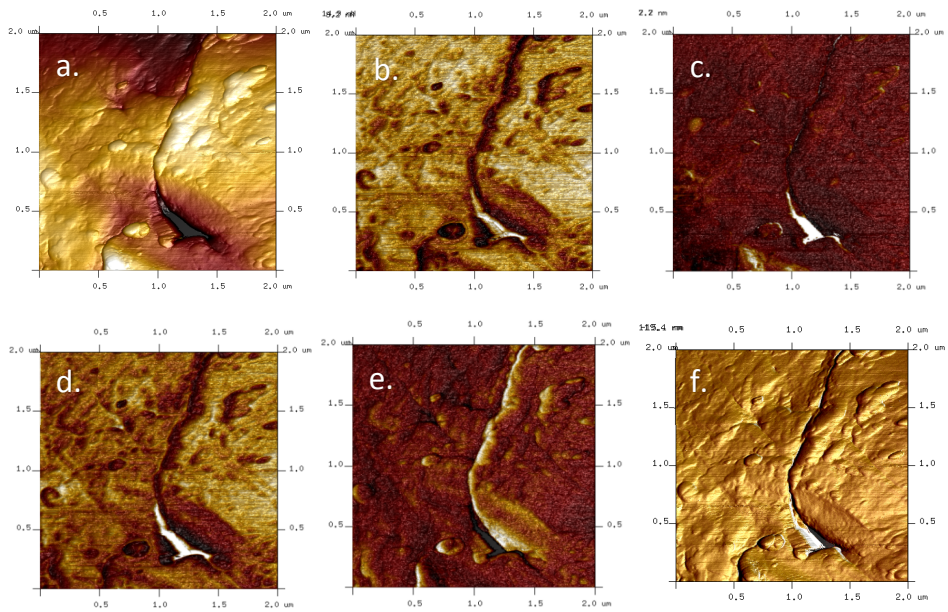

Figure 6. a) Height sensor, b) Adhesion, c) Deformation, d) Dissipation, e) LogDMT Modulus, and f) Peak Force error images of Xiga Left fouled membrane. Scan area: 2×2 µm.

Foulant layers showed a different morphology compared to that of Xiga virgin, where no pores and polymeric structures were observed (Figure 6, S19). First, the mean roughness of the foulant layers, e.g., 51.3 nm (Figure 6a) or 76.1 nm (Figure S19a), were higher than those of Xiga virgin (13.7 nm). The mean LogDMT Modulus values were variable, ranging from 0.065 (Figure 6e) to 0.237 log[Pa]± (Figure S19c). Remarkably, the magnitudes of the mean adhesion forces of these

foulant layers were considerably higher (>1 order of magnitude) than those of Xiga virgin, e.g., 1.87 nN (Figure 6b), 1.20 nN (Figure S19d). The dissipation energies also reached high values, e.g., 943 eV± (Figure 6d) or 588 eV± (Figure S19e). Also, SEM images (Figure S20) supported AFM morphology results. The heterogeneity of the fouling layers was evidenced in each SEM image acquired, ranging from full fouling layers (Figure S20a, S20c) to foulants partially coating the membrane surface, where the membranes pores could be distinguished (Figure S20b, S20d).

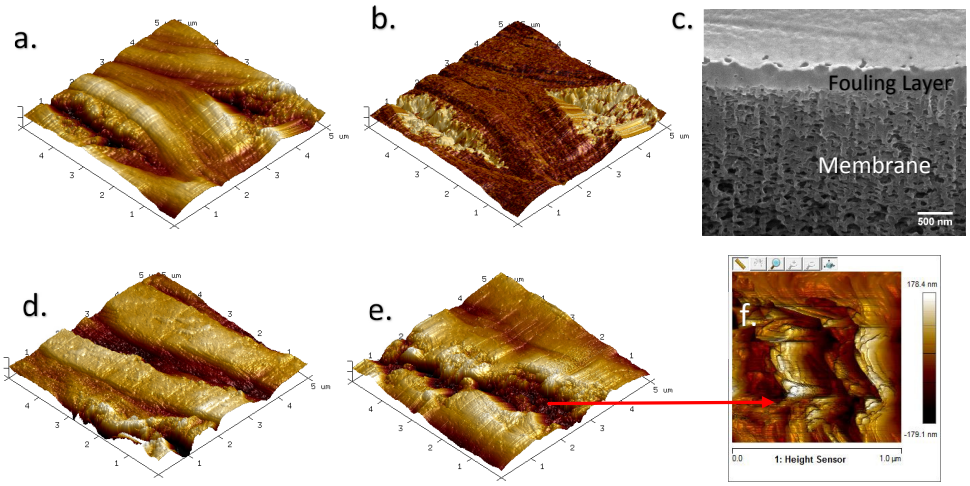

Figure 7. a) Height sensor and b) phase images of fouled Aquaflex middle (scan area: 5×5 µm). c) SEM image of cross section of Aquaflex middle showing a ~300 nm fouling layer. d) Height sensor of fouled Aquaflex membrane (scan area: 5×5 µm). Height sensor of e) fouled Aquaflex membrane showing micro-cracks (scan area: 5×5 µm) and exposing f) membrane surface (scan area: 1×1 µm).

Fouled Aquaflex membranes showed heterogeneous morphologies, surface characteristics, and mechanical properties (Figure 7, S21). Specifically, fouling layers were recorded totally covering scanning areas, where micro-cracks were also detected, i.e., also evidenced in SEM images (Figure S22a-b). Phase images of these fouling layers suggested materials of heterogeneous physicochemical characteristics (Figure 7b). Interestingly, these micro-cracks (i.e., observed in Aquaflex top, middle, and bottom samples) provided crucial information regarding the thickness of the fouling layers. The depth of these crack ranged from 23 nm to 239 nm, where no

membrane material was observed (Figure 7d). This latter result suggests fouling layers thicker than 239 nm. SEM images of cross sections showed foulant layers of similar thickness (Figure 7c). However, other samples showed cracks of few tens of nm where membrane material was detected (Figure 7e-f), indicating the high heterogeneity of fouling layers in terms of thickness. The mean roughness of the foulant layers of used Aquaflex membranes were highly variable, e.g., 130 nm (Figure 7a), 93 nm (Figure 7d), or 51 nm (Figure S21a); while the mean LogDMT Modulus values ranged from 0.081 (Figure S21c) to 0.372 log[Pa]± (Figure 7d). Although variable, the mean adhesion forces of these foulant layers were higher than Aquaflex virgin. However, the mean adhesion forces of foulant layers of Aquaflex membranes were also lower than those of Xiga membranes (e.g., ranging from 0.35 nN to 0.87 nN). Consequently, the dissipation energies of these foulant layers were also lower than those of Xiga membranes, i.e., 220 eV± to 598 eV±. Similar to fouled Xiga membranes, the fouling material of Aquaflex membranes was highly variable in characteristics and nanomechanical properties. Nevertheless, these results indicate that the fouling layer of Aquaflex membranes are rougher, less adhesive, and slightly stiffer that those of Xiga membranes. This latter result would be explained by the feed water quality of the UF-stages. The secondary UF-stage was fed by a more turbid water (coagulant flocs) with significantly higher Particulate Organic Carbon (POC) concentration, although both UF-stages were fed with similar Dissolved Organic Carbon (DOC) concentration (Table S3). Therefore, the remaining fraction of foulant after CEB in both modules may show different structural properties and composition. Nevertheless, it was not possible to statistically distinguish between the foulant layers of harvested Xiga membranes (center, right, or left module) or between the foulant layers of Aquaflex membranes (middle, top, or bottom modules) due to their high heterogeneity in nanomechanical properties.

The pyrolysis GC/MS analysis was conducted on the material recovered from Xiga center (Figure S23a). Comparison with the pyrochromatogram recorded from Xiga virgin (Figure S23b) confirmed the presence of foulant material accumulated at the membrane surface. Pyrolysis by-products such as cyclopentenone and methyl cyclopentenone were indicators of the presence of polysaccharides in the organic layer. Toluene, styrene, pyrrole, and methyl pyrrole confirmed the presence of proteins. The detection of furanmethanol, a DNA pyro-fragment, is an indicator of living or recently dead microorganisms [32]. This pyrolysis fingerprint demonstrates the biological origin (biofilm) of the foulant. Similar results were obtained with the foulant recovered from Aquaflex middle, however the pyro-fragments showed lower relative abundance.

Energy Dispersive X-ray spectroscopy (EDS) analysis of Xiga virgin and Aquaflex virgin revealed peaks of Carbon, Oxygen, and Sulfur present in the spectra (Figure S24), and would originate from the membrane material. The generated spectra and elements (%) observed can be considered as representative of clean membrane surfaces. Conversely, the EDS spectra and elemental analysis of harvested membranes (e.g., Xiga center, Xiga Right) showed additional peaks of Si, Cl, Ca, and Fe (Figure S24), suggesting the presence of foulants.

3.2.4. Change of nanomechanical properties of virgin membranes after chemical cleaning

Xiga virgin and Aquaflex virgin samples were subjected to chemical cleaning. The goal of this control experiment was to study the change in nanomechanical properties of virgin membrane surfaces due to reaction with cleaning agents. The values of mechanical properties of Xiga virgin-chemically cleaned and Aquaflex virgin-chemically cleaned were statistically processed by probability density functions (i.e., Lognormal and Gauss distributions) where no peak values significantly deviated from the fitting functions (Figure S12a-f, S17a-f). A similar trend was observed only for Xiga Virgin and Aquaflex Virgin (Figure 2, S14). Briefly, the mean roughness and adhesion forces of Xiga virgin-chemically cleaned were similar to those of Xiga virgin,

while its mean LogDMT modulus was double in magnitude. Along with a slightly lower deformation and a higher Peak Force, this latter result suggests a stiffer Xiga membrane surface after chemical cleaning. However, an important conclusion extracted from these results is that the type of chemical cleaning process performed in the current investigation did not impact the nanomechanical properties of Xiga virgin to the extent of causing peak values highly deviating from the probability density functions as seen in clean Xiga left, Xiga center, and Xiga Right samples (Figure S9-S11). Thus, these peak values in the mechanical properties of clean Xiga membranes might be the result of a combination of the effect of adsorbed foulant molecules and a more stringent chemical cleaning in the pilot unit (i.e., higher C.t, higher number of CEBs, and acid cleaning) (Table S2-S3). In the same way, the nanomechanical properties of Aquaflex were not significantly impacted by the ageing process. The C.t of the ageing process was similar to that of the chemical cleaning used at the pilot unit. The roughness of Aquaflex virgin-chemically cleaned was lower than Aquaflex virgin (i.e., 8.2 nm and 16.7 nm, respectively), also observed for harvested Aquaflex membranes showing no adsorbed material. Also, the magnitudes of Peak Force, LogDMT Modulus, and adhesion were slightly higher for Aquaflex virgin-chemically cleaned, while the magnitudes of deformation and dissipation were similar for both samples (Table S5). These results indicate that both Aquaflex and Xiga membranes would maintain their mechanical properties after a chemical cleaning process as performed in the current study.

The PES/PVP composition of the Xiga and Aquaflex virgin membranes was recorded by FT-IR analysis (Figure S25a-b). The spectrum recorded for the Xiga virgin-chemically cleaned hollow fiber showed no significant reduction in the intensity of the peak at 1650 cm^{-1} and corresponding to C=O vibration of the PVP amide group, while a strong decrease was observed for the Aquaflex virgin-chemically cleaned membrane. This result indicates a more noticeable impact of

the chemical oxidation on Aquaflex virgin. Interestingly, a small intensity band centered at 1720 cm^{-1} was detected after chemical oxidation (OCl^- at pH 12) of Xiga virgin, which can be attributed to the formation of sucinimide groups [33]. This finding demonstrates that the polymeric matrix of the two PVP/PES hollow fiber membranes present significant structural differences. These latter results are in agreement with the different nanomechanical properties measured between Xiga virgin and Aquaflex virgin membranes (Table S4-S5).

3.2.5. Link between macroscopic properties and nanomechanical characteristics of membranes

The permeability (Figure S26a-b) and transmembrane pressure (TMP) (Figure S26c-d) of UF-1 (Xiga membranes) and UF-2 (Aquaflex membranes) modules were measured during pilot-scale operation. These two macroscopic properties did not experience a significant change during operation. This result indicates that the applied CEB was always able to recover the initial TMP and permeability of the hollow fiber membranes. Also, this result suggests an insignificant presence of irreversible foulants on membrane surface, and membrane characteristics slightly affected by the pilot-scale operation. Although some nanomechanical properties of the membrane samples (Xiga samples) experienced a change during operation (i.e., statistically deviating from the probability density functions), these changes did not considerably impact their macroscopic properties. As future research, a study of nanomechanical characteristics of membranes where their macroscopic properties are affected by pilot-scale operation, would be highly recommended to complement the knowledge achieve in the current study.

4. Conclusions

The current investigation conducted a rigorous analysis of the nanomechanical properties of UF hollow fiber membranes harvested from pilot scale units after extended operation. A Quantitative Nanomechanical Mapping (QNM) of adhesion, dissipation, deformation, and LogDMT modulus

was generated while simultaneously acquiring a topographic image of the membrane samples. From these results, the following key conclusions can be outlined:

- The nanomechanical properties of Xiga and Aquaflex membranes revealed virgin membranes of different characteristics. Also, every nanomechanical map of Xiga virgin and Aquaflex virgin evidenced surfaces of heterogeneous properties at the nano-scale.
- Aquaflex virgin showed higher adhesion to the silica AFM probe, as well as lower deformation and modulus (softer polymeric structure) than Xiga virgin. The dissipation of both virgin membranes was similar, indicating comparable elastic deformation.
- Fouling and chemical cleaning (CEB) exerted different impacts on harvested membranes during pilot tests. The nanomechanical properties of harvested Aquaflex membranes showing no adsorption of foulants were slightly affected compared to Aquaflex virgin. Conversely, the properties of Xiga membranes were highly impacted.
- The operation conditions, feed water quality, and CEB processes would have played an important role in the change of nanomechanical properties of Xiga membranes. Xiga modules were backwashed 267 times while Aquaflex only 37 times using the same CEB procedure. Also, the secondary UF-stage was fed by a more turbid water (coagulant flocs) with a higher POC concentration. Both UF-stages were fed with similar DOC content water.
- The morphology and nanomechanical properties of foulants adsorbed on membranes were highly heterogeneous. Unlike virgin and clean membranes, no statistical analysis could be performed to describe the mechanical properties of foulant layers due to their heterogeneity.
- Foulant layers displayed high roughness, adhesion forces, and dissipation (low elastic deformation), and variable modulus. Interestingly, the fouling layer of Aquaflex membranes

were rougher, less adhesive, and slightly stiffer that those of Xiga membranes. This difference in characteristics would be explained by the feed water quality of the UF-stages.

- The permeability and TMP of both UF-1 and UF-2 modules did not experience a significant change during operation. The change in nanomechanical characteristics of membranes did not considerable impact their macroscopic properties.

Acknowledgements

The financial support of the GenoMembran-project funded by The Swedish Water and Wastewater Association (Swedish Water Development, SVU), Norrvatten, and VIVAB is gratefully acknowledged. Pentair X-Flow is acknowledged for the provision of various test modules and general membrane investigations.

Supplementary Data

Supplementary data associated with this article can be found in the online version at:

References

[1] H.J. Butt, B. Cappella, M. Kappl, Force measurements with the atomic force microscope: Technique, interpretation and applications, Surf. Sci. Rep., 59 (2005) 1-152.
[2] L. Gutierrez, T.H. Nguyen, Interactions between rotavirus and natural organic matter isolates with different physicochemical characteristics, Langmuir, 29 (2013) 14460-14468.
[3] C. Aubry, L. Gutierrez, J.P. Croue, Coating of AFM probes with aquatic humic and non-humic NOM to study their adhesion properties, Water Res., 47 (2013) 3109-3119.
[4] L. Gutierrez, C. Aubry, M. Cornejo, J.-P. Croue, Citrate-Coated Silver Nanoparticles Interactions with Effluent Organic Matter: Influence of Capping Agent and Solution Conditions, Langmuir, 31 (2015) 8865-8872.
[5] L. Gutierrez, C. Aubry, L. Dramas, P. Aimar, J.-P. Croue, Characterization of Skeletonema costatum intracellular organic matter and study of nanomechanical properties under different solution conditions, Colloids Surf., A, 506 (2016) 154-161.
[6] L. Gutierrez, C. Aubry, R. Valladares Linares, J.-P. Croue, Natural organic matter interactions with polyamide and polysulfone membranes: Formation of conditioning film, Colloids Surf., A, 477 (2015) 1-8.
[7] D. Lu, T. Zhang, L. Gutierrez, J. Ma, J.-P. Croué, Influence of Surface Properties of Filtration-Layer Metal Oxide on Ceramic Membrane Fouling during Ultrafiltration of Oil/Water Emulsion, Environ. Sci. Technol., 50 (2016) 4668-4674.
[8] P. Maivald, H.J. Butt, S.A.C. Gould, C.B. Prater, B. Drake, J.A. Gurley, V.B. Elings, P.K. Hansma, Using force modulation to image surface elasticities with the atomic force microscope, Nanotechnology, 2 (1991) 103.

[9] A. Rosa-Zeiser, E. Weilandt, S. Hild, O. Marti, The simultaneous measurement of elastic, electrostatic and adhesive properties by scanning force microscopy: pulsed-force mode operation, Meas. Sci. Technol., 8 (1997) 1333.
[10] M.R. Vanlandingham, S.H. McKnight, G.R. Palmese, R.F. Eduljee, J.W. Gillespie, J.R.L. McCulough, Relating elastic modulus to indentation response using atomic force microscopy, J. Mater. Sci. Lett., 16 (1997) 117-119.
[11] B. Foster, New atomic force microscopy (AFM) approaches life sciences gently, quantitatively, and correlatively, Am. Lab., 44 (2012) 24-28.
[12] K. Sweers, K. van der Werf, M. Bennink, V. Subramaniam, Nanomechanical properties of α-synuclein amyloid fibrils: a comparative study by nanoindentation, harmonic force microscopy, and Peakforce QNM, Nanoscale Research Letters, 6 (2011) 270.
[13] T.J. Young, M.A. Monclus, T.L. Burnett, W.R. Broughton, S.L. Ogin, P.A. Smith, The use of the PeakForce TM quantitative nanomechanical mapping AFM-based method for high-resolution Young's modulus measurement of polymers, Meas. Sci. Technol., 22 (2011) 125703.
[14] J. Adamcik, A. Berquand, R. Mezzenga, Single-step direct measurement of amyloid fibrils stiffness by peak force quantitative nanomechanical atomic force microscopy, Appl. Phys. Lett., 98 (2011) 3701.
[15] P. Trtik, J. Kaufmann, U. Volz, On the use of peak-force tapping atomic force microscopy for quantification of the local elastic modulus in hardened cement paste, Cem. Concr. Res., 42 (2012) 215-221.
[16] A. Pakzad, J. Simonsen, R.S. Yassar, Gradient of nanomechanical properties in the interphase of cellulose nanocrystal composites, Compos. Sci. Technol., 72 (2012) 314-319.
[17] L.C. Powell, N. Hilal, C.J. Wright, Atomic force microscopy study of the biofouling and mechanical properties of virgin and industrially fouled reverse osmosis membranes, Desalination, 404 (2017) 313-321.
[18] S. Homaeigohar, J. Koll, E.T. Lilleodden, M. Elbahri, The solvent induced interfiber adhesion and its influence on the mechanical and filtration properties of polyethersulfone electrospun nanofibrous microfiltration membranes, Separation and Purification Technology, 98 (2012) 456-463.
[19] M.A. Shannon, P.W. Bohn, M. Elimelech, J.G. Georgiadis, B.J. Marinas, A.M. Mayes, Science and technology for water purification in the coming decades, Nature, 452 (2008) 301-310.
[20] L. Zeman, A. Zydney, Microfiltration and Ultrafiltration: Principles and Applications, Taylor & Francis, 1996.
[21] N. Porcelli, S. Judd, Chemical cleaning of potable water membranes: A review, Separation and Purification Technology, 71 (2010) 137-143.
[22] A. Keucken, Y. Wang, K.H. Tng, G.L. Leslie, K.M. Persson, S.J. Köhler, T. Spanjer, Evaluation of novel hollow fibre membranes for NOM removal by advanced membrane autopsy, Water Science and Technology: Water Supply, 16 (2016) 628-640.
[23] A. Touffet, J. Baron, B. Welte, M. Joyeux, B. Teychene, H. Gallard, Impact of pretreatment conditions and chemical ageing on ultrafiltration membrane performances. Diagnostic of a coagulation/adsorption/filtration process, J. Membr. Sci., 489 (2015) 284-291.
[24] E. Filloux, H. Gallard, J.-P. Croue, Identification of effluent organic matter fractions responsible for low-pressure membrane fouling, Water Res., 46 (2012) 5531-5540.
[25] P.F. Greenwood, L.J. Berwick, J.P. Croué, Molecular characterisation of the dissolved organic matter of wastewater effluents by MSSV pyrolysis GC–MS and search for source markers, Chemosphere, 87 (2012) 504-512.
[26] B.V. Derjaguin, V.M. Muller, Y.U.P. Toporov, Effect of contact deformations on the adhesion of particles, J. Colloid Interface Sci., 53 (1975).
[27] N. Lee, G. Amy, J.-P. Croué, H. Buisson, Identification and understanding of fouling in low-pressure membrane (MF/UF) filtration by natural organic matter (NOM), Water Res., 38 (2004) 4511-4523.

[28] J.A. Brant, K.M. Johnson, A.E. Childress, Characterizing NF and RO membrane surface heterogeneity using chemical force microscopy, Colloids Surf., A, 280 (2006) 45-57.
[29] M.T. Khan, C.-L. de O Manes, C. Aubry, L. Gutierrez, J.P. Croue, Kinetic study of seawater reverse osmosis membrane fouling, Environ. Sci. Technol., 47 (2013) 10884-10894.
[30] H. Yamamura, K. Kimura, T. Okajima, H. Tokumoto, Y. Watanabe, Affinity of functional groups for membrane surfaces: Implications for physically irreversible fouling, Environ. Sci. Technol., 42 (2008) 5310-5315.
[31] T. Merle, L. Dramas, L. Gutierrez, V. Garcia-Molina, J.-P. Croué, Investigation of severe UF membrane fouling induced by three marine algal species, Water Res., 93 (2016) 10-19.
[32] A. Bruchet, C. Rousseau, J. Mallevialle, Pyrolysis-GC-MS for investigating high-molecular-weight THM precursors and other refractory organics, Journal (American Water Works Association), (1990) 66-74.
[33] Y. Hanafi, P. Loulergue, S. Ababou-Girard, C. Meriadec, M. Rabiller-Baudry, K. Baddari, A. Szymczyk, Electrokinetic analysis of PES/PVP membranes aged by sodium hypochlorite solutions at different pH, J. Membr. Sci., 501 (2016) 24-32.

Paper II Supplementary information

4.1. Full-scale plant operation and raw water source quality

Kvarnagården WTP (Sweden) is the largest water treatment plant of Varberg municipality. Its raw water consists of 80% surface water and 20% groundwater. The raw water quality parameters were described in Table S1. The surface water source is an oligotrophic lake surrounded by mixed woodland. In line with the ongoing browning of lakes and rivers in large parts of Scandinavia, a rising trend in color and COD has also been observed in the surface water collected by Kvarnagården WTP. No significant reduction of humic substances was achieved with the current treatment process consisting of rapid sand filtration, pH-adjustment, and UV-irradiation.

Due to an increased tendency of browning in raw water and new demands for multiple microbiological barriers, extensive long-term pilot trials for enhanced NOM removal (i.e., which included UF in combination with coagulation) were initiated. In November of 2016 the WTP was upgraded with an UF facility. Briefly, the full-scale plant consists of a two-stage UF membrane filtration process with coagulation upfront of a primary UF membrane stage providing NOM retention and barrier function (Figure S1a). The goal of coagulation was to create flocs of limited size (i.e., pinflocs). Through a minimal dose of inorganic coagulant, the porosity and backwash capacity of the membrane fouling layer were expected to increase. Consequently, even under adverse water quality feed conditions, the filtration flux, backwash, chemical cleaning frequency, and Trans-Membrane Pressure (TMP) would be stabilized and eventually improved. However, because of coagulant residues in the backwash water and limited site sewer capacity, a second stage UF membrane system was installed to increase the recovery of the plant to > 99%.

4.2. Pilot-scale plant operation and sampling points for membrane autopsy

During the construction period of the membrane plant, an extensive test facility was established for various long-term trials to verify the membrane performance of the full-scale design (Figure

S1b). A 40-foot-long container pilot (i.e., designed as a stand-alone unit to mimic the full-scale UF plant) was operated from January 2015 to August 2016 with a treatment capacity of 170 m^3/day (150 m^3/day permeate production). The pilot plant consisted of: a) a primary UF unit (horizontal dead-end filtration) with two membrane modules: Pentair X-Flow XIGA, 55 m^2, and b) a secondary UF unit (vertical dead-end filtration) with one membrane module: Pentair X-Flow AQUAFLEX, 55 m^2. Membranes samples were collected at specific locations of these modules (Figure S2). Raw water was supplied from the intake of the WTP to the primary feed tank by a pressurized line. The feed pump took water from the primary feed tank during filtration of the primary UF unit. If pH correction of feed water was required, coagulants were added in front of the feed pump with optional dosing points for H_2SO_4 and NaOH. During filtration, UF permeate was directed to the permeate tank and discharged by overflow to recipient. Permeate water from the permeate tank was used during backwash of UF units. The backwash waste from the primary UF unit was directed to the secondary feed tank. Chemical waste from the CEB program at the primary UF unit was directed to the chemical waste discharge. During the backwash of the primary UF unit, the secondary feed tank was filled. When the primary UF unit finished a filtration cycle and the secondary feed tank reached a specific level, the primary UF unit stopped after a final backwash. Subsequently, the secondary UF unit was activated and started production. During filtration of the secondary UF unit, the feed pump took water from the secondary feed tank. The secondary permeate was directed to the permeate tank. During the hydraulic cleaning (feed water plus permeate) of the secondary UF unit, the waste water was directed to the non-chemical waste discharge. The waste water of the CEB for the secondary unit was directed to the chemical waste discharge. One feed pump was available for both the primary and the secondary units. Also, one backwash pump ass available for both the primary and

secondary UF units. For the CEBs, dosing systems for H_2SO_4, NaOH, and NaOCl were available. The dosing points were placed in the backwash inlet line and were common for both the primary and the secondary unit. Additionally, caustic/acidic cleaning conditions, module replacements, operational conditions during long-term test runs, and Membrane key performance parameters during pilot trials were summarized in Tables S1-S3.

Table S1. Average feed water quality of primary and secondary UF-stage

Parameters	**Unit**	**Range (UF-stage 1)**	**Range (UF-stage 2)**
Temperature	(°C)	4 – 6.5	3.8 – 4.9
pH	(-)	7.4 – 7.8	7.0 – 7.3
Turbidity	(NTU)	0.3 – 2.0	20.0 – 25.0
Hardness	ºdH	1,6 – 2.0	1.4 – 1.7
Alkalinity	(mg/l HCO_3)	20 – 26	15 – 18
COD	(mg/l O_2)	1.8 – 4.4	19 – 34
TOC	(mg C/l)	2.3 – 8.3	22.0 – 28.0
DOC	(mg C/l)	2.0 – 8.1	4.0 – 4.9
UV_{254}	(/5 cm)	0.235 – 1.083	1.530 – 6.370
Pt-Co	(mg Pt/l)	8 – 31	15 – 25
Conductivity	(µS/cm)	110 – 130	100 – 107
Iron	(mg/l Fe)	0.028 – 0.420	0.480 – 0.680
Manganese	(mg/l Mn)	0.023 – 0.072	0.037 – 0.048
Calcium	(mg/l Ca^{2+})	8.1 - 10	6.6 – 8.3
Magnesium	(mg/l Mg^{2+})	2.2 – 2.9	2.2 – 2.5
Sodium	(mg/l Na^{+})	6.2 – 9.1	8.1 – 9.8
Ammonium	(mg/l $NH4^{+}$)	0.01 – 0.11	0.01 – 0.10
Sulphate	(mg/l SO_4^{2-})	12 – 15	8.5 – 10.0
Nitrate	(mg/l NO_3^{-})	1.5 – 1.8	1.4 – 1.6

Table S2. Operating conditions and process parameters during long-term pilot trials

Parameters	Unit	UF primary	UF secondary
Max. filtration time (t_F)	(min)	90	60
Max. filtration volume	(m^3)	8.4	1.65
Filtration flux (J_F)	(L $m^{-2}h^{-1}$)	65 - 70	45
v_{CF} (cross flow velocity)	(m s^{-1})	-	0.5
R (recovery during filtration)	(%)	100	100
t_{BW} (backwash time)	(s)	30	30
J_{BW} (backwash flux)	(L $m^{-2}h^{-1}$)	250	250
t_{CEFF} (CEB interval)	(days)	1.5	5
CEB1 dosing solution (caustic)	(-)	250-300 ppm NaOCl @ pH 12.2 with NaOH	250-300 ppm NaOCl @ pH 12.2 with NaOH
CEB2 dosing solution (acidic)	(-)	475 mg/l H_2SO_4 @ pH 2.4	475 mg/l H_2SO_4 @ pH 2.4
t_{SOAK} (Soak time CEB)	(min)	10	10

Table S3. Membrane key performance parameters during pilot trials

Parameters	Unit	UF primary	UF secondary
Permeability	(l/m^2hbar @ 20 °C)	350 - 380	600 - 220
Trans membrane pressure	(bar)	0.18 – 0.28	0.12 – 0.25
Total number of CEBs	(-)	267	37
Module age before replacement	(months)	12	14
Installation date	(-)	01.02.2015	08.05.2015
Autopsy date	(-)	17.02.2016	01.08.2016
Total filtration volume (feed water)	m^3	57.150*	2.155**

*150m^3/d x 381 days

** 4,8 m^3/d x 449 days

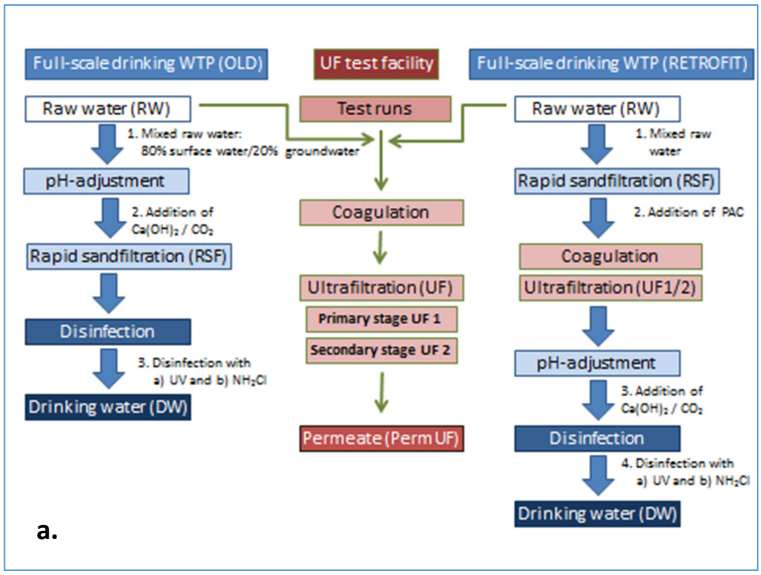

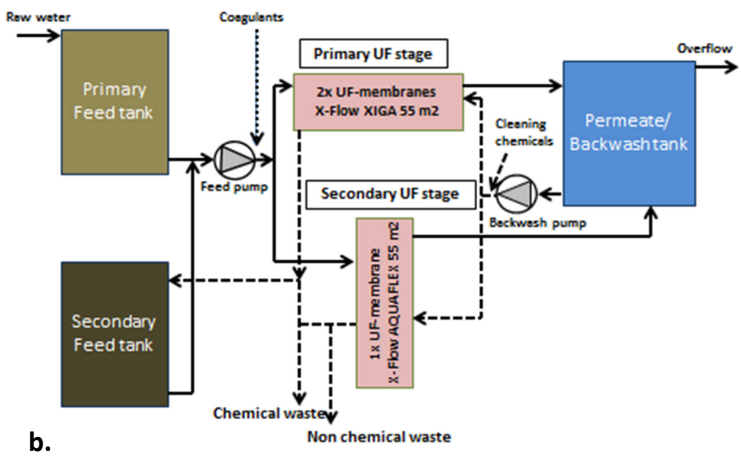

Figure S1: a) Treatment train for full-scale process and test facility at Kvarnagården WTP and b) Schematic overview of the pilot plant process

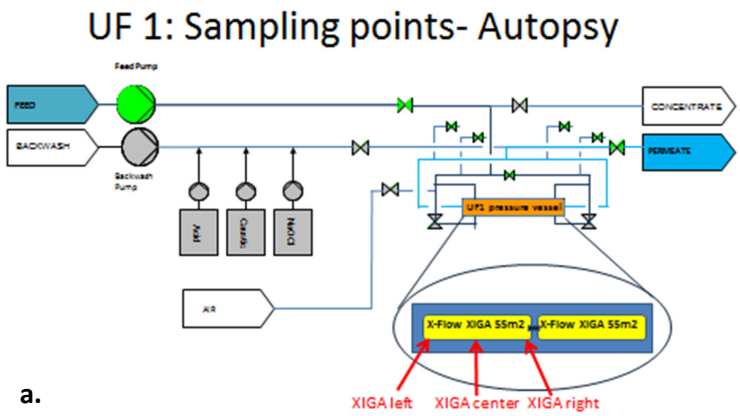

a.

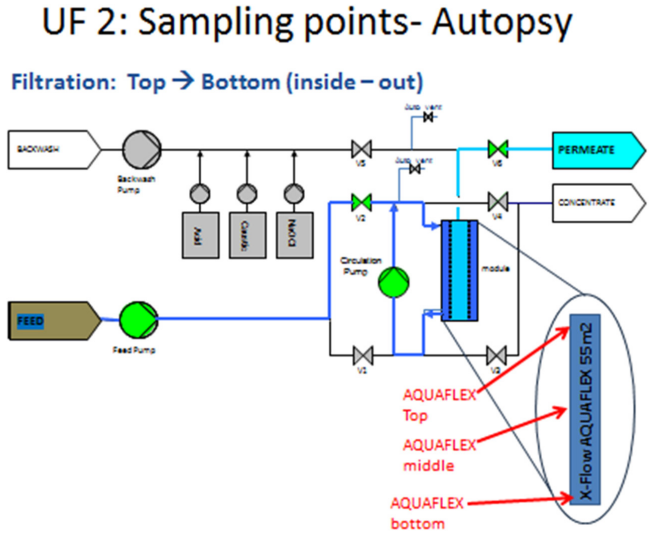

b.

Figure S2: Sampling points for membrane autopsy for a) Xiga and b) Aquaflex membranes

Table S4. Values of mechanical properties of Xiga hollow fiber membrane samples. Mean (μ), variance (σ), and coefficient of determination (R^2) were obtained by probability density functions.

	Roughness (nm)	Peak Force (nN)	LogDMT Modulus (log[Pa]±)	Adhesion Force (nN)	Deformation (nm)	Dissipation (eV±)
Xiga Virgin						
Mean (μ):	13.7	0.12	0.12	0.19	12.2	54.9
Variance (σ):	0.43	0.45	0.55	0.03	0.94	0.37
R^2:	0.98	0.98	0.88	0.97	0.98	0.95
n:	16	16	16	16	16	16
Xiga Center						
Mean (μ):	19.4	0.34	0.33	0.18	8.9	74.6
Variance (σ):	5.06	0.62	0.53	0.07	0.75	0.47
R^2:	0.99	0.99	0.98	0.95	0.98	0.97
n:	23	23	23	23	23	23
Xiga Right						
Mean (μ):	14.9	0.17	0.21	0.10	4.2	36.6
Variance (σ):	0.24	0.28	0.65	0.51	0.67	22.5
R^2:	0.93	0.99	0.99	0.99	0.99	0.97
n:	25	25	25	25	25	25
Xiga Left						
Mean (μ):	18.5	0.20	0.11	0.15	10.6	39.5
Variance (σ):	0.34	0.44	0.18	0.05	0.20	7.97
R^2:	0.98	0.99	0.99	0.88	0.98	0.97
n:	15	15	15	15	15	15
Xiga Virgin Chem-cleaned						
Mean (μ):	11.0	0.16	0.25	0.15	9.5	53.8
Variance (σ):	0.33	0.11	0.53	0.18	0.75	0.35
R^2:	0.97	0.97	0.97	0.96	0.97	0.98
n:	16	16	16	16	16	16

Table S5. Values of mechanical properties of Aquaflex hollow fiber membrane samples. Mean (μ), variance (σ), and coefficient of determination (R^2) were obtained by probability density functions.

	Roughness (nm)	Peak Force (nN)	LogDMT Modulus (log[Pa]±)	Adhesion Force (nN)	Deformation (nm)	Dissipation (eV±)
Aquaflex Virgin						
Mean (μ):	16.7	0.18	0.07	0.36	7.7	59.7
Variance (σ):	0.17	0.26	0.22	0.21	0.5	0.19
R^2:	0.97	0.94	0.98	0.97	0.99	0.93
n:	15	15	15	15	15	15
Aquaflex Middle						
Mean (μ):	11.1	0.14	0.07	0.46	4.5	52.6
Variance (σ):	0.4	0.07	0.43	0.24	0.3	0.31
R^2:	0.98	0.93	0.95	0.82	0.98	0.98
n:	16	16	16	16	16	16
Aquaflex Top						
Mean (μ):	6.2	0.18	0.06	0.37	4.0	48.7
Variance (σ):	0.32	0.36	0.14	0.14	0.48	0.5
R^2:	0.98	0.97	0.99	0.99	0.99	0.97
n:	16	16	16	16	16	16
Aquaflex Bottom						
Mean (μ):	8.8	0.19	0.08	0.52	5.1	54.3
Variance (σ):	0.39	0.22	0.39	0.35	0.29	0.43
R^2:	0.96	0.94	0.98	0.92	0.97	0.94
n:	16	16	16	16	16	16
Aquaflex Virgin Chem-cleaned						
Mean (μ):	8.2	0.22	0.10	0.42	5.9	55.6
Variance (σ):	0.2	0.15	0.29	0.22	0.45	54.1
R^2:	0.97	0.97	0.99	0.99	0.99	0.93
n:	15	15	15	15	15	15

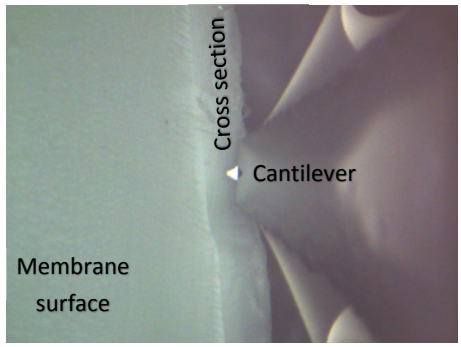

Figure S3. Membrane surface area selected for quantitative nanomechanical mapping. Images were acquired using the high-resolution camera of the AFM.

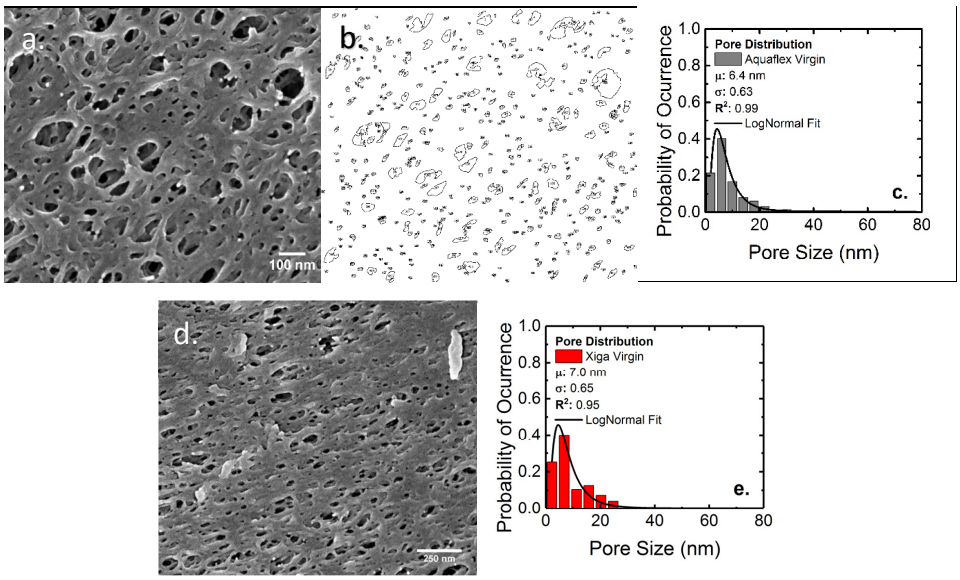

Figure S4. a) SEM image of Aquaflex virgin membrane surface. b) Pores discriminated from membrane surface by ImageJ software. c) Probability density functions describing the pore size distribution of Aquaflex virgin. d) SEM image of Xiga virgin membrane surface. e) Probability density functions describing the pore size distribution of Xiga virgin.

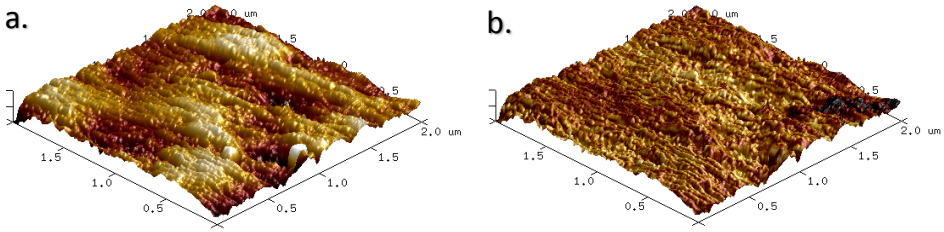

Figure S5. 3D-height sensor of a) topography and b) phase images of Xiga Virgin. Images were acquired in tapping mode in air. Scan area: 2×2 μm.

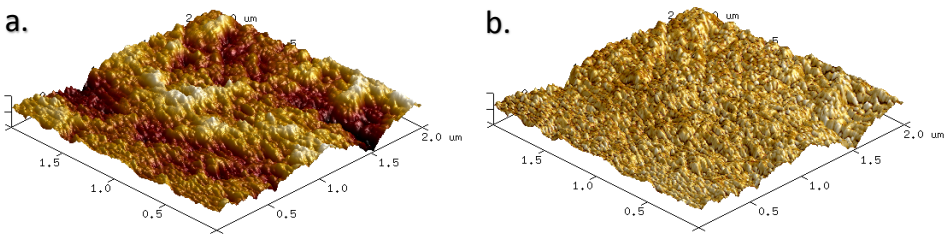

Figure S6. 3D-height sensor of a) topography and b) phase images of Aquaflex Virgin. Images were acquired in tapping mode in air. Scan area: 2×2 μm.

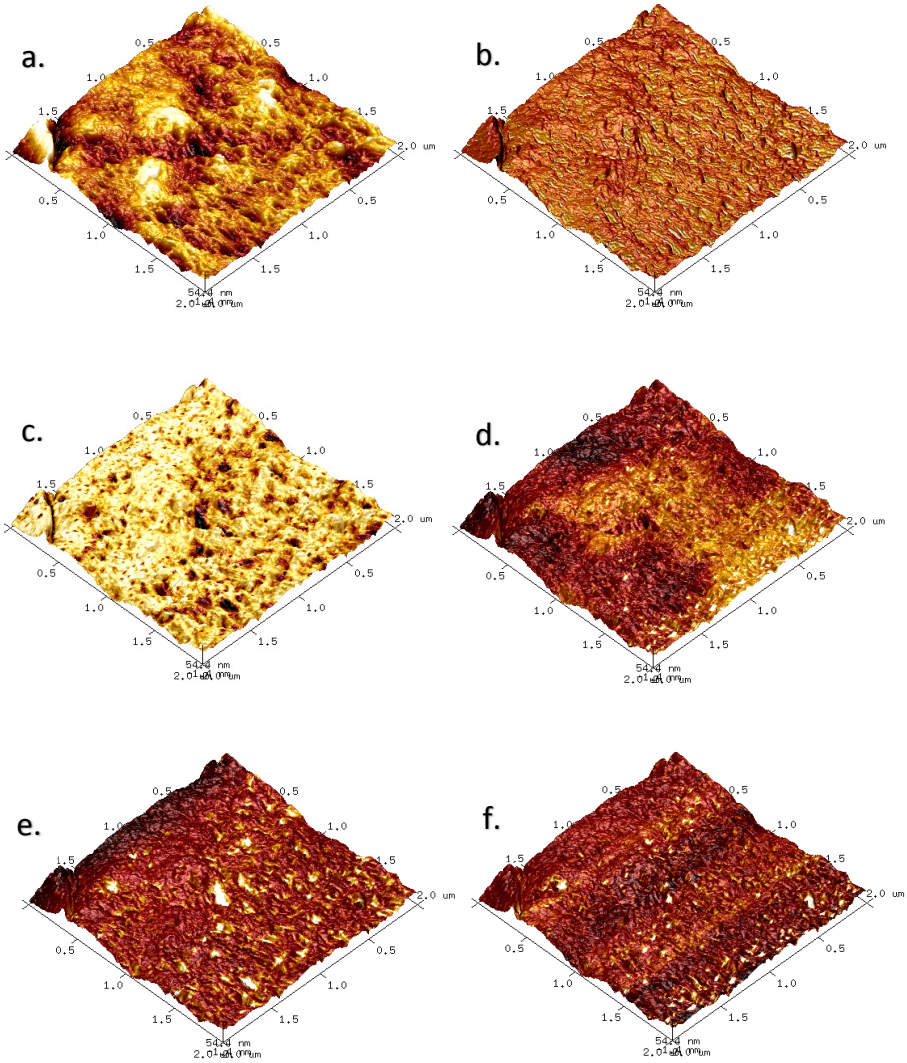

Figure S7. a) Height sensor, b) Peak Force error, c) LogDMT Modulus, d) Adhesion, e) Deformation, and f) Dissipation images of Xiga virgin membrane. Scan area: 2×2 µm.

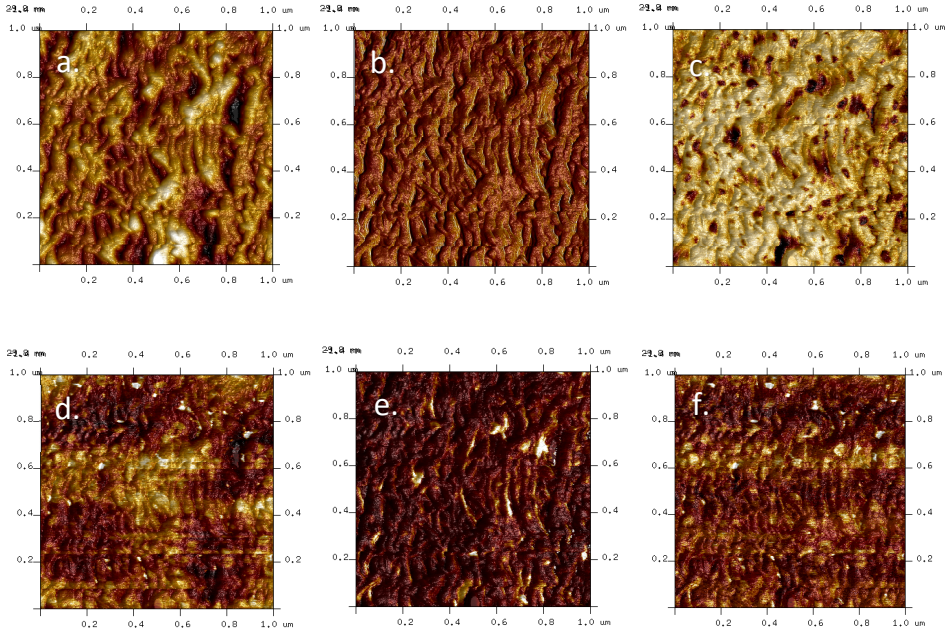

Figure S8. a) Height sensor, b) Peak Force error, c) LogDMT Modulus, d) Adhesion, e) Deformation, and f) Dissipation images of Xiga virgin membrane. Scan area: 1×1 μm.

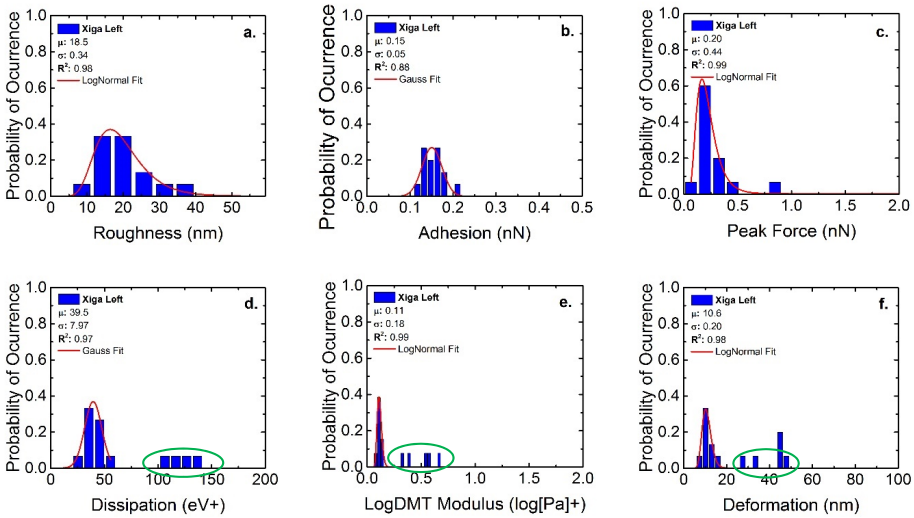

Figure S9. Probability density functions describing a) roughness, b) adhesion, c) Peak Force error, d) dissipation, e) LogDMT Modulus and f) deformation of Xiga left membrane

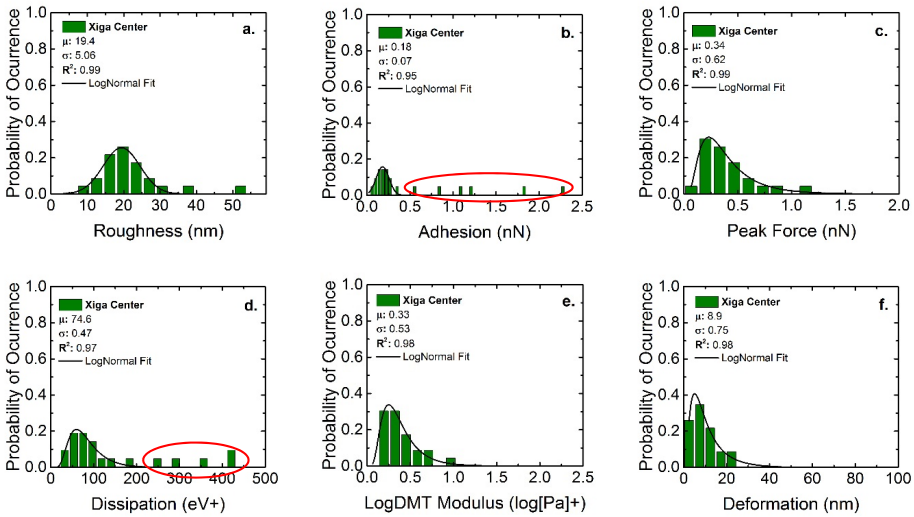

Figure S10. Probability density functions describing a) roughness, b) adhesion, c) Peak Force error, d) dissipation, e) LogDMT Modulus and f) deformation of Xiga center membrane

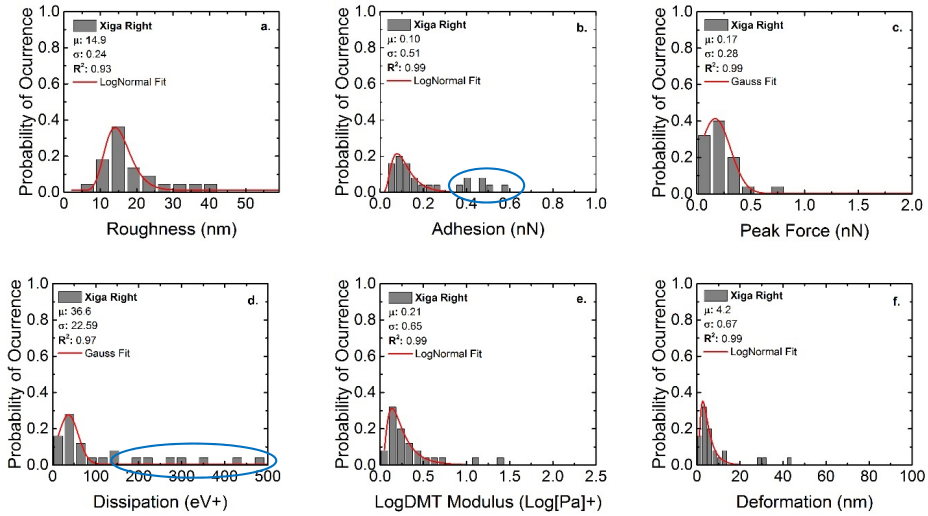

Figure S11. Probability density functions describing a) roughness, b) adhesion, c) Peak Force error, d) dissipation, e) LogDMT Modulus and f) deformation of Xiga right membrane

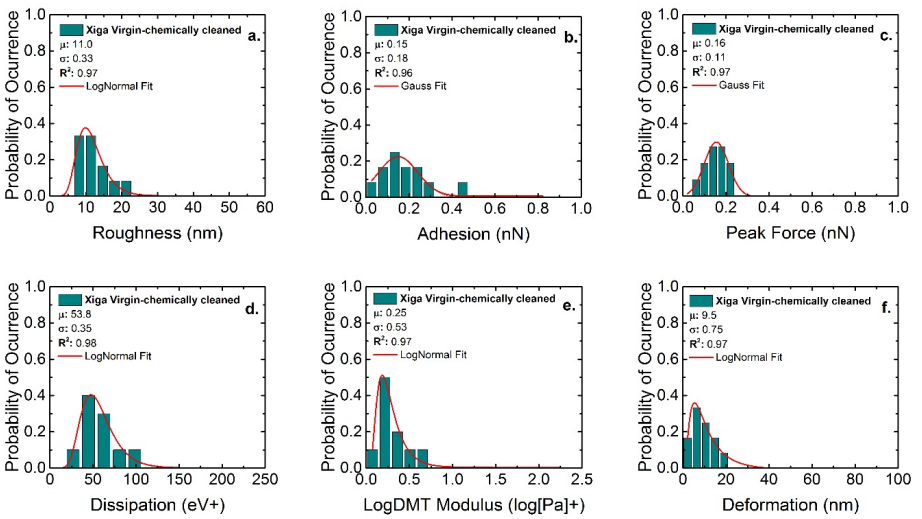

Figure S12. Probability density functions describing a) roughness, b) adhesion, c) Peak Force error, d) dissipation, e) LogDMT Modulus and f) deformation of Xiga virgin-chemically cleaned membrane

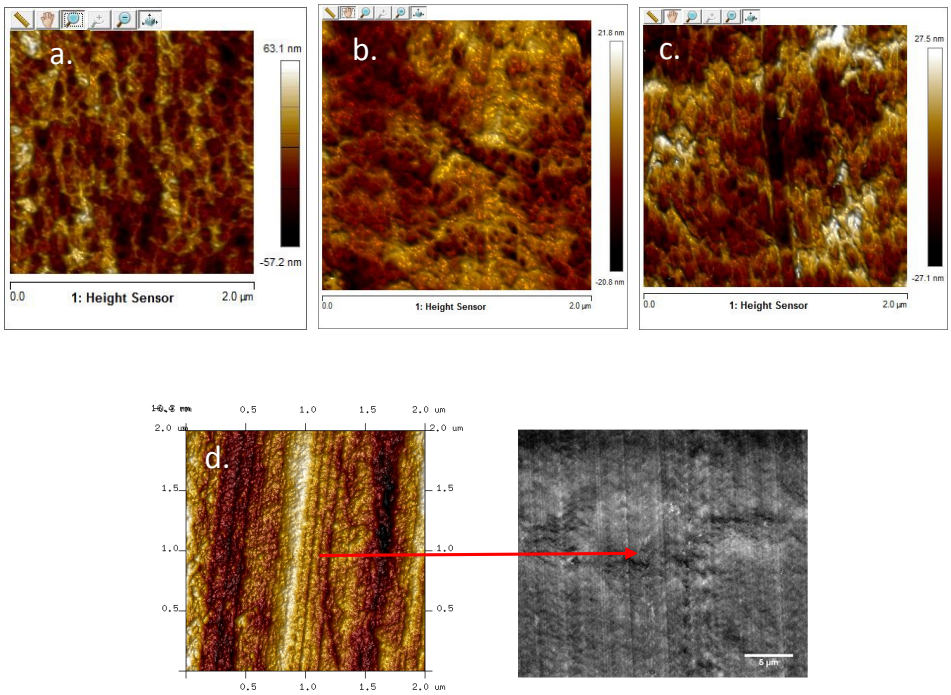

Figure S13. a) QNM-Height sensor image of Xiga center. High resolution images acquired in Soft-Tapping mode of b) Aquaflex virgin and c) Aquaflex middle. QNM-Height Sensor and SEM images depicting the morphology of d) Aquaflex bottom

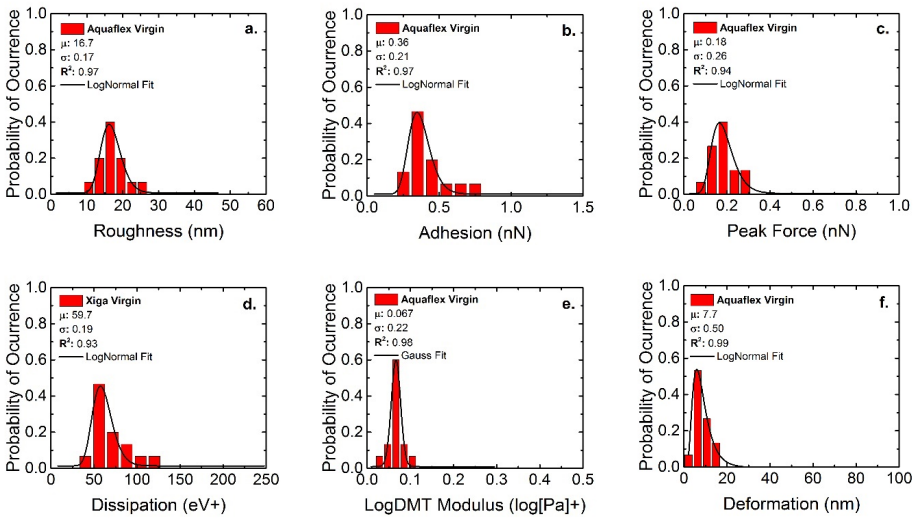

Figure S14. Probability density functions describing a) roughness, b) adhesion, c) Peak Force error, d) dissipation, e) LogDMT Modulus and f) deformation of Aquaflex Virgin membrane.

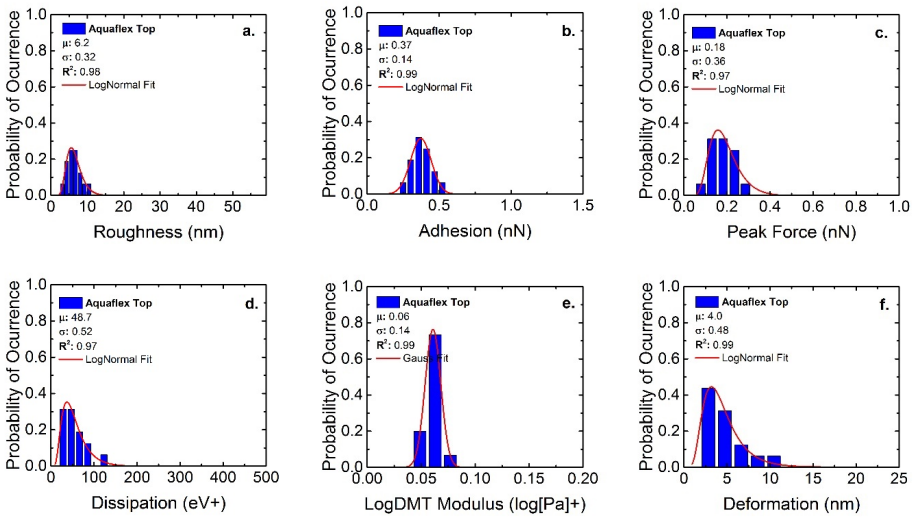

Figure S15. Probability density functions describing a) roughness, b) adhesion, c) Peak Force error, d) dissipation, e) LogDMT Modulus and f) deformation of Aquaflex Top membrane.

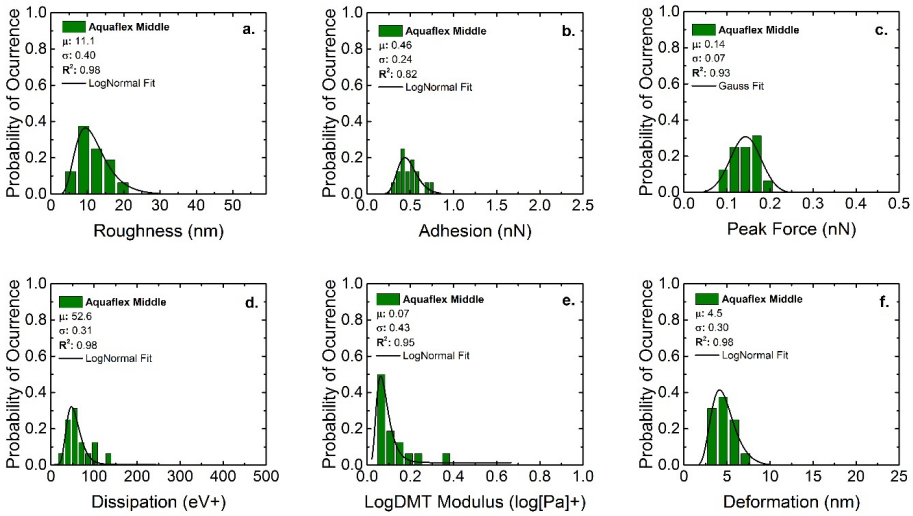

Figure S16. Probability density functions describing a) roughness, b) adhesion, c) Peak Force error, d) dissipation, e) LogDMT Modulus and f) deformation of Aquaflex Middle membrane.

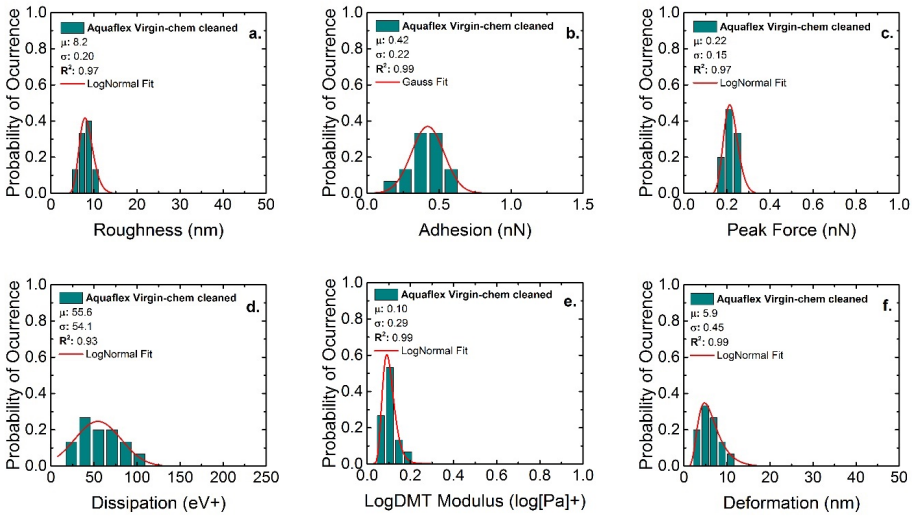

Figure S17. Probability density functions describing a) roughness, b) adhesion, c) Peak Force error, d) dissipation, e) LogDMT Modulus and f) deformation of Aquaflex virgin-chemically cleaned membrane.

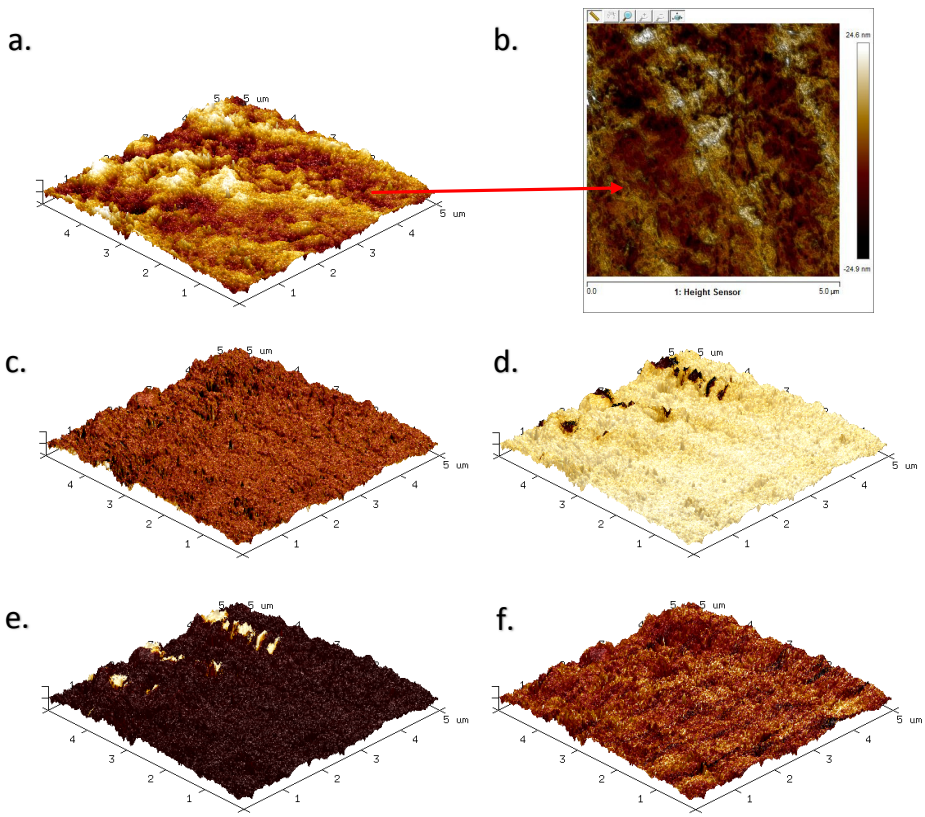

Figure S18. a) 3D-Height sensor, b) 2D-Height sensor, c) Peak Force error, d) LogDMT Modulus, e) Adhesion, and f) Dissipation images of Aquaflex Top membrane. Scan area: 5×5 µm.

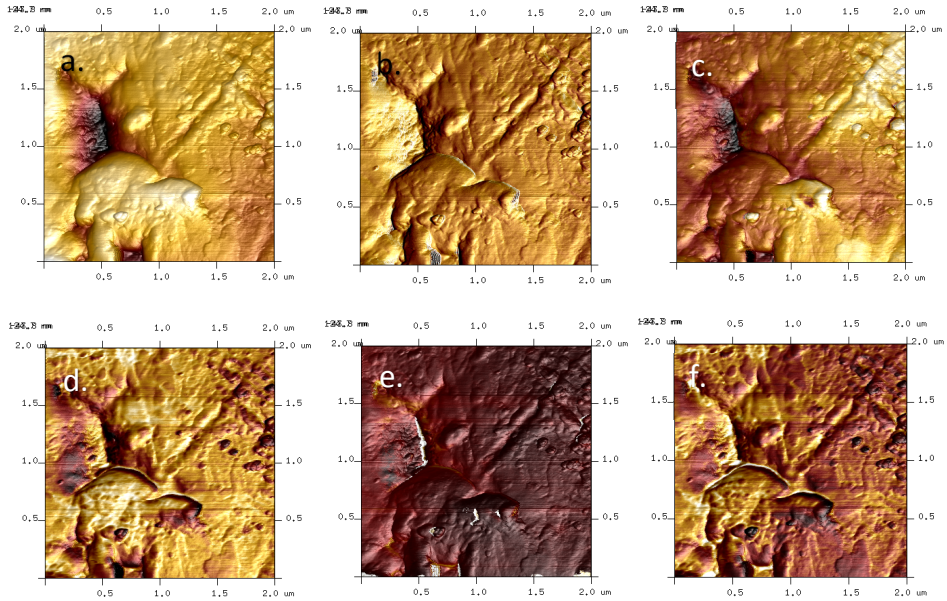

Figure S19. a) Height sensor, b) Peak Force error, c) LogDMT Modulus, d) Adhesion, e) Deformation, and e) Dissipation images of Xiga left fouled membrane. Scan area: 2×2 μm.

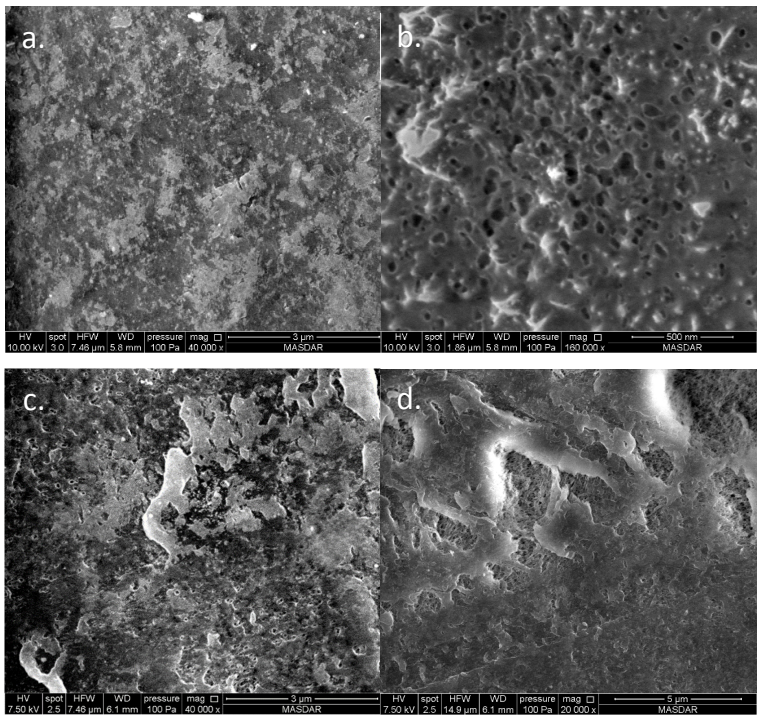

Figure S20. SEM images of a-b) fouled Xiga left membrane, and c-d) fouled Xiga center membrane.

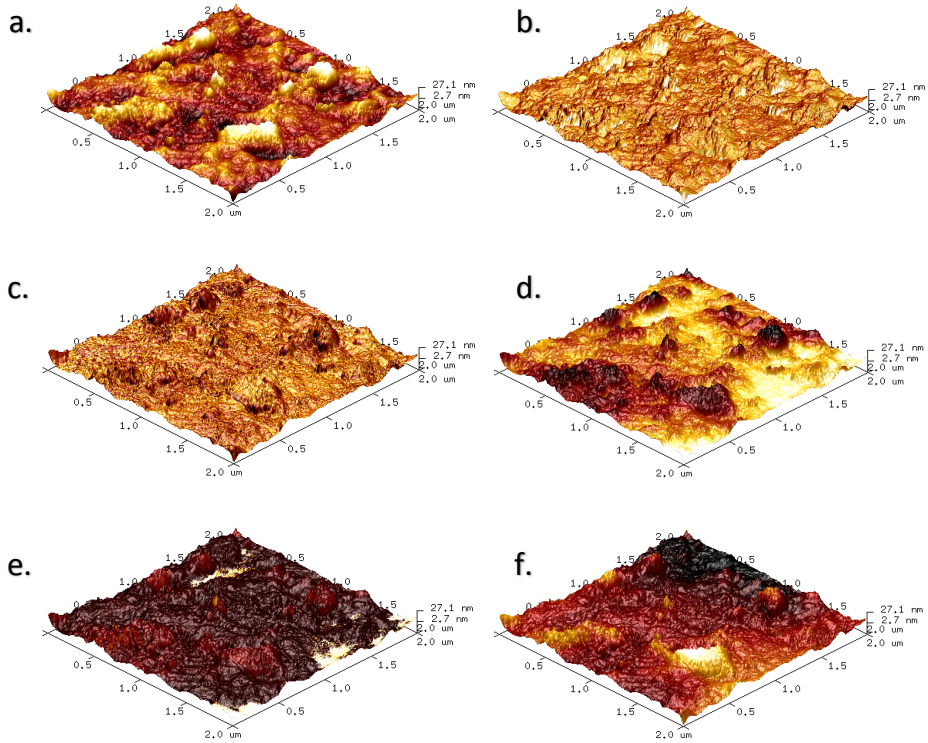

Figure S21. a) Height sensor, b) Peak Force error, c) LogDMT Modulus, d) Adhesion, e) Deformation, and e) Dissipation images of fouled Aquaflex Middle membrane. Scan area: 2×2 µm.

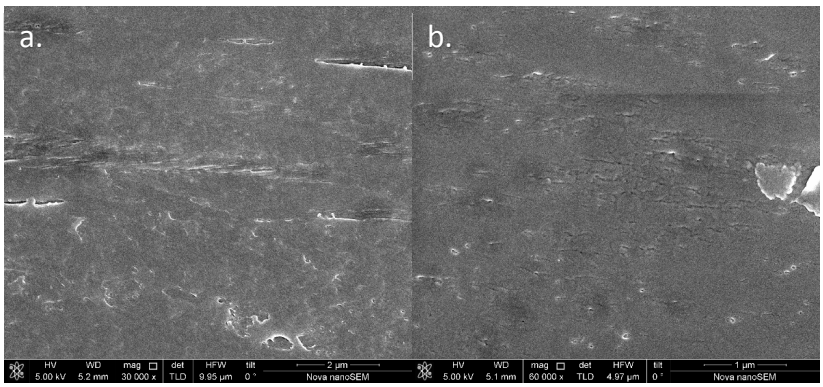

Figure S22. SEM images of fouled a) Aquaflex bottom and b) Aquaflex middle membranes, showing micro-cracks.

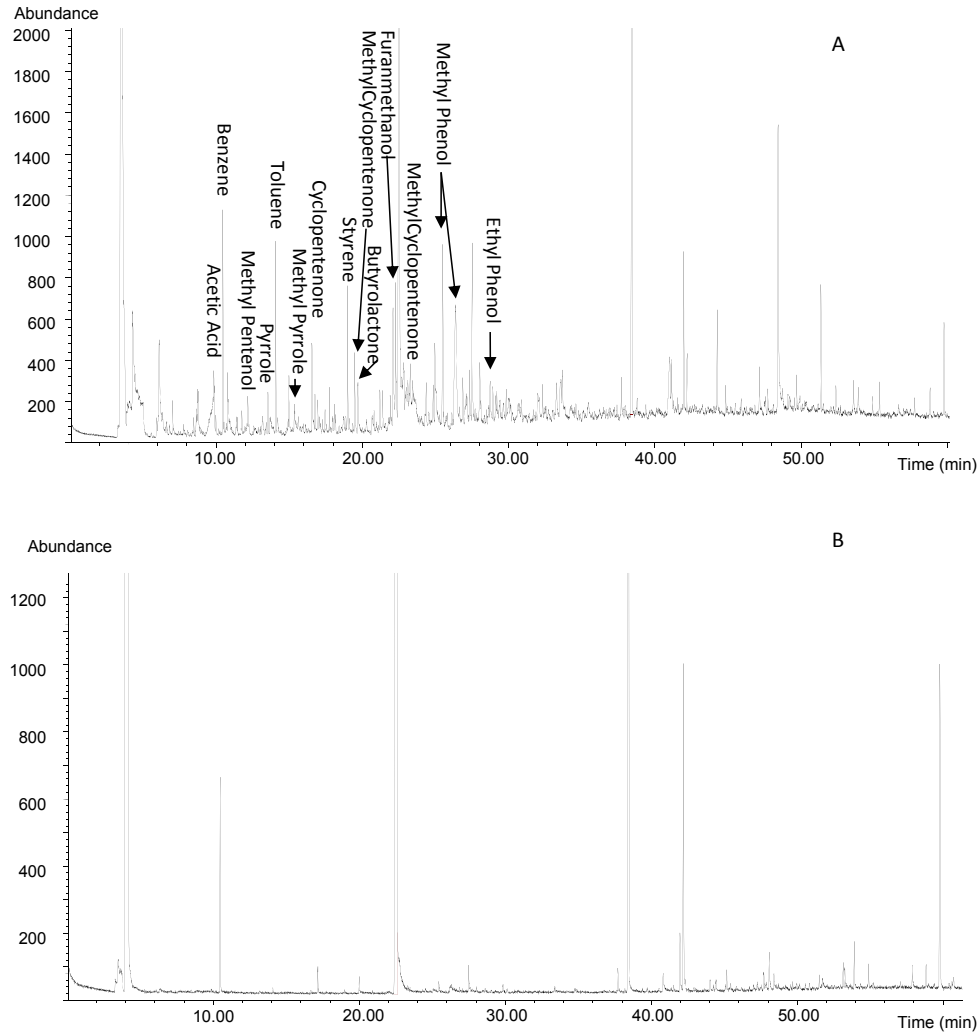

Figure S23. Pyrolysis-GC-MS of a) Xiga center and b) Xiga virgin membrane.

a.

EDAX TEAM

Page1

Xiga

Author: Cyril Aubry
Creation: 01/14/2017 9:58:18 AM
Sample Name: Xiga virgin

Added Spectra

1/14/2017 9:58:18 AM

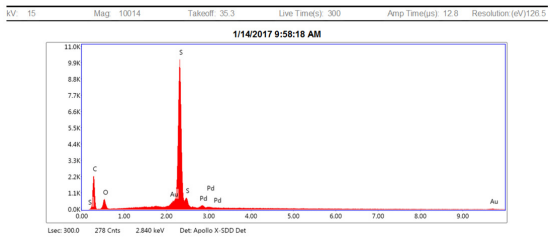

eZAF Smart Quant Results

Element	Weight %	Atomic %	Net Int.	Error %	Kratio	Z	R	A	F
C K	60.75	78.53	44.25	11.08	0.0936	1.0582	0.9684	0.1457	1.0000
O K	5.68	5.51	8.93	13.66	0.0094	1.0075	0.9886	0.1637	1.0000
AuM	0.30	0.02	3.97	26.95	0.0086	0.5703	1.4021	1.3752	3.6405
S K	32.78	15.87	295.79	1.81	0.2928	0.8859	1.0417	1.0042	1.0043
PdL	0.49	0.07	1.63	32.90	0.0033	0.6579	1.2302	1.0111	1.0153

b.

EDAX TEAM

Page1

Xiga

Author: Cyril Aubry
Creation: 01/12/2017 4:08:04 PM
Sample Name: Xiga center

Added Spectra

1/12/2017 4:08:04 PM

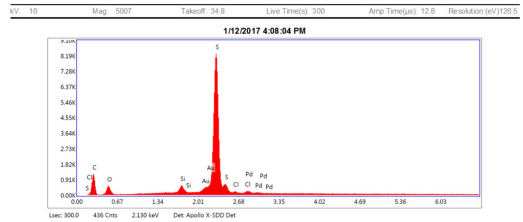

eZAF Smart Quant Results

Element	Weight %	Atomic %	Net Int.	Error %	Kratio	Z	R	A	F
C K	38.63	60.72	21.79	13.45	0.0530	1.1320	0.9430	0.1279	1.0000
O K	1.96	2.44	4.09	17.30	0.0062	1.0715	0.9648	0.2944	1.0000
SiK	0.90	0.64	5.66	9.44	0.0085	0.9534	1.0100	0.9692	1.0218
AuM	1.06	0.11	5.53	20.38	0.0205	0.5627	1.3276	1.1959	2.8654
S K	57.19	35.50	248.06	2.72	0.5305	0.9285	1.0206	0.9957	1.0033
ClK	0.46	0.26	1.44	36.18	0.0036	0.8808	1.0251	0.8799	1.0048
PdL	1.80	0.34	2.61	27.97	0.0117	0.6631	1.1808	0.9664	1.0097

Figure S24. EDS spectra of: a) Xiga virgin and b) Xiga center

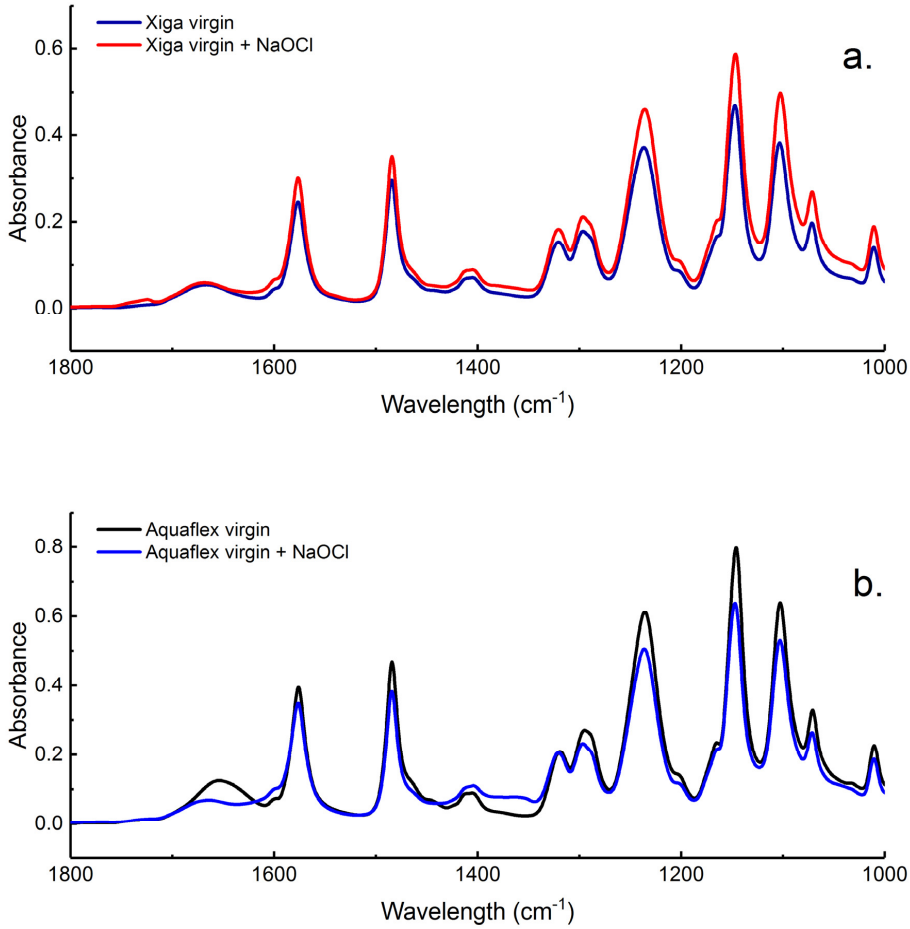

Figure S25. FTIR spectra of a) Xiga virgin and Xiga virgin chemically-cleaned and b) Aquaflex virgin and Aquaflex virgin chemically-cleaned membrane samples.

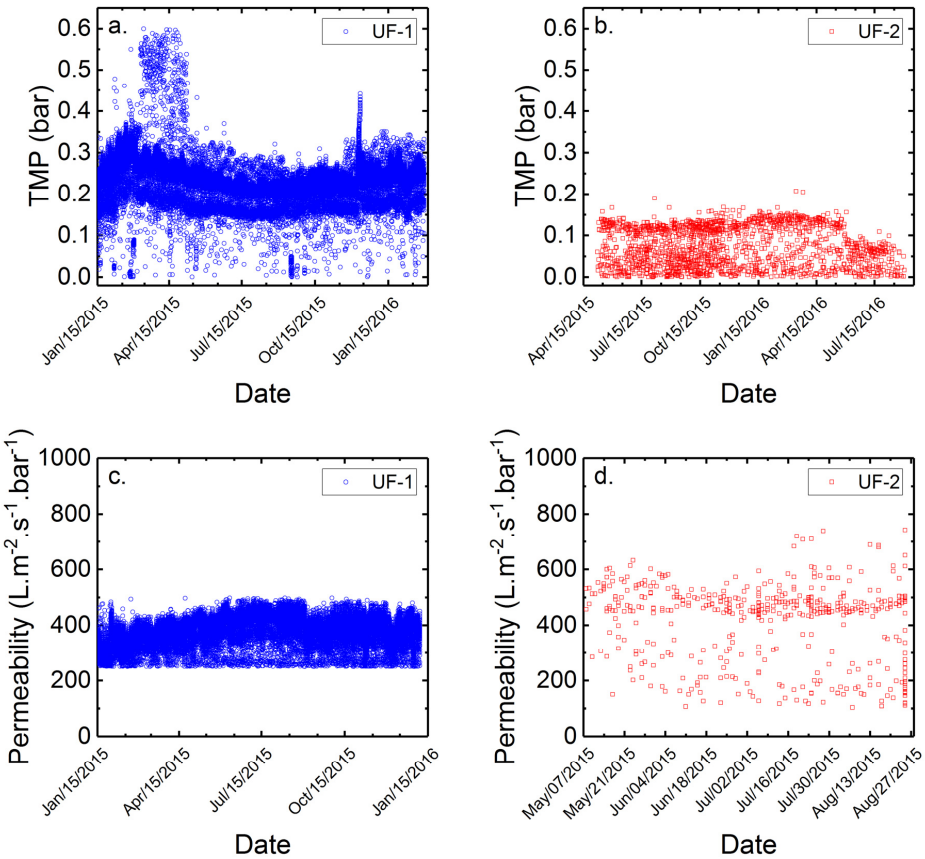

Figure S26. Trans-Membrane pressure of a) UF-1 and b) UF-2 modules, and permeability of c) UF-1 and b) UF-2 modules.

Paper III

water

MDPI

Article

Optimizing Hollow Fibre Nanofiltration for Organic Matter Rich Lake Water

Alexander Keucken [1,2,*], Yuan Wang [3], Keng Han Tng [3], Greg Leslie [3], Tom Spanjer [4] and Stephan J. Köhler [5]

1 Vatten & Miljö i Väst AB (VIVAB), 311 22 Falkenberg, Sweden
2 Water Resources Engineering, Faculty of Engineering, Lund Technical University, 221 00 Lund, Sweden
3 UNESCO Centre for Membrane Science and Technology, University of New South Wales, 2052 Sydney, Australia; yuan.wang@unsw.edu.au (Y.W.); k.h.tng@unsw.edu.au (K.H.T.); g.leslie@unsw.edu.au (G.L.)
4 Pentair X-Flow B.V., 7500 Enschede, The Netherlands; Tom.Spanjer@Pentair.com
5 Department of Aquatic Sciences and Assessment, Swedish University of Agriculture Sciences, 750 07 Uppsala, Sweden; Stephan.Kohler@slu.se
* Correspondence: Alexander.Keucken@vivab.info; Tel.: +46-70-598-99-62

Academic Editor: Stephen Gray
Received: 29 July 2016; Accepted: 26 September 2016; Published: 30 September 2016

Abstract: Over the years, various technologies have been utilized for Natural Organic Matter (NOM) removal with varying degrees of success. Conventional treatment methods comprising of coagulation, flocculation, sedimentation, or filtration are widely used to remove NOM. An alternative to these conventional methods is to use spiral wound membranes. These membranes tend to remove too much hardness whilst being ineffective in disinfection. They also have a low tolerance to chlorine and thus, have limited chemical cleaning options. In this study, we investigated how an alternative and new innovative filtration concept, based on capillary NF membranes from modified polyethersulfone (PES), may be used to treat soft but humus-rich surface waters. Comprehensive performance tests, with a fully automated membrane pilot equipped with a full-scale sized test module (40 m^2 membrane surface), were conducted at WTP Görvälnverket, which is operated by the water utility Norrvatten, providing drinking water from Mälaren (SUVA = 2.7–3.3, TOC = 7.0–10.0 $mg \cdot L^{-1}$) for about 500,000 people in the northern part of the Swedish capital of Stockholm. The removal of both UV and DOC was modeled using a solution diffusion approach. The optimized parameters allow deducing optimal operation conditions with respect to energy, water consumption, and permeate water quality. Optimal cross flow velocity was determined to be 0.75 $m \cdot s^{-1}$ at 80% recovery and a flux of 12–18 $L \cdot m^{-2} \cdot h^{-1}$. Under these conditions, 80% of the UV, 75% of the Humic Substances (MW = 600) and 70% of TOC were removed (from 8 to below 2 $mg \cdot L^{-1}$). A higher cross flow velocity led to marginal improvement (+2%) while both higher and lower membrane fluxes degraded permeate water quality. Apparent optimized diffusion coefficients for UV and TOC were around 1.2–2.4 $\times$ $10^{-10} \cdot m^2 \cdot s^{-1}$ and were similar to values found in the literature. Due to their higher diffusion coefficients and higher permeability coefficient, only 40% of the low molecular weight acids (MW = 300–400) were retained. Approximately 30%–40% of the low molecular weight acids in the permeate can be further removed using GAC post NF. The resulting energy consumption of a hypothetical four-stage design, at average operating temperature of 5.73 °C, was calculated to be around 0.6 $kWh \cdot m^{-3}$ produced water.

Keywords: nanofiltration; hollow fiber; natural organic matter (NOM); solution diffusion model

1. Introduction

Natural organic matter (NOM) is ubiquitous in waters, sediments, and soils. Aquatic NOM is derived both from the breakdown of terrestrial plants as well as the by-product of bacteria, algae,

and aquatic plants. The interrelation between NOM and climate change and notably the rising concentrations of NOM has attracted a lot of attention recently [1–9]. Several potential factors, including an increase in air and surface water temperature, rainfall intensity, and atmospheric CO_2 and/or a decrease in acid deposition, have been proposed to explain the increased amount of NOM [10], but there is yet no scientific consensus on the issue [11].

NOM has a significant impact on drinking water quality directly, by reacting with water treatment chemicals contributing to disinfection by-product (DBP) formation [12,13], and indirectly, by impacting water treatment processes (including fouling of membranes and reducing the effectiveness of activated carbon for contaminant removal). In the recent years, reports worldwide indicate a continuing increase in the color and NOM of the surface water, which in turn, causes an adverse effect on drinking water purification [14]. Changes in the properties of NOM also influence the treatment significantly [15].

Therefore, the water industry has been focusing on improving current treatment processes and developing new applications for enhanced removal of NOM. One of the latest innovations in nanofiltration (NF) for effective removal of NOM, is capillary NF membranes which combine the chemical resistance of hollow fiber membranes with the organic retention of spiral wound nanofiltration [16,17]. This new type of membrane (HFW1000) is suitable for raw waters that have low hardness and contain organic matter that are difficult to flocculate such as lake water. Recent studies indicated that a combined coagulation and NF process removed more than 90% of the dissolved organic carbon (DOC), and 96% of the absorbance at 254 nm in lake water [18], while using direct NF resulted in NOM removal with 93% in UV-absorbance (UVA) retention and 88% TOC retention [19]. An advanced autopsy of the hollow fiber NF membranes was conducted after 12 months of operation with no substantial changes to the membranes detected [20]. These results encouraged us to evaluate dimensioning parameters for the use of these NF membranes for direct lake water filtration.

The transport of NOM through NF membrane pores is influenced either by convection or diffusion, depending on the hydrodynamic conditions and electrostatic interactions between the membrane surface and NOM molecules. Different mechanisms influencing the removal of small organic compounds have been suggested. The polarity and differences in diffusion rates in a non-porous structure may influence the rejection of small organic compounds in NF [21,22]. The solution-diffusion model is the most widely used model of permeation in non-porous polymer membranes [23–25] while the Donnan steric pore model and dielectric exclusion model have also been used to describe mass transfer of electrolytes and neutral solutes through nanofiltration membranes [26] as well as to predict rejections of trace organics by NF membranes [27,28]. The ability of the model to describe all non-porous membrane separation processes has been the subject of several reviews even in the past [23,29,30]. Since the selected capillary NF membrane for this study has been deemed to be a non-porous membrane [31], the solution-diffusion model is used to obtain a design tool for prediction of permeate quality for different settings regarding filtration flux, cross-flow velocity, recovery and for different staging configurations.

This paper describes and evaluates a 6-month (from January 2014 to June 2014) pilot test of hollow fiber nanofiltration by direct filtration of surface water from Lake Mälaren, a drinking water source for more than 2 million citizens. The pilot trials were conducted at Görvälnverket WTP and operated by the water utility, Norrvatten, providing drinking water for about 500,000 people in the northern part of the Swedish capital of Stockholm.

Twenty short-term (<2 h) experiments, at a fixed recovery of 50%, with sufficient variations in filtration flux (5–25 $L \cdot m^{-2} \cdot h^{-1}$) and cross-flow velocity (0.25–1.0 $m \cdot s^{-1}$) were performed with a fully automated pilot plant to determine the solute diffusion coefficient and solute permeability coefficient to predict NOM retention (i.e., DOC). These short term experiments were complemented with a long term performance test of direct filtration at fixed filtration flux of 20 $L \cdot m^{-2}\ h^{-1}$ and fixed cross flow (0.5 $m \cdot s^{-1}$) but at varying recoveries (50%–90%) using the above-mentioned pilot plant. For all experiments, conventional NOM analysis (TOC, DOC, UV absorbance) was combined with LC-OCD

analysis for feed water, concentrate and permeate to elucidate the retention of specific NOM fractions as a function of varying operation conditions.

2. Theory

In theory, both the convection and solution diffusion models might be applicable for the HFW 1000 separation process, since the test membrane is positioned between a dense UF and an open NF (MWCO: ~1000 Da). Recent studies of the capillary nanofiltration membrane for determination of source specific model parameters showed a good fit of experimental results based on the solution diffusion model [31–33]. According to previous research, the selected membrane is a loose and open NF membrane and therefore can be described as a non-porous membrane. The solution-diffusion model, which is based on the film theory, was used for the active membrane layer. When a driving force is applied on the feed solution, the solvent starts to permeate freely while the solute is partially retained by the membrane. As a result, the solute concentration in the permeate (C_p) will be lower compared with the bulk solution (C_b). Retained solutes accumulate near the membrane surface, gradually increasing the local concentration (C_m). This increase in concentration is the driving force for back diffusion into the bulk of the feed and after a given period, steady state conditions are established. Thus, the driving force for solute permeation is assumed to rely solely on diffusion due to a concentration difference between permeate (C_p) and the concentration at the membrane surface (C_m). A schematic representation of the concentration polarization phenomena is given in Figure 1.

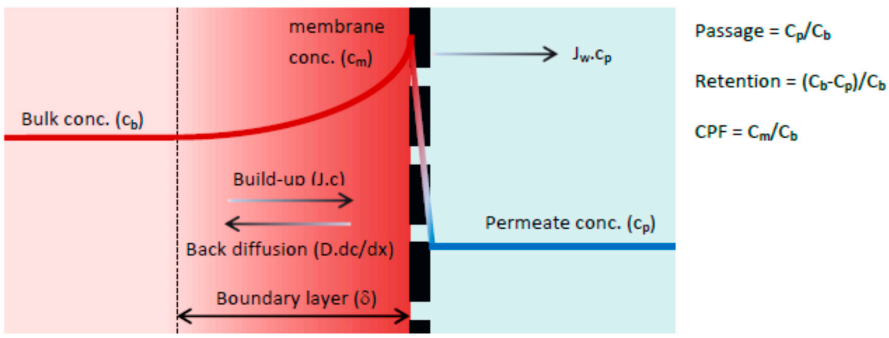

Figure 1. Concentration polarization phenomena [34].

The boundary layer (δ) is defined as the distance from the membrane surface where the solute concentration equals the bulk concentration (complete mixing). In the boundary layer the solute concentration will reach a maximum value at the membrane surface (C_m). The solution diffusion model differs from the convection model in how solute transport through the membrane is defined. The driving forces for solute permeation are assumed to rely solely on diffusion due to a solute concentration difference between permeate (C_p) and concentration at the membrane surface (C_m). The rate of solute permeation is determined by the solute permeability coefficient (B) expressed in ($m \cdot s^{-1}$). By performing a mass balance across the concentration polarization layer, the film model is obtained (Equation (1)). Subsequent substitution of the rate of solute permeation yields Equation (2) which describes the passage for the solution diffusion model [34].

$$\frac{C_m - C_p}{C_b - C_p} = e^{\left(\frac{l\delta}{D}\right)} = e^{\left(\frac{l_w}{k}\right)} \quad (1)$$

$$\frac{C_p}{C_b} = \frac{e^{\left(\frac{l_w}{k}\right)}}{\frac{J_w}{B} + e^{\left(\frac{l_w}{k}\right)}} \quad (2)$$

$$\frac{C_m}{C_b} = \frac{e^{\left(\frac{J_w}{k}\right)}}{1 + \frac{1}{\frac{J_w}{B}+1} - \frac{1}{\frac{J_w}{B}+1} e^{\left(\frac{J_w}{k}\right)}} \quad (3)$$

$$k = 1.62 v^{\frac{1}{3}} d^{-\frac{1}{3}} D^{\frac{2}{3}} L^{-\frac{1}{3}} \quad (4)$$

where,

C_p = Concentration in the permeate (e.g., TOC in $mg \cdot L^{-1}$ or UV extinction in m^{-1})
C_b = Concentration in the bulk (actual feed)
C_m = Concentration at the membrane surface
J_w = Filtration flux ($m^3 \cdot m^{-2} \cdot s^{-1}$)
k = Mass transfer coefficient ($m \cdot s^{-1}$)
v = Cross flow velocity ($m \cdot s^{-1}$)
d = Hydraulic membrane diameter (m)
L = Membrane length (m)
B = Solute permeability coefficient ($m \cdot s^{-1}$)
D = Solute diffusion coefficient ($m^2 \cdot s^{-1}$)

The solution diffusion model has two unknown parameters, the solute diffusion coefficient, D, and the solute permeability coefficient, B. These two latter parameters were fitted using the experimental results from pilot trials.

Model fitting was performed through an iterative process with the initial value of solute diffusion coefficient, D, based on the literature value reported by Park et al. [35]. Mass transfer coefficients, k, were calculated using Equation (4) for laminar flow conditions at four different crossflow velocities, ranging from 0 to 3.0 $m \cdot s^{-1}$ with corresponding Reynolds numbers of 0 to 2400 for 0.8 mm membrane fibres. The TOC and UV_{254} of the permeate were calculated using Equation (1) and compared with experimentally measured values. The final model fitting parameters of D, and B were determined using the Least Square Error method through the 'Generalized Reduced Gradient' (GRG2) algorithm in Excel (Solver).

It should be noted that only the concentrations of fraction (II) of the TOC were used for the model calibration as fraction (I) was only present in the feed water and concentrate, and fractions (III) was present in the same quantitative amount in the feed water and permeate.

3. Material and Methods

3.1. NOM Removal Concept Based on Capillary Nanofiltration

The core of the enhanced NOM removal concept is the innovative HFW 1000 membrane based on a capillary nanofiltration platform developed by X-Flow and recently commercialized by Pentair According to SEM pictures (Figure 1), the structure becomes denser towards the membrane surface which is advantageous for an inside-out filtration process.

Figure 2B illustrates the integrated top-layer with a thickness of approximately 100 nm. By optimizing the membrane production and polymer blend, a thin nanolayer is created at the inner wall of the membrane, which is completely integrated with the open membrane backbone structure and provides the required strength to withstand the applied forces during the filtration process and hydraulic membrane cleaning. Contrary to conventional spiral wound membrane modules, the integrated top-layer allows hydraulic cleaning of the HFW 1000 membrane by backwashing. Since the membrane material is based on modified PES, the HFW 1000 membrane properties can be characterized as highly chemical tolerant and chlorine resistant. This HFW membrane is designed for enhanced and selective removal of organics from surface water. The main characteristics of the selected test membrane are presented in Table 1.

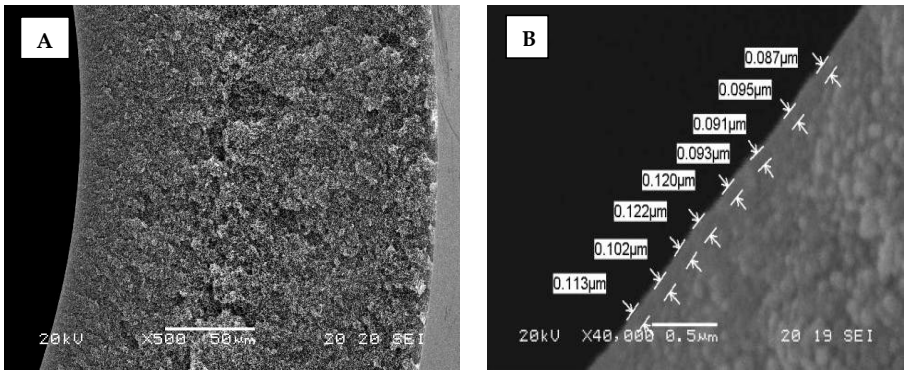

Figure 2. SEM images of the HFW membrane: (**A**) Cross-section; (**B**) Top-layer with replicated measurements of layer thickness.

Table 1. Manufacturer reported specified properties of the hollow fibre membranes.

Parameter	Unit	Key Performance Values
Membrane material	Sulfonated polyethersulfone (PES)	
Permeability	$L/m^2 \cdot h \cdot bar$	~10
MWCO based on PEG #	Da	~1000
Diameter (internal)	mm	0.80
Diameter (external)	mm	1.15
Membrane area	m^2	40
Collapse pressure	bar	>18
Burst pressure	bar	>20
Module hydraulic diameter	m	0.20
Module length	m	1.50
NOM removal:		Retention behavior
DOC	%	70–80
UV_{254}	%	80–90
Color	mg·Pt/L	90–95
Hardness removal (Ca^{2+}, Mg^{2+})	%	<20
Monovalent ions (Na^+, K^+)	%	~0
Sunset yellow retention@ Re = 3500	%	>97

Note: # PEG = Polyethylene glycol unit of molecular weight around 1000 Dalton.

3.2. The Pilot Plant and Description of Experimental Trial Periods

3.2.1. The Pilot Plant

For all trials, a 20-foot-long container pilot is used that was designed as a stand-alone unit and equipped with one element adapter for 8-inch commercial size membrane modules. The pilot plant consists of the following main sections (Figure 3):

- Feed section including coagulation dosing and chemical dosing for pH correction (not used during the trial period).
- Membrane system (one adapter for UF or NF test modules) including air integrity testing.
- Permeate and backwash section including the chemical dosing for membrane cleaning.

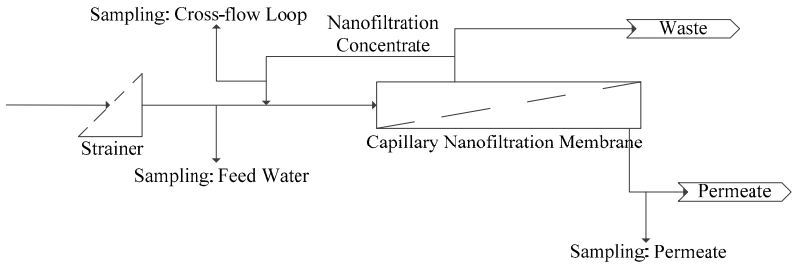

Figure 3. Schematic diagram of the pilot plant and sampling points.

The system design of the pilot plant was based on feed and bleed, with a slight cross-flow. By applying a minor bleed flow, the fouling layer on the membrane surface was minimized and the fouling potential of the membranes was significantly reduced. The pilot plant was equipped with a computer for systems control and runs automatically. All necessary process parameters were logged and trended on the computer, which can be observed and evaluated on the display. The plant also allowed remote access providing the same functionality as local access, except for Cleaning in Place (CIP) feasibilities. Besides hydraulic cleaning of the membranes via a combined backwash with forward flush, several automatic cleaning sequences have been pre-programmed for specific cleaning protocols. In general, cleaning took place on an elapsed time interval. A cleaning cycle consisted of flushing with clean water (permeate) followed by soaking with a maximum of two different cleaning agents (acidic and caustic). For the particular pilot trials, the feed water section was connected to an external feed pump located in the inlet of the WTP Görväln drinking water treatment plant. Regular membrane cleaning was performed using hydraulic backwash/forward flushing (every 60 min) and chemical enhanced cleaning with sodium hypochlorite and sodium hydroxide (after 72 h).

The average feed water parameters during the comprehensive pilot trial at the treatment work Görvälnverket of Norvatten are shown in Table 2.

Table 2. Average feed water quality.

Parameters	Unit	Range
Temperature	°C	2–12
pH	(-)	7.2–8.2
Turbidity	(NTU)	2–5
Conductivity	(µS/cm)	150–230
UV_{254}	(/5·cm)	1.09–1.44
Pt-Co	(mg·Pt/L)	28–33
DOC	(mg·C/L)	7.3–9.8
TOC	(mg·C/L)	7.3–9.9

3.2.2. Experimental Conditions

After an initial system stabilization period in February 2014 (trial 1) at 10 and 15 $L \cdot m^{-2} \cdot h^{-1}$ and fixed recovery of 50%, a large number of short term trails were conducted (trial 2, "short term"). Five sets of experiments with different cross-flow velocities from 0.25 to 1.0 $m \cdot s^{-1}$ at filtration fluxes between 5 and 25 $L \cdot m^{-2} \cdot h^{-1}$ were performed in random order to minimize the effect of changing water qualities. During those experiments the system recovery was kept constant at 50% (Table 3). Subsequently experiments at increasing filtration flux at a fixed cross flow of 0.5 $m \cdot s^{-1}$ (trial 3 "filtration flux") were performed. The final two trials consisted of a longer term performance test in March and April 2014 (trial 4, "long-term") at 20 $L \cdot m^{-2} \cdot h^{-1}$ at 50% recovery and a period where recovery was changed while keeping the filtration flux constant (trial 5, "recovery"). Operating conditions during pilot trials can be found in Table 4.

During the short-term trials, samples were taken from four sample points: feed water from Lake Mälaren (pre-filtered with 300 μm strainer), circulation loop, concentrate and permeate (Figure 3). Steady state conditions at the moment of sampling were ensured by on-line measurements of conductivity in the circulation loop and permeate line. Between the two experiments, the concentrate and permeate side were completely drained including the membrane module to diminish the influence of previous experiments.

Table 3. Summary of the short-term trial conditions.

Experiment Number	Crossflow Setpoint ($m \cdot s^{-1}$)	Filtration Flux Setpoint ($L \cdot m^{-2} \cdot h^{-1}$)	Recovery Setpoint (%)
1	0.25	5	50
2	0.25	10	50
3	0.25	15	50
4	0.25	20	50
5	0.25	25	50
6	0.50	5	50
7	0.50	10	50
8	0.50	15	50
9	0.50	20	50
10	0.50	25	50
11	0.75	5	50
12	0.75	10	50
13	0.75	15	50
14	0.75	20	50
15	0.75	25	50
16	1.00	5	50
17	1.00	10	50
18	1.00	15	50
19	1.00	20	50
20	1.00	25	50

Table 4. Operating conditions and process parameters during different pilot trials.

Parameters	Unit	Short Term Trial	Filtration Flux Trial	Recovery Trial
Filtration time (t_F)	(min)	90–180	60–90	60–90
Filtration flux (J_F)	($L \cdot m^{-2} \cdot h^{-1}$)	5–25	15–20	20
v_{CF} (cross flow velocity)	($m \cdot s^{-1}$)	0.25–1	0.5	0.5
R (recovery during filtration)	(%)	50	50	50–90
t_{BW} (backwash time)	(s)	60	60	60
J_{BW} (backwash flux)	($L \cdot m^{-2} \cdot h^{-1}$)	40	40	40
t_{CEFF} (CEFF * interval)	(days)	0	3	1–3
CEFF * dosing solution	(-)		200 ppm NaOCl @ pH 12 with NaOH	200 ppm NaOCl @ pH 12 with NaOH
t_{SOAK} (Soak time CEFF *)	(min)	0	60	60

Note: * CEFF—Chemically Enhanced Forward Flushing.

3.3. Characterization of Organic Fractions in Feed Water and Treated Water

3.3.1. Determination of UV, TOC and DOC

Total organic carbon (TOC) and dissolved organic carbon (DOC) were determined using an Elementar (SRN) Vario TOC Cube analyzer with a precision of 0.2 $mg \cdot L^{-1}$. UV absorbance at 254 nm was determined with a 5 cm cuvette.

3.3.2. Evaluation of NOM Retention by Liquid Chromatography-Organic Carbon Detection (LC-OCD)

The nature of the organics presented in the raw water to the WTP, feedwater to the pilot plant, and effluent from the WTP and the pilot plant were characterised using UV absorbance at 254 nm and

using a DOC-LABOR Liquid Chromatography-Organic Carbon Detection (LC-OCD). LC-OCD utilizes a polymethacrylate, size-exclusion column (Toso, Japan) coupled with three detectors (Organic Carbon, Organic Nitrogen and UV-absorbance). This technique allows for subdivision of organic matter into six major sub-fractions: biopolymers, Humic substances, building blocks, low molecular-weight acids, low molecular-weight neutrals, and hydrophobic organic carbon. From the results, the biopolymer's and humic substances' nitrogen content can be estimated. The measurement of the protein content of the biopolymer fraction allows for the amount of bound nitrogen to be determined using the UV-detector, while Humic Substances (HS) can be further characterised using the HS-diagram which plots the aromaticity of HS against its nominal molecular weight. Detailed information of the LC-OCD technique can be found in the paper previously published [36].

3.4. Prediction of Removal Efficiency of Full-Scale Plant (First Stage Process)

In order to predict the removal efficiency of the first stage and full-scale processes, mass balance calculations were used. The full-scale design is not based on the full-scale flow and only illustrates the mass balances over the different membrane stages. The objective of staging is to lower the average bulk concentration at the feed side. This is achieved with the first stages operating at a lower overall recovery compared to that of an equivalent single stage process.

According to previous studies [17], TOC analysis can be used as a key parameter for the determination of the solute diffusion coefficient (D) and the solute permeability coefficient (B). As for membrane retention, the TOC can be divided into three fractions; (I) 100% retained; (II) partially retained (based on current process conditions, membrane geometry and membrane properties); and (III) 0% retained. Different mass balances were calculated for all three water fractions. The TOC levels of feed water and permeate were corrected in order to eliminate the influence of fractions (I) and (III). Since fraction (I) was only present in the feed water and concentrate, the TOC level of the feed was corrected by subtracting fraction (I) from the total feed TOC value. Fraction (III) was present in the same quantitative amount in the feed and permeate, and therefore, was also subtracted to obtain the corrected TOC concentration for fraction (I) and (III). Correction factors (C) were determined via a Pentair-developed design tool that utilized trend-line regression. The design tool took into account the effects of filtration flux, and cross-flow velocity on the membrane retention. Based on the fixed membrane retention, the design tool then calculated removal efficiencies for the first stage and a typical 4-stage, full-scale process (Equations (5) and (6)). The number of membrane modules per stage only indicates the ratio of membrane modules over the stages. For example, with the current module ratio 20-10-6-4 (40 modules), a skid could be designed with 80-40-24-16 modules (160 modules in total) for stage 1 to 4.

$$\begin{gathered} \eta_{\text{First Stage}} = 1 - \left(x_{II}\left(1 - C_{\text{mem}\rightarrow 1\text{Stage}}\right) + x_{III}\right) \\ C_{\text{mem}\rightarrow 1\text{Stage}} = 0.4542\eta_{\text{mem}}^3 - 0.0187\eta_{\text{mem}}^2 + 0.5633\eta_{\text{mem}} - 0.0026 \end{gathered} \tag{5}$$

$$\begin{gathered} \eta_{\text{Full-scale}} = 1 - \left(x_{II}\left(1 - C_{\text{mem}\rightarrow \text{Full-scale}}\right) + x_{III}\right) \\ C_{\text{mem}\rightarrow \text{Full-scale}} = 0.7415\eta_{\text{mem}}^4 - 0.5488\eta_{\text{mem}}^3 + 0.5439\eta_{\text{mem}}^2 + 0.2617\eta_{\text{mem}} \end{gathered} \tag{6}$$

where,

η = Removal efficiency (%);
χ_{II} = Partly-retained feed fraction;
χ_{III} = Non-retained feed fraction;
C = Correction Factor.

In the applied design tool, in each stage, two modules were operated in series. In this double-pass loop, the concentrate of the first module was the feed for the second module. Between the second and the first module, the circulation pump, pressurized feed line and concentrate line were connected. This setup halves the circulation flow rate, because two modules were operated in series, which resulted in smaller circulation pipes/headers. The disadvantage of this setup was the different Transmembrane

Pressure (TMP) for both the modules, due to the pressure drop over the two modules. This caused a filtration flux deviation between the first and second module, which depended on the membrane permeability, filtration flux and cross-flow velocity. The first module was thereby running at the highest filtration flux and limiting the design based on the maximum allowable filtration flux. For the full-scale design, the pilot data and solution diffusion models were used to calculate the mass balances.

4. Results and Discussion

4.1. Long-Term Experiments

4.1.1. Hydraulic Membrane Performance

The hydraulic performance of the membrane module for the entire pilot period from 23 January 2014 to 12 June 2014 was presented in Figure 4. Membrane resistance data showed a stable filtration performance during the entire 4.5 month pilot period, except the period from 10 May 2014 to 15 May 2014 (Table 5). During this period, an issue occurred due to precipitation while dosing the chemical cleaning solution, resulting in scaling. This scaling was caused by the insufficient rinsing of the concentrate loop before the caustic/oxidizer cleaning solution was dosed. Scaling was removed with one standard chemical cleaning with hydrochloric acid at pH 2 with a soak time of 60 min. Implementing the pilot automation, alleviated the scaling issue and the process appeared to be stable with a caustic/oxidizer chemical cleaning only.

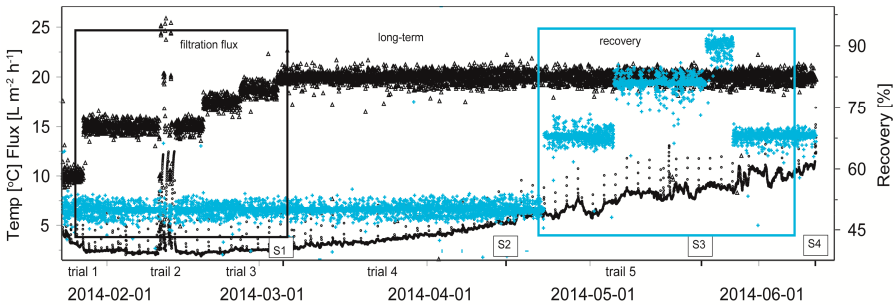

Figure 4. Hydraulic performance of the capillary NF container test module for time period January to June 2014 at WTP Görvälnverket, Norrvatten. At times (S1, S2, S3 and S4 samples were taken for LC-OCD analysis. Periods of increase infiltration flux and increase of recovery are marked with black and blue frames respectively. Temperature (°C) and flux ($L \cdot m^{-2} \cdot h^{-1}$) on the left scale with white circles (○) and white triangles (Δ) respectively and recovery (%) with grey markers (+).

Table 5. Variation of membrane performance and parameters during long-term pilot trials.

Parameters	Unit	Range
Membrane permeability	($L \cdot m^{-2} \cdot h^{-1} \cdot bar^{-1}$, 20 °C)	11–13.6
Membrane resistance × 10^{13}	(m^{-1})	2.65–3.23
Trans membrane pressure	(bar)	1.1–2.8
Pressure loss module (V_{CF} = 0.5 m/s)	(bar)	0.5–0.7

During first trial period ("increase in filtration flux") with increasing filtration fluxes from 10 to 20 $L \cdot m^{-2} \cdot h^{-1}$, an increase in the resistance built-up was observed over time between two chemical cleanings. This increase in resistance built-up was caused by the higher filtration fluxes (higher local forces towards the membrane) and larger filtration volumes per filtration run. However, this increase in resistance built-up was not major and chemical cleaning could easily restore the membrane

resistance to ensure stable filtration performances. In the third trial period ("increase in recovery") with increasing recoveries from 50% to 90%, an increase in the resistance built-up was not observed over time between two chemical cleanings, which suggests that the fouling rate is probably independent of the recovery up to 90%, while the bulk concentration of the organics significant increases with increasing recovery. Therefore, the fouling rate is only affected by the filtration flux and probably not by the used recovery rate (bulk concentration of organics). This fact resulted in equal fouling rates for all the stages in the full-scale process, which led to stable and equal flux distributions over the several stages in time during the filtration cycles. These results are also in line with the measured pressure drop over the module, which was stable during the entire pilot period, indicating no significant risk for fiber plugging during filtration and cleaning.

Membrane retention was shown as a function of the filtration flux and cross-flow velocity for the entire pilot period from 23 January 2014 to 12 June 2014. Membrane retention decreases with increasing filtration flux in the first period ("increase of filtration flux"). After the period with increasing filtration fluxes up to 20 $L \cdot m^{-2} \cdot h^{-1}$, the membrane resistance was stable and fluctuated only in a small range possibly due to measurement inaccuracies (Figure 5). Even when the recovery was increased from 22 April 2014, the membrane resistance was constant over time. The membrane retentions for UV_{254} varied between 87.6% and 91.6%, for Pt-Co between 87.5% and 97.5% and for TOC between 82% and 89% during the trial period. The range of membrane retentions achieved in the experimental matrix for the models were broader, with membrane retentions for UV_{254} between 88.0% and 94.7%, for Pt-Co between 87.5% and 98.4% and for TOC between 79.7% and 92.2% (Table A1).

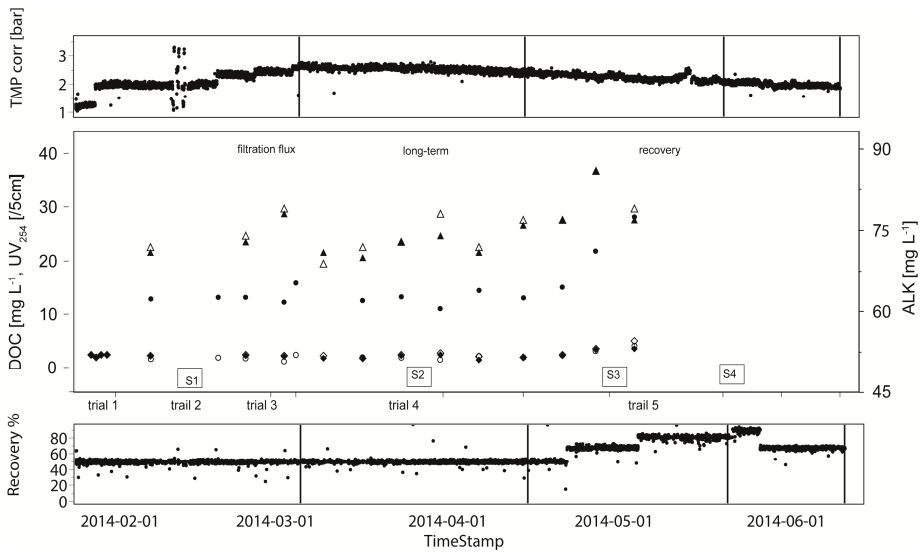

Figure 5. Membrane performance with respect to DOC ($mg \cdot L^{-1}$) (in ● and out ○), Alkalinity (right scale ($mg \cdot L^{-1}$) (ALK_{in} ▲, ALK_{out} Δ) and UV_{254} (UV_{in} ◆ and UV_{out} ◇) of the capillary NF container test module for time period January to June 2014 at WTP Görvälnverket, Norrvatten. S1–S4 and bars as in Figure 3.

4.1.2. Effects of Cross-Flow Velocity and Recovery

Membrane filtration performance suggested that membrane retentions were strongly affected by the filtration flux and cross-flow velocity. Decreasing cross-flow and increasing recovery deteriorated water quality. The membrane removal was highest for biopolymeres (>95% removal), followed by Humics (>80% removal). This was in accordance with earlier experiments performed [18] using

similar types of membranes [37]. LC-OCD results showed that while incoming molecular weight of Humic substances is 660 Dalton, the small fraction of permeating Humic substances have a molecular weight of around 530 Dalton. Due to their low molecular weight of below 500 Dalton, the removal of building blocks (between 65% and 80% removal) and low molecular weight substances (<60%) is poorer. Both the low molecular weights neutrals and the Humic substances follow a similar pattern (Figure 6). At a cross flow velocity of 0.5 $m \cdot s^{-1}$, recoveries of above 50% significantly deteriorated water quality. Permeate quality improved when the crossflow was increased to 0.8 $m \cdot s^{-1}$, above which no further improvement was observed. The low molecular weight neutrals (LMWN) were below the molecular cutoff of the HFW1000 membrane with at least 40% passing through into the permeate. This corresponds to LMWN in the range of 1300 ppb in the influent and around 300 ppb detected in the permeate. Post NF Granulated Activated Carbon (GAC) filters should be used to remove these DOC fractions. Earlier experiments using the same type of membrane and source water [18] indicated that at least half of the permeating LMW substances can be removed by GAC filters.

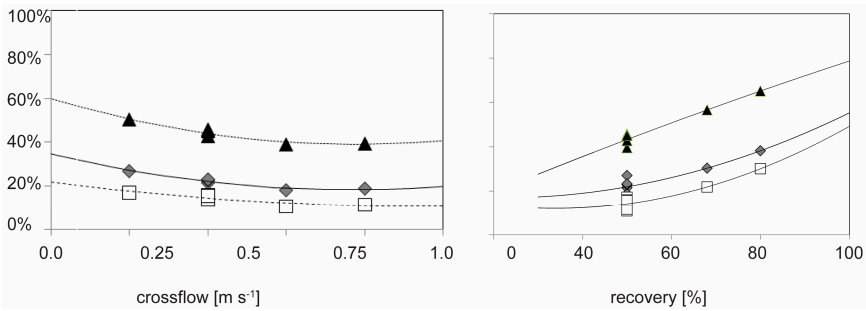

Figure 6. Effect of recovery rate on the fraction of DOC in the permeate for DOC (◆), Humic substances (□) and Low molecular weight neutrals (▲) at a fixed cross flow of 0.5 $m \cdot s^{-1}$ in the pilot plant (**left**, samples S1–S4) and effect of cross flow on the fraction of DOC in the permeate for DOC at fixed recovery of 50%, Humic substances and low molecular weight acids, neutrals for the container plant experiments (**right**) The lines are second-degree order fits to the data to highlight the trends.

Data points that overlap in the above figure at crossflow of 0.5 $m \cdot s^{-1}$ and at recovery of 50% are replicate samples at similar conditions but sampled under the short-term experiment described below.

4.2. Short Term Experiments

In Figure 7, UV, DOC and LC-OCD fractionations are shown at four different cross-flow velocities (0.25, 0.50, 0.75 and 1.0 $m \cdot s^{-1}$) and filtration flux of 15 $L \cdot m^{-2} \cdot h^{-1}$ at 50% recovery. Comprehensive LC-OCD data is shown in Table A2, while Figures A3–A6 show the membrane performance during short term trials.

Although the membrane retention increases with increasing cross-flow velocities, the relative DOC composition of the permeate does not change in terms of retention behavior of humics and building blocks (Figure 6). Increased cross-flow velocities (increased mass-transfer coefficients) affected the membrane retention on the several DOC fractions with comparable magnitudes, the lines in Figure 6 are close to parallel despite the molecular mass being significantly for those DOC fractions.

In accordance with the long-term experiments, crossflow velocities of above 0.8 $m \cdot s^{-1}$ do not improve water quality with the exception of the UV-absorbance 254. We have no explanation for the slight improvement of UV and must speculate that factors other than DOC or Humics affected the decrease in UV in those experiments. We have no explanation to why UV did not change at filtration fluxes of 5 $L \cdot m^{-2}$ h^{-1} and the occurrence of unsystematic variation of DOC at crossflow of 0.5 $m \cdot s^{-1}$.

Part of that variation may be due to the precision of the DOC measurements, which is in the order of 0.3 mg·L^{-1}.

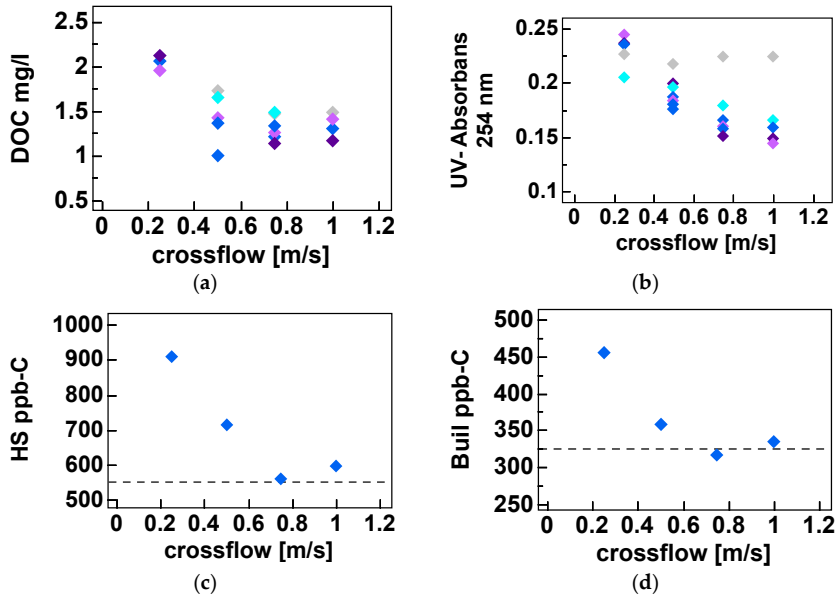

Figure 7. Membrane performance of the capillary NF pilot test module and effect of crossflow and filtration flux for permeate quality for both UV_{254} and DOC for all experiments ((**a**) and (**b**) respectively) and those where LC-OCD were available for HS and building blocks ((**c**) and (**d**) respectively). Different filteration fluxes (L·m^{-2}·h^{-1}) are distinguished with grey (◆5), light blue (◆10), dark blue (◆15), light violet (◆20) and dark violet (◆25) markers.

4.3. Water Fractions and Solution Diffusion Model Parameters

4.3.1. Prediction of Membrane Retention Based on TOC and UV Absorbance, UVA_{254}

With initial guesses for fraction (I), fraction (III), solute diffusion coefficient and solute permeability coefficient, the measured membrane passages and predicted membrane passages, based on the solution diffusion model, were fitted with the GRG non-linear solver in Excel. In contradiction to the UV model, the TOC model fitted best with one water fraction only. The total feed concentration was thereby assumed as partly retained based on process conditions and membrane properties. In the UV model, 1.5% of the feed concentration was assumed to permeate unaffected through the membranes and 98.5% are considered as being partly retained. The water fractions and model parameters from the model fitting based on UV_{254} and TOC are listed in Table 6.

Table 6. Water fractions and model parameters for UV_{254} and TOC.

	Model Parameter: UV_{254}	**Model Parameter: TOC**
Fraction (I)	0	0
Fraction (II)	0.985	1
Fraction (III)	0.015	0
D (solute diffusion coefficient)	1.74×10^{-10} (m^2·s^{-1}) *	1.65×10^{-10} (m^2·s^{-1}) *
B (solute permeability coefficient)	1.01×10^{-7} (m·s^{-1})	1.69×10^{-7} (m·s^{-1})

Note: * comparable with diffusion coefficients in the literature [26].

According to the calculations of the model parameters, the solute diffusion coefficients were comparable for UV_{254} and TOC, while the solute permeability coefficient for TOC was higher compared with the permeability coefficient for UV_{254}. This resulted in lower TOC retentions compared to retentions based on UV_{254}, which was also expected.

The graphs in Figure 8 show the results of the measured membrane passages (data points) and predicted membrane passages (data lines) based on DOC. The four different lines in the figure above indicate the predicted performance when using various cross-flow velocities. It can be seen that the measured and predicted membrane passages are well fitted with probably some outliers. For instance, the fitting is improved with 25%, based on the average error per data point, if experiment 8.1 was not used in the model (vCF: 0.5 $m \cdot s^{-1}$, Jf: 15 $L \cdot m^{-2} \cdot h^{-1}$; passage 20%). It can also be pointed out that the membrane passage increases if the cross-flow velocity is decreased. With a certain cross-flow velocity, the passage first decreases when the flux is increased. However, if the filtration flux is further increased the passage increases again. This effect is similar to the UV-retention, caused by the dilution effect (permeate flux) and concentration polarization. Based on the predicted membrane passages, the retention of the first stage (50% recovery) can be calculated by using mass balances. In Figure 8, the measured retentions (raw feed water to permeate) and predicted retentions are shown for the four applied cross-flow velocities. The predicted retentions compare well with the measured retentions with an outlier at 65% retention and filtration flux of 15 $L \cdot m^{-2} \cdot h^{-1}$. The calculations also indicate that the expected first stage retentions, with 0.5 m/s cross-flow velocity and filtration fluxes between 10 and 20 $L \cdot m^{-2} \cdot h^{-1}$, are in the range of 78%–80% based on TOC. The first stage retentions could be increased further to 83% by increasing the cross-flow velocity towards 1 $m \cdot s^{-1}$. From an operational perspective, a cross-flow velocity of 0.5 $m \cdot s^{-1}$ with a flux-range from 8 to 22 $L \cdot m^{-2} \cdot h^{-1}$ is the most optimal setting based on the passage and energy consumption.

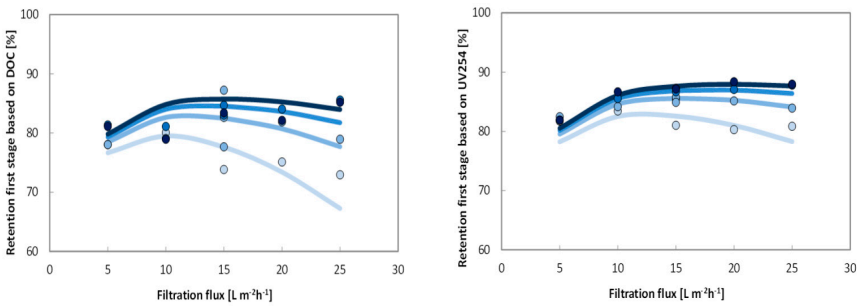

(**a**) (**b**)

Figure 8. Model fit of membrane passage of capillary NF pilot test module for DOC (first stage: 50% recovery, (**a**)) and on UV_{254} (first stage: 50% recovery, (**b**)) as a function of filtration flux. Cross flows increases from 0.25 to 1.0 $m \cdot s^{-1}$ from light to dark blue (●, ●, ●, ● from bottom to top). Best fit model performance of first stage removal and using the parameters displayed in Table 7 for both UV and DOC are displayed with lines in both figures.

4.3.2. Uncertainties

The solver function succeeds in finding a local minimum for the sum of errors for both UV and DOC experimental data. During the optimization procedure, it became evident that a number of combinations of D and B led to acceptable fits with sum of errors close to the local minimum. This was tested by systematically varying B and D stepwise in the range of 0.42–1.42 (0.2 per step) for B and 1.36–2.76 (0.2 per step) for D. The resulting matrix of the sum of errors is displayed in the appendix (Figure A1). Based on that matrix, we could establish a relationship between D and B that covers the

area of smallest sum of errors. This also allowed us to evaluate the potential effect of the optimum operation range (Figure A2).

4.4. Modelling of Full-Scale Process Design for Direct Nanofiltration

Figure 9 shows the predicted full-scale retentions for a typical three stage process, whereby all stages operates at 50% recovery, resulting in overall recovery of 82.5%. The predicted full-scale TOC retention is shown for the four applied cross-flow velocities. The overall TOC retention, with 0.5 $m \cdot s^{-1}$ cross-flow velocity and filtration fluxes between 10 and 20 $L \cdot m^{-2} \cdot h^{-1}$, was in the range of 67%–69%. Figure 8 also illustrates the comparison of the UV_{254} and TOC retention, which could be achieved in the above mentioned full-scale installation (3 stages at 50% recovery, overall recovery of 82.5%) at a cross-flow velocity of 0.5 $m \cdot s^{-1}$. According to the calculations the optimum flux range based on retentions is between 10 and 20 $L \cdot m^{-2} \cdot h^{-1}$, with the predicted UV_{254} retention rate corresponding to 78% and the predicted TOC retention reaching approximately 67% to 69%. In general, the TOC retention with a cross-flow velocity of 0.5 $m \cdot s^{-1}$ is 10% lower compared to the UV retention. Therefore, this shows that by using the adapted models based on UV_{254} and TOC, the permeate quality and energy consumption of full-scale configurations can be calculated.

The ranges of membrane retentions, achieved in the experimental matrix, were used to calculate process retentions of a four-stage system with 90.2% recovery during filtration. Membrane (process-) retention were on average 88%–95% (72%–87%) of the UV_{254}, 88%–98% (72%–96%) for color ($mg \cdot Pt \cdot L^{-1}$) and between 80% and 92% (58%–81%) for TOC ($mg \cdot C \cdot L^{-1}$).

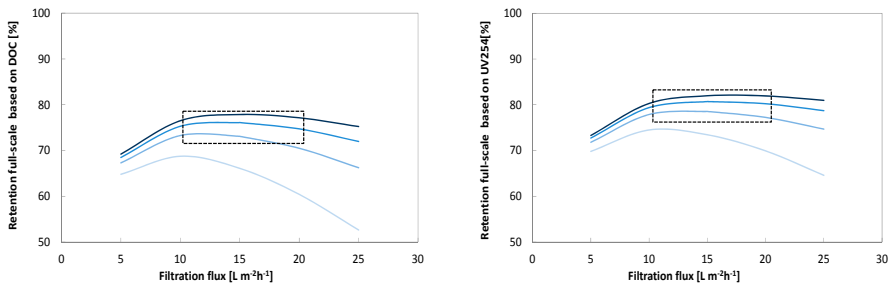

Figure 9. Influence of filtration flux (5–25 $L \cdot m^{-2} \cdot h^{-1}$) and cross-flow velocity (0.25–1.0 $L \cdot s^{-1}$) for a full-scale three stage process with 82.5% overall recovery on membrane passage of DOC (**a**) based on UV_{254} (**b**). The area within the square indicate the range of optimum conditions.

Based on the results of on-going pilot trials, feasibility studies and sensitivity analyses have been conducted with the aim to develop a preliminary full-scale process design for direct nanofiltration at WTP Görvälnverket. For this purpose, the characteristics for feed water, the required permeate quality and minimum recovery rate were defined. For calculation of mass balances current pilot data and requirements by the utility Görvälnverket were used as listed in Table 7.

Table 7. Design criteria for preliminary full-scale process design for WTP Görvälnverket.

Design Parameter	Design Value
Overall system retention, based on UV_{254}	80%
Overall system recovery, based on the raw feed	85%
Average design temperature	5.73 °C
Membrane permeablility	10 $L \cdot m^{-2} \cdot h^{-1} \cdot bar^{-1}$
Max. filtration flux	20 $L \cdot m^{-2} \cdot h^{-1}$
Max Chemical enhanced forward flushing interval	2 days
Cross-flow velocity (at the end of the 2nd module)	0.5 $m \cdot s^{-1}$

The most important design criteria for process optimization have been ranked as follows:

1. Permeate quality
2. Recovery rate
3. Operational costs (including energy) and investments

Preliminary calculations indicated a total membrane surface area in the range of 314,000 to 524,000 m^2 for the given flow rates of the actual plant capacity. In order to meet the design criteria a four-stage membrane system is proposed. It consists of 7862 modules for 120 $m^3 \cdot day^{-1}$ and 13,103 modules for 200 $m^3 \cdot day^{-1}$ with an estimated module ratio of 10-5-3-2 for stage 1 to 4. This meant that a 160-module membrane skid could be designed with a 80-40-24-16 per stage configuration. For the full-scale design of the membrane plant, it is assumed that two modules are operated in series for each membrane stage. The selected process configuration enables a double-pass loop, which means that the concentrate of the first module will be the feed water of the second module. The circulation pump as well as the pressurized feed and concentration line are connected between the second and first module. This setup halves the circulation flow rate due to the fact that two modules are operated in series resulting in smaller pipes and headers for the circulation. However, also results in different TMPs for both of the modules due to the pressure drop over the two modules, therefore, resulting in a filtration flux deviation between the first and second module, depending on the membrane permeability, filtration flux and cross-flow velocity. In this case, the first module is running at the highest flux and thus, limits the process design based on the filtration flux. The output of the projection tool for the proposed retrofit of WTP Görvälnverket for direct nanofiltration is summarized in Table 8.

Table 8. Calculated design parameters for retrofit of WTP Görvälnverket.

Design Parameter	Output of Design Tool
Overall system retention, based on UV_{254}	80.0%
Overall plant recovery, based on the raw water flow rate	85.1%
Net permeate flux	15.9 $L^{-1} \cdot m^{-2} \cdot h^{-1}$
Recovery during filtration in the 1st stage	45.1%
Overall recovery during filtration in the 2nd stage	67.6%
Overall recovery during filtration in the 3rd stage	81.2%
Overall recovery during filtration in the 4th stage	90.2%
Membrane permeability	10 $L^{-1} \cdot m^{-2} \cdot h^{-1} \cdot bar^{-1}$
Average TMP (@5.73 °C)	2.65 bar
Pressure loss over the two module in double-pass loop (@5.73 °C)	1.27 bar
Filtration flux, 1st module in the double-pass loop	20.0 $L^{-1} \cdot m^{-2} \cdot h^{-1}$
Filtration flux, 2nd module in the double-pass loop	15.7 $L^{-1} \cdot m^{-2} \cdot h^{-1}$
Average cross-flow velocity	0.53 $m \cdot s^{-1}$
Overall pump efficiency	75%
Pressure loss over the membrane skid	0.2 bar
Additional pressure loss over the circulation line	0.2 bar
Energy consumption for pressurization *	0.12 $kWh \cdot m^{-3}$ produced water
Energy consumption for circulation *	0.42 $kWh \cdot m^{-3}$ produced water
Total energy consumption *	0.54 $kWh \cdot m^{-3}$ produced water

Note: * corrected calculation with the additional pressure losses and pump efficiencies.

Sensitivity analyses were performed to investigate the effects of several design parameters on the full-scale process. In the appendix (Figure A7 Appendix A), the energy consumption per cubic meter of produced water (permeate) versus the feed water temperature, with a fixed retention of 80% based on UV_{254} is shown. The energy consumptions are corrected at an overall pump efficiency of 75% and for additional pressure losses over the skid and the circulation line. It can be seen that the energy consumption is significant affected by the temperature with the energy consumption for feed water temperatures of 0.5, 5.73 and 18 °C were 0.63, 0.54 and 0.4 $kWh \cdot m^{-3}$ respectively. Given that the average feed water temperature was 5.73 °C, the predicted average energy consumption would be 0.54 $kWh \cdot m^{-3}$ of produced water for the proposed full-scale process at WTP Görvälnverket.

5. Conclusions

Pilot studies are valuable to find optimal conditions for nanofiltration of lake water rich in organic material. The NOM removal based on capillary NF membranes from modified polyethersulfone (PES) proved to be suitable for direct nanofiltration of surface water from Lake Mälaren with high removal of NOM and minimal removal of salts.

The influence of filtration and cross flow velocity on permeate quality can be described using the solution diffusion model. Therefore, the HFW1000 membrane can be categorized as a non-porous membrane with respect to NOM removal.

Employing the solution diffusion model, the model parameters 'B' and 'D' can be determined. For surface water from Lake Mälaren source specific model parameters were calculated based on TOC analysis as:

$$B = 1.69 \times 10^{-7} \ m \cdot s^{-1}$$

$$D = 1.65 \times 10^{-10} \ m^2 \cdot s^{-1}$$

These model parameters can be used to design full-scale plants.

The permeate quality was greatly improved after nanofiltration. Preferential removal of UV over HS as compared to DOC was observed. Only low molecular acids and low molecular non-charged matter passed through the membrane, while high molecular compounds were retained.

Optimal cross flow was close to 0.75 $m \cdot s^{-1}$ at 80% recovery with a flux of 12–18 $L \cdot m^{-2} \cdot h^{-1}$. Under these conditions, around 80% of the UV, 75% of the Humic substances (Mw = 600) and 70% of TOC (from 8 to below 2 $mg \cdot L^{-1}$) were removed. Higher cross flow velocities led to a marginal improvement (+2%) while increasing and decreasing membrane flux degraded permeate water quality. Apparent optimized diffusion coefficients for UV and TOC were around 1.2–2.4 $\times$ 10^{-10} $m^2 \cdot s^{-1}$ and are close to values found in the literature. Due to their higher diffusion coefficients and higher permeability coefficient only around 40% of the low molecular weight acids (MW = 300–400) were retained. Between 30% and 40% of the low molecular acids that permeate the membrane can be removed with post nanofiltration via granulated activated carbon.

The resulting energy consumption of a hypothetical four-stage design, at average operating temperature of 5.73 °C, for the proposed full-scale process was calculated to be 0.54 $kWh \cdot m^{-3}$ produced water.

Acknowledgments: Financial support of the GenoMembran-project funded by The Swedish Water and Wastewater Association (Swedish Water Development, SVU) is gratefully acknowledged. Pentair X-Flow is acknowledged for the provision of various test modules. The authors would also like to acknowledge Kristina Dahlberg for her contribution of reagents, materials, and analytical tools, as well as Kenneth M. Persson for advise on data analysis.

Author Contributions: Alexander Keucken and Tom Spanjer designed and planned the experiments; Alexander Keucken performed the experiments; Tom Spanjer and Alexander Keucken contributed analysis tools. All the authors analyzed the data and wrote the paper.

Conflicts of Interest: The authors declare no conflict of interest. The funding sponsors had no role in the design of the study; in the collection, analyses, or interpretation of data; in the writing of the manuscript, and in the decision to publish the results.

Glossary of Terms

The following abbreviations are used in this manuscript:

Term	Definition
B	Solute Permeability Coefficient
C	Correction Factor
C_b	Concentration of Bulk
CEFF	Chemically Enhanced Forward Flushing
CIP	Cleaning In Place

$\mathbf{C_p}$	Concentration of Permeate
D	Hydraulic Membrane Diameter
D	Solute Diffusion Coefficient
DBP	Disinfection By-Product
DOC	Dissolved Organic Carbon
GAC	Granulated Activated Carbon
HS	Humic Substances
$\mathbf{J_{BW}}$	Backwash Flux
$\mathbf{J_F}$	Filtration Flux
K	Mass Transfer Coefficient
L	Membrane Length
LC-OCD	Liquid Chromatography-Organic Carbon Detection
LMWN	Low Molecular Weight Neutrals
MW	Molecular Weight
MWCO	Molecular Weight Cut-Off
NF	Nanofiltration
NOM	Natural Organic Matter
PES	Polyethersulfone
R	Recovery Rate
SEM	Scanning Electron Microscopy
SUVA	Specific Ultraviolet Absorbance
TMP	Transmembrane Pressure
TOC	Total Organic Carbon
UF	Ultrafiltration
$\mathbf{V_{CF}}$	Cross Flow Velocity
WTP	Water Treatment Plant
H	Removal Efficiency
χ_{II}	Partly-retained Fraction
χ_{III}	Non-retained Fraction

Appendix A

Table A1. All data (UV, DOC, TOC) and relevant data on container plant.

Experiment No.	Actual Order	[m·s^{-1}]	[L·m^{-2}·h^{-1}]	[%]	UV Feed	UV Concentrate	UV Permeate	TOC Feed	TOC Concentrate	TOC Permeate	DOC Feed	DOC Concentrate	DOC Permeate
1	3	0.25	5	50	2.086	2.139	0.226	13.1	13.3	2.16	13.0	12.7	1.72
2	1	0.25	10	50	1.972	2.137	0.205	12.8	13.1	2.01	12.4	12.5	1.56
3	13	0.25	15	50	1.888	2.108	0.235	12.1	13.1	2.15	10.8	12.8	2.05
4	7	0.25	20	50	1.76	2.008	0.244	12.1	14.8	2.06	11.2	13	1.95
5	12	0.25	25	50	1.636	1.911	0.237	10.4	12.5	2.32	10.1	11.5	2.12
6	6	0.5	5	50	2.13	2.146	0.217	12.6	12.9	2.19	12.4	12.6	1.72
7	16	0.5	10	50	2.183	2.223	0.196	14.6	15.1	1.65	14.5	15.1	1.64
8.1	0	0.5	15	50	2.078	2.218	0.18	13.2	13.7	2.7	11.9	12.5	1.75
8.2	9	0.5	15	50	1.996	2.143	0.176	13.6	13.7	1.7	12.5	13.2	1.36
8.3	21	0.5	15	50	2.083	2.236	0.187	14.3	15.2	1.25	14.2	15.2	1
9	8	0.5	20	50	1.963	2.117	0.184	14.1	15.4	1.75	12.3	13.5	1.42
10	4	0.5	25	50	1.994	2.21	0.199	13	13.8	1.78	12.7	13.1	1.65
11	14	0.75	5	50	2.095	2.118	0.224	13.8	14.2	1.52	13.5	14.2	1.46
12	17	0.75	10	50	2.19	2.21	0.179	14.7	15.2	1.5	14.5	15.2	1.48
13	10	0.75	15	50	2.155	2.267	0.158	15.5	16	1.68	13.5	13.8	1.2
13.1	22	0.75	15	50	2.189	2.264	0.165	13.9	14.3	1.43	14.4	15.3	1.33
14	20	0.75	20	50	2.23	2.219	0.16	14.5	15.5	1.31	14.4	15.5	1.25
15	11	0.75	25	50	2.059	2.191	0.151	14.4	15.8	1.6	13.2	13.5	1.13
16	15	1	5	50	2.125	2.146	0.224	14.2	14.3	1.48	14	14.3	1.48
17	2	1	10	50	2.09	2.222	0.165	13.2	13.5	1.66	12.2	12.8	1.65
18	18	1	15	50	2.183	2.28	0.159	14.1	14.2	1.48	14.8	15.2	1.3
19	5	1	20	50	2.078	2.194	0.144	12.5	13.1	1.52	12.6	12.8	1.4
20	19	1	25	50	2.118	2.279	0.149	14.5	15.6	1.18	14.4	15.5	1.16

Table A2. All data (UV, DOC, LC-OCD) on pilot scale plant (B/D experiments).

EXP	DOC ppb-C	HOC ppb-C	CDOC ppb-C	Bioply ppb-C	HS ppb-C	SUVA HS L/(mg·m)	MW g/mol	Buil ppb-C	LMW Neut ppb-C	LMW Acids ppb-C	Colloid (m^{-1})
A 3	7939	274	7666	457	183	3.86	632	1165	763	n.q.	0.082
B 3	12,114	417	11,697	371	281	3.83	658	1845	1249	n.q.	0.096
C 3	13,108	815	12,293	372	309	3.96	660	1932	1086	n.q.	0.131
D 3	2146	379	1768	8	32	3.15	511	455	384	12	0.001
A 13.1	7945	430	7515	259	172	3.98	658	1273	756	n.q.	0.077
B 13.1	13,892	656	13,237	456	318	3.75	658	2122	1082	n.q.	0.150
C 13.1	14,287	412	13,876	609	340	3.81	659	2165	1201	n.q.	0.112
D 13.1	1433	223	1209	25	17	3.30	534	316	295	13	0.010
A 8.2	7896	375	7521	215	184	3.87	653	1273	787	n.q.	0.052
B 8.2	13,607	483	13,124	640	314	3.69	659	2002	1117	n.q.	0.093
C 8.2	13,718	393	13,324	601	327	3.82	655	2048	1156	n.q.	0.090
D 8.2	1700	248	1452	18	22	3.14	506	358	359	2	0.001
A 18	7911	374	7537	251	177	3.95	668	1320	794	n.q.	0.060
B 18	14,076	259	13,816	540	322	3.80	658	2155	1479	n.q.	0.120
C 18	14,183	307	13,876	628	333	3.80	658	2160	1207	n.q.	0.110
D 18	1488	205	1284	30	23	3.37	537	334	314	10	0.000
A-S1	8496	392	8103	383	171	4.10	675	1054	750	42	0.055
B-S1	13,260	346	12,913	589	279	4.10	698	1608	1027	47	0.095
C-S1	14,437	600	13,837	659	297	4.14	696	1734	1079	33	0.101
D-S1	1944	293	1651	7	16	3.75	559	350	321	34	0.001
A-S2	8657	180	8477	313	183	3.99	689	1242	766	53	0.014
B-S2	14,484	481	14,003	473	303	3.91	711	2005	1068	38	0.015
C-S2	15,535	321	15,213	483	328	3.93	717	2209	1171	59	0.006
D-S2	2013	282	1731	2	19	3.34	563	386	345	41	0.002
A-S3	9027	141	8886	365	184	3.83	694	1200	722	75	0.075
B-S3	30,028	419	29,610	1439	652	3.75	746	3279	1667	50	0.334
C-S3	32,544	683	31,861	1733	643	3.67	727	3270	1759	n.q.	0.213
D-S3	3447	308	3139	17	42	3.27	579	637	470	53	0.002
A-S4	9033	93	8939	413	189	3.76	712	1228	756	21	0.076
B-S4	21,003	485	20,518	999	475	3.82	741	2697	1437	n.q.	0.219
C-S4	22,346	633	21,712	1090	503	3.83	703	2584	1410	n.q.	0.234
D-S4	2740	304	2436	5	32	3.38	567	548	428	29	0.005

Note: n.q. stands for concentrations not quantifiable or below the detection limit.

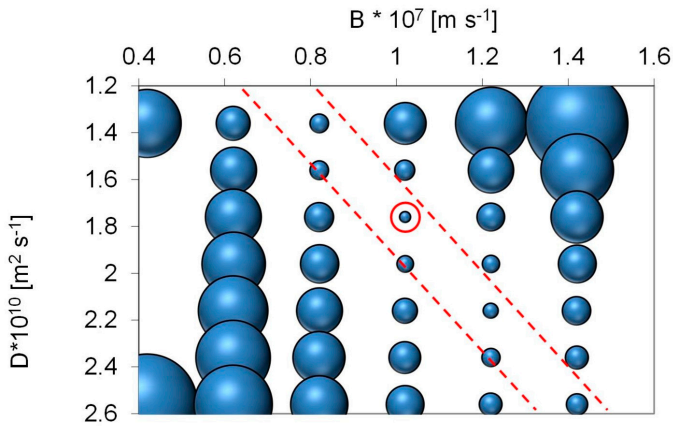

Figure A1. Plot of sum of systematic change of errors between modelled predicted and experimental DOC data when changing both D and B in increments of 0.2 units. D was varied from 1.36 to 2.76 and B between 0.22 and 1.22. An approximately linear relation exists between D and B ($D = -0.28 + 2 \times B$) that describes in which area space optimum conditions for B and D occur. Points between the two red lines have sum of errors that are within a factor of two with respect to the local minimum for $B = 1.02 \times 10^{-7}$ and $D = 1.76 \times 10^{-10}$.

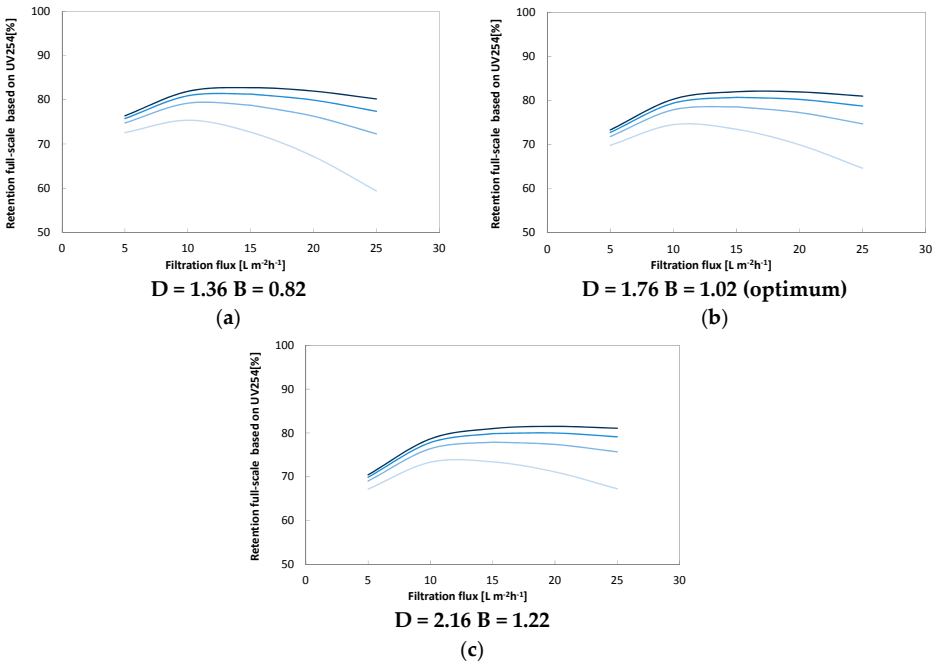

Figure A2. Illustration of potential outcome of varying optimum conditions for B and D along the optimum line presented above. Small values for both D and B (**a**), D and B decrease the optimum (**b**) window while larger values (**c**) D and B increase the apparent optimum range of operation. Overall this effect is smallest for cross flow rates between 0.5 and 0.75 $L \cdot s^{-1}$ and larger deviations occur for both the lowest (0.25 $L \cdot s^{-1}$) and the highest crossflow ($L \cdot s^{-1}$).

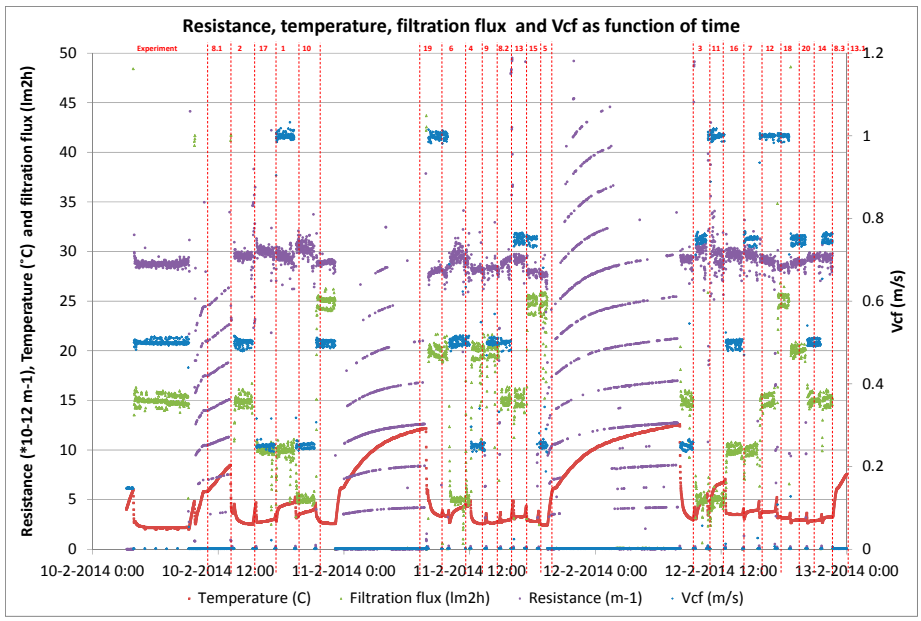

Figure A3. Membrane performance during short term trials for determination of B/D coefficients.

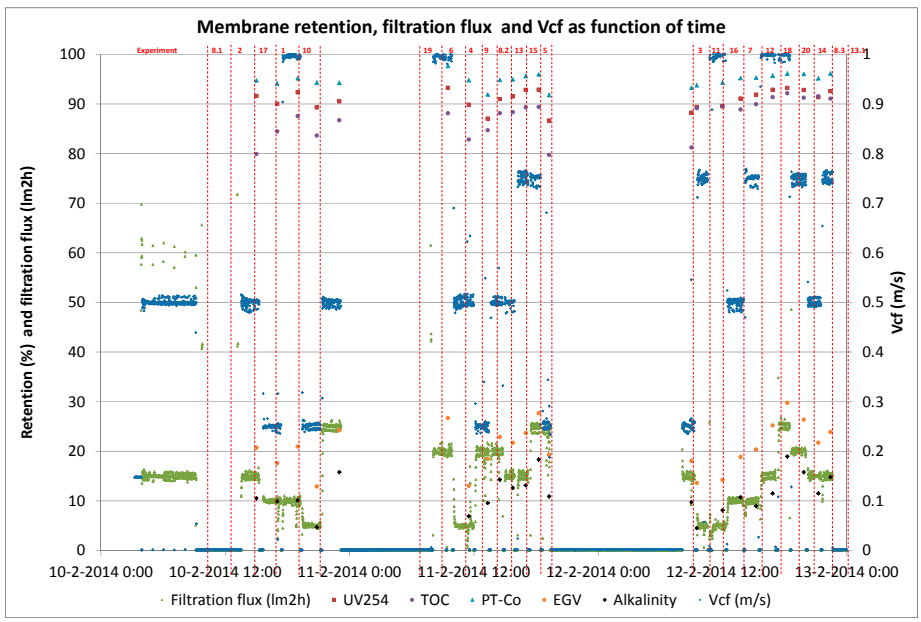

Figure A4. Retention behavior during short term trials for determination of B/D coefficients.

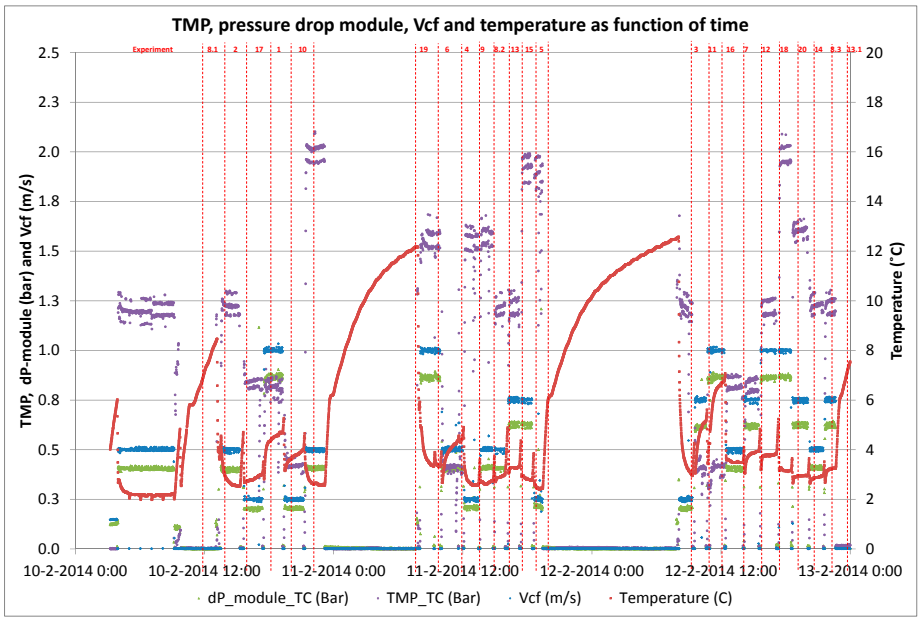

Figure A5. Membrane performance during short term trials for determination of B/D coefficients.

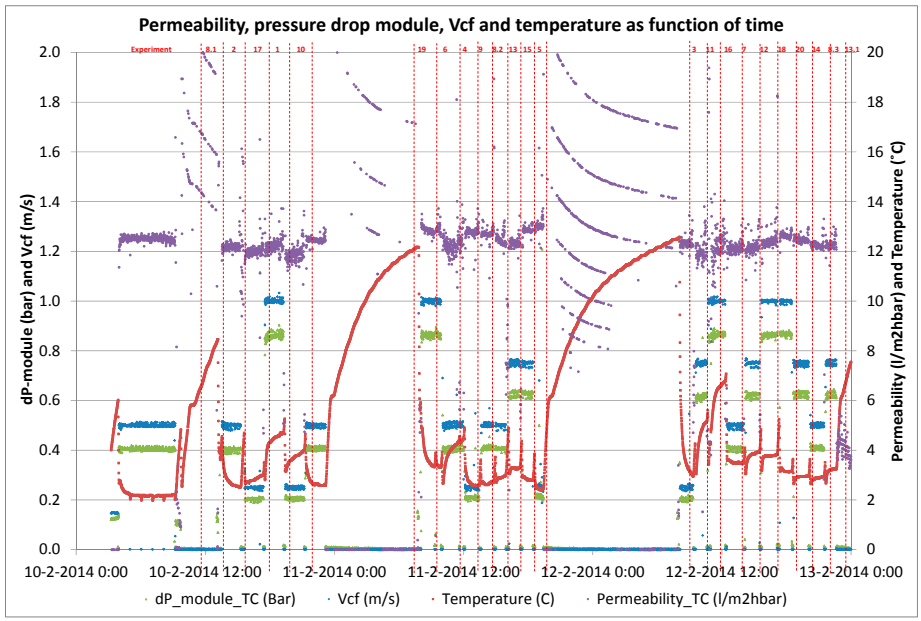

Figure A6. Membrane performance during short term trials for determination of B/D coefficients.

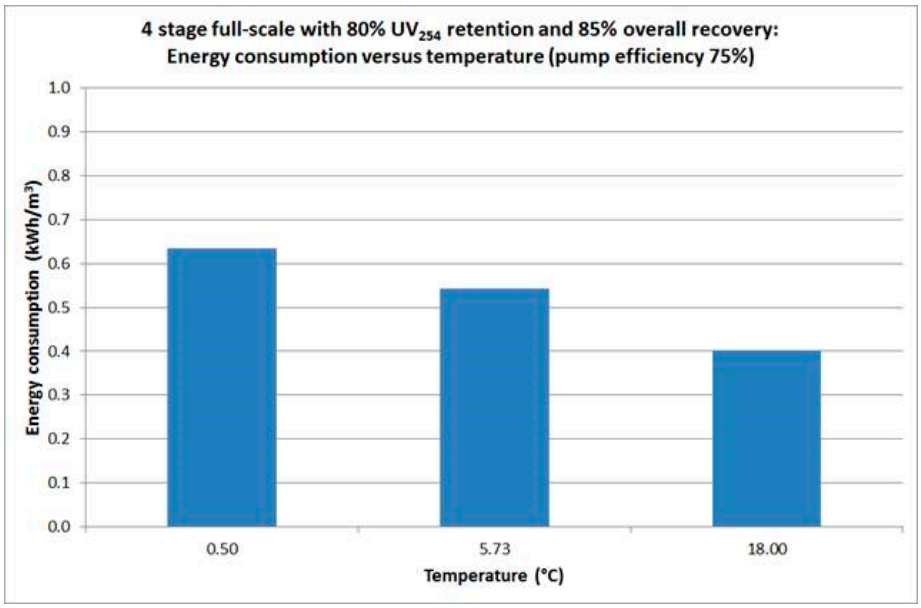

Figure A7. Influence of temperature related to energy consumption for retrofit design.

References

1. Granskog, M.; MacDonald, R.; Mundy, C.-J.; Barber, D. Distribution, characteristics and potential impacts of chromophoric dissolved organic matter (CDOM) in Hudson Strait and Hudson Bay. Canada. *Cont. Shelf Res.* **2007**, *27*, 2032–2050. [CrossRef]
2. Park, J.H.; Kang, S.-Y.; Kim, S.-Y. Hydroclimatic controls on dissolved organic matter (DOM) chararcteristics and implications for trace metal transport in Hwangryoong River Watershed, Korea, during a summer monsoon period. *Hydrol. Process.* **2007**, *21*, 3025–3034. [CrossRef]
3. Clements, W.; Brooks, M.; Kashian, D.; Zuellig, R. Changes in dissolved organic material determine exposure of stream benthic communities to UV-B radiation and heavy metals: Implications for climate change. *Glob. Chang. Biol.* **2008**, *14*, 2201–2214. [CrossRef]
4. Köhler, S.J.; Buffam, I.; Seibert, J.; Bishop, K.H.; Laudon, H. Dynamics of stream water TOC concentrations in a boreal headwater catchment: Controlling factors and implications for climate scenarios. *J. Hydrol.* **2009**, *373*, 44–56. [CrossRef]
5. Sulzberger, B.; Durisch-Kaiser, E. Chemical characterization of dissolved organic matter (DOM): A prerequisite for understanding UV-induced changes of DOM absorption properties and bioavailability. *Aquat. Sci.* **2009**, *71*, 104–126. [CrossRef]
6. Pautler, B.; Woods, G.; Dubnick, A.; Simpson, A.; Sharp, M.; Fitzimons, S.; Simpson, M. Molecular characterization of dissolved organic matter in glacial ice: Coupling natural abundance 1H NMR and fluorescence spectroscopy. *Environ. Sci. Technol.* **2012**, *46*, 3753–3761. [CrossRef] [PubMed]
7. Brezonik, W.; Arnold, W. Water chemistry: Fifty years of change and progress. *Environ. Sci. Technol.* **2012**, *46*, 5650–5657. [CrossRef] [PubMed]
8. Diem, S.; von Rohra, M.; Heringa, J.; Kohlera, H.-P.; Schirmera, M.; von Gunten, U. NOM degradation during river infiltration: Effects of the climate variables temperature and discharge. *Water Res.* **2013**, *47*, 6585–6595. [CrossRef] [PubMed]
9. Ritson, J.P.; Grahamb, N.J.D.; Templetonb, M.R.; Clark, J.M.; Gough, R.; Freemand, C. The impact of climate change on the treatability of dissolved organic matter (DOM) in upland water supplies: A UK perspective. *Sci. Total Environ.* **2014**, *473–474*, 714–730. [CrossRef] [PubMed]

10. Monteith, D.T.; Stoddard, J.L.; Evans, C.D.; de Wit, H.A.; Forsius, M.; Høgåsen, T.; Wilander, A.; Skjelkvåle, B.L.; Jeffries, D.S.; Vuorenmaa, J.; et al. Dissolved organic carbon trends resulting from changes in atmospheric deposition chemistry. *Nature* **2007**, *450*, 537–539. [CrossRef] [PubMed]
11. Delpla, I.; Jung, A.-V.; Baures, E.; Clement, M.; Thomas, O. Impacts of the climate change on surface water quality in relation to drinking water production. *Environ. Int.* **2009**, *35*, 1225–1233. [CrossRef] [PubMed]
12. Trang, V.; Phuong, L.; Dan, N.; Thanh, B.; Visvanathan, C. Assessment on the trihalomethanes formation potential of Tan Hiep Water Treatment Plant. *J. Water Sustain.* **2012**, *2*, 43–53.
13. Lavonen, E.E.; Gonsior, M.; Tranvik, L.J.; Schmitt-Kopplin, P.; Köhler, S.J. Selective chlorination of natural organic matter: Identification of previously unknown disinfection byproducts. *Environ. Sci. Technol.* **2013**, *47*, 2264–2271. [CrossRef] [PubMed]
14. Eikebrokk, B.; Vogt, R.D.; Liltved, H. NOM increase in Northern European source waters: Discussion of possible causes and impacts on coagulation/contact filtration processes. *Water Sci. Technol.* **2004**, *4*, 47–54.
15. Sharp, E.; Jarvis, P.; Parsons, S.; Jefferson, B. Impact of fractional character on the coagulant of NOM. *Colloids Surf. A. Physicochem. Eng. Asp.* **2006**, *286*, 104–111. [CrossRef]
16. Futselaar, H.; Schonewille, H.; Meer, W.V.D. Direct filtration nanofiltration—A new high-grade purification concept. *Desalination* **2002**, *145*, 75–80. [CrossRef]
17. Spenkelink, F.J. Capillary Nanofiltration—Influence of Membrane Characteristics & Process Parameters on Permeate Quality. Master's Thesis, UNESCO-IHE, Delft, The Netherlands, January 2012.
18. Köhler, S.J.; Lavonen, E.E.; Keucken, A.; Schmitt-Kopplin, P.; Spanjer, T.; Persson, K.M. Upgrading coagulation with hollow-fibre nanofiltration for improved organic matter removal during surface water treatment. *Water Res.* **2016**, *89*, 232–240. [CrossRef] [PubMed]
19. Lidén, A.; Persson, K.M. Comparison between ultrafiltration and nanofiltration hollow-fiber membranes for removal of natural organic matter—A pilot study. *J. Water Supply Res. Technol.-Aqua* **2015**, *65*. [CrossRef]
20. Keucken, A.; Wang, Y.; Tng, K.H.; Leslie, G.L.; Persson, K.M.; Köhler, S.J.; Spanjer, T. Evaluation of novel hollow fiber membranes for NOM removal by advanced membrane autopsy. *Water Sci. Technol. Water Supply* **2016**, *16*, 628–640.
21. Van der Bruggen, B.; Schaep, J.; Wilms, D.; Vandecasteele, C. Influence of molecular size, polarity and charge on the retention of organic molecules by nanofiltration. *J. Membr. Sci.* **1999**, *156*, 29–41. [CrossRef]
22. Van der Bruggen, B.; Vandecasteele, C. Removal of pollutants from surface water and groundwater by nanofiltration: Overview of possible applications in the drinking water industry. *Environ. Pollut.* **2003**, *122*, 435–445. [CrossRef]
23. Wijmans, J.G.; Baker, R.W. The solution-diffusion model: A review. *J. Membr. Sci.* **1995**, *107*, 1–21. [CrossRef]
24. Wijmans, J.G. The role of permanent molar volume in the solution-diffusion model transport equations. *J. Membr. Sci.* **2004**, *237*, 39–50. [CrossRef]
25. Hoek, E.M.; Elimelech, M. Cake-enhanced concentration polarization: A new fouling mechanism for salt-rejecting membranes. *Environ. Sci. Technol.* **2003**, *37*, 5581–5588. [CrossRef] [PubMed]
26. Bandini, S.; Vezzani, D. Nanofiltration modeling: The role of dielectric exclusion in membrane characterization. *Chem. Eng. Sci.* **2003**, *58*, 3303–3326. [CrossRef]
27. Wang, X.M.; Li, B.; Zhang, T.; Li, X.Y. Performance of nanofiltration membrane in rejecting trace organic compounds: Experiment and model prediction. *Desalination* **2015**, *370*, 7–16. [CrossRef]
28. Kong, F.X.; Yang, H.W.; Wang, X.M.; Xie, Y.F. Assessment of the hindered transport model in predicting the rejection of trace organic compounds by nanofiltration. *J. Membr. Sci.* **2016**, *498*, 57–66. [CrossRef]
29. Kataoka, T.; Tsuru, T.; Nakao, S.I.; Kimura, S. Permeation equations developed for prediction of membrane performance in pervaporation, vapour permeation and reverse osmosis based solution-diffusion model. *J. Chem. Eng. Jpn.* **1991**, *24*, 326–333. [CrossRef]
30. Nagy, E.; Kulcsár, E.; Nagy, A. Membrane mass transport by nanofiltration: Coupled effect of the polarization and membrane layers. *J. Membr. Sci.* **2011**, *368*, 215–222. [CrossRef]
31. Spenkelink, F.J.; Wennekes, W.B.; Blankert, B.; Knops, F.; Dekker, R.; Potreck, J. New Developments in Hollow Fiber Nanofiltration. In Proceedings of the 2nd Dissemination Workshop of the Nano4water Cluster, Chalkidiki, Greece, 24–25 April 2012.
32. Romera, C.A.; Davis, R.H. Global model of crossflow microfiltration based on hydrodynamic diffusion. *J. Membr. Sci.* **1988**, *39*, 117. [CrossRef]

33. Thorsen, T. Concentration polarization by natural organic matter (NOM) in NF and UF. *J. Membr. Sci.* **2004**, *233*, 79–91. [CrossRef]
34. Mulder, M. *Basic Principles of Membrane Technology*, 2nd ed.; Technical University of Twente: Enschede, The Netherlands, 1996.
35. Park, N.; Cho, J. Natural organic matter diffusivity for transport characterizations in nanofiltration and ultrafiltration membranes. *J. Membr. Sci.* **2008**, *315*, 133–140. [CrossRef]
36. Huber, S.A.; Balz, A.; Abert, M.; Pronk, W. Characterisation of aquatic humic and non-humic matter with size-exclusion chromatography-organic carbon detection-organic nitrogen detection (LC-OCD-OND). *Water Res.* **2011**, *45*, 879–885. [CrossRef] [PubMed]
37. Laurell, P.; Sivonen, K.; Poutanen, H.; Vuorileto, V.-P.; Hesampour, M.; Kettunen, V.; Tuutijärvi, T.; Vahala, R. Applicability of loose nanofiltration membranes for the removal of natural organic matter from soft surface water. In Proceedings of the 5th IWA Specialist Conference on Natural Organic Matter in Water, Malmö, Sweden, 7–10 September 2015.

Paper IV

Simulation of NOM removal by capillary NF: A numerical method for full-scale plant design

Alexander Keucken [1,2], Xuefei Liu[3], Boyue Lian [3], Yuan Wang [3], Kenneth M. Persson [2,4], Greg Leslie*[3]

[1] Vatten & Miljö i Väst AB (VIVAB), Box 110, 311 22 Falkenberg, Sweden

[2] Water Resources Engineering, Faculty of Engineering, Lund technical University, Box 118, SE-221 00 Lund, Sweden

[3] UNESCO Centre for Membrane Science & Technology, University of New South Wales, Sydney 2052, Australia

[4] Sweden Water Research AB, Ideon Science Park, SE 223 60 Lund, Sweden

Submitted to Journal of Membrane Science

October 2017

* Corresponding author: Greg Leslie: g.leslie@unsw.edu.au

Highlights

- NOM transfer in novel NF membrane modules was successfully modelled using CFD
- The impact of double –pass loop operation mode on the efficiency of NOM removal was evaluated
- The performance of a hypothetical four-stage full-scale plant was predicted showing higher NOM removal than a three-stage plant at same water recovery.

Abstract

The removal of natural organic matter (NOM) from boreal lake water by a novel capillary nanofiltration (NF) membrane was predicted using a computational fluid dynamics(CFD). The 2-dimensional axis-symmetric model was based on a 48 m^3/day NF pilot plant operating in cross-flow mode on water containing 8 mg/L total organic carbon (TOC) at fluxes ranging from 10 – 25 l/m^2/h and velocities ranging from 0.25 to 1.0 m/s. A "mass jump" source code developed using the solution diffusion model was used to simulate water flux and variations in NOM content as a function of axial and radial position in the capillary fibres. The model was validated within 3% accuracy using pilot data for filtrate TOC and UV254 absorbance and longitudinal pressure drop. The model was subsequently used to compare the effect of module length and number of stages on the design performance of a 110.000 m^3/day NF plant. Simulations indicated that 1.5 m long modules operated in a double pass configuration removed 33% more NOM compared with 3.0 m long modules in a single pass. Moreover, the use of 1.5 m modules in the full-scale plant configured in a 10:5:3:2 four stage array achieved greater NOM removal than a 10:5:3 three stage at the same plant water recovery (90.5%) using lower recycle rates and lower net energy consumption. The paper demonstrates that the combination of experimental and numerical methods can be an effective tool for the design of nanofiltration plants for NOM removal.

Keywords: NOM removal, Nanofiltration, Computational Fluid Dynamics

1. Introduction

The increase of natural organic matter (NOM) concentration in surface water was first identified in the late 1980s when Forsberg reported a link between increased amount of humic substance and the darkening of Sweden lakes [1]. In the ensuing decades the effect has been reported in other countries in Europe, the Americas and Asia [2-4], and attributed to a variety of causes, including increased surface temperatures, variations in rainfall intensity and decline in acid rain[5, 6]. Elevated NOM levels in surface waters presents a suite of problems for potable supplies, including (i) poor aesthetics associated with colour, taste and odor, (ii) higher treatment cost due to increased coagulant and disinfectant dose requirements, which in turn results in increased sludge (iii) increased health risks due to increased potential for disinfection by-product (DBP) formation and biological growth in distribution system, and increased levels of complexed heavy metals and adsorbed organic pollutants [7]. Therefore, increasing the efficacy of drinking water treatment processes to deal with elevated NOM is critical.

The most common and economically feasible method of NOM removal is coagulation and flocculation followed by sedimentation/flotation and filtration. NOM removal through coagulation, however, is selective and affected by the NOM composition[8, 9]. Recently we reported variable NOM removal ranging from 50% to 52% NOM using coagulation/sedimentation and filtration at the Gorvaln WTP in Sweden [10]. In contrast at the same plant, a pilot scale combined coagulation/membrane filtration process using a recently developed chemically resistant capillary fibre NF membrane, was found to achieve a more than 90% removal of the dissolved organic carbon (DOC), and 96% removal of the DOC-normalised absorbance at 254 nm with little change on water hardness. Additionally, no substantial changes on membrane were detected after 12 months of operation through membrane autopsy [11]. Water recovery comparable to conventional filtration could be achieved with the pilot NF by operating single modules in multiple pass mode, while coagulant consumption was lower in NF compared to conventional filtration because it was not necessary form a settleable or filterable floc [10]. However, operating in multiple pass mode increases power consumption per cubic meter (kWh/m^3). Therefore, scale up of NF system for NOM removal at

municipal water treatment scale necessitates configuring the modules in multiple stages and operating in a double pass[12]. In staged designs, each module in series will operate on feedwater with a high concentration as water is recovered and NOM retained. As a result, the resistance of the retained NOM, the water flux and the filtrate quality will differ for each module. Consequently, in order to optimize power consumption, water recovery and filtrate quality it is necessary to predict NOM spatial variations in each module in the multi-stage system. This requires a detailed understanding of NOM rejection by the NF membrane as a function of design flux and cross flow velocity.

Several theories and models have been developed to describe the rejection of anions and cations by NF [13-21]. The literature teaches that NOM rejection in this process will depend on: (i) transport through concentration polarization (CP) layer, (ii) partitioning phenomena at membrane interfaces and, (iii) solute transport through membrane pores [13]. Previous numerical models for the NF process include empirical mass-balance/black box approach to models based on irreversible thermodynamics [14] and deterministic models based on the Extended Nernst–Planck equation (ENP) [15]. Deterministic models account for properties of both the membrane and hydraulic conditions in the module that can alter the spatial concentrations. For example, mass transfer models derived from space charge (SC) modeling [16] assume radial homogeneity of ionic concentration and potential across the pores, which is valid in the case of small surface charge densities and sufficiently narrow pores, maintained under most NF conditions. Pore transport models have also been built upon the ENP equation. Bowen and Mukhtar suggested a hybrid model based on ENP with a Donnan condition at membrane-electrolyte interfaces and the hindered nature of transport through membranes[17]. This hybrid model was subsequently modified to include a “Donnan-steric-pore model” (DSPM) [18]. Further modifications to the DSPM account for the effects of pore size distribution on the rejection of uncharged solutes and NaCl for hypothetical NF membranes incorporating dielectric constant variations between bulk and pore to calculate ionic distribution between bulk and pore solutions[19]. Different approaches are proposed to include dielectric exclusion (DE) in the modeling, namely DSPM&DE [20] and SEDE (steric-electric-dielectric exclusion) [21]. However, all these mathematical models simplify the hydraulic conditions that influence the NOM convection and

diffusion and ignore the effects of module geometry. This limited the application of these models for predicting NOM transport in complicated hollow fibre membrane modules.

Computational Fluid Dynamics (CFD) methods have been used to link rejection fundamentals with hydraulic conditions to predict NOM transport in NF systems [22]. CFD modelling of NF process requires the coupling of water and NOM transport modelling in a specific module geometry with a transmembrane model for water and NOM transport across the membrane. However, a feature of CFD models for NF processes is the assumption that the membrane behaves as animpermeable, "no-slip" wall [23]. This approach neglects the water flux and concentration polarization near membrane surface. Recently, Liang et al. developed a 2D simulation of an electro-osmosis enhanced bench-scale membrane filtration by combinng a permeable wall model, based on the approach of Kedem and Katchalsky, to simulate the water flux and a solute mass balanced model based on Neumann boundary conditions [24, 25] for solute mass balance on membrane surface This permeable wall model required the simulation of flow field in membrane which resulted in significant computational effort. Carlos et al. recently used a dissolving wall boundary condition to simulate water and solute transfer in a NF small device [26]. The successful development of numerical models for bench-scale NF process indicates the potential to evaluate the performance of full scale, multi-stage NF plant designs using CFD techniques. The challenge is to verify the accuracy of the model by validating simulated data with independent empirical observations using full scale membrane modules.

Therefore, in this paper, we have used a novel "mass jump" method [27] in a CFD model to assess NOM removal efficiency of a single NF membrane and NF modules operated in a double-pass loop mode. The model was validated using experimental data derived from previous short-term experiments and long-term pilot trials at the Gorvaln WTP in Sweden [12]. The model was subsequently used to predict the performance of a full-scale multi-stage NF membrane system (Figure 1).

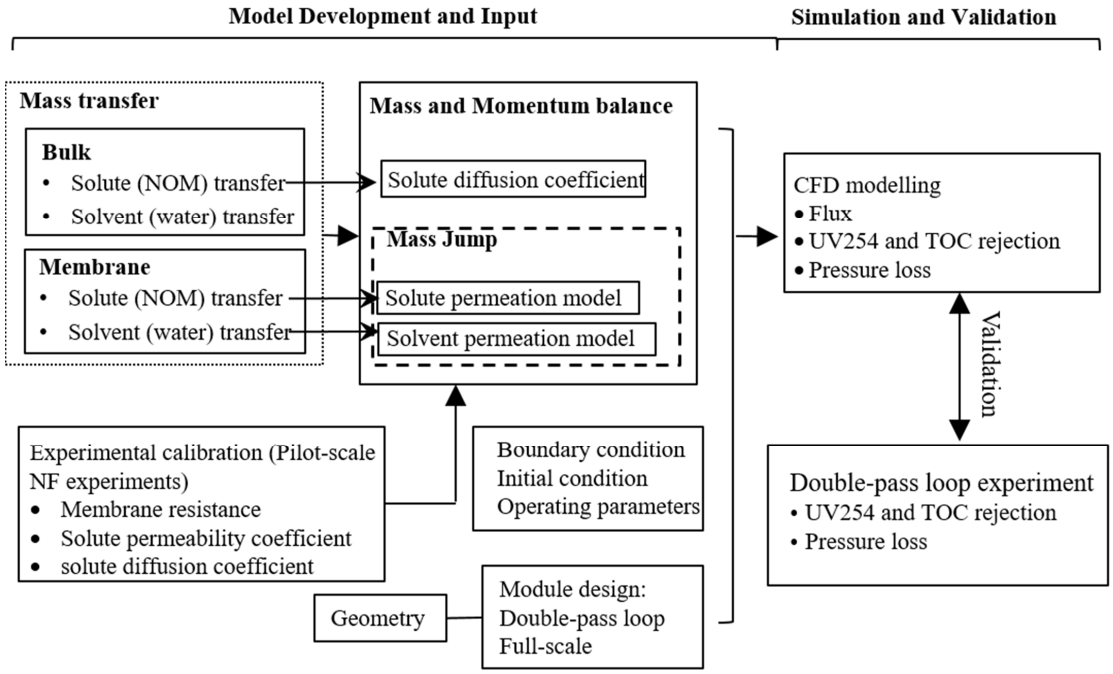

Figure 1: Workflow diagram for CFD modelling of hydraulic properties of NF process

2. Model development

CFD modelling of NOM separation from boreal lake water using NF membrane involves the simulation of solvent (water) transport and solute (NOM) transport in bulk and through membrane. Mass transfer was simulated by mass and momentum balance, with experimentally calibrated submodels and coefficients including solute diffusion coefficient for solute transfer in bulk, solvent permeation model for solvent transfer through membrane and solute permeability model for solute transfer through membrane (Figure 1).

In terms of governing equations, the transport of solvent in bulk can be expressed by the Navier-Stokes (NS) equations. While the solvent transportation through membrane was solved by adding a mass sink, S_m, and a momentum source terms, S_v, on membrane surface, expressed as,

$$S_m = -\frac{J \cdot A}{V}, at\ r = r_0; \quad \text{Equation 1}$$

$$S_v = -\frac{J \cdot A \cdot v}{V}, at\ r = r_0. \quad \text{Equation 2}$$

Where A is area. Solvent transport is driven by the difference between transmembrane pressure and osmotic pressure, and expressed as a mass flux J using the approach of Kedem and Katchalsky as,

$$J = \frac{1}{\mu R_m}(\Delta P - \Delta \Pi) \quad \text{Equation 3}$$

Where R_m is membrane resistance, μ is fluid viscosity, ΔP is transmembrane pressure, ΔΠ is osmotic pressure induced by solute concentration at membrane surface.

Comparatively, solute transportation in bulk was solved by conservation equation with consideration of the convection-diffusion effects, expressed as,

$$\frac{\partial \rho}{\partial t} + \nabla \cdot (\rho v) = -\nabla \cdot J_{sd} \quad \text{Equation 4}$$

Where J_{sd} is the diffusion flux. Solute permeation through the non-porous NF membrane was simulated by adding a mass sink at membrane surface, S_s, espressed as,

$$S_s = -\frac{J_s \cdot A}{V}, at\ r = r_0$$ Equation 5

The solute flux, J_s, is driven by the concentration difference between permeate and the concentration at membrane surface. For a neutral solute at low concentration (i.e. NOM in surface water), it can be calculated using an expression intuitively related to Fick's Law [28], defined as,

$$J_s = P_s(C_m - C_p)$$ Equation 6

Where P_s is the solute permeability coefficient, C_p is the solute concentration in permeate.

3 Method

3.1 Physical NF process

A pilot scale NF plant was operated in Görväln water treatment plant (WTP) to treat water from Lake Mälaren, Sweden. The pilot plant was configured with 8 inch commericial size capillary nanofiltration membrane modules (40 m^2 effective surface area) employing the innovative HFW 1000 membrane (Pentair®) with an external diameter of 1.15 mm and an internal diameter of 0.80 mm. With the separating layer located at the lumen side of the capillary membrane fibre, the membrane module was operated in an inside-out filtration mode. The whole pilot plant was operated in a double-pass loop mode based on two membrane modules connected in series (Figure 2). The concentrate of the first module was the feed for the second module. And the concentrate of the second module was circulated back to the feed of the first module. This setup halves the circulation flow rate and resulted in smaller circulation pipes/headers. Further details of the pilot plant can be found elsewhere [10, 12].

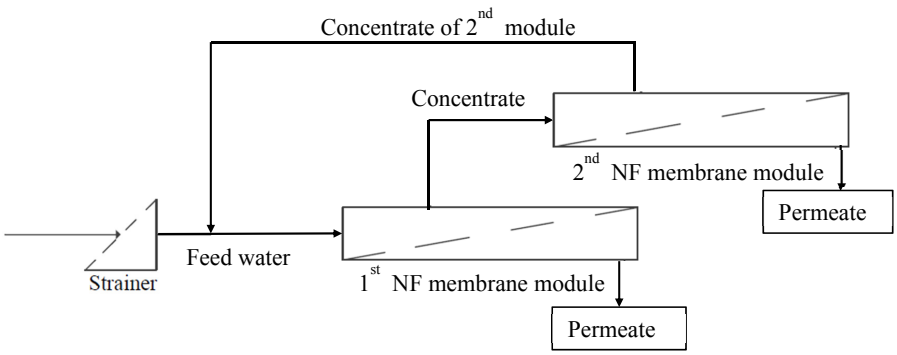

Figure 2: Simplified flow diagram of the HFW 1000 unit

The multi-stage full scale plant was designed to be comprised of stages which were connected in series (Figure 3). In other word, the concentrate of the previous stage was the feed for the later stage. In each stage, membrane modules were operated in the double-pass loop mode and in parallel. The performance of a full scale plant in a configured 10:5:3:2 four stage array was compared to a typical three-stage full plant configured in a stage ratio of 10:5:3.

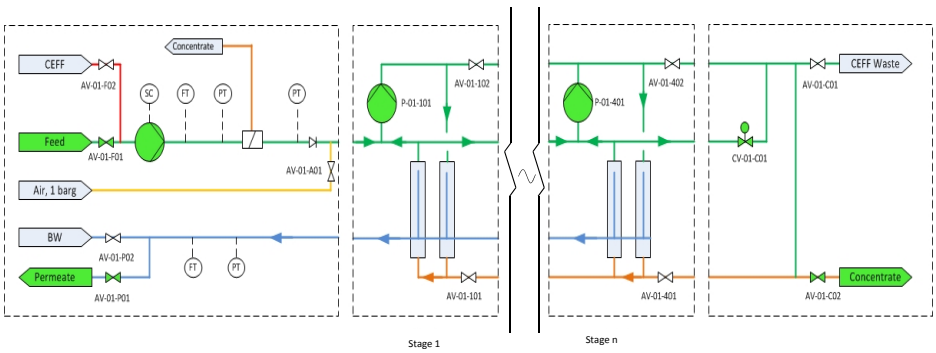

Figure 3: Simplified flow diagram of full-scale plant

3.2 CFD simulation

The commercial CFD software ANSYS Fluent 16.2® was employed to simulate the flow field in the pilot-scale HFW 1000 unit. For the inside-out membrane unit, the geometry was simplified as single fibre employing a two-dimensional axisymmetric geometry. The model was used to evaluate the impact of the double-pass loop operation mode on NOM removal efficiency. Elements of the model of the single module were expanded to evaluate the performance of various multi-stage full scale plant operations.

Five inflation layers with a first layer thickness of 5×10^{-5} m and a growth rate of 1.2 × per layer were set near the liquid-membrane interfaces, ensuring the zones where concentration polarization and transport phenomena occur were simulated using a higher mesh resolution (Figure 4). The sweeping method was employed along fibre length with a 5 mm mesh size along the axis selected according the

grid-independence test (Figure S1), resulting in a total of 50000 elements and an average aspect ratio of 0.25.

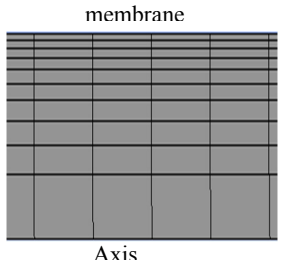

Figure 4: Mesh for lumen side fluid

Reynolds number of the feed flow varied from the minimum value of 225 at the crossflow velocity of 0.25 m/s, to the maximum value of 899 at the crossflow velocity of 1.0 m/s, indicating the flow profile follows laminar flow behaviour. The laminar model was employed to simulate the flow inside membrane fibre. Solute was simulated as a species with the mixing simulated following the volume-weighted mixing law. Membrane filtration process was simulated using a "mass jump" method developed by Lian et al. (2016), which utilizes source terms S_m and S_v to define mass and momentum sinks of the solvent and one more source term S_s to define mass sink of the solute at the membrane and feed interface. Details of the" mass jump" method were described elsewhere [27] (Supplementary S1).

All simulations were carried out using the SIMPLE (Semi-Implicit Method for Pressure Linked Equations) algorithm for pressure–velocity coupling and Second Order Up-wind algorithm for discretization of the conservation equations. No slip wall with conjugated heat transfer was used for the wall boundary conditions. All simulations were performed at steady-state conditions with a convergence level of 10^{-5} for the solvent continuity and 10^{-6} for the continuity of the solute.

3.3 Experimental calibration and model validation

Twenty short-term experiments (<2 hours) different cross-flow velocities from 0.25 to 1.0 m/s at filtration fluxes between 10 - 25 L/m^2/hr (LMH) were performed on the pilot plant for model calibration and validation. For each experiment, water samples of feed, concentrate and permeate were collected when steay stete conditions reached which is ensured by on-line measurements of conductivity in the circulation loop and permeate line. The total organic carbon (TOC) and dissolved organic carbon (DOC) were determined using a Elementar (SRN) Vario TOC Cube analyzer with a precision of 0.2 mg L^{-1}. UV absorbance at 254nm was determined with a 5 cm cuvette. During the operation period, the TOC of the feed water ranges from 7.3 mg/ L to 9.8 mg/L. The UV_{254} adsorbance ranges from 1.09 to 1.44. Details on feed water quality can be found in Table 1.

Table 1: Average feed water quality

Parameters	Unit	Range
Temperature	°C	2–12
pH	(-)	7.2–8.2
Turbidity	(NTU)	2–5
Conductivity	(μS/cm)	150–230
UV_{254}	(/5·cm)	1.09-1.44
Pt-Co	(mg·Pt/L)	28–33
DOC	(mg·C/L)	7.3–9.8

Further details of the experiment operations in pilot plant can be found elsewhere [10, 12]. The solute diffusion coefficient and the solute permeability coefficient (Table 2) deduced using solution diffusion model [12] were used to calibrate the diffusion coefficient in Equation 4 and Equation 6, and experimentally measured membrane resistance were imported in Equation 3. It should be noted that with the short-term experimental data incorporated into CFD modelling which neglected membrane fouling, this model cannot predict long-term membrane performance.

Experimentally measured solute retention and pressure drop along fibre length [12] were used for model validation.

Table 2: Parameters for model calibration

Parameters	Values
Membrane resistance $*10^{13}$ (m^{-1})	2.65
TOC diffusion coefficient (m^2s^{-1})	1.65×10^{-10}
UV254 diffusion coefficient (m^2s^{-1})	1.74×10^{-10}
TOC permeability coefficient (ms^{-1})	1.69×10^{-7}
UV254 permeability coefficient (ms^{-1})	1.01×10^{-7}

4. Results and Discussion

4.1 Model validation

System performance was evaluated at fluxes ranging from 10 - 25 LMH at cross flow velocities ranging from 0.25 to 1.0 m/s. Simulated performance differed from experimental observation by 1.9% for retention of UV254 (Figure 5a), 2.1% for retention of TOC (Figure 5b) and 1.0 % for pressure drop (Figure 5c).

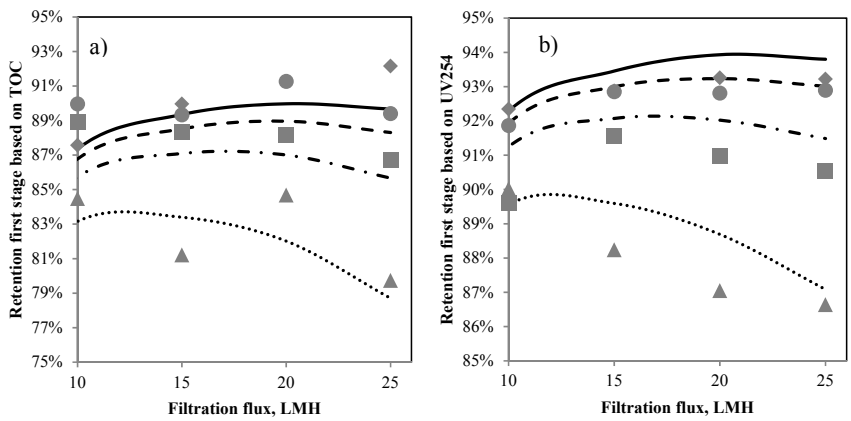

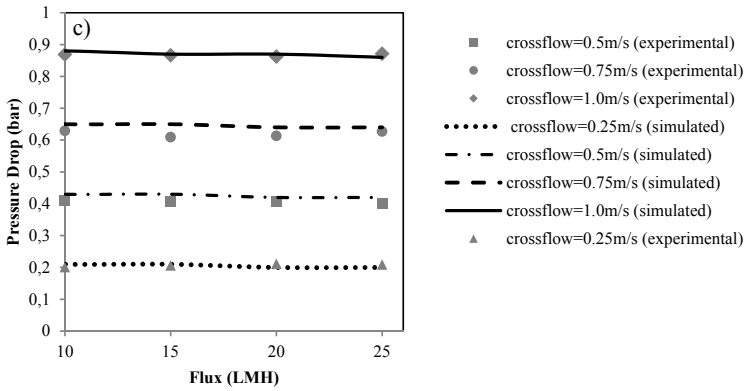

Figure 5: Comparison between experimental and simulated (a) TOC retention, (b) UV254 retention and (c) pressure drop at different cross-flow velocities ranging from 0.25 to 1.0 m/s at filtration fluxes between 5 - 25 LMH

The simulated solute retention based on TOC and UV254 was found to be larger than 78.7% and 87.1%, respectively, for all cases with different cross-flow velocities from 0.25 to 1.0 m/s at filtration fluxes between 10 - 25 LMH (Figure 5 a and b). Increasing the cross- flow velocity significantly increased the TOC retention from 78.7% at 0.25 m/s to 89.4% at 1.0 m/s when the flux was kept constant at 25 LMH. The impact of flux on NOM recovery was more complicated. At comparatively higher cross-flow velocity, for example 1.0 m/s, the solute retention based on TOC increased gradually from 87.6% to 89.4% when the water flux increased from 10 LMH to 25 LMH. An opposite trend was observed at 0.25 m/s cross-flow velocity with TOC retention decreased from 83.2% at 10 LMH flux to 78.7% at 25 LMH flux. A similar but less pronounced trend was obtained for UV254. For example, the largest increase in retention from 87.1% to 93.2% was obtained by increasing the cross-flow velocity from 0.25 m/s to 1.0 m/s at 25 LMH flux. This indicated the increase of cross-flow velocity contribute more on the removal of colourless NOM.

The pressure drop along fibre length significantly increased around 4 times from 0.21 bar under 0.25m/s cross-flow to 0.88 bar under 1.0 m/s cross-flow at a flux of 10 LMH (Figure 5c). Increasing flux from 10 LMH to 20 LMH at different cross-flow velocities from 0.25 to 1.0 m/s had no impact on pressure drop. This is expected as the maximum flux is approximately 2.2×10^{-3} times lower than

the minimum cross-flow velocity and has negligible impact on pressure drop in this inside-out HF membrane.

4.2 Single module

Water flux as a function of position along fibre length was simulated under four cross-flow velocities ranging from 0.25 to 1.00 m/s at an inlet TMP of 2.6 bar (Figure 6). Flux declined linearly as a function of position. The maximum flux decline of 10.4 LMH, equivalent to 40% of the average flux was observed at the highest cross-flow velocity of 1.0 m/s. The flux decline was less pronounced at lower cross-flow velocities (Figure 6).

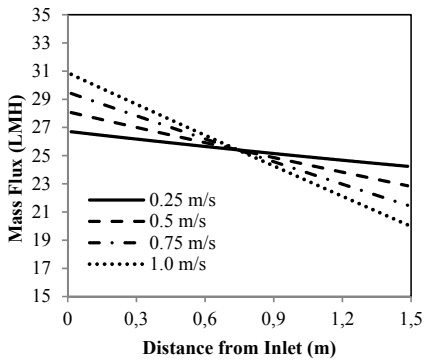

Figure 6: water flux distribution along module length at different cross-flow velocities

TOC increased as a function of position from a concentration of 8.0 mg/L at the inlet (position 0) at cross-flow velocities ranging from 0.25 to 1.0 m/s (Figure 7a). A maximum TOC of 80.2 mg/L was simulated at the the outlet of membrane module at a cross-flow velocity of 0.25 m/s (Figure 7a). Increasing the cross flow velocity to 0.5 m/s resulted in a 42% decrease to 46.6 mg/L at the outlet. Increasing the cross-flow velocity to 0.75 m/s and 1.0 m/s reduced the TOC at the outlet to 35.1 mg/L and 29.6 mg/L, respectively.

Similar trends were observed for solute flux distribution along fibre length (Figure 7b), since the local solute flux was determined by the local concentration difference between the feed side and permeate side. The solute flux increased along fibre length from an initial flux of 1.9 mg/m^{2}hr to the maximum

solute flux of 17.1 mg/m^{2}hr and the minimum solute flux of 6.2 mg/m^{2}hr at cross-flow velocity of 0.25 m/s and 1.0 m/s, respectively.

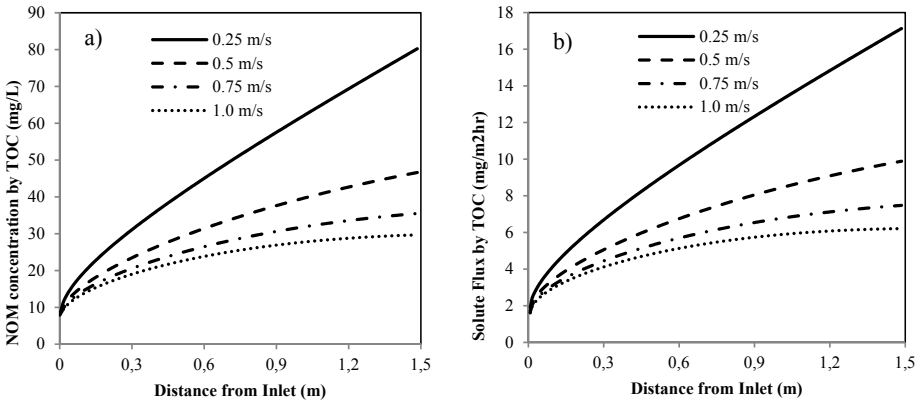

Figure 7: solute concentration at the lumen side of membrane (a) and solute flux (b) as a function of fibre length at different cross-flow velocities

4.3 Double-pass loop operation mode

Water flux distribution in membrane modules was simulated for operation under a double-pass loop mode. Neglecting the local head loss at the connector of the 1st module and 2nd module, the mass flux at the outlet of the 1st module was found to be the same with that at the inlet of the 2nd module (Figure 8). This indicated that the water flux distribution in the double –pass loop membrane modules comprised of two 1.5 m membrane modules was the same as a single 3 m long membrane module. Starting with an initial TMP of 2.42 bar and a cross-flow velocity of 0.57 m/s, the water flux declined linearly from 25.3LMH near the inlet of the 1st module to 13.8 LMH near the outlet of the 2nd module (Figure 8).

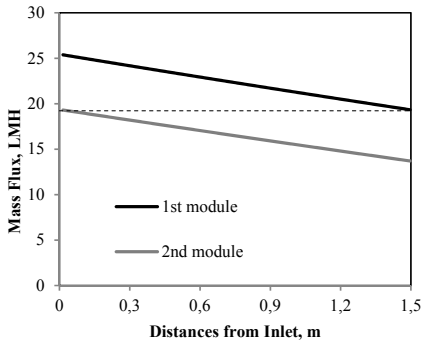

Figure 8: Comparison of water flux distribution along module length between 1st module and 2nd module

Concentration polarisation near membrane, *CP,* expressed as $(C_m - C_P)/(C_b - C_p)$, experienced a obvious decline from 6.1 at the outlet of the 1st module to 1.0 at the inlet of the 2nd module (Figure 9). This was based on a C_m of 56.76 mg/L at the outlet of the 1st module and a C_m of 9.85 mg/L at the inlet of the 2nd module (equivalent to C_b value at the same location (Figure 9). This indicated that the flow mixing without filtration at the connector disrupts the concentration polarisation near the outlet of 1st module. A single 3.0 m long module would exihibt higher concentration polarisation compared to two 1.5 m modules operating in series.

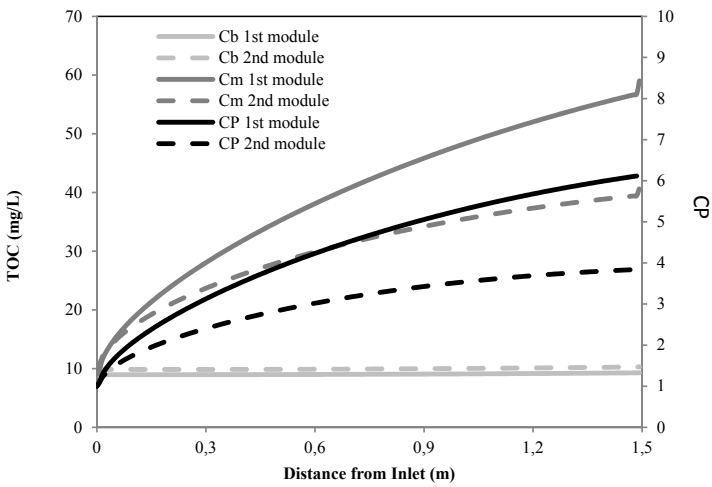

Figure 9: Comparison of TOC in bulk solution C_b, TOC near membrane C_m and concentration polarisation at membrane *CP* along module length between 1st module (solid line) and 2nd module (dash line)

Similarly, operating two 1.5 m modules in series produces a lower solute flux profile than a single 3.0 m module (Figure 10). Simulated solute flux was 50% lower at the outlet of two 1.5 modules in series (10 mg/m^2.hr) compared to a single 3.0 m module (20 mg/m^2.hr) (Figure 10). Operation of two 1.5 m modules in series reduces the solute flux 17.1 mg/m^2.hr at the outlet of the 1st module to 2.9 mg/m^2.hr at the inlet of the 2nd module. This produces approximately a 33% decrease in final permeate TOC (Figure 10). Therefore, for the same water recovery NF modules operated in double-pass can operate at higher flux and produce better quality water than a single module of twice the length.

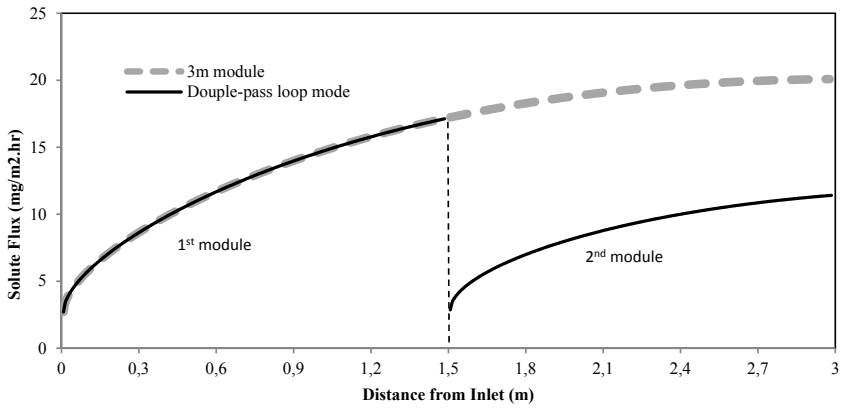

Figure 10: solute flux distribution along fibre length in membrane module operated in double-pass loop vs. a single 3m long membrane module

4.4 Full-scale NF process

The performance of a three-stage plant configured with 7200 NF modules in a module ratio of 10-5-3 was compared to a a 10:5:3:2 four stage configuration (Table 3). All NF processes were operated on feedwater containing 8.0 mg/L of TOC at double-pass loop mode with an initial TMP of 2.42 bar at the inlet of the 1st membrane module for each stage and a cross flow velocity of 0.57 m/s.

NOM removal was estimated to be 66.8% (based on TOC) and 76.3% (based on UV254) for a three stage plant operating at an overall recovery of 90.5%, with each stage set to a recovery of 50.3% (Table 2). In contrast, a four stage plant achieved a slightly higher NOM removal of 69.3% (TOC)

and 78.4% (UV254) at the same overall recovery (90.5%) , but with a recovery per stage of only 45.3%. The low recovery for each stage resulted in a reduced recycle rate of the retentate of the 2nd module to the inlet of the 1st module when the double-pass filtration was operated at a constant cross flow velocity of 0.57 m/s, this reduced the NOM concentration at the feed side which increased NOM removal. For example, the TOC retention in stage 1 of the 3-stage plant with a 4.75 recycle rate was estimated to be 80.9%, lower than the 82.3% obtained for stage 1 of the 4-stage plant with a 3.7 recycle rate. More importantly, reducing the recycle rate reduced energy consumption. Therefore, operated at a constant overall recovery of 90.5%, the 110.000 m^3/day 4-stage full-scale NF plant removes more NOM using less energy than the 3-stage full-scale plant at the same recovery. Details of the estimated influent and effluent water quality of the two full plant were presented in appendix (Table S1).

Table 3: The performance of four stage process vs. three stage process

Full-scale plants	Stage No	Number of modules	TOC retention	UV254 retention	Water recovery
3-stage plant	Stage 1	4000	80.9%	86.9%	50.3%
	Stage 2	2000	65.0%	75.3%	25.1%
	Stage 3	1200	22.7%	42.5%	15.1%
	Overall	**7200**	**66.8%**	**76.3%**	**90.5%**
4-stage plant	Stage 1	3600	82.3%	88.0%	45.3%
	Stage 2	1800	71.8%	80.5%	22.6%
	Stage 3	1080	54.9%	67.8%	13.6%
	Stage 4	720	19.8%	40.9%	9.1%
	Overall	**7200**	**69.3%**	**78.4%**	**90.5%**

5. Conclusion

Two-dimensional axisymmetric CFD model was successfully developed to investigate the influence of water flux and cross-flow velocity in the performance of the novel inside-out NF membrane module. The model was validated using data generated at a pilot plant operating at the Görväln WTP.

The simulated results showed that the cross-flow velocity and water flux had significant influences in solute retention. The solute retention can reach a maximum 89.4% in TOC, 93.2% in UV254 with an optimisation of water flux ranging from 5 LMH to 25 LMH and cross-flow velocity ranging from 0.25 m/s to 1.0 m/s.

The NF modules operated in a double-pass loop mode have a better performance in permeate quality with a 33% decrease in TOC of effluent compared to single membrane modules with double fibre length.

A four-stage full scale NF process operated at a a 90.5% water recovery was found to remove 69.3% of TOC and 78.4% of UV254 in feed water, superior to a typical three-stage full plant operated at the same overall recovery.

The CFD model developed in this study provided accurate prediction of the inside-out NF process for NOM removal over a wide range of operating condition. It can be used to assist the design and evaluation of different full scale NF systems treating different water sources with experimentally calibrated solute permeability and diffusion coefficients and membrane resistance.

Acknowledgments

Financial support of the GenoMembran-project funded by The Swedish Water and Wastewater Association (Swedish Water Development, SVU) is gratefully acknowledged. Pentair X-Flow is acknowledged for the provision of various test modules and access to design tools. The authors would also like to acknowledge Kristina Dahlberg (Norrvatten) for her contribution of reagents, materials, and analytical tools, as well as Tom Spanjer (Pentair) for advise on data analysis.

Glossary of terms

Symbols

A	area (m^2)
BW	backwashing of membranes

C_m	solute concentration at membrane surface (mg/L)
CP	concentration polarisation
C_p	solute concentration in permeate (mg/L)
CEFF	chemical enhanced forward flushing of membranes
J	mass flux (LMH)
J_s	solute flux (mg/m^2/hr)
P_s	solute permeability coefficient
ΔP	transmembrane pressure (Pa)
R_m	membrane resistance (m^{-1})
r	distance to the axis of HF membrane (m)
r_0	interal radius of HF membrane (m)
S_m	mass source term (kg/m^3/s)
S_v	momentum source term (kg/m^2/s^2)

Greek symbols

μ	fluid viscosity (Pa.s)
$\Delta\Pi$	osmotic pressure (Pa)

References

[1] C. Forsberg, R. Petersen Jr., A darkening of Swedish lakes due to increased humus inputs during the last 15 years, Verh..Internat. Verein. Limnol, 24 (1990) 289-292.
[2] B. Eikebrokk, R. Vogt, H. Liltved, NOM increase in Northern European source waters: discussion of possible causes and impacts on coagulation/contact filtration processes, Water Science and Technology: Water Supply, 4 (2004) 47-54.

[3] C. Evans, D. Monteith, D. Cooper, Long-term increases in surface water dissolved organic carbon: observations, possible causes and environmental impacts, Environmental Pollution, 137 (2005) 55-71.
[4] F. Worrall, T. Burt, Trends in DOC concentration in Great Britain, Journal of Hydrology, 346 (2007) 81-92.
[5] I. Delpla, A.-V. Jung, E. Baures, M. Clement, O. Thomas, Impacts of climate change on surface water quality in relation to drinking water production, Environment International, 35 (2009) 1225-1233.
[6] S. Köhler, I. Buffam, J. Seibert, K. Bishop, H. Laudon, Dynamics of stream water TOC concentrations in a boreal headwater catchment: Controlling factors and implications for climate scenarios, Journal of Hydrology, 373 (2009) 44-56.
[7] J.G. Jacangelo, J. DeMarco, D.M. Owen, S.J. Randtke, Selected processes for removing NOM: an overview: Natural organic matter, Journal-American Water Works Association, 87 (1995) 64-77.
[8] A. Matilainen, M. Sillanpää, Removal of natural organic matter from drinking water by advanced oxidation processes, Chemosphere, 80 (2010) 351-365.
[9] J.L. Weishaar, G.R. Aiken, B.A. Bergamaschi, M.S. Fram, R. Fujii, K. Mopper, Evaluation of specific ultraviolet absorbance as an indicator of the chemical composition and reactivity of dissolved organic carbon, Environmental science & technology, 37 (2003) 4702-4708.
[10] S.J. Köhler, E. Lavonen, A. Keucken, P. Schmitt-Kopplin, T. Spanjer, K. Persson, Upgrading coagulation with hollow-fibre nanofiltration for improved organic matter removal during surface water treatment, Water research, 89 (2016) 232-240.
[11] A. Keucken, Y. Wang, K. Tng, G. Leslie, K.M. Persson, S.J. Köhler, T. Spanjer, Evaluation of novel hollow fibre membranes for NOM removal by advanced membrane autopsy, Water Science and Technology: Water Supply, 16 (2016) 628-640.
[12] A. Keucken, Y. Wang, K.H. Tng, G. Leslie, T. Spanjer, S.J. Köhler, Optimizing Hollow Fibre Nanofiltration for Organic Matter Rich Lake Water, Water, 8 (2016) 430.
[13] S. Déon, P. Dutournié, P. Bourseau, Transfer of monovalent salts through nanofiltration membranes: A model combining transport through pores and the polarization layer, Industrial & Engineering Chemistry Research, 46 (2007) 6752-6761.
[14] R. Levenstein, D. Hasson, R. Semiat, Utilization of the Donnan effect for improving electrolyte separation with nanofiltration membranes, Journal of Membrane Science, 116 (1996) 77-92.
[15] T. Tsuru, S.-i. Nakao, S. Kimura, Calculation of ion rejection by extended Nernst–Planck equation with charged reverse osmosis membranes for single and mixed electrolyte solutions, Journal of chemical engineering of Japan, 24 (1991) 511-517.
[16] R.J. Gross, J. Osterle, Membrane transport characteristics of ultrafine capillaries, The Journal of chemical physics, 49 (1968) 228-234.
[17] W.R. Bowen, H. Mukhtar, Characterisation and prediction of separation performance of nanofiltration membranes, Journal of Membrane Science, 112 (1996) 263-274.
[18] W.R. Bowen, A.W. Mohammad, N. Hilal, Characterisation of nanofiltration membranes for predictive purposes—use of salts, uncharged solutes and atomic force microscopy, Journal of Membrane Science, 126 (1997) 91-105.
[19] W.R. Bowen, J.S. Welfoot, P.M. Williams, Linearized transport model for nanofiltration: development and assessment, AIChE journal, 48 (2002) 760-773.
[20] S. Bandini, D. Vezzani, Nanofiltration modeling: the role of dielectric exclusion in membrane characterization, Chemical engineering science, 58 (2003) 3303-3326.
[21] A. Szymczyk, P. Fievet, Investigating transport properties of nanofiltration membranes by means of a steric, electric and dielectric exclusion model, Journal of membrane science, 252 (2005) 77-88.
[22] V.t. Geraldes, V. Semião, M.N. de Pinho, Flow and mass transfer modelling of nanofiltration, Journal of Membrane Science, 191 (2001) 109-128.
[23] F. Cortés-Juan, B. Balannec, T. Renouard, CFD-assisted design improvement of a bench-scale nanofiltration cell, Separation and purification technology, 82 (2011) 177-184.
[24] Y.Y. Liang, M.B. Chapman, G.A. Fimbres Weihs, D.E. Wiley, CFD modelling of electro-osmotic permeate flux enhancement on the feed side of a membrane module, Journal of Membrane Science, 470 (2014) 378-388.

[25] Y.Y. Liang, G. Fimbres Weihs, R. Setiawan, D. Wiley, CFD modelling of unsteady electro-osmotic permeate flux enhancement in membrane systems, Chemical Engineering Science, 146 (2016) 189-198.
[26] C. Completo, V. Semiao, V. Geraldes, Efficient CFD-based method for designing cross-flow nanofiltration small devices, Journal of Membrane Science, 500 (2016) 190-202.
[27] B. Lian, Y. Wang, P. Le-Clech, V. Chen, G. Leslie, A numerical approach to module design for crossflow vacuum membrane distillation systems, Journal of Membrane Science, 510 (2016) 489-496.
[28] A.L. Hines, R.N. Maddox, Mass transfer: fundamentals and applications, Prentice-Hall Englewood Cliffs, NJ, 1985.

Supplementary Information

The "mass jump" method

The transport of solvent and solute in NF process can be expressed by the Navier-Stokes (NS) equations, where,

the continuity equation,

$$\nabla \cdot \left(\rho \vec{V}\right) = S_m \qquad \text{Equation S1}$$

the momentum transport equation,

$$\nabla \cdot \left(\rho \vec{V} \vec{V}\right) = -\nabla \cdot P + \nabla \cdot (\bar{\bar{\tau}}) + \rho g + S_v \qquad \text{Equation S2}$$

A novel computational code, named the "mass jump" method, was developed for simultaneous calculation of solvent and solute transfer across the membrane. The "mass jump" method utilizes the source terms in Eqs S1 and S2 to define a mass and momentum sink of the solvent and solute at the membrane and feed interface. The "mass jump" method could reduce the computational demand by eliminating the simulation of the porous membrane.

A self-developed User Define Function(UDF) was compiled in ANSYS Fluent® to calculate mass and momentum transport of solvent and solute at membrane boundaries. Based on the calling sequence of Fluent, at the start of each iteration, a user Define Adjust Function(DAF) was used to calculate the transmembrane solvent and solute flux (Eq 3 and 4) for a given pressure, and solute concentration profile at the feed-membrane interface. User Defined Memory(UDM) was applied to record the fluxes calculated from DAF and deliver these data to the "Define Source" functions which is utilized in the governing Eqs S1 and S2 for continuity and momentum calculation. All UDMs were updated at the end of each iteration and transferred back to the DAF to recalculate the mass flux until a convergence result is achieved for continuity and momentum.

Table S1: The influent and effluent quality of four-stage process vs. three-stage process

Full-scale plants	Stage No	Module No	TOC			UV_{254}		
			Feed concnetration (mg/L)	Influent concentration (mg/L)	Permeate concentration (mg/L)	Feed concentration (mg/L)	Influent concentration (m^{-1})	Permeate concentration (m^{-1})
3-stage plant	Stage 1	1st module	12.60	8.00	1.53	12.94	8.00	1.05
		2nd module	13.57			13.99		
	Stage 2	1st module	23.00	14.54	2.80	24.45	15.04	1.98
		2nd module	24.78			26.43		
	Stage 3	1st module	51.00	26.56	6.19	57.09	28.41	4.61
		2nd module	54.94			61.72		
4-stage plant	Stage 1	1st module	11.65	8.00	1.41	11.90	8.00	0.96
		2nd module	12.55			12.86		
	Stage 2	1st module	18.49	13.45	2.25	19.34	13.82	1.56
		2nd module	19.92			20.90		
	Stage 3	1st module	29.76	21.35	3.61	31.89	22.46	2.58
		2nd module	32.06			34.48		
	Stage 4	1st module	52.92	34.36	6.42	58.51	37.05	4.73
		2nd module	57.01			63.25		

Paper V

water

MDPI

Article

Combined Coagulation and Ultrafiltration Process to Counteract Increasing NOM in Brown Surface Water

Alexander Keucken [1,2,*], Gerald Heinicke [3], Kenneth M. Persson [2,4] and Stephan J. Köhler [5]

1 Vatten & Miljö i Väst AB (VIVAB), 311 22 Falkenberg, Sweden
2 Water Resources Engineering, Faculty of Engineering, Lund Technical University, 221 00 Lund, Sweden; Kenneth.Persson@sydvatten.se
3 DHI, Agern Allé 5, 2970 Hørsholm, Denmark; ghe@dhigroup.com
4 Sweden Water Research AB, Ideon Science Park, 223 60 Lund, Sweden
5 Department of Aquatic Sciences and Assessment, Swedish University of Agriculture Sciences, 750 07 Uppsala, Sweden; Stephan.Kohler@slu.se
* Correspondence: Alexander.Keucken@vivab.info; Tel.: +46-70-598-99-62

Received: 14 August 2017; Accepted: 7 September 2017; Published: 13 September 2017

Abstract: Membrane hybrid processes—coagulation coupled with ultrafiltration (UF)—have become a common method to comply with the legal, chemical, and microbiological requirements for drinking water. The main advantages of integrating coagulation with membrane filtration are the enhanced removal of natural organic matter (NOM) and reduced membrane fouling. With in-line coagulation, coagulants are patched into the feed stream directly prior to the membrane process, without removing the coagulated solids. Compared with conventional coagulation/sedimentation, in-line coagulation/membrane reduces the treatment time and footprint. Coagulant dosing could be challenging in raw water of varying quality; however, with relatively stable specific ultraviolet absorbance (SUVA), dosing can be controlled. Recent studies indicate that *UV* absorbance correlates well with humic substances (HS), the major fraction to be removed during coagulation. This paper describes and evaluates a 30-month UF pilot trial on the surface water of Lake Neden (Sweden), providing drinking water to 60,000 residents. In this study, automatic coagulant dosing based on online measurement was successfully applied. Online sensor data were used to identify the current optimal aluminium coagulation conditions (0.5–0.7 mg L^{-1}) and the potential boundaries (0.9–1.2 mg L^{-1}) for efficient future (2040) NOM removal. The potential increase in NOM could affect the Al dose and drinking water quality significantly within 20 years, should the current trends in dissolved organic carbon (DOC) prevail. *UV* absorbance, the freshness index, and liquid chromatography-organic carbon detection (LC-OCD) measurements were used to optimise the process. Careful cross-calibration of raw and filtered samples is recommended when using online sensor data for process optimisation, even in low-turbidity water (formazin nephelometric unit (FNU) < 5).

Keywords: ultrafiltration; hollow fibre; natural organic matter (NOM); coagulation; optical sensors

1. Introduction

In the late 1980s, an increase of natural organic matter (NOM) concentration was first reported in Swedish surface waters as a link between increased amount of humic substances (HS) and the darkening of Swedish lakes [1]. Over the last few decades, several other reports have confirmed that the occurrence of NOM in water (browning of surface waters) was a worldwide phenomenon [2–4]. Changes in the climate (temperature, quality, and amount of precipitation) [5] and the decline in acid deposition are reasonable explanations for the increasing NOM concentrations [6]. NOM is a complex mixture of organic compounds present in all fresh water, particularly surface water [7].

The presence of NOM could have severe effects on drinking water quality and its treatment processes. These problems include (i) negative effects on water quality relevant to colour, taste, and odour; (ii) increased disinfectant dose requirements, which in turn result in potential harmful disinfection by-product (DBP) production [8]; (iii) promoted biological growth in the distribution system; and (iv) increased levels of complex heavy metals and adsorbed organic pollutants [9].

Among the available technologies to remove NOM, the most common and economically feasible method is coagulation and flocculation, followed by sedimentation/flotation and filtration. Other treatment options for NOM removal include the magnetic ion exchange resin (MIEX®) technique, activated carbon filtration, advanced oxidation processes, and membrane filtration [10–15].

Early studies of filtration processes showed that membranes were effective in removing dissolved organic matter (DOM)—including precursors of trihalomethane (THM)—from surface- and groundwater sources [16]. Over the last decade, the combination of membrane processes with other unit processes has become a common way to achieve the removal of NOM and function as a barrier against microorganisms.

Recently, several studies have focused on evaluating NOM removal by capillary nanofiltration (NF) in Swedish surface water sources. These studies indicate that a process combining coagulation and NF could remove more than 90% of the dissolved organic carbon (DOC), and 96% of the *UV* absorbance at 254 nm from lake water [17]. Using direct NF resulted in 93% removal of *UV*-absorbance (UV_{abs}), and 88% total organic carbon (TOC) [18].

Membrane processes need pre-treatment for enhanced NOM removal and decreased membrane fouling. Hybrid processes may therefore be superior to the individual processes. The integration of coagulation with membrane filtration has two main advantages: enhanced removal of NOM molecules and reduction of membrane fouling. The most recent mode of combining coagulant with microfiltration (MF) or ultrafiltration (UF) is to add coagulant into the feed stream immediately prior to the membrane process, without removal of the coagulated solids (in-line coagulation). The advantages of in-line coagulation are the reduced footprint and lower coagulant dose, as settleable flocs are not needed [19]. Coagulant selection and dosing can be optimised specifically for NOM removal, as particle removal is assured by the membrane [20]. Careful dosing is required to produce large enough flocs to avoid pore blocking, while avoiding increased fouling [21].

Coagulant dosing can be challenging in raw water, with large variations in water quality. In raw water sources with relatively stable specific ultraviolet absorbance (SUVA), dosing can be controlled with the *UV* signal in the incoming raw water. *UV* has been shown to correlate well with the presence of HS [17], which compose the major fraction removed during coagulation. In this instance, the use of optical sensors for dose control could be a viable method of process control. In this study, a combination of sensor-based in-line coagulation was investigated for the removal of NOM by UF. A 30-month pilot test was carried out on surface water from Lake Neden, a drinking water source for more than 60,000 residents on the west coast of Sweden.

This study aims to evaluate a combined coagulation/UF process, with respect to

- Its sensitivity and the limits of the coagulant dose for NOM removal
- The use of optical sensors for online dosing of coagulants
- Its vulnerability to a further decrease in raw water quality.

The merit of this research is to advance our operational understanding of the effect of membrane hybrid processes, combining UF and in-line coagulation for efficient NOM removal. Particular focus was on dosing control by optical sensors.

2. Material and Methods

2.1. Raw Water Source Quality

The raw water source used in this study was a mixture (20%/80%) of water from a nearby alkaline groundwater well (pH 8, TOC = 0.6 mg L^{-1}, σ = 380 μS cm^{-1}) and a slightly acidic clear-water lake (pH = 6.7, TOC = 3.4 mg L^{-1}, and σ = 60 μS cm^{-1}). The surface water source was an oligotrophic lake, surrounded by mixed woodland. The average feed water quality of the various pilot trials is described in Table A1. Lake Neden was heavily contaminated by acid rain during the 1980s and 1990s, and was subsequently treated with lime, as were most of the lakes in that area of southwestern Sweden. As a result, the organic matter concentration was suppressed temporarily but is currently recovering to its natural values, similar to many other lakes in the area [22]. In this area, it was observed that the water colour more than doubled during 2007–2012 [23]. The time series of colour (Abs_420) and TOC indicated an increase in colour and carbon content during 1995–2010 in several lakes in the area (Figures A1 and A2). In addition, it is assumed that prolonged vegetation periods will cause higher concentrations of organic matter in the future [24]. Compared with the other lakes in the area, the water of Lake Neden is clear, low in TOC (3.4 ± 0.4 mg L^{-1}), and has a comparatively low SUVA value (3.2 ± 0.4). The removal of organic matter by flocculation is limited by the amount of HS in the water. This characteristic can be determined by using either the SUVA value or by using more advanced DOC characterisation techniques [7]. In all of our experiments, conventional NOM analyses (TOC, DOC, and *UV* absorbance) and fluorescence excitation emission matrices (EEMs) [7] were combined with liquid chromatography-organic carbon detection (LC-OCD) analysis for feed water, concentrate, and permeate. This was done to elucidate the retention of specific NOM fractions as a function of varying operating conditions.

Consistent with the continuing browning of lakes and rivers in large parts of Scandinavia, a rising trend in colour and chemical oxygen demand (COD) has been observed in the surface water abstracted by the Kvarnagården water treatment plant (WTP). No significant reduction in HS was achieved with the old full-scale treatment process, consisting of rapid sand filtration, pH-adjustment, and *UV* irradiation.

2.2. UF Full-Scale Design and Pilot Studies

2.2.1. Retrofit of Full-Scale Plant and Pilot Trials

Preliminary pilot trials with one-stage UF (UF-HF-P1) and hollow-fibre NF (NF-HF-P) were performed from June 2010 to May 2012 [25,26]. More extensive field testing with a two-stage UF pilot plant has been carried out since January 2015. An overview of the pilot studies is given in Table 1.

Table 1. Summary of different pilot studies at Kvarnagården water treatment plant (WTP). HF: hollow fibre; NF: nanofiltration; PES: polyethersulfone; UF: ultrafiltration.

Pilot Plant Type (Module Type)	Code	Scale	Start	End	Membrane Type
UF HF one-stage (KOCH, HF 10-48 35)	UF-HF-P1	Pilot	1 June 2010	15 August 2011	PES
UF-HF two-stage (Pentair, XIGA/AquaFlex)	UF-HF-P2	Pilot	1 January 2015	Running	PES
NF (Pentair, HFW 1000)	NF-HF-P	Pilot	2 November 2011	4 May 2012	PES
UF-HF two-stage HF (Pentair, XIGA/AquaFlex)	UF-HF-F	Full	15 February 2017	Running	PES

In November 2016, the WTP was upgraded with a UF facility (capacity of 1080 m^3 h^{-1} net permeate flow rate). In brief, the full-scale plant consists of a two-stage UF membrane filtration process, with in-line coagulation of a primary UF membrane stage that provides NOM retention and a barrier function against microorganisms (Figure 1). Because of coagulant residues in the backwash water and the limited sewer capacity of the site, a second-stage UF membrane system was installed to increase the recovery of the plant to >99%.

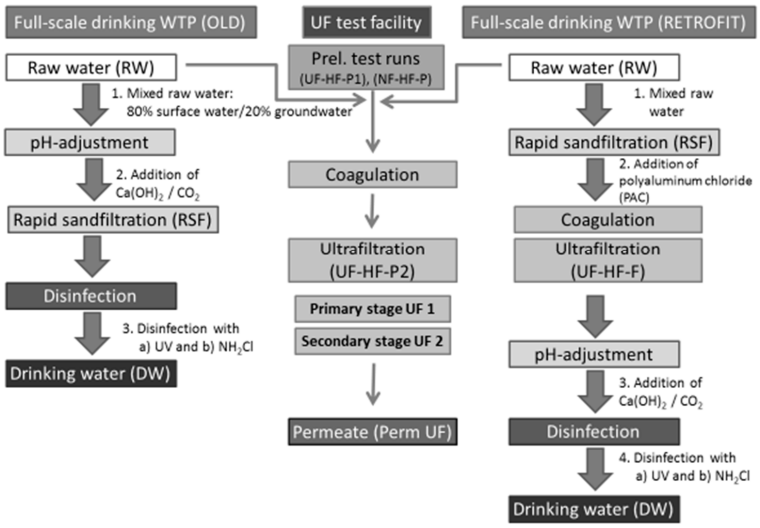

Figure 1. Treatment train for full-scale process and test facility at Kvarnagården WTP.

2.2.2. Control Philosophy of Pin-Floc Coagulation for Full-Scale UF Plant

For the full-scale plant, the coagulation philosophy was to create "pin flocs" (i.e., flocs of limited size) for the operation of the UF hybrid process. On the one hand, these pin flocs are of sufficient size to be retained by the UF membranes and to create a relatively open cake structure on the membrane surface. On the other hand, the floc size required could be limited because the removal of solids is determined by the size difference between the flocs and the membrane pores, and does not depend on gravitational separation. The critical parameters for optimum pin-floc coagulation are proper distribution of the coagulant into the UF feed stream, a sufficiently high mixing energy at the coagulant dosing point during a minimum contact time, and an optimum pH depending on the coagulant selected. The specific coagulation dosing conditions for the UF full-scale plant in the present study are shown in Figure 2. A similar but more simplified set-up was applied for the UF pilot studies.

Based on extended UF-trials [25] (year 2011), the effective coagulant concentration required to improve UF operation was found to be in the range 0.4–1.5 mg Al L^{-1}. As the efficiency of pin-floc coagulation strongly depends on the absolute number of collisions at the dosing point, the proper distribution of these relatively low coagulant concentrations and UF feed water is vital. For this reason, a maximum dilution factor of 500 was applied in the present study. This means that direct dosing of the coagulant stock concentration into the UF feed stream was avoided. Instead, a small separate dispersion pump was installed to create a carrier water supply, which obtained water from the UF feed line. The coagulant stock concentration was dosed into the suction line of the dispersion pump. For operational flexibility, the coagulant dosing pump was frequency controlled to enable flow-ratio dosing control based on the actual UF feed flow.

At the coagulant dosing point, the mixing energy should be sufficiently high to maximize the absolute number of collisions and consequent pin flocs. This was achieved by installing a static in-line mixer, providing a plug-flow contacting environment. A residence time of 10 s between the coagulant dosing point and the first UF unit was sufficient to allow for a limited flocculation period.

If pH correction of the UF feed stream was required, a frequency-controlled dosing pump for acid/caustic chemicals would be necessary to achieve stable pH control, based on pH and flow fluctuations of the UF feed stream. Since coagulant dosing influenced the pH of the UF feed, pH was measured downstream of the static mixer. For proper mixing of the acid/caustic chemicals into the

UF feed stream, a low-pressure drop static in-line mixer was installed upstream of the coagulant dosing point.

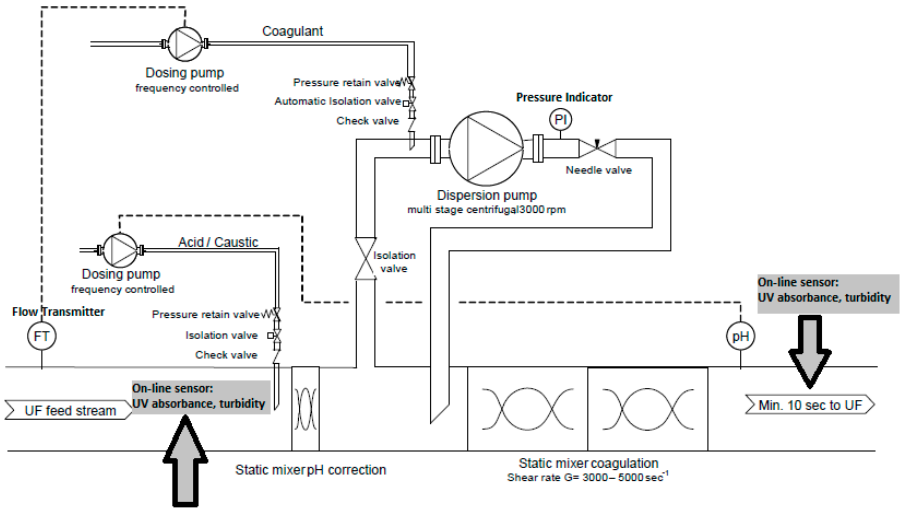

Figure 2. Design for in-line coagulation of full-scale process at Kvarnagården WTP.

2.2.3. Two-Stage UF Test Facility (UF-HF-P2)

During the construction period of the membrane plant, an extensive test facility was established for various long-term trials to verify the membrane performance of the full-scale design (Figure 3).

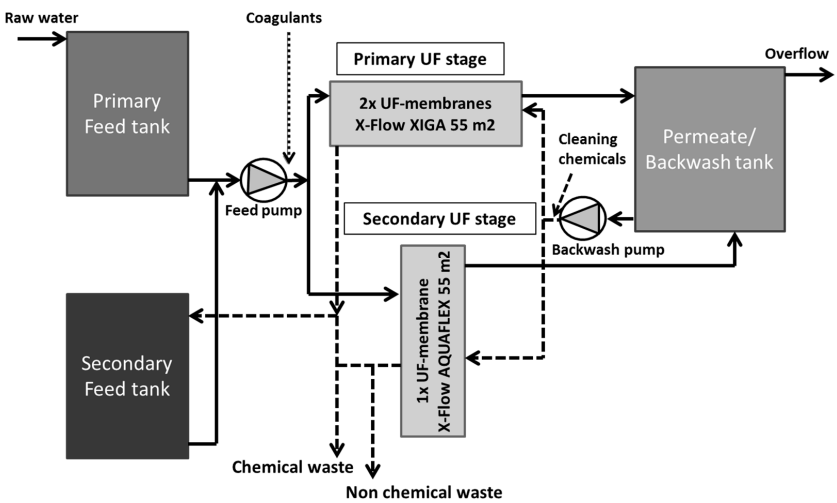

Figure 3. Schematic overview of the pilot plant process for the two-stage UF test facility (UF-HF-P2).

A 40 foot (12 m)-long container pilot plant (designed as a stand-alone unit to mimic the full-scale UF plant) has been in operation since January 2015, with a treatment capacity of 170 m^3/day (150 m^3/day permeate production). The pilot plant consists of the following main sections:

- Feed section, including dosing equipment for coagulant and chemicals for pH correction,
- Membrane system (two-stage UF), including air integrity testing,
- Permeate and backwash section, including chemical dosing for membrane cleaning.

The pilot plant was equipped with a computer for systems control and automatic operation. All the necessary process parameters were logged and trended on the computer. The plant allowed remote access, providing the same functionality as local access.

The two-stage membrane system comprised (a) a primary UF unit (horizontal dead-end filtration), with two membrane modules (Pentair X-Flow XIGA, 55 m^2); and (b) a secondary UF unit (vertical dead-end filtration), with one membrane module (Pentair X-Flow AQUAFLEX, 55 m^2). The raw water was supplied from the intake of the WTP to the primary feed tank by a pressurised line. The feed pump obtained water from the primary feed tank during the filtration of the primary UF unit. If pH correction of feed water was required, both H_2SO_4 and NaOH were added in front of the feed pump to obtain an optimal pH window for coagulants. During filtration, the UF permeate was directed to the permeate tank and discharged by overflow to the recipient. Permeate water from the permeate tank was used during backwashing of the UF units. The backwash waste from the primary UF unit was directed to the secondary feed tank. Chemical waste from the chemically-enhanced backwashing (CEB) programme at the primary UF unit was directed to the chemical waste discharge. During the backwash of the primary UF unit, the secondary feed tank was filled. When the primary UF unit finished a filtration cycle and the secondary feed tank reached a specific level, the primary UF unit stopped after a final backwash. Subsequently, the secondary UF unit was activated and started production. During filtration of the secondary UF unit, the feed pump obtained water from the secondary feed tank. The secondary permeate was directed to the permeate tank. During the hydraulic cleaning (feed water plus permeate) of the secondary UF unit, the waste water was directed to the non-chemical waste discharge facility. The waste water of the CEB for the secondary unit was directed to the chemical waste discharge facility. One feed pump was available for both the primary and the secondary units. In addition, one backwash pump was available for both the primary and secondary UF units. For the CEBs, dosing systems for H_2SO_4, NaOH, and NaOCl were available. The dosing points were placed in the backwash inlet line, and were used by both the primary and secondary units.

In addition to the hydraulic cleaning of the membranes with a combined backwash and forward flush, several automatic cleaning sequences were pre-programmed for specific cleaning protocols. In general, cleaning took place on an elapsed-time interval. A cleaning cycle consisted of flushing with clean water (permeate), followed by soaking with a maximum of two cleaning agents (acidic and caustic). The average feed water quality, cleaning protocols, and operational conditions during long-term test runs are summarised in Tables A2 and A3, whereas the membrane key performance parameters and manufacturer-reported properties of the hollow fibre membranes are listed in Table A4.

2.2.4. Coagulant Dosing System for UF Test Facility

The online measurements of turbidity and *UV* absorbance (254 nm) in feed water (UV_{Raw}) were used to control the coagulation dosing rate in the feed line in order to meet the target values for NOM removal and permeate quality. The dosing rate of coagulants could be adjusted depending on current feed water quality and flow rates, according to Equation (1). The dependence was derived based on empirical evaluations of laboratory experiments and pilot studies, as part of the current study and previous studies by the authors [25].

$$Dos_{Coag} = A + B * ^{(TURB)} + C * ^{(UV\ abs)} \quad (1)$$

where

- Dos_{Coag} is the coagulant dosing concentration (mg Metal L^{-1})
- B is the conversion factor for turbidity [-] (was set to zero during the pilot trials)

- C is the conversion factor for UV absorbance [-] (range: 0.005–0.035)
- $TURB$ is the feed water turbidity (FTU)
- $UV\ abs$ is the feed water UV absorbance (m^{-1})
- A is a set point for the base coagulant dosage (range: 0.2–2.0).

2.2.5. Evaluation of Coagulation Efficiency

The variation of and differences in UV signals between the raw (UV_{Raw}) and permeate (UV_{Perm}) is the most efficient way to evaluate the removal efficiency of the UF flocculation process. The removal efficiency of UV absorbance at different coagulant dosing situations was evaluated by comparing the absolute change in UV absorbance (Equations (2)–(4)).

$$\Delta\ UV = UV_{Raw} - UV_{Perm}. \quad (2)$$

The observed values for UV were subsequently plotted as a function of the aluminium dose and fitted to a power relationship of the form:

$$\Delta\ UV = a + \ b * Al_{DOS} + c * Al_{DOS}{}^{2} \quad (3)$$

With a, b, and c used as empirical fitting factors to describe the observed curvature. In addition, a change in the UV removal efficiency that is normalised to the target coagulant dose (Al_{DOS*}) under regular operational conditions of 0.6 mg L^{-1} was calculated as:

$$UV_{norm} = \Delta \frac{UV}{Al_{DOS(t)}} * Al_{DOS*} \quad (4)$$

After initial separate treatment of the data from experiments UF-HF-P1 and UF-HF-P2 (Table 1), the datasets were combined, as the resulting curvature from the experiments was not different.

2.3. Characterisation of Organic Fractions in Feed Water and Treated Water

2.3.1. Determination of UV, TOC, and DOC

The following three measurements were done by a commercial laboratory. The UV absorbance at 254 nm was measured with a 5-cm cuvette ($UV_{\text{Lab2 unfilt}}$) using a Hach DR 5000 UV-Vis spectrophotometer (Loveland, CO, USA). The TOC and dissolved organic carbon (DOC) were determined using an Elementar Vario TOC Cube analyser (Langenselbold, Germany), with precision of 0.2 mg L^{-1}.

2.3.2. Evaluation of NOM Retention by LC-OCD

The composition of the organics that were present in the water samples of this study were characterised by using UV absorbance at 254 nm and DOC-LABOR liquid chromatography-organic carbon detection (LC-OCD). The LC-OCD technique is based on a polymethacrylate size-exclusion column (Toso, Japan), coupled with three detectors (organic carbon, organic nitrogen, and UV-absorbance). This technique facilitates the subdivision of organic matter into six major subfractions: biopolymers, HS, building blocks, low-molecular-weight acids, low-molecular-weight neutrals, and hydrophobic organic carbon. Detailed information on the LC-OCD technique is available from the following studies [17,27,28].

2.3.3. Absorbance and Fluorescence Characterisation and Additional DOC and TOC

The presence of organic carbon was determined on unfiltered (TOC) and filtered samples (DOC) by using pre-combusted (4 h at 450 °C) GF/F filters (effective pore size of 0.7 µm) and acidified to pH 2 by using 37% HCl on a Shimadzu TOC-VCPH (Kyoto, Japan). The TOC and DOC were within the

analytical precision parameters of the measurements (0.3 mg L^{-1}). Fluorescence excitation emission matrices (EEMs) were collected by using an Aqualog (Horiba, Edison, NJ, USA) spectrofluorometer [7]. Previously established indices were calculated from the corrected EEMs—namely humification index (HIX), fluorescence index (FI), and freshness index (β:α) according to Cory and McKnight [29]; Ohno [30]; and Parlanti et al. [31]. The freshness index (β:α) has been shown to be particularly valuable for the characterisation of coagulation [7,17].

2.4. Optical Sensors for Online Process Control and Dosing

Two online instruments (i::scan™; s::can Messtechnik GmbH, Vienna, Austria) were installed to detect the changes in the *UV* absorbance, colour, and turbidity in the feed water after the groundwater and lake water had been mixed (UF_{Feed}), and alternatively, in the permeate from both UF stages (UF_{Perm}). In addition to the *UV* absorbance probes, pH-sensors, pressure transmitters, flow meters, and temperature sensors were used for online monitoring of membrane performance and water quality. The absorbance spectra in the wavelength range 230–350 nm were acquired, with the online sensor using a flow-cell with a path length of 35 mm. The empirical relationships from particle-rich waters were used to calibrate the absorbance measurements against both TOC and turbidity, with algorithms developed by the probe manufacturer (so-called global calibration).

The correctness of the absorbance values of the online sensors were monitored by using three other independent *UV* absorbance measurements. On a biweekly basis, the *UV* was measured directly in unfiltered water samples by the operators at the WTP, using a 4-cm cuvette ($UV_{Lab1\ unfilt}$) and at a commercial laboratory ($UV_{Lab2\ unfilt}$; see Section 2.3.1). Furthermore, the filtered water samples were sent to an external research laboratory and measured by using a 1-cm flow-through cuvette ($UV_{Lab3\ filt}$) in combination with a high-precision combined fluorescence/absorbance spectrophotometer (Aqualog Horiba Jobin Yvon). During the second year of the study, an internal standard (60 ppm K-phthalate, with approximately A = 0.7 @ 254 nm) was added to all the sample runs to determine whether *UV* lamp drift had occurred.

The correctness of the calculated turbidity values of the online sensors were monitored with regular laboratory measurements of turbidity, using a HACH Model 2100N IS® Turbidimeter (Loveland, CO, USA), designed for turbidity measurement in accordance with ISO 7027.

The presence of particles probably led to deposition on the sensor, particularly on the raw water side. To prevent the degradation of the online signals, both probes were cleaned at regular intervals by following the procedures suggested by the manufacturer. For automatic cleaning, a rotating brush was mounted inside the flow cell in such way that the brush fibres reached the measuring windows on both sides of the measurement path of the spectrometer probes. The optimal autobrush cleaning settings were defined to 10 brush rotations every 20 min for the permeate and 10 brush rotations every 5 min for the feed water. Manual cleaning of the probes was carried out preventively once a month by using a mild alkaline cleaning agent provided by the manufacture and cleaning tissue. In the event of persistent fouling, pure alcohol (ethanol) and 3% hydrochloric acid (to prevent a mineral film/residue forming on the measuring windows) were used as cleaning liquids. The observed changes in *UV* absorbance and the calculated turbidity before and after manual cleaning typically ranged between 0.2 and 0.3 m^{-1} and 0.1 and 0.2 FTU, respectively.

3. Results and Discussion

3.1. Preliminary Membrane Trials Using NF (NF-HF-P) and UF (UF-HF-P1)

Preliminary feasibility tests were carried out between 2010 and 2012 with several membrane processes to reduce the NOM concentration in the drinking water. Ultrafiltration with and without coagulant dosage was compared with hollow-fibre NF. The results from these test runs are summarised in Table 2.

Whereas UF alone did not remove NOM sufficiently, UF with in-line coagulation and hollow-fibre NF produced permeate that complied with the regulatory requirements for colour and COD.

Three operational modes of the UF pilot plant (UF-HF-P1) were investigated during the feasibility tests, namely: (1) dead-end filtration; (2) cross-flow with continuous bleed; and (3) cross-flow with intermittent flush. Dead-end filtration with raw water resulted in rapid increase of trans-membrane pressure (TMP). Cross-flow with continuous bleed produced approximately 20% of the feed flow as concentrate, requiring further treatment or having to be discarded. The operational mode that facilitated constant, high flux, and high recovery was cross-flow with intermittent flush. The UF was run with a polyaluminium coagulant dose of 1 mg/L Al per cubic metre of raw water [25].

UF with in-line coagulation could be run at a flux of approximately 60 L/m^2/h (LMH), which was four times the flux for capillary NF. This has major implications related to investment costs and the footprint of the plant. Accordingly, it was decided to continue the investigation focusing on a retrofit of the old full-scale plant with a UF hybrid process, with the aim of achieving NOM removal (as UV_{abs}) of at least 50% and feed water recovery of at least 99%.

Table 2. Comparison of water quality parameters in raw water, current drinking water, and after membrane treatment (median and standard deviations) during the feasibility tests year 2010–2012. The NF was run as one stage, with a recovery rate of 50%. During the early UF and NF trials, most turbidity values in permeate were below the detection limit. For the NF, most total organic carbon (TOC) and dissolved organic carbon (DOC) values were below the detection limit (affected values in italics). Values below the detection limit were reported as half the detection limit. COD: chemical oxygen demand; SUVA: specific ultraviolet absorbance.

Parameter	Raw Water	Drinking Water (Full-Scale WTP OLD)	UF without Coagulant	UF with Coagulant	$NF_{50\%}$	Target Value
Code	RAW	DW	UF-HF-P1	UF-HF-P1	NF-HF-P	
COD (mg/L)	2.2 ± 0.2	2.1 ± 0.2	2.1 ±0.1	1.3 ± 0.2	0.9 ± 0.5	<4 limit
TOC (mg/L)	2.6 ± 0.2	2.7 ± 0.2	2.5 ± 0.2	2.1 ± 0.3	*1.0*	
DOC (mg/L)	2.5 ± 0.2	2.4 ± 0.2	2.3 ± 0.1	2.0 ± 0.2	*1.0*	
UV_{254} (L/m)	8.7 ± 0.5	8.1 ± 0.5	7.3 ± 0.2	3.7 ± 0.5	2.8 ± 0.1	
SUVA (L/mg, m)	3.6 ± 0.4	3.3 ± 0.4	3.3 ± 0.1	1.8 ± 0.3	*2.8*	
$Colour_{405nm}$ (mg Pt/L)	14.0 ± 1.2	13.0 ± 1.3	10.0 ± 0.7	2.5 ± 1.3	2.0 ± 0.8	<15 limit <5 rec.
Turbidity (FNU)	0.21 ± 0.06	0.22 ± 0.05	0.05	0.05	0.04	<0.5 limit <0.1 rec.
pH	7.6 ± 0.1	8.1 ± 0.1			7.4 ± 0.1	7.5–9 limit

3.2. Pilot Trials Using the Two-Stage UF Pilot Plant Test Facility (UF-HF-P2)

The pilot trials with primary and secondary UF were used to identify the optimal operating conditions for the full-scale plant. At the design flux of 65 LMH and with a CEB interval after 20 filtration cycles, the primary UF stage showed stable operational conditions at permeability of approximately 400 LMH/bar over a period of 30 months. In this context, three episodes were analysed further, as they related to the robustness of the process. These are:

1. Impact of in-line coagulation on NOM removal and membrane performance
2. Effect of operation at high flux (maxflux and subsequent regaining of permeability)
3. Varying feed water quality (e.g., surface water only or variation in surface water NOM content).

3.2.1. Pilot Trials (UF-HF-P2): Episode 1—Effect of in-Line Coagulation

Initial trials with various coagulants (PAX XL 100 and PLUSPAC 1465) and varying doses resulted in long-term settings for coagulant dosing, Dos_{coag} = 0.6 mg Al L^{-1} (base coagulants dosage, A = 0.25; and a correction factor for *UV* absorbance, C = 0.035).

Over a period of four days (7–11 December 2015), the pilot plant was operated without coagulant dosing, at a flux of 65 LMH. During that time, the permeability before the daily CEB quickly decreased from approximately 400 to below 250 L m^{-2} h^{-1} bar^{-1} @ 20 °C. After two extended

CEBs, the permeability prior to the daily CEB started increasing slowly again. However, the initial permeability of 400 L m^{-2} h^{-1} bar^{-1} @ 20 °C could not be restored completely within a week after the incident (Figure 4).

The simulated shutdown of coagulant dosing caused an instant decrease in the permeability of the primary UF, which could not be recovered fully by subsequent CEBs. The membrane obviously had lower "critical flux" without the coagulant. The critical flux of the membrane should be quantified for relevant feed water quality and coagulant dosing conditions in order to avoid irreversible loss of permeability. Investigation should be conducted to determine whether the permeability lost during such incidents could be recovered by a cleaning-in-place (CIP). Moreover, process strategies should be formulated on whether to reduce the flux automatically when a sudden loss of coagulant dosage occurs.

Once the full-scale plant is in stable operation, the pilot plant could be used to adjust the CEB and CIP conditions to ensure effective yet mild cleaning of the membranes. Furthermore, there should be a balance between the level of NOM removal and effective cleaning protocols, as well as the mechanical and chemical long-term stability of the membrane [26].

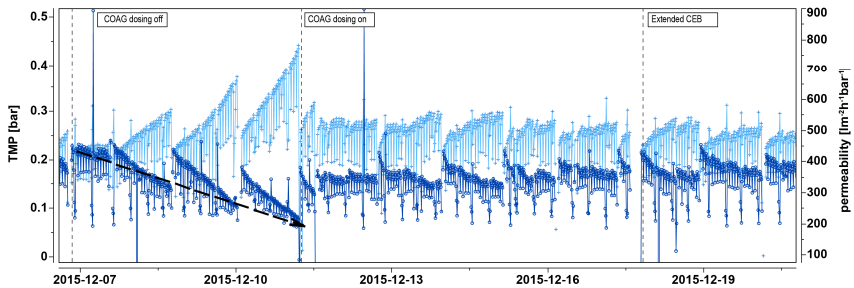

Figure 4. Hydraulic performance of the UF stage-1 container test modules at Kvarnagården WTP for the period 7–19 December 2015. Periods with an increase in transmembrane pressure (TMP; bar) (light blue on left y-axis) and a decrease in permeability (L m^{-2} h^{-1} bar^{-1} @ 20 °C) (dark blue on right y-axis) are shown in relation to in-line coagulation (before, during, and after a stop in coagulant dosing, as displayed with vertical lines) and chemically-enhanced backwashing (CEB) cycles.

3.2.2. Pilot Trials (UF-HF-P2): Episode 2—High-Flux Testing

Over a period of six days (15–21 March 2016), the flux over UF stage-1 was increased from 65 to 70 LMH (i.e., by 7.7%), with a coagulation dosing concentration of 0.6 mg Al L^{-1} (Figure 5). Before this specific episode, the permeability was stable at approximately 400 L m^{-2} h^{-1} bar^{-1} @ 20 °C, with only minor reduction during a filter run, and 80 L m^{-2} h^{-1} bar^{-1} @ 20 °C between daily CEBs. In addition, the permeability was restored by the CEB and was maintained in the long term. At 70 LMH, the permeability drop during a filter run was more rapid (40 L m^{-2} h^{-1} bar^{-1} @ 20 °C), and there was a tendency toward decreasing permeability with every passing day (120 L m^{-2} h^{-1} bar^{-1} @ 20 °C between daily CEBs). There was a strong indication that a certain maximum flux should not be exceeded in the long-term operation. These boundaries should be quantified by using the pilot plant for varying raw water qualities and temperatures. At the end of the high-flux testing period, a change in the raw water quality occurred (increase of *UV* absorbance from 10 to 11.5 m^{-1}), which resulted in a further decrease in permeability (below 300 L m^{-2} h^{-1} bar^{-1} @ 20 °C), although the coagulant dose was automatically adapted to 0.7 mg Al L^{-1} in accordance with the current *UV* correction factor and ordinary flux settings (65 LMH). The membrane system recovered first, after a further two days of normal operation, regaining levels of permeability and TMP comparable with the operational conditions prior to the testing period.

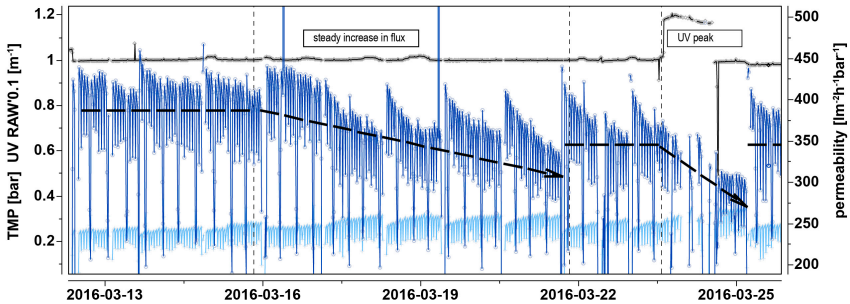

Figure 5. Hydraulic performance of the UF stage-1 container test modules at Kvarnagården WTP for the period 13 to 25 March 2016. The increase in flux was 65 to 70 L/m^2/h (LMH) during the period 15 to 21 March 2016. The TMP and permeability before, during, and after the increase in flux and *UV* absorbance are indicated with vertical lines. The TMP (bar) on the left-hand scale is indicated with light-blue lines, and permeability (L m^{-2} h^{-1} bar^{-1} @ 20 °C) on the right-hand scale with dark-blue lines. *UV* absorbance (0.1*m^{-1}) on the left-hand scale is indicated with black lines.

3.2.3. Pilot Trials (UF-HF-P2): Episode 3—Varying Feed Water Quality

During a period of 21 h (23–24 March 2016), the feed water consisted of surface water only (no addition of alkaline groundwater). As shown in Figure 6, the change in the quality of the raw water resulted in an increase in TMP from 0.18 to 0.35 at a flux of 65 LMH. Despite recurring backwashing and one CEB during this period, the TMP could not be stabilised and the high levels could not be brought down, even after the addition of mixed raw water. The change in the feed water had no further effect on the removal efficiency of NOM, but the filtration behaviour indicated a tendency towards membrane fouling. Therefore, the cleaning protocols had to be adapted with regard to frequency and choice of cleaning chemicals.

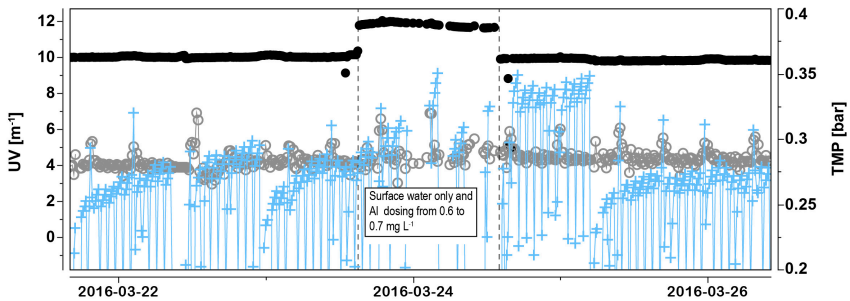

Figure 6. Membrane performance and natural organic matter (NOM) removal efficiency of the UF stage-1 container test modules at Kvarnagården WTP for the period 23 to 26 March 2016. A change occurred in the feed water quality for a period of 21 h. TMP (bar) is indicated on the right-hand scale (+), and *UV* absorbance (m^{-1}) on the left-hand scale: (●) UV_{Raw}, (○) UV_{Perm}.

3.3. Characterisation of Organic Matter in the Raw and Permeated Water

3.3.1. Absorbance and Fluorescence Data Evaluation

The temporal changes in the organic matter concentration and character of the raw water source of Lake Neden were minor compared with other surface-water drinking-water plants in Sweden (e.g., Görväln WTP, Råberga WTP, and Ringsjö WTP) [18,32]. The turnover time of close to five years

probably allowed for substantial removal of terrestrial-derived carbon, similar to the process observed in a larger Swedish lake, Lake Mälaren [33]. The comparatively low SUVA (2.97 ± 0.05) and high freshness (0.63 ± 0.01) in the raw water (Table 3) were indicative of mixing both with groundwater with low SUVA (2.0 ± 0.18, Table 4) and with lake water containing internally produced carbon. This source water was more difficult to flocculate compared with many other boreal lakes, with shorter turnover times and a higher proportion of forest cover on the catchment. This notion is corroborated by the observation of a comparably high fraction (3%) of biopolymers in the lake water (Table 4).

The *UV* absorbance at 254 nm was measured with four different devices: online (UV_{Sensor}), in the laboratory of the WTP ($UV_{\text{Lab1 unfilt.}}$), in a commercial laboratory ($UV_{\text{Lab2 unfilt.}}$), and on filtered samples in a research laboratory ($UV_{\text{Lab3 filt.}}$). Because of differences during the trials, the data were evaluated for the entire period and for each year (Table 3). The results are discussed in more detail in Section 3.4.

Table 3. Median and standard deviation for *UV* absorbance @254 nm (m^{-1}), DOC (mg L^{-1}), fluorescence index (FI), freshness index (β:α), and SUVA (L/mg*m) for the period 2015–2016. Regarding the *UV* absorbance, four different measurements are available, namely those of three laboratories ($UV_{\text{Lab1–3}}$) and the sensor data (UV_{Raw}). The samples for laboratory 3 are all filtered (0.7 µm glass fibre filters, GFF) samples. Missing results are marked n.d., and DELTA (%) is the percentage of removal of *UV* calculated as $\Delta UV/UV$.

Sample	UV_{Raw}	$UV_{\text{Lab1 unfilt.}}$ [$]	$UV_{\text{Lab2 unfilt.}}$ [$]	$UV_{\text{Lab3 filt.}}$ [#]	DOC_{Lab3}	FI_{Lab3}	$\beta/\alpha_{\text{Lab3}}$	$SUVA_{\text{Lab3}}$
Raw 2015	9.40 ± 0.46	9.23 ± 0.44	9.30 ± 0.38	8.57 ± 0.36	n.d.	n.d.	n.d.	n.d.
Raw 2016	9.90 ± 0.17	9.30 ± 0.37	9.04 ± 0.48	8.60 ± 0.39	n.d.	n.d.	n.d.	n.d.
Raw	9.80 ± 0.23	9.40 ± 0.45	9.11 ± 0.41	8.59 ± 0.37	2.89 ± 0.07	1.47 ± 0.02	0.63 ± 0.01	2.97 ± 0.05
Feed	n.d.	n.d.	n.d.	5.93 ± 1.48	2.26 ± 0.30	1.58 ± 0.05	0.71 ± 0.03	2.51 ± 0.32
Perm	4.00 ± 0.78	4.00 ± 1.00	4.53 ± 1.02	4.41 ± 1.05	2.05 ± 0.22	1.61 ± 0.05	0.73 ± 0.03	2.12 ± 0.25
DELTA	59%	57%	50%	48%				
Perm 2015	4.10 ± 0.74	4.03 ± 0.76	4.50 ± 1.09	4.23 ± 1.07	n.d.	n.d.	n.d.	n.d.
Perm 2016	3.80 ± 0.34	4.01 ± 0.33	4.62 ± 0.95	4.43 ± 1.57	n.d.	n.d.	n.d.	n.d.

Notes: [$] Measured in a 4-cm cuvette. [#] Measured in a 1-cm cuvette.

On average, less than 30% of the DOC and slightly more than 50% of the *UV* absorbance (UV_{Raw}) were removed during the coagulation UF process (Table 3). The SUVA decreased from approximately 3 to close to 2. Owing to a potential analytical error in the DOC (±0.2 mg L^{-1}) and the filtered absorbance determined in a 1-cm cuvette (±0.5 m^{-1}), the estimated error in SUVA for laboratory 3 was on the order of 0.3. The stability of the SUVA values over the entire period is shown in a DOC–SUVA plot in Figure A3. Of the three derived fluorescence indices, the freshness index (β:α) was found to be an extremely valuable tool for evaluating removal as a function of the Al dose. The time series of freshness for both the raw water and the permeate indicated stable and reproducible time series (Figure A4). In addition, the excellent correlation of the Al dose and the freshness index facilitated the use of the freshness index as a superior indicator of the coagulation efficiency (Figure A5). This indicator is superior to SUVA, as it has higher precision and requires only one measurement compared with the two parameters for SUVA. This finding confirmed the results obtained by Köhler et al. [17] on the use of the freshness index.

3.3.2. LC-OCD Data Evaluation

Most of the LC-OCD measurements conducted over the last five years indicated quite stable conditions for both ground- and lake water (Table 4). On average, the raw water consisted of approximately 60% humic acids, only half of which could be removed by the current process.

Table 4. Average and standard deviation of liquid chromatography-organic carbon detection (LC-OCD) analysis for (*n*) samples of the groundwater well (Well), the lake (Neden), the feed (Feed, values in bold for comparison), and the UF and NF permeate (Perm), NF concentrate (Conc), and the drinking water from the retrofitted UF full-scale water treatment plant (DV). Missing results are marked as n.d. LMW: low molecular weight.

Code	Sample	*n*	TOC (ppb-C)	DOC (ppb-C)	Biopolymers (ppb-C)	HS (ppb-C)	Building Blocks (ppb-C)	$LMW_{neutrals}$ (ppb-C)	LMW_{acids} (ppb-C)	SUVA (L mg^{-1} m^{-1})
NF-HF-P	Lake	3	n.d.	3235 ± 81	121 ± 8	2034 ± 54	568 ± 67	398 ± 33	9 ± 9	3.92 ± 0.03
UF-HF-P1	Lake	4	3126 ± 202	3021 ± 204	100 ± 23	1919 ± 119	558 ± 49	401 ± 20	20 ± 9	3.82 ± 0.24
UF-HF-P1	GW	2	600 ± 73	546 ± 213	5 ± 26	260 ± 85	0 ± 7	0 ± 2	0 ± 0	2.02 ± 0.18
UF-HF-P1	Feed	4	2578 ± 402	2423 ± 343	72 ± 37	1603 ± 273	444 ± 57	344 ± 33	23 ± 11	3.65 ± 0.8
UF-HF-P1	Perm	3	1655 ± 85	1714 ± 111	35 ± 10	855 ± 140	418 ± 28	315 ± 38	5 ± 7	2.62 ± 0.18
UF-HF-F	Feed	2	2541 ± 77	2337 ± 16	72 ± 10	1513 ± 10	409 ± 3	302 ± 5	42 ± 4	3.43 ± 0.22
UF-HF-F	Perm	2	1679 ± 34	1496 ± 24	27 ± 4	756 ± 53	424 ± 68	281 ± 1	17 ± 9	2.31 ± 0.26
NF-HF-P	Feed	3	n.d.	2593 ± 167	93 ± 2	1638 ± 55	508 ± 13	334 ± 19	0 ± 3	3.83 ± 0.04
NF-HF-P	Perm	3	n.d.	1158 ± 268	7 ± 3	592 ± 185	244 ± 56	210 ± 49	0 ± 3	3.09 ± 0.18
NF-HF-P	Conc	3	n.d.	4502 ± 1317	162 ± 99	2940 ± 980	804 ± 171	476 ± 123	1 ± 0	4.09 ± 0.16
UF-HF-F	DV	2	1742 ± 194	1473 ± 7	31 ± 1	754 ± 66	411 ± 70	272 ± 4	11 ± 5	1.88 ± 0.41

The DOC removal percentage and the stable conditions were in accordance with the minor changes in the inflowing raw water observed during the two-year trial period. The measured variation in DOC was in accordance with the two-year data time series presented above. The LC-OCD analysis indicated a lower DOC in the permeate (1.7 mg L^{-1}) compared with that of the classical DOC analysis (2.1 mg L^{-1}), but a higher DOC in the feed (2.5 mg L^{-1}) compared with that of the classical DOC analysis (2.3 mg L^{-1}). According to the LC-OCD, the combined coagulation/ultrafiltration processes removed approximately 30% of the DOC and 50% of the HS. However, all the other compounds (building blocks and low-molecular-weight (LMW) acids) remained unchanged compared with the feed and permeate composition. The removal of HS resulted in a decrease of SUVA from 3.4–3.7 to 2.3–2.6 compared with the LC-OCD, as well as a decrease from 3 to 2 compared with the classical DOC analysis. These differences fall just outside the analytical error of the classical method, and we are currently unable to explain why the LC-OCD-derived SUVA was higher throughout. In addition, the LC-OCD results indicated that both the biopolymers and the low molecular-weight neutrals ($LMW_{neutrals}$) originated from the lake water. Half of the biopolymers but none of the LMW acids were removed in the treatment process. These carbon fractions have the potential to cause regrowth in the distribution system, which in view of climate change, could probably have implications for the future adaptation of the process (see Section 3.6.2).

All the results from the pilot-scale trial (UF-HF-P1) conducted in 2011 agreed with the data obtained from the most recent (2017) full-scale process (UF-HF-F). This is a most satisfactory result, as it indicates that (a) the full-scale plant was successfully implemented and trimmed to resemble the pilot-scale plant closely and (b) the LC-OCD results were reproducible over time.

3.4. UV Sensor Data Evaluation

The removal of organic matter is controlled by the addition of aluminium salts, of which the dosage is a function of the variation of the incoming *UV* absorbance in the raw water. The differences in the *UV* absorbance in the raw water and the permeate can subsequently be used to assess the efficiency of the removal over time. As the online *UV* sensor signal in the raw water (UV_{Raw}) could be affected by the presence of particles and changes in the optical behaviour owing to fouling, several control measurements were implemented to follow the *UV* signal over time (Table 3). Two of the additional laboratory determinations (Lab 2 and Lab 3, also displayed in Table 3) of the *UV* absorbance are compared with the online data in Figure 7.

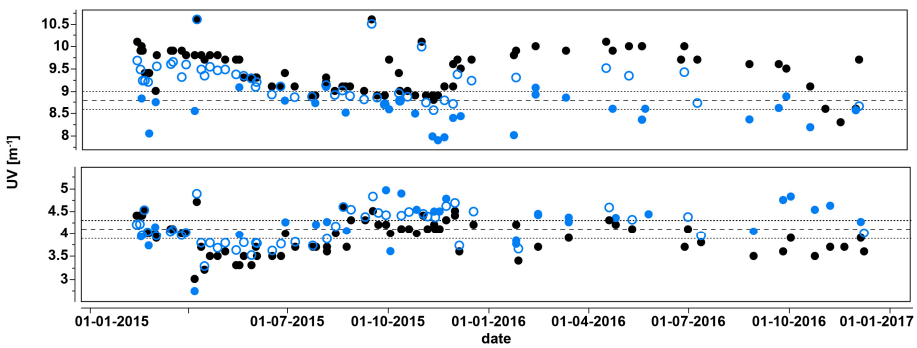

Figure 7. Time series of *UV* (m^{-1}) measured over time using the *UV* sensor (UV_{Raw}, ●), the unfiltered data of Lab 2 ($UV_{Lab2\ unfilt}$, ○), and the filtered data of Lab 3 ($UV_{Lab3\ filt}$, ●) for the raw water (above) and the permeate (below).

The four *UV* measurement methods differed significantly—especially with respect to the raw water (Table 3). The $UV_{Lab2\ unfilt}$ (9.1) and $UV_{Lab3\ filt}$ (8.6) had lower values for the feed water compared

with both the $UV_{\text{Lab1 unfilt}}$ (9.3) and the sensor UV_{Raw} (9.9). From the above time series, it is concluded that a systematic deviation between the different signals was obtained, especially in the later period (Figure 7). All three laboratories found systematically lower *UV* values in the raw water compared with the sensor (UV_{Raw}). Regarding the permeate, the differences in *UV* absorbance were still systematic, with a lower *UV* signal for the sensor compared with that of the laboratory analysis, but they were much less pronounced. The time series of measured differences between the sensor (UV_{Raw}) and $UV_{\text{Lab3 filt}}$ are shown in Figure A6, which confirm these systematic differences over time. These differences highlight the importance of cross-calibration. In particular, the significant difference in the measured values between the sensor (UV_{Raw}) and the filtered samples from Lab 3 ($UV_{\text{Lab3 filt}}$, 1.2 m^{-1} in Table 3) in relation to the raw water was considered unusual. This is because the difference in the TOC and DOC was below 0.05 mg L^{-1} on average (i.e., within the error of the method). Absolute and systematic differences in the different laboratory photometer signals should be excluded, as the filtered samples were not systematically lower for Lab 3 ($UV_{\text{Lab3 filt}}$ 4.4 > 4.0 m^{-1} UV_{Raw}). As the data from Lab 3 were obtained with a 1-cm cuvette, error margins of 0.4 m^{-1} could be avoided only with extreme precaution. In the instance of higher precision being required, a 5-cm cuvette had to be used in a separate measurement of the filtered samples. However, currently, no commercial 5-cm cuvette is available for coupled fluorescence–absorbance measurements similar to those performed in our study. The internal quality control in Lab 3 using K-phthalate standards revealed absolute differences in the monthly samples, which were below 3% on average (Figure A7). Furthermore, we could not exclude the possibility of some smaller fraction of the *UV* absorbance being lost between the time of sampling and the time of analysis (within a few days for most of the samples). The values of both Lab 2 and Lab 3 were lower than were those of Lab 1 measured onsite.

The presence of turbidity in the raw water (on average 0.6 FTU), in addition to the fouling on the sensor ($UV_{\text{Lab2 unfilt}} < UV_{Raw}$)—particularly later (from the spring of 2016, Figure 7)—could be the origin of the observed differences between the sensor, laboratory, and filtered data. Turbidity affected both the calculated *UV* signal and the modelled colour (Figure A8 of the Appendix A). Based on the average measured turbidity in the raw water (0.6 FTU), it was possible to estimate a systematically higher *UV* value of 0.3 m^{-1} (0.6 × 0.523 = 0.34) in the unfiltered samples by using the established equation between turbidity and measured *UV* (Figure A8). The remaining difference in the *UV* absorbance between the raw water (0.9 m^{-1}) and the filtered sample could be ascribed to smaller but reasonably systematic differences (up to 0.4 m^{-1}). This could be related to fouling and the removal of some of the extremely dark hydrophobic fractions during filtration (TOC − DOC = 0.15 mg L^{-1} in Table 4), requiring the removal of approximately 0.5 m^{-1}. This latter observation was corroborated by our own observations on the removal of *UV* when no Al dosage was applied. The observed difference ($UV_{Raw} - UV_{\text{Lab3 filt}}$) of 1.2 m^{-1} was therefore split into three fractions, which were 0.3 m^{-1} caused by turbidity, 0.4 m^{-1} potentially caused by a systematic error between the sensors, and 0.5 m^{-1} caused by filtration or fouling.

This evaluation revealed that the sensor data alone were not enough to track the performance of this UF process (DELTA in Table 3 varies between 48% and 59%) and that the use of both filtered and unfiltered control samples was required to support and calibrate the sensor data. At WTPs with higher turbidity and a higher fraction of particulate organic carbon, measurements that are even more precise would be required.

3.5. DOC Removal Efficiency

The sensor data and coagulant dosing were used to identify the optimal coagulation conditions over the entire pilot period. For this purpose, the variation in the observed *UV* signals between the feed and permeate was plotted against the utilised coagulant dose. The observed relationship was nonlinear, with decreasing efficiency of *UV* removal when the Al dose was increased. This behaviour could be mimicked with a second-degree curve, as shown in Figure 8.

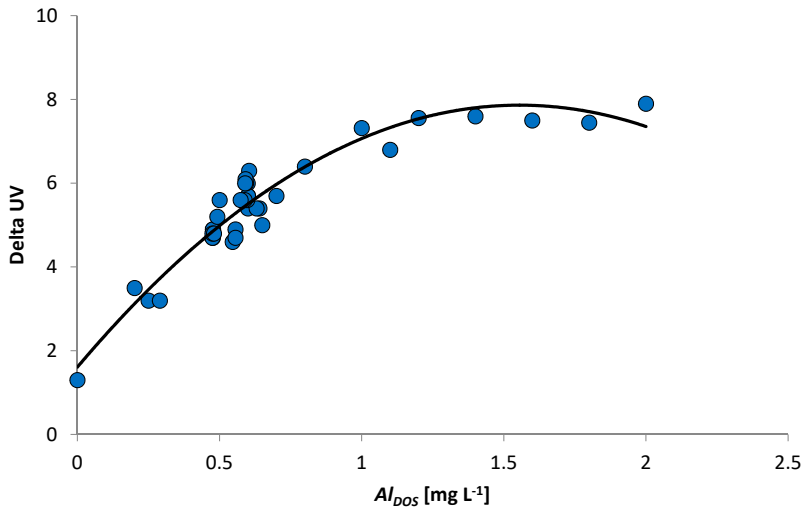

Figure 8. Sensor-based change in *UV* signal between the feed and permeate, as a function of added Al. $\Delta UV = 2.63 + 5.15$*Al dose $- 4.30$*(dose $- 0.529)^2$.

Based on this relationship, all the results related to dosing could be benchmarked. Occurrences of removal (ΔUV) at least 25% below the optimum removal (according to the fitted equation) are coloured red, whereas those at least 10% lower (but within 25% of the optimal performance) are marked black (Figure A9). Most such data points occurred in the initial trimming phase of the pilot experiment, during the first three months. The increasing coagulation efficiency as a function of time is evident. During the first three months, a larger number of data points had a coagulation efficiency below 75%, whereas almost all the data points were above 90% after the nine-month trial.

The available sensor data and those obtained from the extra trials could be used to identify the potential limits of the coagulation dosing beyond 0.6 mg Al L^{-1} currently applied. While there was a somewhat linear relationship between the dose and change in *UV* (Delta *UV*) in the range 0 to 0.7 mg Al L^{-1}, the relationship flattened out at higher doses. Dosing above 1.2–1.4 mg Al L^{-1} did not bring about further reductions in *UV* (Figure 8). This limit was related to the raw water content in the HS and the low SUVA, as was described earlier (Table 4).

The evaluation of normalised coagulation efficiency (Equation 4) could help to determine the efficiency of increasing the dosage compared with the current dose of 0.6 mg Al L^{-1}. These data revealed the sharply decreasing efficiency of Al addition (Figure A10), and in accordance with Figure 8, the curve flattened out at higher doses. It could be calculated how much *UV* was removed with an increase in the dose ($\Delta UV/\Delta$Al). Dosing at 0.95 mg L^{-1} (1.4 mg L^{-1}) achieved only 80% (respectively 66%) of the *UV* removal per dose achieved with the current dose (0.6 mg L^{-1}). Furthermore, higher doses produced more sludge, which from both an environmental and economical viewpoint was not a desired result. Based on the other limitations of the process (e.g., changes in TMP and flux), it was concluded that the current process with the current raw water probably had an optimal technical and economic dosing limit of close to 0.95 mg L^{-1}. This value was used in the scenario below for assessing the potential deterioration in water quality (see Section 3.6.2).

3.6. Adaptation and Resilience of the UF Process (UF-HF-P2)

3.6.1. Determination of Maximum Coagulation Dosage

The critical operational conditions were evaluated during a one-week stress testing period (25 June 2017 to 4 July 2017). This was done to define the maximum coagulation dosage for enhanced NOM removal, in consideration of the overall membrane performance (Table 5). Whereas the membrane performance at the primary UF stage was stable regardless of the incremental increase in the coagulant dosage, the secondary UF stage reached a critical level at 2.0 mg Al L^{-1}. This resulted in a distinct decrease in the permeability during a single filtration cycle (from 740 to 150 L m^{-2} h^{-1} bar^{-1} @ 20 °C). Furthermore, doubling of the coagulant dosage (1 to 2 mg Al L^{-1}) resulted in a limited decrease in *UV* absorbance in the permeate with (0.55 m^{-1}), raising concerns about the economic and operational aspects of process strategies for higher NOM removal.

Table 5. The effect of incremental increase of the coagulant dose on *UV* absorbance and membrane performance. Data for TMP and permeability relate to an ordinary filtration cycle for UF stage-1 and UF stage-2 of the UF test facility (UF-HF-P2) at Kvarnagården WTP.

Dose (mg Al L^{-1})	**1.00**		**1.40**		**1.60**		**1.80**		**2.00**	
UF stage	UF1	UF2	UF1	UF2	UF1	UF2	UF1	UF2	UF1	UF2
Flux (LMH)	49	33	49	33	49	33	49	33	49	33
TMP (bar)	0.16–0.19	0.05–0.14	0.17–0.19	0.06–0.17	0.16–0.18	0.06–0.22	0.16–0.18	0.06–0.24	0.16–0.19	0.06–0.25
Permeability (L m^{-2} h^{-1} bar^{-1} @ 20 °C)	420–360	760–320	420–360	760–240	420–370	740–200	420–360	740–170	420–360	740–150
Feed water, UV_{254} (m^{-1})	10.02	n.a.	9.9	n.a.	9.8	n.a.	9.7	n.a.	10.05	n.a.
Permeate, UV_{254} (m^{-1})	2.70	4.1	2.3	3.2	2.3	2.8	2.25	2.7	2.15	2.8

3.6.2. Scenario Analysis and Evaluation of UF Performance during Constant Rise of DOC

The DOC concentrations have been rising in large parts of the boreal zone, with trends reported to be in the range 0.1 to 0.2 mg L^{-1} per year, and significant changes in the water colour over time.

The following scenario was based on the *UV* data obtained from Lab 1 ($UV_{\text{Lab1 unfilt}}$), assuming an initial *UV* value of 9.4 m^{-1} and a removal level down to approximately 4 m^{-1} using a dose of 0.6 mg L^{-1}. In this projection, it is assumed that the current character of DOC in the raw water sources from Lake Neden and the current groundwater well (i.e., SUVA) would not change over time, while a steady increase for DOC is defined with 0.05 mg L^{-1} per year in the surface water from Lake Neden. This low annual increase, in comparison with the other sites in the area [22], was chosen to account for the potential breakdown of terrestrial TOC during the five-year turnover time. In addition to this change in DOC, the effect of increasing the fraction of groundwater to raw water (i.e., 20% and 25%, instead of the current 15% contribution) was studied. The exact assumptions for the values of DOC and SUVA are shown in Table A5. These three scenarios gave rise to a change in Al dosing that are shown below. A constant rise in DOC over time from the current DOC of 3 mg L^{-1} (2015) to 4.25 (2040) would imply a sharp rise in the required Al dose over time, if the quality of the drinking water (UF permeate) was to remain the same (Figure 9). In 2031, as Al dosing would reach its maximum removal capacity (1.6 mg L^{-1}), the model predicted a decrease in the drinking water quality, as the rising DOC could not be removed any further. Increasing the fraction of GW from 15% to 20% would postpone this eventuality to 2040 and even beyond 2040, if 25% of the raw water could be obtained from the groundwater source. The fourth scenario assumed that the economic limit of Al dosing would be reached at a dose of approximately 0.95 mg L^{-1}. In this scenario, the Al dose would rise until the maximum dose was reached, leading to a deterioration of the *UV* absorbance in the drinking water from the current 4 m^{-1} to approximately 6.3 m^{-1} in 2040.

This analysis (Figure 9) clearly reveals that comparatively minor but reasonable changes in DOC over time owing to climate change or continuing recovery from acid rain would require adaptations to the process. Therefore, careful monitoring of changes in the raw water sources in future is

recommended, similar to that currently being conducted by the regular Swedish lake-monitoring programme that is coordinated by the Swedish EPA.

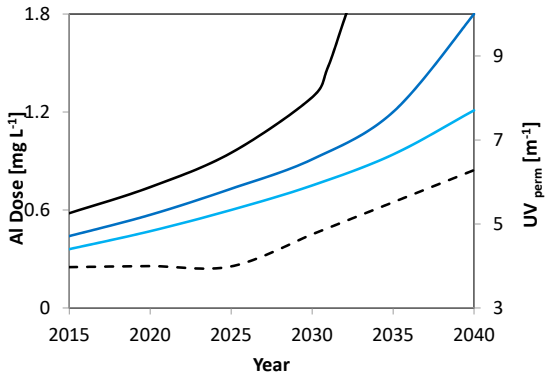

Figure 9. Predicted Al dose as a function of time for current mixing conditions (15% groundwater (GW), 85% surface water, black line), optional (20% GW and 80% surface water, dark-blue line), and increased (25% GW and 75% surface water, light-blue line), assuming constant SUVA in both sources over time, but an increase of 0.05 mg DOC L^{-1} per year in the surface water (Lake Neden) over time. The black stippled line shows the predicted *UV* absorbance in the permeate (UF perm) from the retrofitted UF full-scale water treatment plant, if current mixing conditions were maintained and the maximum economically feasible dosing was assumed to be 0.95 mg Al L^{-1}.

4. Conclusions

Long-term pilot studies are valuable to determine the optimal conditions for ultrafiltration of mixed raw water rich in organic material, with minor seasonal variations. The NOM removal based on in-line coagulation combined with UF membranes from modified polyethersulfone (PES) proved to be suitable for direct ultrafiltration of surface water from Lake Neden, with high removal of NOM and minimal membrane-fouling potential. The major findings of the study are:

- The in-line coagulation/UF process produced stable water quality and facilitated the calculation of a dose–response curve for optimal dosing conditions (0.5–0.7 mg Al L^{-1}) and potential boundaries (0.9–1.2 mg Al L^{-1}).
- The secondary UF stage reached a critical level at 2.0 mg Al L^{-1}, resulting in a distinct decrease in permeability during a single filtration cycle (from 740 to 150 L m^{-2} h^{-1} bar^{-1} @ 20 °C).
- Doubling the coagulant dosage (1.0 to 2.0 mg Al L^{-1}) resulted in a limited decrease in *UV* absorbance in the permeate (0.55 m^{-1}), raising concerns about the economic and operational aspects of process strategies to facilitate higher NOM removal.
- Systematic differences in the sensor and laboratory data must be taken into account for the different procedures to allow for the correct calculation of removal efficiency (quality control).
- The surface-water quality scenarios (up to the year 2040) indicated a potential increase in NOM, with significant effects on the coagulant dose and the quality of drinking water.

Acknowledgments: The financial support of the GenoMembran-project, funded by the Swedish Water and Wastewater Association (Swedish Water Development, SVU) is gratefully acknowledged. The financial support for S.J. Köhler for the duration of this study was assured through DRICKS (Framework programme for drinking water research at Chalmers University in Gothenburg, Sweden). Pentair X-Flow (The Netherlands) is acknowledged for the provision of various test modules. The authors would also like to acknowledge Jennie Lindgren for her contribution of reagents, materials, and analytical tools, as well as Erik Scharenborg for advice on data analysis.

Author Contributions: Alexander Keucken and Gerald Heinicke designed and planned the experiments; Alexander Keucken performed the experiments; Stephan J. Köhler, Kenneth M. Persson, and Alexander Keucken contributed the analysis tools. All the authors analysed the data and contributed to writing the paper.

Conflicts of Interest: The authors declare no conflict of interest. The funding sponsors had no role in the design of the study; in the collection, analyses, or interpretation of the data; in the writing of the manuscript; or in the decision to publish the results.

Glossary

Term	Definition
BB	Building Blocks
CEB	Chemical Enhanced Backwashing
CEEF	Chemical Enhanced Forward Flushing
CIP	Cleaning-in-Place
COD	Chemical Oxygen Demand
Da	Dalton
DBP	Disinfection By-Product
DOC	Dissolved Organic Carbon
FNU	Formazin Nephelometric Unit
GW	Groundwater
HS	Humic Substances
LC-OCD	Liquid Chromatography–Organic Carbon Detection
LMWneutrals	Low Molecular Weight Neutrals
MW	Molecular Weight
MWCO	Molecular Weight Cut-Off
NF	Nanofiltration
NOM	Natural Organic Matter
PES	Polyethersulfone
SUVA	Specific Ultraviolet Absorbance
TMP	Transmembrane Pressure
TOC	Total Organic Carbon
UV_{abs}	Absorption of *UV* light at 254 nm
UF	Ultrafiltration
WTP	Water Treatment Plant

Appendix A

Table A1. Feed water quality (median and standard deviations) of primary and secondary UF stages (UF-HF-P2).

Parameters	Unit	Range (UF-Stage 1)	Range (UF-Stage 2)
Temperature	°C	4.5 ± 0.7	4.6 ± 0.5
pH	(-)	7.4 ± 0.1	7.1 ± 0.2
Turbidity	(FTU)	0.6 ± 0.2	20.0 ± 2.9
Hardness	°dH	1.5 ± 0.10	1.6 ± 0.15
Alkalinity	(mg/L HCO_3)	19.0 ± 2.1	18.0 ± 3.0
COD	(mg/L O_2)	2.0 ± 0.1	25.0 ± 7,5
TOC	(mg C/L)	2.9 ± 0.06	27.0 ± 3.2
DOC	(mg C/L)	2.6 ± 0.1	4.4 ± 0.45
UV_{254}	(/5 cm)	0.380 ± 0.22	3.955 ± 3.3
Pt-Co	(mg Pt/L)	13 ± 1.0	15.0 ± 5.8
Conductivity	(µS/cm)	110 ± 6.9	110 ± 5.7
Iron	(mg/L Fe)	0.026 ± 0.02	0.57 ± 0.1
Manganese	(mg/L Mn)	0.035 ± 0.01	0.044 ± 0.01

Table A2. Operating conditions and process parameters during long-term pilot trials (UF-HF-P2).

Parameters	Unit	UF Primary	UF Secondary
Max. filtration time (t_F)	(min)	90	60
Max. filtration volume	(m^3)	8.4	1.65
Filtration flux (J_F)	(L m^{-2} h^{-1})	65–70	45
V_{CF} (cross flow velocity)	(m s^{-1})	-	0.5
R (recovery during filtration)	(%)	100	100
t_{BW} (backwash time)	(s)	30	30
J_{BW} (backwash flux)	(L m^{-2} h^{-1})	250	250
t_{CEFF} (CEB interval)	(days)	1.5	5
CEB1 dosing solution (caustic)	(-)	250–300 ppm NaOCl @ pH 12.2 with NaOH	250–300 ppm NaOCl @ pH 12.2 with NaOH
CEB2 dosing solution (acidic)	(-)	475 mg/L H_2SO_4 @ pH 2.4	475 mg/L H_2SO_4 @ pH 2.4
t_{SOAK} (Soak time CEB)	(min)	10	10

Table A3. Membrane key performance parameters during pilot trials.

Parameters	Unit	UF Primary	UF Secondary
Permeability	(L m^{-2} h^{-1} bar^{-1} @ 20 °C)	350–380	600–220
Transmembrane pressure	(bar)	0.18–0.28	0.12–0.25
Total number of CEBs	(-)	267	37
Module age before replacement	(months)	12	14
Total amount of filtration volume (feed water)	m^3	57.150 [1]	2.155 [2]

Notes: [1] 150 m^3/day × 381 days, [2] 4.8 m^3/day × 449 days.

Table A4. Manufacturer-reported properties of the hollow fibre membranes.

Parameter	Unit	Key Performance Values
Membrane Material	**Sulfonated Polyethersulfone (PES)**	
Max. backflush pressure	kPa	300
MWCO based on PEG [1]	kDa	100
Diameter (internal)	mm	0.80
Nominal pore size	nm	20
Membrane area	m^2	55
Number of fibres		~15,000
Reduction of bacteria	log	6 (*Pseudomonas diminuta*)
Reduction of virus	log	4 (MS2 coliphages)
Module hydraulic diameter	mm	220.0
Module length	mm	1537.5

Notes: [1] PEG = Polyethylene glycol unit of molecular weight approximately 1000 dalton. MWCO: molecular weight cut-off.

Table A5. Scenario analysis (year 2040): Assumptions for source water values regarding DOC and SUVA (DELTA [DOC] 0.05 mg DOC/year).

Year	GW DOC (mg L^{-1})	GW SUVA (L/mg*m)	GW *UV* abs (m^{-1})	Neden DOC (mg L^{-1})	Neden SUVA (L mg^{-1} m^{-1})	Neden *UV* (m^{-1})	GW Fraction (%)	UVabs MIX (m^{-1})	DOC MIX (mg L^{-1})	Al_{DOS} S1 (mg L^{-1})	Al_{DOS} S2 (mg L^{-1})	Al_{DOS} S3 (mg L^{-1})	Delta *UV* [1]	Delta *UV* [1]	Uvabs Permeate (m^{-1})	Al DOS Max Dose (mg L^{-1})
2015	0.65	2	1.3	3	3.6	10.8	0.15	9.375	2.6475	0.58			5.40	5.40	3.97	0.58
2020	0.65	2	1.3	3.25	3.6	11.7	0.15	10.14	2.86	0.74			6.14	6.14	3.99	0.74
2025	0.65	2	1.3	3.5	3.6	12.6	0.15	10.905	3.0725	0.95			6.92	6.91	3.98	0.95
2030	0.65	2	1.3	3.75	3.6	13.5	0.15	11.67	3.285	1.29			6.92	7.68	3.98	0.95
2031	0.65	2	1.3	3.8	3.6	13.68	0.15	11.823	3.3275	1.48			6.92	7.84	3.97	0.95
2033	0.65	2	1.3	3.9	3.6	14.04	0.15	12.129	3.4125	>2			6.92	<8	>4	0.95
2035	0.65	2	1.3	4	3.6	14.4	0.15	12.435	3.4975	>2			6.92	<8	>4	0.95
2040	0.65	2	1.3	4.25	3.6	15.3	0.15	13.2	3.71	>2			6.92	<8	>4	0.95
2015	0.65	2	1.3	2.9	3.6	10.44	0.2	8.612	2.45		0.44			4.64	3.96	
2020	0.65	2	1.3	3.15	3.6	11.34	0.2	9.332	2.65		0.57			5.35	3.98	
2025	0.65	2	1.3	3.4	3.6	12.24	0.2	10.052	2.85		0.73			6.10	3.95	
2030	0.65	2	1.3	3.65	3.6	13.14	0.2	10.772	3.05		0.91			6.78	3.98	
2035	0.65	2	1.3	3.9	3.6	14.04	0.2	11.492	3.25		1.2			7.53	3.95	
2040	0.65	2	1.3	4.15	3.6	14.94	0.2	12.212	3.45		>2			<8	>4	
2015	0.65	2	1.3	2.9	3.6	10.44	0.25	8.155	2.3375			0.36		4.16	3.98	
2020	0.65	2	1.3	3.15	3.6	11.34	0.25	8.83	2.525			0.47		4.81	4.01	
2025	0.65	2	1.3	3.4	3.6	12.24	0.25	9.505	2.7125			0.6		5.50	4.00	
2030	0.65	2	1.3	3.65	3.6	13.14	0.25	10.18	2.9			0.75		6.18	3.99	
2035	0.65	2	1.3	3.9	3.6	14.04	0.25	10.855	3.0875			0.94		6.88	3.97	
2040	0.65	2	1.3	4.15	3.6	14.94	0.25	11.53	3.275			1.21		7.55	3.97	

Note: [1] Delta $UV = -2.5864*Al_{DOS}{}^2 + 8.0452*Al_{DOS} + 1.6065$.

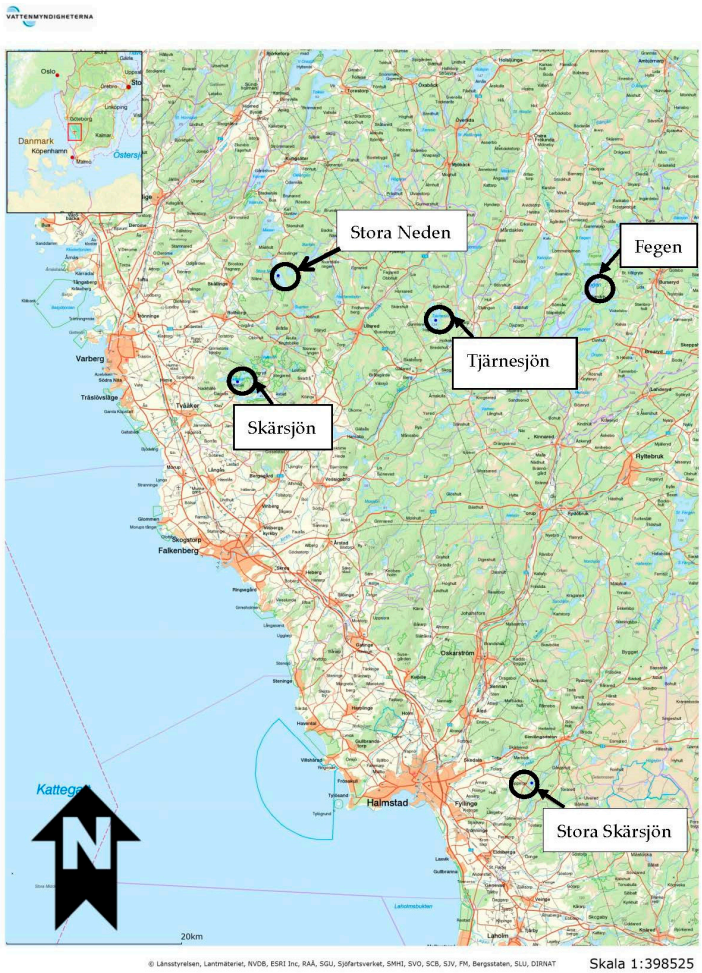

Figure A1. Geographical location of lakes in the region for which long-term monitoring data from the Swedish monitoring programme are available.

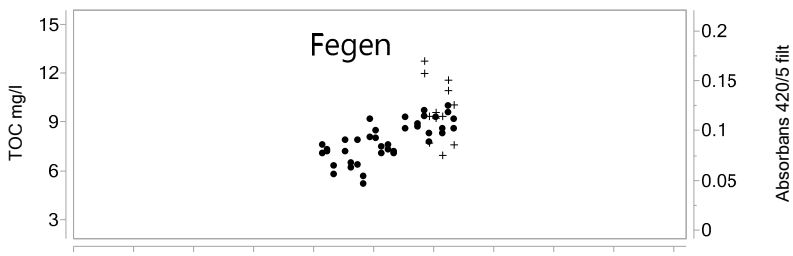

Figure A2. *Cont.*

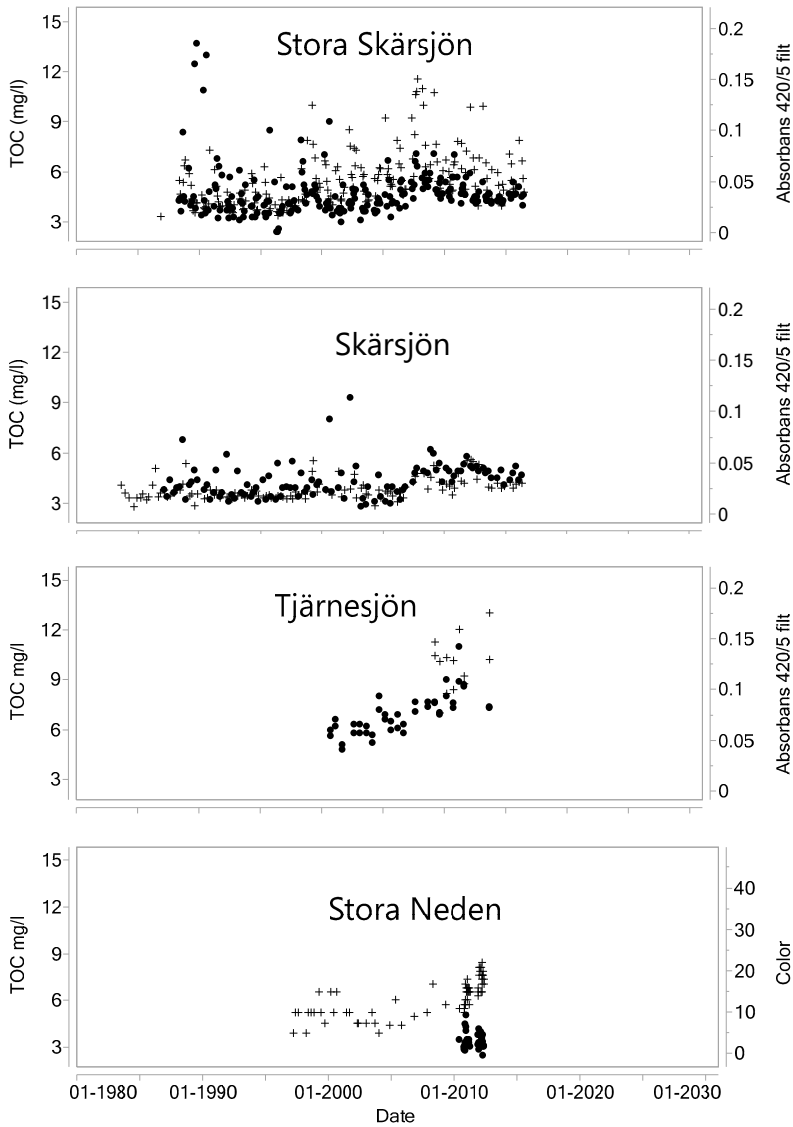

Figure A2. Time series of trends in TOC (+, left scale, mg L^{-1}) and colour measured as Abs_420 (●, right scale) or, as in the instance of Lake Stora Neden, in Pt colour that were acquired by the Swedish lake monitoring programme.

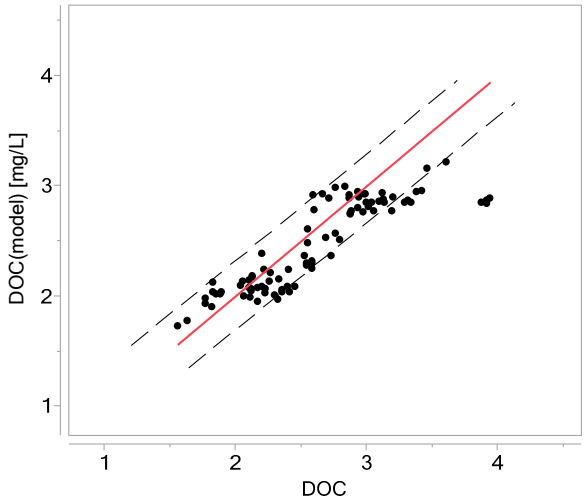

Figure A3. Measured DOC (mg L^{-1}) against predicted DOC (DOC (model) = a + b * $UV_{\text{Lab3 filt}}$). The close linear relationship is proof of extremely stable SUVA over time.

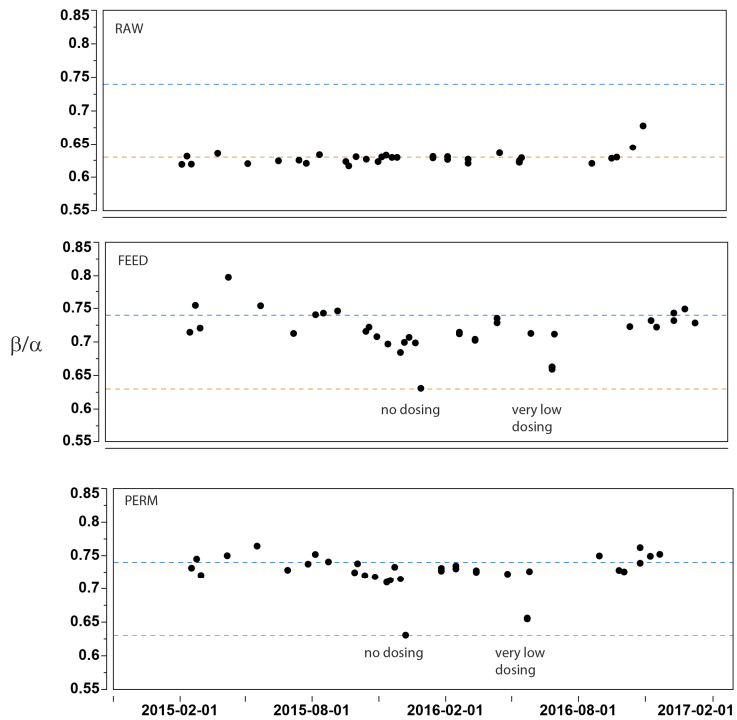

Figure A4. Time series of the freshness index of raw water (above), feed water (middle), and permeate (below) for 2015–2016.

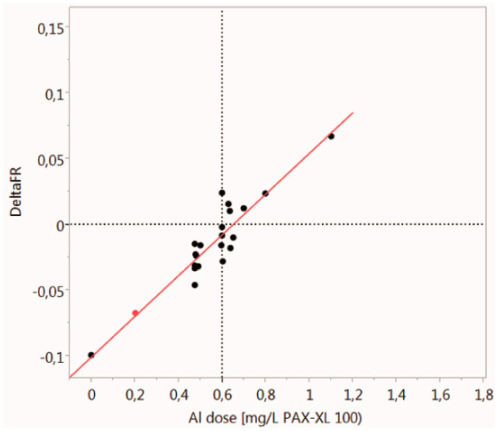

Figure A5. Change in the freshness index (DeltaFR) when comparing higher and lower doses than the current optimal dose of 0.6 mg L^{-1}. DeltaFR = −0.100117 + 0.154*Al DOS (mg L^{-1} PAX-XL 100); R2 = 0.872, RMSE = 0.012.

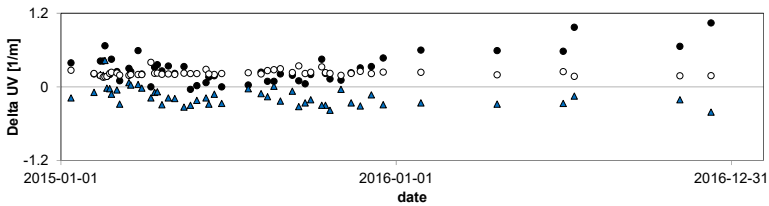

Figure A6. Comparison of *UV* signal from the sensor (UV_{Raw}, ●) Lab 2 ($UV_{\text{Lab2 unfilt}}$, ○), and from Lab 3 ($UV_{\text{Lab3 filt}}$, ▲) over time.

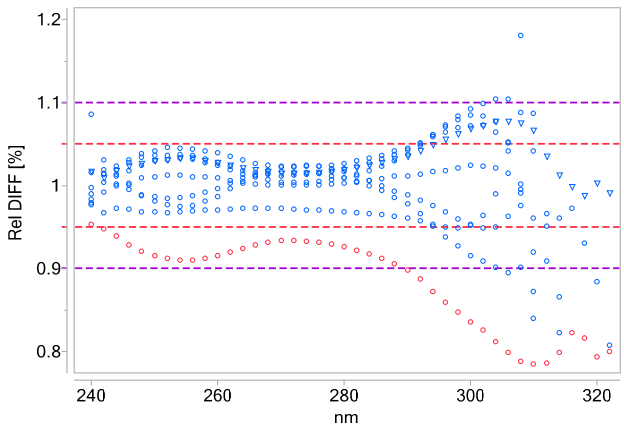

Figure A7. Differences in spectra normalised to average spectra of the K-phthalate internal standard solutions (60 ppm), as a function of wavelength that were measured monthly during 2016 for quality control purposes. On average, the relative deviation is below 3% in the *UV* range 240–290 nm. Different blue markers indicate the different sample months. One extreme sample is marked in red.

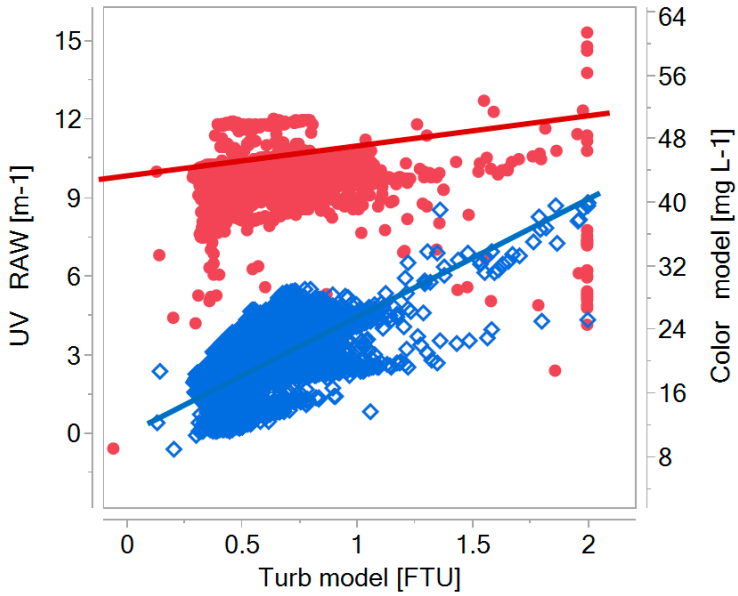

Figure A8. Estimation of effects of sensor-modelled turbidity (FTU) on sensor-modelled colour (◇), and sensor-measured *UV* (●). $UV = 9.30 + 0.523 * Turb_{model}$. Per one unit of modelled turbidity, approximately half a unit of *UV* is added, which is in accordance with unpublished stream data from the Fyris River (Uppsala, Sweden). At turbidity of 2, an additional *UV* signal of 1 is captured that is not related to the DOC. The offset 9.3 is extremely close to the average raw water *UV*. Regarding the colour, this effect is more pronounced, such that a turbidity of 2 could give rise to additional colour of 36 mg L^{-1}, therefore dominating the signal. $Color = 11.6 + 18.4 * Turb_{model}$.

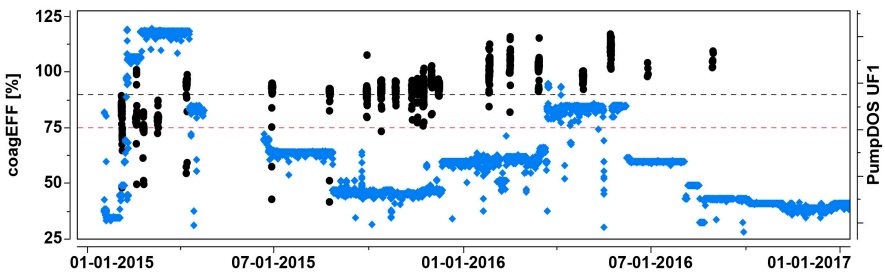

Figure A9. Change in coagulation efficiency (● coagEFF [%]) and dosing (◆ Al Dosing INT [L/h]) signal as a function of time for the two-year study period. The black and red horizontal lines highlight 90% and 75% coagEFF.

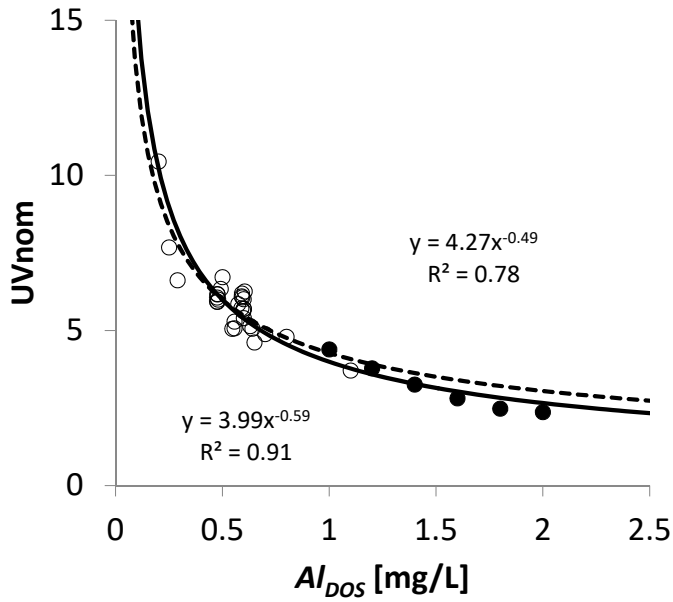

Figure A10. Estimation of normalised *UV* removal as a function of Al dose based on Equation (4). Black circles (●) are additional high-dose experiments, while white circles (○) are those from the optimization period. Two regression lines including (below) or excluding the additional points are displayed (above).

References

1. Forsberg, C.; Petersen, R., Jr. A darkening of Swedish lakes due to increased humus inputs during the last 15 years. *Verhandlungen des Internationalen Verein Limnologie* **1990**, *24*, 289–292.
2. Eikebrokk, B.; Vogt, R.; Liltved, H. NOM increase in Northern European source waters: Discussion of possible causes and impacts on coagulation/contact filtration processes. *Water Sci. Technol. Water Supply* **2004**, *4*, 47–54.
3. Worrall, F.; Burt, T. Trends in DOC concentration in Great Britain. *J. Hydrol.* **2007**, *346*, 81–92. [CrossRef]
4. Evans, C.D.; Monteith, D.T.; Cooper, D.M. Long-term increases in surface water dissolved organic carbon: Observations, possible causes and environmental impacts. *Environ. Pollut.* **2005**, *137*, 55–71. [CrossRef] [PubMed]
5. Köhler, S.J.; Buffam, I.; Seibert, J.; Bishop, K.H.; Laudon, H. Dynamics of stream water TOC concentrations in a boreal headwater catchment: Controlling factors and implications for climate scenarios. *J. Hydrol.* **2009**, *373*, 44–56. [CrossRef]
6. Delpla, I.; Jung, A.-V.; Baures, E.; Clement, M.; Thomas, O. Impacts of climate change on surface water quality in relation to drinking water production. *Environ. Int.* **2009**, *35*, 1225–1233. [CrossRef] [PubMed]
7. Lavonen, E.E.; Kothawala, D.N.; Tranvik, L.J.; Gonsior, M.; Schmitt-Kopplin, P.; Köhler, S.J. Tracking changes in the optical properties and molecular composition of dissolved organic matter during drinking water production. *Water Res.* **2015**, *85*, 286–294. [CrossRef] [PubMed]
8. Lavonen, E.E.; Gonsior, M.; Tranvik, L.J.; Schmitt-Kopplin, P.; Köhler, S.J. Selective Chlorination of Natural Organic Matter: Identification of Previously Unknown Disinfection Byproducts. *Environ. Sci. Technol.* **2013**, *47*, 2264–2271. [CrossRef] [PubMed]
9. Jacangelo, J.; DeMarco, J.; Owen, D.; Randtke, S. Selected processes for removing NOM: An overview. *J. Am. Water Works Assoc.* **1995**, *87*, 64–77.
10. Jacangelo, J.G.; Rhodes Trussell, R.; Watson, M. Role of membrane technology in drinking water treatment in the United States. *Desalination* **1997**, *113*, 119–127. [CrossRef]

11. Singer, P.; Bilyk, K. Enhanced coagulation using a magnetic ion exchange resin. *Water Res.* **2002**, *36*, 4009–4022. [CrossRef]
12. Matilainen, A.; Iivari, P.; Sallanko, J.; Heiska, E.; Tuhkanen, T. The role of ozonation and activated carbon filtration in the natural organic matter removal from drinking water. *Environ. Technol.* **2006**, *27*, 1171–1180. [CrossRef] [PubMed]
13. Zularisam, A.; Ismail, A.; Salim, R. Behaviours of natural organic matter in membrane filtration for surface water treatment—A review. *Desalination* **2006**, *194*, 211–231. [CrossRef]
14. Toor, R.; Mohseni, M. UV-H2O2 based AOP and its integration with biological activated carbon treatment for DBP reduction in drinking water. *Chemosphere* **2007**, *66*, 2087–2095. [CrossRef] [PubMed]
15. Matilainen, A.; Sillanpää, M. Removal of organic matter from drinking water by advanced oxidation processes: A review. *Chemosphere* **2010**, *80*, 351–365. [CrossRef] [PubMed]
16. Amy, G.L.; Alleman, B.C.; Cluff, C.B. Removal of dissolved organic matter by nanofiltration. *J. Environ. Eng.* **1990**, *116*, 200–205. [CrossRef]
17. Köhler, S.J.; Lavonen, E.E.; Keucken, A.; Schmitt-Kopplin, P.; Spanjer, T.; Persson, K.M. Upgrading coagulation with hollow-fibre nanofiltration for improved organic matter removal during surface water treatment. *Water Res.* **2016**, *89*, 232–240. [CrossRef] [PubMed]
18. Lidén, A.; Persson, K.M. Comparison between ultrafiltration and nanofiltration hollow-fiber membranes for removal of natural organic matter—A pilot study. *J. Water Supply Res. Technol. AQUA* **2015**, *65*. [CrossRef]
19. Jung, C.-W.; Kang, L.-S. Application of combined coagulation-ultrafiltration membrane process for water treatment. *Korean J. Chem. Eng.* **2003**, *20*, 855–861. [CrossRef]
20. Vickers, J.; Thompson, M.; Kelkar, U. The use of membrane filtration in conjunction with coagulation processes for improved NOM removal. *Desalination* **1995**, *102*, 57–61. [CrossRef]
21. Tran, T.; Gray, S.; Naughton, R.; Bolto, B. Polysilicato-iron for improved NOM removal and membrane performance. *J. Membr. Sci.* **2006**, *280*, 560–571. [CrossRef]
22. Valinia, S.; Futter, M.; Fölster, J.; Cosby, B.; Rosén, P. Simple models to estimate historical and recent changes of total organic carbon concentrations in lakes. *Environ. Sci. Technol.* **2015**, *49*, 386–394. [CrossRef] [PubMed]
23. Vattenkvalitet i Hallands Sjöar 2012. *Resultat Från Omdrevsprogrammet 2007–2012 Länsstyrelsen i Hallands län Enheten för Naturvård & Miljöövervakning Meddelande*; Vattenkvalitet i Hallands Sjöar: Hallands Sjöar, Swedish, 2013; ISSN 1101-1084.
24. Finstad, A.; Blumentrath, S.; Tømmervik, H.; Andersen, T.; Larsen, S.; Tominaga, K.; Hessen, D.; De Wit, H. From greening to browning: Catchment vegetation development and reduced S-deposition promote organic carbon load on decadal time scales in Nordic lakes. *Sci. Rep.* **2016**, *6*, 31944. [CrossRef] [PubMed]
25. Keucken, A.; Heinicke, H. NOM characterization and removal by water treatment processes for drinking water and ultra pure process water. In Proceedings of the 4th IWA Speciality Conference on Natural Organic Matter, Costa Mesa, CA, USA, 27–29 July 2011.
26. Keucken, A.; Donose, B.-C.; Persson, K.-M. Membrane fouling revealed by advanced autopsy. In Proceedings of the 8th Nordic Drinking Water Conference, Stockholm, Sweden, 18–20 June 2012.
27. Keucken, A.; Wang, Y.; Tng, K.H.; Leslie, G.L.; Spanjer, T.; Köhler, S.J. Optimizing hollow fibre nanofiltration for organic matter rich lake water. *Water* **2016**, *8*, 430. [CrossRef]
28. Huber, S.A.; Balz, A.; Abert, M.; Pronk, W. Characterisation of aquatic humic and non-humic matter with size-exclusion chromatography–organic carbon detection–organic nitrogen detection (LC-OCD-OND). *Water Res.* **2011**, *45*, 879–885. [CrossRef] [PubMed]
29. Cory, R.; McKnight, D. Fluorescence spectroscopy reveals ubiquitous presence of oxidized and reduced quinones in dissolved organic matter. *Environ. Sci. Technol.* **2005**, *39*, 8142–8149. [CrossRef] [PubMed]
30. Ohno, T.; Bro, R. Dissolved organic matter characterization using multiway spectral decomposition of fluorescence landscapes. *Soil Sci. Soc. Am. J.* **2006**, *70*, 2028–2037. [CrossRef]
31. Parlanti, E.; Woerz, K.; Geoffroy, L.; Lamotte, M. Dissolved organic matter fluorescence spectroscopy as a tool to estimate biological activity in a coastal zone submitted to anthropogenic inputs. *Org. Geochem.* **2000**, *31*, 1765–1781. [CrossRef]

32. Lidén, A.; Keucken, A.; Persson, K.M. Uses of fluorescence excitation-emissions indices in predicting water efficiency. *J. Water Proc. Eng.* **2017**, *16*, 249–257. [CrossRef]
33. Köhler, S.J.; Kothawala, D.; Futter, M.N.; Liungman, O.; Tranvik, L. In-Lake Processes Offset Increased Terrestrial Inputs of Dissolved Organic Carbon and Color to Lakes. *PLoS ONE* **2013**, *8*, e70598. [CrossRef] [PubMed]

Paper VI

Water Research 89 (2016) 232–240

Contents lists available at ScienceDirect

Water Research

journal homepage: www.elsevier.com/locate/watres

Upgrading coagulation with hollow-fibre nanofiltration for improved organic matter removal during surface water treatment

Stephan J. Köhler [a, *], Elin Lavonen [a], Alexander Keucken [b, c], Philippe Schmitt-Kopplin [d, e], Tom Spanjer [f], Kenneth Persson [c, g]

[a] Department of Aquatic Sciences and Assessment, Swedish University of Agricultural Sciences, Box 7050, Uppsala, Sweden
[b] Vatten & Miljö i Väst AB (VIVAB), Box 110, SE-311 22, Falkenberg, Sweden
[c] Water Resources Engineering, Faculty of Engineering, Lund Technical University, Box 118, SE-221 00, Lund, Sweden
[d] Analytical BioGeoChemistry, German Research Center for Environmental Health, Helmholtz Zentrum München, 85764, Neuherberg, Germany
[e] Chair of Analytical Food Chemistry, Technische Universität München, 85354, Freising-Weihenstephan, Germany
[f] Pentair X-Flow B.V., P.O. 739, 7500, AS Enschede, The Netherlands
[g] Sydvatten AB, Skeppsgatan 19, SE 211 19, Malmö, Sweden

ARTICLE INFO

Article history:
Received 4 July 2015
Received in revised form
17 November 2015
Accepted 20 November 2015
Available online 27 November 2015

Keywords:
Nanofiltration (NF)
Hollow fibre
Humic substances (HS)
Drinking water
Fluorescence EEM
GAC

ABSTRACT

Rising organic matter concentrations in surface waters in many Nordic countries require current drinking water treatment processes to be adapted. Accordingly, the use of a novel nanofiltration (NF) membrane was studied during a nine month period in pilot scale at a large drinking water treatment plant in Stockholm, Sweden. A chemically resistant hollow-fibre NF membrane was fed with full scale process water from a rapid sand filter after aluminum sulfate coagulation. The combined coagulation and NF process removed more than 90% of the incoming lake water dissolved organic carbon (DOC) (8.7 mg C L^{-1}), and 96% of the absorbance at 254 nm (A254) (0.28 cm^{-1} incoming absorbance). Including granulated active carbon GAC) filter, the complete pilot plant treatment process we observed decreases in DOC concentration (8.7–0.5 mg C L^{-1}), SUVA (3.1–1.7 mg^{-1} L m^{-1}), and the average nominal molecular mass (670–440 Da). Meanwhile, water hardness was practically unaffected (<20% reduction). Humic substances (HS) and biopolymers were almost completely eliminated (6510–140 and 260 to 10 μg C L^{-1} respectively) and low molecular weight (LMW) neutrals decreased substantially (880–190 μg C L^{-1}). Differential excitation emission matrices (EEMs), which illustrate the removal of fluorescing organic matter (FDOM) over a range of excitation and emission wavelengths, demonstrate that coagulation removed 35 ± 2% of protein-like material and 65 ± 2% of longer emission wavelength, humic-like FDOM. The subsequent NF treatment was somewhat less selective but still preferentially targeted humic-like FDOM (83 ± 1%) to a larger extent than protein-like material (66 ± 3%). The high selectivity of organic matter during coagulation compared to NF separation was confirmed from analyses with Fourier transform ion cyclotron resonance mass spectrometry (FT-ICR-MS), and liquid chromatography with organic carbon detection (LC-OCD), as coagulation exclusively targeted oxidized organic matter components while NF removed both chemically reduced and oxidized components. DOC removal and change in DOC character in the GAC filters showed marked differences with slower saturation and more pronounced shifts in DOC character using NF as pre-treatment. Fluorescence derived parameters showed a similar decrease over time of GAC performance for the first 150 days but also indicated ongoing change of DOM character in the post NF GAC filtrate over time even after LC-OCD indicated steady state with respect to outgoing carbon. During our trial iron concentrations were low (<30 ppb) and thus A254 could be directly related to the concentration of HS ($R^2 = 0.9$). The fluorescence derived freshness index (β:α) proved to be an excellent variable for estimating the fraction of HS present in all samples. Given the recommended limit of 4 mg L^{-1} for chemical oxygen demand (COD) for Swedish drinking water, coagulation will need to be supplemented with one or more treatment steps irrespective whether climate change will lead to drier or wetter conditions in order to maintain sufficient DOC removal with the current increasing concentrations in raw waters.

* Corresponding author.
E-mail address: stephan.kohler@slu.se (S.J. Köhler).

http://dx.doi.org/10.1016/j.watres.2015.11.048
0043-1354/

1. Introduction

Rising levels of dissolved organic matter (DOM) in boreal and north European surface waters (Hongve et al. 2004) pose a number of technical and chemical challenges for drinking water production. Water treatment costs have increased and are expected to continue to rise, especially when using coagulation techniques which require higher chemical doses that results in more sludge (Eikebrokk et al. 2004). In addition, climate change is expected to lead to larger fluctuations in dissolved organic carbon (DOC) concentrations, commonly used as a proxy for DOM, and thus, further degradation of raw water quality in the future (Delpla et al., 2009). Intensity, timing and duration of fluctuations in DOC concentration and composition in surface waters are of vital economic interest for drinking water producers but difficult to foresee. DOC removal through coagulation treatment, which is the most commonly used method at Swedish water treatment plants (WTPs), is affected by organic matter composition and the removal efficiency is commonly reported to increase with the DOC-normalized absorbance at 254 nm (SUVA), an indicator of aromatic carbon and a terrestrial origin (Matilainen et al. 2010; Weishaar et al. 2003). The fraction of terrestrially derived DOC decrease with water turnover time in lakes (Gondar et al. 2008; Tang et al. 2013; Köhler et al. 2013), leading to lowered removal efficiency during the coagulation treatment. Lakes with varying turnover times are thus more prone to temporal changes in DOC character. This is the case for Mälaren, the third largest lake in Sweden, which is used as raw water source for three large WTPs supplying the Swedish capital city Stockholm with drinking water. Raw water DOC concentration is currently approximately 9 mg C L^{-1}, of which only roughly half can be removed through coagulation treatment. Lake water retention time has been identified as a key driver of DOM quality in this lake (Köhler et al. 2013; Lavonen et al. 2015). In Sweden, WTPs have to comply with a recommended limit of around 4 mg C L^{-1} organic matter measured as chemical oxygen demand (COD) for drinking water. In the case of Mälaren this is equivalent to 5 mg C L^{-1} DOC. Future climate or land use driven changes in DOC concentration and composition are thus large challenges for drinking water producers. Lower outgoing DOC will lead to decreased unwanted consumption of disinfectant and, reduced microbial regrowth potential in the distribution network. Improved DOC removal prior to treatment with granular activated carbon (GAC) filters may furthermore decrease fouling by irreversibly bound DOM components which diminish the ability of GAC filters to remove micro-pollutants such as perfluorooctanesulfonic acid (PFOS), algal degradation products or fuel residues, all which may occur in Mälaren.

High pressure (>10 bar), NF membranes with low molecular weight cut-off (<300 Da) have been used for a number years to remove organic matter for drinking water purposes (Meylan et al. 2007). These tight membranes are efficient in removing DOC and hardness (e.g. Ca^{2+}, Mg^{2+}, >80% removal) as well as a number of organic micro-pollutants (Zhang et al. 2006). Commercially available spiral wound NF membranes are designed for DOC removal at the expense of undesirable retention of hardness for drinking water production from soft raw waters. Furthermore, the spiral wound membranes are characterized by low chlorine stability, limited disinfection and chemical cleaning possibilities, e.g. pH 3–8 for cellulose acetate filters as compared to pH 2–12 for polysulfonate (Regula et al. 2014). Intensive pre-treatment is necessary due to limited hydraulic cleaning options. Capillary, hollow fibre NF membranes have been applied for direct filtration of highly colored surface water during the last decade (Meylan et al. 2007). One of the latest concepts in NF for highly effective removal of organic matter, the so called Color Removal Package, is based on capillary NF membranes, combining the chemical resistance of hollow fibre membranes with the organic carbon retention of spiral wound units (De Grooth, 2015). These membranes are modified for enhanced organic matter removal and limited retention of bivalent metal ions from the feed water. As they are operated using outside in flow, they may be flushed inside out which is ideal when retrofitting an existing treatment scheme. They do not require pretreatment other than 300 micron safety screen and can directly be fed with raw surface water. In summer 2013, a HFW 1000 membrane pilot plant was installed at Görväln WTP, situated in Stockholm, Sweden, to evaluate the organic matter removal and performance of NF filtration following conventional coagulation and rapid sand filtration. Organic matter quality and quantity in all steps from raw to drinking water were evaluated with a large range of analytical techniques. These included total and dissolved organic carbon (TOC, DOC), online ultraviolet and visible (UV-VIS) absorbance (250–700 nm), 3D fluorescence, Fourier transform ion cyclotron resonance mass spectrometry (FT-ICR-MS) and liquid chromatography with organic carbon detection (LC-OCD).

This study aims to a) evaluate the performance of a retrofitted new generation HFW 1000 nanofilter membrane, b) study the selective removal of DOM fractions in the combined coagulation NF process and the currently used coagulation technique; c) identify DOM characterization techniques that are informative for validating membrane and GAC performance, and d) use the acquired data to estimate removal of DOC with varying composition in the studied raw water as a function of lake water retention time.

2. Material and methods

2.1. NF pilot plant

The membrane material is composed of sulfonated polyether sulfone. The presence of sulfonate groups on the benzene ring structure renders them hydrophilic and leads to a negative zeta potential at pH above 5. The zeta potential further decrease to around −20 mV with the raw water pH 7.5 used in our study and the membrane therefore effectively rejects molecules with negatively charged functional groups such as DOC (De Grooth, 2015). The separating layer of the membrane is on the inside of the fibres, thus allowing operating inside-out. The internal hydraulic diameter of the membrane fibres is 0.8 mm and the molecular weight cut-off is approximately 1000 Da based on Dextran permeation.

The HFW 1000 NF membrane module is 0.20 m (8″) in diameter and 1.54 m (60.5″) long. It contained 40 m^2 of membrane surface area with the 0.8 mm fibres. The test module was equipped with surface flow collectors. The test facility (a QuickScan pilot plant, supplied by Pentair X-Flow) had a capacity of 600 L h^{-1} (permeate production). During the pilot trials the test membrane was continuously operated at feed flow rate of 1.2 m^3 h^{-1} with a flux range of around 15 L m^{-2} h^{-1}, a cross-flow velocity of 0.5 m s^{-1}, an intermittent forward flushing interval of every 60 min and a recovery rate of 50%. We chose to protect the membrane and operate at this low recovery even if higher recoveries of up to 80 were successfully tested, With operating pressures around 4 bar and permeability rates of 10 L m^{-2} h^{-1} bar^{-1} the transmembrane pressure typically increased with 0.17 bar and the permeability decreased with 1.0 L m^{-2} h^{-1} bar^{-1} at low water temperatures of around 1–3 °C during a filtration period of 42 days. The cleaning procedure is explained in detail in the appendix.

2.2. Mälaren as drinking water source

Görväln WTP is located in the eastern part, close to the outlet of Lake Mälaren, Sweden, where water from a northern basin (16%)

and the large western basin (84%) mix. Varying water quality in the raw water intake is due to different processing of DOC within the lake (Köhler et al. 2013). Mälaren raw water (2002–2013) has high pH (7.6–7.8), high alkalinity (1.3 mM) and a DOC that varies between 6 and 12 mg L^{-1}. Raw water turbidity varies between 2 and 10 FNU depending on the raw water intake depth. A more detailed description of the water quality and different water sources that contribute to the raw water at Görväln WTP can be found in Ericsson et al. 1984.

2.3. Full scale drinking water plant

The raw water (RAW) from Mälaren is taken in at two different intake depths (−4 and −22 m) depending on the water quality. After passing a micro sieve (200 μm nominal pore size) the water is coagulated with $Al_2(SO_4)_3$ at doses varying from 40 to 70 mg L^{-1}. The coagulant dose is controlled by measuring turbidity after the following rapid sand filtration (SF) (0.6 m h^{-1}), which is used to remove residual flocs. Downstream, the water is filtered through a Norit 1240 W GAC bed (CF), and disinfected with UV irradiation (25 mJ cm^{-2}) and monochloramine (NH_2Cl; 0.2–0.35 mg L^{-1}) to produce drinking water (DW) as shown on the left side in Fig. 1.

2.4. Pilot scale drinking water treatment plant

The feed water for the NF pilot plant water is recovered from the SF full-scale plant as displayed in the right side of Fig. 1. NF membrane module was followed by a pilot scale GAC filter (CF2). A fraction of the rapid sand filtrate was filtered directly by another GAC filter (CF4) so that the effect of NF on the activated carbon filter could be compared under the same conditions regarding GAC age (Fig. 1). Granulated activated carbon (GAC) filter beads of approximately 2.5 m height were filled with 1 m GAC (Norit 1240 W) and at a hydraulic load of 10 m h^{-1} this resulted in an empty bed contact time of approximately 6 min at a flow rate of 1 L min^{-1} in accordance with the full scale plant conditions. This setup was studied from August 2013 to May 2014.

2.5. Online sensors

The pilot plant was equipped with a number of sensors including an S:can absorbance probe (spectro:lyser™; s:can Messtechnik GmbH), pH-meter, pressure transducers and a conductivity probe. Absorbance spectra was acquired with the S:can sensor using a flow through cell with 4 cm path length in the wavelength range 230–750 nm. Empirical relationships from particle rich waters were used to calibrate the absorbance measurements against both TOC and turbidity.

2.6. Organic matter characterization

Organic matter was characterized using a number of techniques. Regular and compulsory samples monitoring the WTP performance ($n > 30$) between treatment steps were analyzed for pH, alkalinity and UV absorbance at 254 nm. S:can recorded absorbance spectra at the raw water intake for the period July 2010 to June 2014 with one minute resolution. Additionally, grab samples ($n = 20$) were analyzed for a number of DOC characteristics at eight different sampling points throughout the drinking water train (Fig. 1). Samples were taken every month and at specific days prior to or after important adjustments in the setup, such as change of active carbon in the filters or change of intake depth from level A to level B (15.01.2013: 22 m → 4 m, 25.04.2013: 4 m → 22 m, 04.02.2014: 22 m → 4 m, and 25.02.2014: 4 m → 22 m), shown as vertical lines in Fig. A1. All samples were analyzed for total and dissolved organic carbon (TOC and DOC) using a Shimadzu TOC-V_{CPH}. DOC samples were filtered using pre-washed (MilliQ water, <18.2 Ω cm^{-1}) cellulose acetate 0.45 μm filters (Minisart, Sartorius). Filter blanks were within 0.1 mg C L^{-1} of the DOC content of MilliQ water. As TOC and DOC were always within the analytical precision of the measurement (0.3 mg L^{-1}) we will only mention DOC in the subsequent text. Fluorescence excitation emission matrices (EEMs) were collected using an Aqualog (Horiba Jobin Yvon) spectrofluorometer (Lavonen et al. 2015). Previously established indices were calculated from the corrected EEMs, namely HIX, fluorescence index (FI) and β:α according to Ohno 2002, Cory and McKnight 2005, and Parlanti et al. 2000. Changes in fluorescence spectra over the whole measured range were assessed using differential EEMs (Lavonen et al. 2015) for the coagulation, NF and GAC treatments. To compare the removal of shorter emission wavelength, protein-like autochthonous FDOM and longer emission wavelength, terrestrially derived humic-like FDOM we looked at the % decrease in fluorescence signal (differential EEM divided by measured EEM before a treatment process) at excitation = 276 nm, emission = 320 nm (protein-like) and excitation = 350 nm, emission = 550 nm (humic-like). As the raw water was low in dissolved iron (<30 ppb) and all treatment processes studied here involved only small changes in pH ($6.6 < pH < 7.2$) we expect no significant effect on the fluorescence spectra from the chemical conditions of the samples.

Approximately 1–20 L samples (depending on DOC concentration) were filtered through pre-combusted (4 h at 450 °C) GF/F

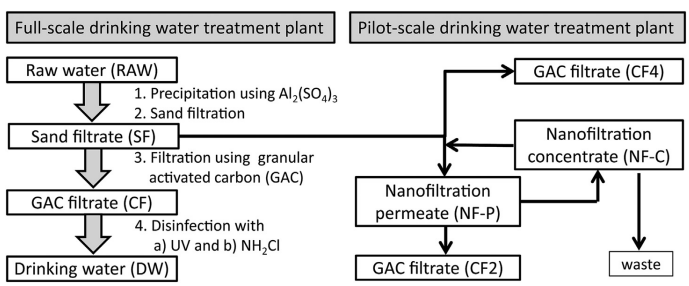

Fig. 1. Water treatment train for the full scale drinking water plant and the pilot scale drinking water plant at Görväln waterworks. The codes for raw water (RAW), sand filter (SF), full scale active carbon filter (CF), nanofilter concentrate (NF–C), nanofilter permeate (NF–P), the other two carbon filters (CF2 and CF4) and drinking water (DW) are used throughout the paper.

filters (effective pore size of 0.7 μm) and acidified to pH 2 using 37% HCl, p.a., before gravitationally loaded to solid phase extraction cartridges (Agilent Bond Elut PPL). DOM was eluted with methanol according to Dittmar et al. 2008. The methanol extracts were kept in a freezer until analyses were conducted. Ultrahigh resolution MS analyses were performed at the Helmholtz Centre in Munich using a 12 T SOLARIX FT-ICR mass spectrometer (Bruker, Bremen, Germany) with an Apollo II electrospray ionization source in negative ion mode. Chemical formulas were assigned to the *m*/*z* peaks based on $^{12}C_{0-100}$, $^{16}O_{0-80}$, $^{1}H_{0-\infty}$, $^{14}N_{0-3}$, $^{32}S_{0-2}$. For further details regarding FT-ICR-MS analyses, formula assignment and data processing, see Lavonen et al. 2015. Relative abundances of *m*/*z* peaks were calculated by dividing the signal intensities by the intensity of the most abundant peak in each sample. Changes in relative abundance during the different treatment processes are expressed in percentage points by subtracting the relative abundance of an *m*/*z* peak in the sample after treatment from that in the sample before treatment. Following Lavonen et al., 2015, where the same mass spectrometer was used, we only considered changes in relative abundance by more than 2.5 percentage points as significant, based on measurements of double samples where differences between signal intensities were, on average, 0.9 ± 1.5 percentage points.

Liquid chromatograph organic carbon detection (LC-OCD) was used to analyze a large number of samples (n = 100) from the pilot plant and the full scale process. LC-OCD quantifies the elution as a function of size and column affinity of carbon and nitrogen from a Sephadex column using a buffered (pH = 6.85 using a potassium-dihydrogenphosphate and sodium-hydrogenphosphate buffer with an ionic strength of 2.5 mM) carrier solution (Huber et al. 2011). This method has been calibrated using both standard IHSS and polystyrene sulfonate standards and widely applied (Baghoth et al. 2011). UV absorbance (254 nm), C and N are measured online, and allow quantifying the elution of DOC over time. The acquired chromatogram is separated into different apparent size fractions using the Chrom_CALC software (Huber et al. 2011) that divides DOC into the following apparent size fractions as a function of elution time: Biopolymers, HS, building blocks, low molecular weight neutrals and low molecular weight acids that are noted together as LMW.

3. Results and discussion

3.1. Performance of the retrofitted NF pilot plant

The pilot scale membrane plant produced treated water with constant water quality during the whole 9 month experimental period, thus fulfilling one of the main objectives of the study: stable removal of color and DOC over time. The stable DOC character is exemplified by the data in Tables 2 and 3 and Fig. A1 Both outgoing DOC concentration (0.6 ± 0.1 mg C L^{-1}) and DOC character (i.e β:α = 0.95 ± 0.04) of the NF permeate are very stable during the whole study period. Raw water DOC concentration of around 8–11 mg C L^{-1} was reduced to below 0.5 mg C L^{-1} after NF. Of this removal, the full scale coagulation treatment accounted for approximately 50% while NF removed additionally 40% of the DOC, only slightly lower than what can be achieved using conventional spiral would membranes (Meylan et al. 2007; Schafer et al. 2004; Metsamuuronen et al. 2014). In contrast to the former membranes, the hollow fibre NF membranes used here succeeded to retain less than 80% of incoming hardness (results not shown), as is desirable for soft raw waters, thus avoiding a post-membrane alkalinisation step. DOC concentration in the GAC filter feed was significantly reduced (compare SF and NF–P in Table 2). Incoming DOC in the water fed to the pilot plant GAC was eight times lower than that of the full scale GAC, which was approximately 4 mg C L^{-1}. Across the whole pilot plant around 93% of incoming HS, 86% of incoming DOC and 87% of A254 was removed.

Table 1
Correlations between different relationships that concern changes in DOC or, character of DOC used in this study.

No	Equation
1	COD_{Mn} [mg L^{-1}] = 0.666 + 5.26*A_{254}; r^2 = 0.94 RMSE = 0.5 [mg L^{-1}]; n = 115
2	%DOC removed = 0.788–0.00489*Al_{DOS} [mg L^{-1}]; r^2 = 0.91 RMSE = 1.3%; n = 249
3	%DOC removed = 2–2.09*HS_{frac};r^2 = 0.75 RMSE = 2.2%; n = 24
4	HS [ppb] = 307 + 21800*A_{254}; r^2 = 0.99 RMSE = 200 [ppb]; n = 29
5	SUVA-HS = 16.2–8.19*FI; r^2 = 0.93 RMSE = 0.17; n = 28
6	MW-HS [Dalton] = −4190 + 5240*HIX; r^2 = 0.80 RMSE = 38 [Dalton]; n = 29
7	LMW neutrals [ppb] = 124 + 0.489*Build-Blocks [ppb]; r^2 = 0.86, RMSE = 99 [ppb]; n = 29
8	%HS = 1.52–1.33*β:α; r^2 = 0.86, RMSE = 0.032; n = 29

3.2. Selective removal of DOC across the whole and pilot plant treatment train

3.2.1. DOC concentration in the raw water

Raw water DOC varied between 8.1 and 11.1 mg L^{-1} (10–90% quartiles respectively) during our experiment period and was composed of approximately 70% HS (Table 2, Table A1 and Fig. 2). The observed variation in DOC during the study period is thus very relevant for dealing with the recently increasing raw water DOC (Fig. A7) and for testing how retrofitting a NF membrane may counteract this rise in DOC.

3.2.2. Changes in DOC composition during coagulation

DOC characterization using LC-OCD indicates that the coagulation treatment was, apart from small quantities of large biopolymers, almost exclusively removing HS from the raw water (Fig. 2). A selective removal of UV-absorbing substances (Fig. 2, SUVA in Table 2) is in accordance with many previous studies (Baghoth et al. 2011; Shutova et al. 2014). Within the HS fraction, larger compounds were preferentially removed during the coagulation step. Median nominal molecular weight for HS was 452 ± 30 Da after coagulation, compared to 660 ± 70 Da in the incoming water (Table 2). Targeted removal of larger components was also seen from the FT-ICR-MS data were the average nominal molecular weight of CHO components that decreased significantly (were selectively removed) was 440 Da (range from 302 to 578 Da) while the average mass for components that increased significantly (were not/poorly removed) was 380 Da (range from 256 to 454 Da). There was, furthermore, a clear shift in abundance from components with a positive average carbon oxidation state to those with negative values (more reduced), in accordance with a previous study of another WTP (Lovö) that also use eastern Mälaren as raw water source and the same coagulation chemical as Görväln WTP (Lavonen et al. 2015). Comparing the components that decreased during coagulation at Görväln and Lovö WTP formula by formula showed that 82% (n = 114) of those decreasing with >2.5 percentage points at Görväln also decreased significantly at Lovö despite being sampled different years and seasons. This shows that coagulation is a rather stable process, repeatedly targeting similar components. Differential EEMs indicate a strong preferential removal of terrestrial FDOM with emission at long wavelengths (Fig. 3 and Fig. A4), as demonstrated by low β:α (0.48 ± 0.01) and FI 1.37 ± 0.02, and HIX close to 1 (0.94 ± 0.01) for the calculated removed fraction (Table 3), in line with Lavonen et al. 2015. Removal ranged from 35 ± 2% for protein-like material to 65 ± 2% of

Table 2
Median DOC, A254, SUVA and DOC character during the different treatment steps for the period August 2013 to end of May 2014 (5–9 measurements per treatment). Pilot scale sampling sites in brackets (nanofiltration permeate (NF–P), activated carbon filtrate for pilot column fed with NF permeate (CF2), activated carbon filtrate for pilot column fed with rapid sand filtrate from the full scale process (CF4) and concentrate from the nanofiltration NF–C).

Sample	DOC (mg C L^{-1})	A_{254} (m^{-1})	SUVA (L mg^{-1} m^{-1})	%HS	MW_{HS} (Da)	%Build	%LMW
Raw	8.8 ± 0.1	26.7 ± 3.5	3.1 ± 0.1	71 ± 3	660 ± 70	3.1	9.4
SF	4.3 ± 0.1	8.9 ± 0.5	2.1 ± 0.1	50 ± 4	450 ± 50	3.6	15.0
NF–P	0.6 ± 0.0	1.1 ± 0.2	1.7 ± 0.3	27 ± 3	420 ± 40	1.4	34.9
CF2[a]	0.5 ± 0.1	0.5 ± 0.6	1.2 ± 1.3	30 ± 14	420 ± 50	2.1	36.3
NF–C	8.1 ± 0.3	17.4 ± 1.5	2.0 ± 0.2	54 ± 4	450 ± 50	3.3	13.7
CF4[a]	4.2 ± 0.8	8.4 ± 0.7	2.1 ± 0.2	54 ± 4	450 ± 50	3.2	14.8
DW	4.4 ± 0.2	8.6 ± 0.4	1.9 ± 0.1	52 ± 4	407 ± 60	3.5	15.2

[a] These data have clear trends over time when fresh granular activated carbon is used but are displayed as median values in this table.

longer emission wavelength, terrestrially derived FDOM (Fig. 3, left).

3.2.3. GAC in full and pilot scale

Detailed analysis of full scale or pilot scale long term experiments involving GAC filters are rare (Gibert et al. 2013). In the full scale treatment Görväln WTP aims to use their GAC filter as a chemical barrier. However, due to the relatively high DOC concentration in the GAC feed (4.8 ± 0.3 mg C L^{-1}), the filters commonly become saturated with irreversibly bound DOM compounds within 1 month after regeneration (Matilainen et al. 2006) and do not remove any DOC (Table A1). The current GAC thus functions as a biofilter, where microbes adsorbed to the GAC surface remove e.g. compounds causing taste and odor, and in some case smaller amounts of DOC e.g. (Camper, 2004; Matilainen et al. 2006; Gibert et al. 2013). The pilot reference GAC filter (CF4) reduced 75% of the incoming DOC when the activated carbon was new, but after being used for just 1 month the removal had been lowered to 11% (0.5 mg C L^{-1}). After one additional month until the end of the experiment period hardly any (0.1 ± 0.8 mg C L^{-1}) was removed (Fig. A6). The pilot GAC filter that was fed with NF permeate (CF2) showed a similar reduction in DOC removing capacity over time with the largest removal when the activated carbon was new (72% = 1.4 mg C L^{-1}), which decreased to 0.5 mg C L^{-1} removal the next coming two months and thereafter the reduction in DOC was only 0.1 mg C L^{-1} until the end of the trial period, similar to CF4. Both GAC filters in the pilot plant initially removed large amount of both humic-like (77 and 96% for CF4 and CF2 respectively) and protein-like FDOM (70 and 61% respectively) (Fig. 4, left panel). Our LC-OCD analysis confirmed the results from Gibert et al. 2013 who also observed preferential removal of HS during the early phase (Fig. 4, right panel). The Norit 1240 W seems to have a higher affinity for HS than Norit Row 0.8 supra used in Gibert et al. 2013 under the given conditions. This was not studied further but could be due to differences in water quality such as pH, presence of cations that change the conformation of HS in solution (Schafer et al., 2004) and differences in the GAC pore size distribution. According to Camper 2004, HS may support the same amount of microbial growth in a biofilm as readily available smaller LMW substances. Even if no change in DOC could be quantified across the full scale GAC filter, there was still a clear pattern in FDOM removal demonstrated by a decrease in 15 ± 11% for protein-like material and 3 ± 1% for humic-like material, indicating that the GAC mainly had acted as a biofilter as humic material primarily is removed through adsorption (Velten et al. 2011; Matilainen et al. 2006): Both fluorescence and LC-OCD data are thus valuable for indicating changes in GAC saturation and functioning.

3.2.4. Changes in DOC concentration and composition across the NF membrane

In the pilot plant 40% of the incoming DOC was removed with the NF membrane. The two main fractions that were retained (>90%) were biopolymers and HS (Fig. 2). Similar or higher removals are observed in tighter spiral wound membranes (Schafer et al. 2004) and (Meylan et al. 2007). Up to 80% of the smaller constituents – building blocks and low molecular weight compounds were removed (Table 2, Table A1). UV absorbing compounds were removed slightly more than bulk DOC with SUVA decreasing from 2.1 to 1.7 (Table 2). This and the significant increase in FI and β:α during membrane treatment demonstrates selective removal of terrestrial DOM (Table 3). FI in the treated water was 1.84 ± 0.03 which indicates that so much terrestrial DOM was removed in the combined coagulation NF treatment that the permeate (Table 3) resembled organic compounds from extracellular release and leachate from algae and bacteria defined as a microbial endmember (McKnight et al. 2001). Even if NF was selectively removing terrestrial DOM, indices calculated from

Table 3
Median and standard deviation for fluorescence derived data of raw and processed water (SF = sand filtrate, NF–P = nanofiltration permeate). Indices from differential EEMs (Raw/SF = coagulation and SF/NF–P = nanofiltration) demonstrate characteristics of the removed FDOM. The step NF/CF2 is not included here as DOC is very low and we observed clear trends over time.

Sample	FI	HIX	β:α
Raw	1.48 + 0.02	0.91 + 0.01	0.61 + 0.02
SF	1.68 + 0.03	0.88 + 0.01	0.76 + 0.02
Raw/SF	1.37 ± 0.02	0.94 ± 0.01	0.48 ± 0.01
NF–P	1.84 + 0.06	0.83 + 0.02	0.95 + 0.04
SF/NF–P	1.65 ± 0.02	0.90 ± 0.01	0.70 ± 0.02
CF	1.67 ± 0.03	0.88 ± 0.01	0.75 ± 0.01
SF/CF	1.80 ± 0.25	0.84 ± 0.09	1.07 ± 0.22
DW	1.67 ± 0.03	0.88 ± 0.01	0.75 ± 001

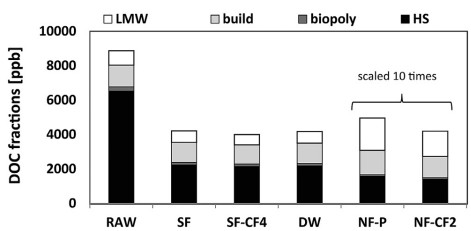

Fig. 2. Selected results of median values for changes in DOC [ppb] quantity and quality across the WTP and pilot plant from the raw water (RAW) through the sand filter (SF), the nanofilter (NF–P) and through the full scale activated carbon (SF-CF4) to the final drinking water (DW) and after the activated carbon filter of the pilot plant (NF-CF2) for all samples in the period August 2013–June 2014. DOC quality parameters in order of decreasing molecular size are codes as biopoly = Biopolymers, HS = Humic substances; LMW = low molecular weight neutrals; build = building blocks.

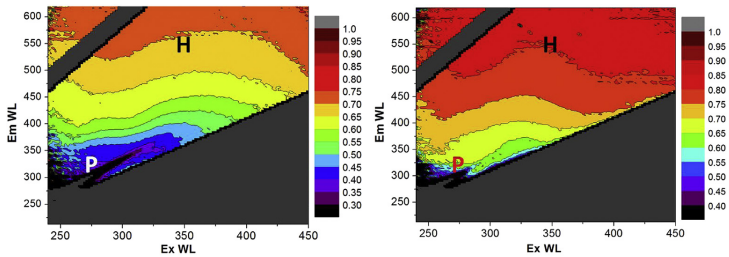

Fig. 3. Fraction of removed fluorescent dissolved organic matter for coagulation (left) and NF (right) treatments. Dark red colors indcate strong removal (>75%) while blue–purple colors indicate less removal (<40%). The excitation/emission wavelength pairs chosen to represent humic-like (Ex = 350 nm, Em = 550 nm, marked "H" in the EEMs) and protein-like (Ex = 276 nm, Em = 320 nm, marked "P" in the EEMs). (For interpretation of the references to color in this figure legend, the reader is referred to the web version of this article.)

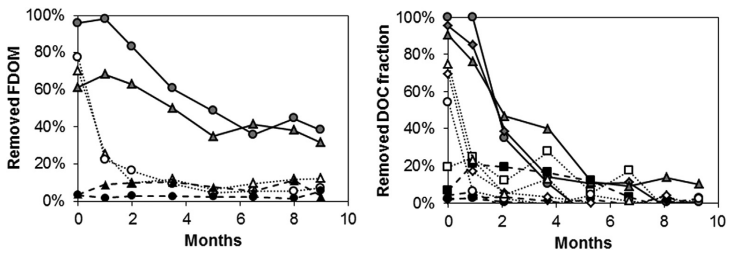

Fig. 4. Removal (left panel) of protein-like (triangles) and humic-like (circles) fluorescent dissolved organic matter and (right panel) removal of low molecular neutrals (triangles), humic substances (circles), building blocks (diamonds) and biopolymers (squares) across granulated activated carbon (CF) filters in the full scale treatment (black symbols), as well as the pilot plant reference (CF4, white symbols), and downstream from the NF membrane (CF2, gray symbols).

differential EEMs show that the removed DOC still had a rather microbial fingerprint (high FI (1.64 ± 0.02) and β:α (0.71 ± 0.02)). This demonstrates that NF can remove a wide range of DOM components, reflected in 83 ± 1% removal of humic-like FDOM and 66 ± 3% reduction in protein-like material (Fig. 3). This is supported by FT-ICR-MS results, showing that more than 90% of the components that decreased significantly in relative abundance during coagulation (n = 139) further decreased with NF. Also, 93 components that were not targeted during coagulation decreased significantly during NF. The coagulation treatment was highly selective towards oxidized components with a weighted (against the relative abundance) mean average carbon oxidation state ($\overline{C_{os}}$) of 0.35 for decreasing components (maximum 0.78 and minimum −0.10 for components that decreased significantly). Meanwhile, NF removed a wider range of both reduced and oxidized components (weighted mean $\overline{C_{os}} = -0.05$, maximum 0.63 and minimum −0.61 for components decreasing significantly). Hence, we can show that NF with the employed membrane is more efficient than coagulation, both continuing to remove material reactive during coagulation, as well as additional components. All components that increased in relative abundance during NF treatment had $m/z < 400$ Da (Fig. 5). This indicates that these components do not aggregate significantly and

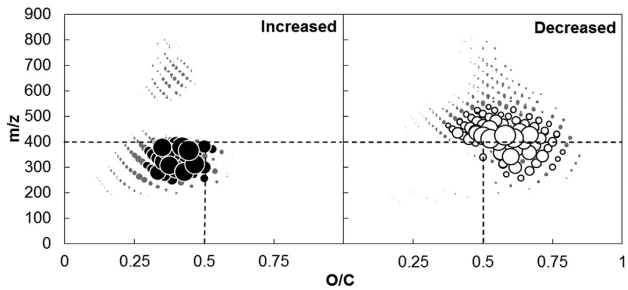

Fig. 5. CHO components that increased (left) and decreased (right) during the pilot scale nanofiltration of, with chemical coagulation, treated water. White and black bubbles demonstrate significant changes in relative abundance while gray bubbles show non significant changes. Bubble size represents the magnitude of the change in relative abundance (maximum 52 percentage point's decrease and 24 percentage point's increase).

have therefore not been removed through size exclusion. There were also components that had m/z < 400 Da that decreased in abundance, however, these had significantly higher O/C (>0.50) (right panel in Fig. 5). A higher removal of smaller but highly charged molecules is in line with expected repulsion on negatively charged membranes (Schafer et al. 2004).

3.3. Identifying useful spectroscopic information for DOC character

From August 2012 the S:can was used to control the $Al_2(SO_4)_3$ dosing for improved DOC removal in the full scale WTP. From then on dosing efforts were increased and controlled by the online UV signal. Two thirds of HS were removed using a coagulant dose of around 50 mg/l $Al_2(SO_4)_3$. The removed DOC was almost entirely composed of HS (96%) (Fig. 2). This explains why the relative removal of DOC is well correlated to both %HS, Al_{DOS} and to A254 (Table 1). On average, the online sensor controlled dosing was higher than the turbidity controlled dosing (75 versus 50 mg L^{-1} $Al_2(SO_4)_3$ and led to a 12% higher DOC removal (around 1 mg L^{-1} on average). Controlling the coagulant dose with absorbance measured online will allow the WTP to remove more DOC under periods with high A254 when DOC is easy to coagulate as shown below.

Due to the importance of HS for DOC removal during coagulation we analyzed whether any of the optical parameters could be coupled to the LC-OCD data. When comparing the average β:α with average fraction of HS of total DOC in the raw water, rapid sand filtrate and NF permeate and concentrate as well as the drinking water we obtained a linear relationship (Fig. 6). Using average data (Table 3) from delta EEMs from raw water to coagulation (RAW/SF) and from coagulation to NF (SF/NF–P) we may produce two additional data points using mass balance calculations of changes in HS (Fig. 6). There were a number of other interesting relationships (e.g. prediction of molecular weight of HS as a function of increasing HIX, HS as a function of A254 (Table 1) in line with the results of (Baghoth et al. 2011). We focused on another important aspect for finished drinking water, notably the presence of low molecular weight compounds (LMW) in the permeate. In our study we found that LMW determined by LC-OCD in the permeate may be estimated from HIX and β:α (Fig. A6). In line with Baghoth et al. 2011 and Baker et al. 2008 our results confirm that fluorescence signals may be coupled to NOM properties.

Both GAC and membrane performance may thus be followed using fluorescence as a faster and cheaper indicator of DOC quality on site. While these relationships (e.g. UV versus DOC (Fig. A2), DOC versus building blocks etc.) are useful for individual WTPs, we agree with Shutova et al. 2014 that further work is needed to exclude that they are only site specific. Complicating factors in such an analysis would be the presence of dissolved iron (Weishaar et al. 2003), pH (Pace et al. 2012) and presence of cations (Schafer et al. 2004) that all may influence absorbance and fluorescence due to either changes in organic matter conformation or metal binding.

3.4. Effect of lake water retention time on coagulation efficiency as one aspect of climate adaptation

Both Gondar et al. 2008 and Köhler et al. 2013 have noted that lake water NOM may be described as two endmembers that are mainly controlled by lake turnover and flow. Dry spells may have a significant effect of lake water quality as lake water NOM during those periods usually contain more hydrophilic NOM (Tang et al. 2013; Ritson et al. 2014) and less of hydrophobic HS. Removal of incoming DOC during coagulation treatment is controlled by the fraction of HS present in the raw water. The abundance of HS can be estimated from A254 (Fig. A3). A254 is, however, affected by the presence of iron (Weishaar et al. 2003) and during periods of high iron concentrations (>300 ppb) as was observed in the year 2000 (personal communication Görväln WTP) this relationship will fail. Both β:α and DOC concentration, however, have previously been shown (Fig. 6) to be controlled by lake water retention time (Köhler et al. 2013) This information could be combined to estimate how shorter or longer lake water retention times may control raw water DOC concentrations and $Al_2(SO_4)_3$ doses. Using a series of linear regression that relate age with DOC and β:α (Fig. 7), β:α with HS (Fig. 6) and HS with dosing and DOC removal (Table 1) we may estimate outgoing DOC from raw water DOC and β:α that both change with the age of incoming raw water. As β:α proved to be an excellent indicator of the percentage of HS present, we selected this optical variable to further evaluate its usefulness to assess coagulation treatability of DOM. Two different scenarios with varying water age as surrogates for high respective low flow conditions and varying DOC concentration and their respective β:α and %HS are displayed in Fig. 7. Despite varying incoming DOC in our scenario (7–14 mg C L^{-1}), drinking water DOC is expected to vary between 3.3 and 4.7 requiring $Al_2(SO_4)_3$ doses between below 10 to almost 100 mg L^{-1}, twice the average dose used today. Wet years with short lake WRT (<1 year) will lead to exceptionally high $Al_2(SO_4)_3$ dosing due to the increased presence of HS while dry years with long WRT (>3 years) will lead to low $Al_2(SO_4)_3$ dosing but almost similar outgoing DOC. Should the current observed trend of increasing DOC that has been recorded at the outlet of Mälaren (Fig. A7), and large areas of Sweden and Norway continue for several years, outgoing DOC will be above 5 mg L^{-1} irrespective of the chosen scenario.

Another important question of interest is how the fraction of hydrophilic and neutral DOC giving rise to biologically degradable

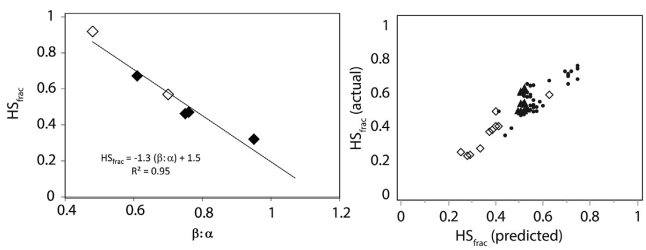

Fig. 6. Left: Measured fraction of humic substances (HS_{frac}) for Raw, SF, DW and NF–P as a function of β:α (black diamonds) and mass balance derived HS_{frac} for the material that was removed during coagulation and NF treatments versus β:α calculated from differential EEM (white diamonds). The regression line is very close to that estimated from all individual data shown to the right. HS_{frac} (predicted) was estimated using β:α (HS_{frac} = 1.52–1.33*β:α) for all samples except CF2 where DOC concentrations were low.

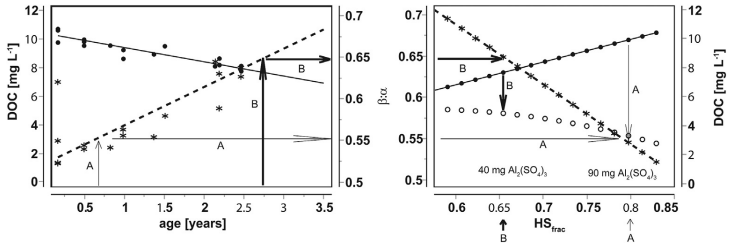

Fig. 7. Measured and fitted DOC and β:α across Mälaren as a function of water age to the left (Data from Köhler et al., 2013). Black circles and black stars display measured DOC and measured β:α respectively (left panel). Both DOC and β:α are read out as a function of water age (x-axis in left panel) using the horizontally pointing arrows in the left panel. On the right: predicted fraction of DOC composed of HS (HS_{frac}) (x-axis) estimated from as a function of incoming β:α (left y-axis) (blacks stars) and DOC (right y-axis) (black circles) using eqs. 2,3, and 8 in Table A1 that relate β:α, HS, DOC and aluminum dose. Vertically downwards pointing arrows indicate the amount of DOC (difference between black and white circles) that can be removed through coagulation treatment for two different situations (A and B); The predicted outgoing DOC (white circles in the right panel) is illustrated for A (a "young" water 0.7 months of age with high DOC and high $HS_{frac} = 0.8$, requiring around 90 mg L^{-1} $Al_2(SO_4)_3$ and outgoing DOC of around 3.3 mg L^{-1}) and B (an "old water" with lower DOC, lower $HS_{frac} = 0.65$ leading to a low dose of 40 mg L^{-1} $Al_2(SO_4)_3$ and outgoing DOC of around 4.7 mg L^{-1}).

organic carbon will vary in the future. The most relevant fraction is probably that determined as LMW through LC-OCD. Applying the regression in Fig. A6 and using lake water HIX and β/α LMW decreases from 0.8 to 0.6 mg L^{-1} across the lake. Lake water retention time thus only has a minor effect on LMW. Future studies will need to address that question in more detail.

3.5. Remaining questions and challenges with hollow fibre membrane filtration

Fluorescence EEMs and LC-OCD analyses indicate that the NF permeate consists of microbial derived low molecular weight components, rich in organic nitrogen that might affect the biological activity (regrowth potential) and chemical reactivity (disinfectant stability, corrosion of pipes) in the distribution network. There are recurrent algal blooms in Mälaren and the lake also receives waste water from a number of smaller cities and one large hospital within the catchment. The NF membrane used in this study would allow removing at least some of the larger hydrophilic micropollutants such as microcystines and large PFCAs (Perfluorodecanoate 513 Da) and PFOS (Perfluorooctane sulfonic acid 500 Da). Other typically occurring, smaller compounds such as ketoprofene ($pK_a = 4.5$, 250 Da), or danofloxazine ($pK_a = 6.0$, 360 Da) might permeate. In the future we will analyze the fate of a number of micro pollutants through todays and the new proposed water treatment train to test the ability of NF to either retain or improve the removal efficiency of GAC filters.

4. Conclusions

Improved removal of organic matter from surface water is important for surface waters in Nordic countries that currently undergo show increasing trends of organic carbon. Stockholm produces its drinking water from raw water (DOC = 9 mg L^{-1}) taken in Mälaren, Swedens third largest lake. DOC has increased over the last 19 years from 6 to 10 mg L^{-1} and we expect larger temperature and flow driven variations in DOC concentration and character over time in the future. At current full scale operation using aluminum coagulation indicate removal of larger (>500 Da and HS only) terrestrial (FI = 1.4, β:α = 0.5) and with a higher mean average carbon oxidation state ($\overline{C_{os}} = 0.5$) carbon. Using β:α that relates to the presence of HS in the studied water we may estimate the outgoing DOC concentration as a function of incoming DOC character in the incoming water based on established coagulation dose DOC and color relationships. The existing aluminum coagulation (outgoing DOC 4.5 mg C L^{-1}) and granular active carbon (outgoing DOC 4.0 mg C L^{-1}) process alone might not be able to handle these future changes. Longer water retention times during dry spells will decrease the fraction of hydrophobic DOC that is easy to flocculate.

We chose to use a novel and more resistant hollow-fibre polysulfone nanofilter (HFW 1000) instead of spiral wound membranes as they would affect hardness too much in the studied soft waters. The coupled coagulation-NF pilot plant produced stable outgoing water quality (0.5 mg L^{-1}) during the nine month test trial. The removal of carbon with a much larger range of size (350–500 Da) and properties ($\overline{C_{os}} = -0.07$, FI = 1.65, β:α = 0.5) during NF as compared to coagulation was confirmed using a large array of methods including LC-OCD, FT-ICR-MS and fluorescence. Even if the fluorescence derived parameters and correlations probably are site specific they are reliable, fast to determine and comparably cheap complement to the more advanced techniques used here (FT-ICR-MS and LC-OCD). DOC removal and change of DOC character in the GAC filters in full scale, the current coagulation scheme and pilot plant setup showed marked differences with slower saturation and larger changes in DOC character using fresh GAC. The removal of potentially elevated concentrations of organic contaminants such as diesel, microcystines or persistant organic micropollutants in Mδlaren may thus improve using the proposed new scheme.

Acknowledgments

Chemical analysis and the working time of S.J, Köhler was financed by two research grants, grant number 11–112 Genomembran and through the research network DRICKS that are financed by the Swedish Water and waste water association. Elin Lavonen was financed through the FORMAS grant Color of water.

Appendix A. Supplementary data

Supplementary data related to this article can be found at http://dx.doi.org/10.1016/j.watres.2015.11.048.

References

Baghoth, S.A., Sharma, S.K., Amy, G.L., 2011. Tracking natural organic matter (NOM) in a drinking water treatment plant using fluorescence excitation-emission matrices and PARAFAC. Water Res. 45 (2), 797–809.

Baker, A., Tipping, E., Thacker, S.A., Gondar, D., 2008. Relating dissolved organic matter fluorescence and functional properties. Chemosphere 73 (11),

1765–1772.
Camper, A.K., 2004. Involvement of humic substances in regrowth. Int. J. Food Microbiol. 92 (3), 355–364, 1.
Cory, R.M., McKnight, D.M., 2005. Fluorescence spectroscopy reveals ubiquitous presence of oxidized and reduced quinones in dissolved organic matter. Environ. Sci. Technol. 39 (21), 8142–8149.
De Grooth, J., 2015. A Tale of Two Charges: Zwitterionic Polyelect Rolyte Multilayer Membranes. Ph.D.. Twente University, Twente.
Dittmar, T., Koch, B., Hertkorn, N., Kattner, G., 2008. A simple and efficient method for the solid-phase extracion of dissolved organic matter (SPE-DOM) from seawater. Limnol. Oceanogr. Methods 6, 230–235.
Eikebrokk, B., Vogt, R.D., Liltved, H., 2004. NOM increase in Northern European source waters: discussion of possible causes and impacts on coagulation/contact filtration processes. Water Sci. Technol. 4 (4), 47–54.
Ericsson, P., Hajdu, S., Willén, E., 1984. Vattenkvaliteten i Görväln. En dynamisk Mälarfjärd. Vattenkemi och växtplankton i ett fyrtioårigt perspektiv. Vatten 40, 193–211 (in Swedish).
Gibert, O., Lefevre, B., Fernandez, M., Bernat, X., Paraira, M., Pons, M., 2013. Fractionation and removal of dissolved organic carbon in a full-scale granular activated carbon filter used for drinking water production. Water Res. 47 (8), 2821–2829.
Gondar, D., Thacker, S., Tipping, E., Baker, A., 2008. Functional variability of dissolved organic matter from the surface water of a productive lake. Wat. Res. 42 (1–2), 81–90.
Hongve, D., Riise, G., Kristiansen, J.F., 2004. Increased colour and organic acid concentrations in Norwegian forest lakes and drinking water – a result of increased precipitation? Aquat. Sci. 66, 231–238.
Huber, S.A., Balz, A., Abert, M., Pronk, W., 2011. Characterisation of aquatic humic and non-humic matter with size-exclusion chromatography – organic carbon detection – organic nitrogen detection (LC-OCD-OND). Water Res. 45 (2), 879–885.
Köhler, S.J., Kothawala, D., Futter, M.N., Liungman, O., Tranvik, L., 2013. In-Lake processes offset increased terrestrial inputs of dissolved organic carbon and color to lakes. Plos One 8 (8).
Lavonen, E.E., Kothawala, D.N., Tranvik, L.J., Gonsior, M., Schmitt-Kopplin, P., Köhler, S.J., 2015. Ultra-high resolution mass spectrometry explains changes in the optical properties of dissolved organic matter during drinking water production. Water Res. (in review for).
Matilainen, A., Vepsäläinen, M., Sillanpää, M., 2010. Natural organic matter removal by coagulation during drinking water treatment: a review. Adv. Colloid Interface Sci. 159 (2), 189–197.
Matilainen, A., Vieno, N., Tuhkanen, T., 2006. Efficiency of the activated carbon filtration in the natural organic matter removal. Environ. Int. 32 (3), 324–331.
McKnight, D.M., Boyer, E.W., Westerhoff, P.K., Doran, P.T., Kulbe, T., Andersen, D.T., 2001. Spectrofluorometric characterization of dissolved organic matter for indication of precursor organic material and aromaticity. Limnol. Oceanogr. 46 (1), 38–48.
Metsamuuronen, S., Sillanpaa, M., Bhatnagar, A., Manttari, M., 2014. Natural organic matter removal from drinking water by membrane technology. Sep. Purif. Rev. 43 (1), 1–61.
Meylan, S., Hammes, F., Traber, J., Salhi, E., von Gunten, U., Pronk, W., 2007. Permeability of low molecular weight organics through nanofiltration membranes. Water Res. 41 (17), 3968–3976.
Ohno, T., 2002. Fluorescence inner-filtering correction for determining the humification index of dissolved organic matter. Environ. Sci. Technol. 36 (4), 742–746.
Pace, M., Reche, I., Cole, J., Fernández-Barbero, A., Mazuecos, I., Prairie, Y., 2012. pH change induces shifts in the size and light absorption of dissolved organic matter. Biogeochemistry 108 (1–3), 109–118.
Parlanti, E., Worz, K., Geoffroy, L., Lamotte, M., 2000. Dissolved organic matter fluorescence spectroscopy as a tool to estimate biological activity in a coastal zone submitted to anthropogenic inputs. Org. Geochem. 31 (12), 1765–1781.
Regula, C., Carretier, E., Wyart, Y., Gesan-Guiziou, G., Vincent, A., Boudot, D., Moulin, P., 2014. Chemical cleaning/disinfection and ageing of organic UF membranes: a review. Water Res. 56, 325–365.
Ritson, J.P., Graham, N.J.D., Templeton, M.R., Clark, J.M., Gough, R., Freeman, C., 2014. The impact of climate change on the treatability of dissolved organic matter (DOM) in upland water supplies: a UK perspective. Sci. Total Environ. 473, 714–730.
Schafer, A.I., Pihlajamaki, A., Fane, A.G., Waite, T.D., Nystrom, M., 2004. Natural organic matter removal by nanofiltration: effects of solution chemistry on retention of low molar mass acids versus bulk organic matter. J. Membr. Sci. 242 (1–2), 73–85.
Shutova, Y., Baker, A., Bridgeman, J., Henderson, R.K., 2014. Spectroscopic characterisation of dissolved organic matter changes in drinking water treatment: from PARAFAC analysis to online monitoring wavelengths. Water Res. 54, 159–169.
Tang, R., Clark, J.M., Bond, T., Graham, N., Hughes, D., Freeman, C., 2013. Assessment of potential climate change impacts on peatland dissolved organic carbon release and drinking water treatment from laboratory experiments. Environ. Pollut. 173, 270–277.
Velten, S., Knappe, D.R.U., Traber, J., Kaiser, H.-P., von Gunten, U., Boller, M., Meylan, S., 2011. Characterization of natural organic matter adsorption in granular activated carbon adsorbers. Water Res. 45 (13), 3951–3959.
Weishaar, J.L., Aiken, G.R., Bergamaschi, B.A., Fram, M.S., Fujii, R., Mopper, K., 2003. Evaluation of specific ultraviolet absorbance as an indicator of the chemical composition and reactivity of dissolved organic carbon. Environ. Sci. Technol. 37 (20), 4702–4708.
Zhang, Y., Causserand, C., Aimar, P., Cravedi, J.P., 2006. Removal of bisphenol A by a nanofiltration membrane in view of drinking water production. Water Res. 40 (20), 3793–3799.

Printed by Media-Tryck, Lund 2017 NORDIC ECOLABEL, 3041 0903

Alexander Keucken is a research manager at the public utility Vatten & Miljö i Väst AB (VIVAB).

Alexander Keucken has been enrolled at the division of Water Resources Engineering, Lund University for his Ph.D. studies. His research subject is membrane technology for drinking water treatment processes. Alexander started his career as a water professional in 1995 by graduating in a German training program within environmental engineering, focusing on advanced water treatment. Alexander has acquired an extensive range of environmental and technical knowledge over his 20 years of work experience in the Swedish public water sector. Alexander is engaged in the water industry, both nationally and internationally, as member of the Swedish national committee in the International Water Association (IWA Sweden). Furthermore, Alexander represents the Swedish Water & Wastewater Association (SWWA) in the committee on drinking water within the European Federation of National Association of Water Services (EurEau).

LUND UNIVERSITY

Faculty of Engineering
Department of Building & Environmental Technology
Division of Water Resources Engineering

ISBN 978-91-7753-459-4 (print)
ISBN 978-91-7753-460-0 (pdf)
Report: 1072